RESILIENCY AND VULNERABILITY OF BOREAL PEATLANDS TO WILDLAND FIRE: IDENTIFYING PATTERNS THROUGH DEPTH OF BURN, CARBON LOSS, AND ENVIRONMENTAL CONTROLS

KAILYN NELSON
Bachelor of Science, University of Lethbridge, 2017

A thesis submitted
in partial fulfilment of the requirements for the degree of

DOCTOR OF PHILOSOPHY

in

EARTH, SPACE, AND PHYSICAL SCIENCE

Department of Geography and Environment
University of Lethbridge
LETHBRIDGE, ALBERTA, CANADA

RESILIENCY AND VULNERABILITY OF BOREAL PEATLANDS TO WILDLAND FIRE: IDENTIFYING PATTERNS THROUGH DEPTH OF BURN, CARBON LOSS, AND ENVIRONMENTAL CONTROLS

KAILYN NELSON

Date of Defense: November 28, 2025

Dr. L. Chasmer Thesis Supervisor University of Lethbridge Lethbridge, Alberta	Associate Professor	Ph.D.
Dr. C. Hopkinson Thesis Examination Committee Member University of Lethbridge Lethbridge, Alberta	Professor	Ph.D.
Dr. D. Thompson Thesis Examination Committee Member Canadian Forest Service Sault Ste. Marie, Ontario	Research Scientist	Ph.D.
Dr. K. Millard Thesis Examination Committee Member Carleton University Ottawa, Ontario	Associate Professor	Ph.D.
Dr. R. Petrone Thesis Examination Committee Member University of Waterloo Waterloo, Ontario	Professor	Ph.D.
Dr. N. Coops External Examiner University of British Columbia Vancouver, British Columbia	Professor	Ph.D.
Dr. Kevin McGeough Chair, Thesis Examination Committee	Co-Chair/Professor	Ph.D.

DEDICATION

For my parents, who supported me through every challenge and celebrated every success. Who encouraged me from day one to pursue my passions, and taught me resiliency, integrity, and the value of doing things that are important to you. For my husband, whose steadfast support, eternal patience, and unwavering confidence in me allowed me to pursue my Ph.D. while we built our family. And for Noah – my moon and my stars – who encompasses everything that is good in this world and brings me more joy than I knew possible.

ABSTRACT

Boreal peatlands are globally significant carbon (C) sinks that have accumulated C over millennia but are increasingly threatened by climate-driven changes in fire regimes and moisture levels. Soil C losses from peat combustion remain uncertain due to challenges in quantifying below-ground combustion, limiting representation in global C budgets and models. This thesis 1) quantifies spatial variability in C loss during boreal peatland fires, and 2) identifies ecological conditions driving variability and peatland resistance or vulnerability to combustion. Research integrates field data, bi-temporal airborne lidar, and statistical modelling from the 2016 Horse River Wildfire in Alberta's Boreal Plains.

A synthesis of existing knowledge produced conceptual models of pre- and post-fire feedbacks impacting peatland combustion and recovery. These frameworks define two conceptual peatlands: resilient – hydrologically connected with low soil bulk density and moderated water tables, resulting in low severity combustion and moisture-retaining negative feedbacks; and vulnerable – fragmented or drained, with high bulk density, fluctuating water tables, and shrub encroachment, resulting in deep burns and drying positive feedbacks.

Lidar ground classification accuracy assessments across unburned and burned, regenerating peatlands revealed negligible mean offsets: 0.00 m in burned to 0.01 m in unburned peatlands, with RMSEs of 0.09 m to 0.19 m, respectively. These findings support the utility of lidar for detecting elevation changes from peat combustion.

Using these validated data, depth of burn (DOB) was estimated across peatland types and ecotones, averaging 0.08 ± 0.06 m, with deepest combustion in bog ecotones

(0.09 ± 0.07 m). Statistical models revealed that top drivers of DOB variability depended on peatland type. In bogs, DOB was associated with topography and morphology, while in fens and swamps, where groundwater connectivity reduces the influence of topography on water tables, differences were associated with vegetation, hydrology, and disturbance.

C losses across peatlands estimated using field-based soil C data and lidar-derived DOB showed that soil C losses (-2.11 ± 5.09 kg m^{-2}) were substantially greater than vegetation losses (-0.38 ± 0.32 kg m^{-2}), with bog ecotones identified as hotspots for C combustion loss (-16.5 kg m^{-2}). Comparison with Landsat differenced Normalized Burn Ratio (dNBR) revealed that while vegetation losses related moderately to dNBR, soil losses did not, demonstrating the limitations of optical indices for below-ground combustion. Comparisons with estimates from the Canadian Model for Peatlands highlighted the need to explicitly include ecotones in C models – particularly under a changing climate.

CONTRIBUTIONS OF AUTHORS

This thesis comprises four manuscript-style chapters, two of which have been published in peer-reviewed journals. Chapter 2 was published by Elsevier under CC BY-NC-ND 4.0. Chapter 3 was published by MDPI under CC BY 4.0. Both manuscripts have undergone minor formatting changes to meet thesis requirements (e.g., re-formatting of reference style to APA 7th edition); no content has been altered. Chapters 4 and 5 are original, unpublished manuscripts that have been written with the intent to submit for publication following thesis submission. Due to the nature of manuscript-based theses, each chapter can be read independently, while also following a natural progression of research, where each builds upon the last, developing a cohesive narrative. I am the sole author of this thesis and lead author on each manuscript, though each chapter is the result of collaborative learning with co-authors, which are attributed below.

Chapter 2: Peatland-Fire Interactions: A Review of Wildland Fire Feedbacks and Interactions in Canadian Boreal Peatlands

Citation: Nelson, K., Thompson, D., Hopkinson, C., Petrone, R., & Chasmer, L. (2021). Peatland-fire interactions: A review of wildland fire feedbacks and interactions in Canadian boreal peatlands. *Science of the total environment*, *769*, 145212. https://doi.org/10.1016/j.scitotenv.2021.145212.

Publication status: Published May 15, 2021 in *Science of The Total Environment* (Elsevier).

Author contributions:

- Conceptualization: Nelson, Chasmer, Thompson, Hopkinson, Petrone
- Methodology: Nelson, Chasmer, Thompson, Hopkinson, Petrone
- Investigation: Nelson
- Formal Analysis: Nelson
- Visualization: Nelson
- Writing – Original Draft Preparation: Nelson
- Writing – Review & Editing: Nelson, Chasmer, Thompson, Hopkinson, Petrone
- Project Administration: Chasmer
- Supervision: Chasmer
- Resources: Chasmer, Hopkinson
- Funding Acquisition: Chasmer, Hopkinson, Nelson

Chapter 3: Quantifying Lidar Elevation Accuracy: Parameterization and Wavelength Selection for Optimal Ground Classifications Based on Time since Fire/Disturbance

Citation: Nelson, K., Chasmer, L., & Hopkinson, C. (2022). Quantifying LiDAR elevation accuracy: Parameterization and wavelength selection for optimal ground classifications based on time since fire/disturbance. *Remote Sensing*, *14*(20), 5080.

Publication status: Published October 11, 2022 in *Remote Sensing* (MDPI).

Author contributions:

- Conceptualization: Nelson, Chasmer, Hopkinson
- Methodology: Nelson, Chasmer, Hopkinson
- Investigation: Nelson
- Data Curation: Nelson
- Formal Analysis: Nelson
- Visualization: Nelson
- Writing – Original Draft Preparation: Nelson
- Writing – Review & Editing: Nelson, Chasmer, Hopkinson
- Project Administration: Chasmer
- Supervision: Chasmer
- Resources: Chasmer, Hopkinson
- Funding Acquisition: Chasmer, Hopkinson, Nelson

Chapter 4: Drivers of Peat Combustion as Indicators of Carbon Loss and Fire Resilience in Boreal Peatlands

Authors: Nelson, et al. (Author order yet to be finalized. Tentatively: Nelson, K., Thompson, D., Hopkinson, C., Millard K., & Chasmer L.)

Publication status: Unpublished, in preparation. Author list and contributions are not finalized.

Author contributions (provisional):

- Conceptualization: Nelson, Chasmer, Thompson, Hopkinson, Millard

- Methodology: Nelson, Thompson, Millard, Chasmer (developed lidar-to-AGB models), Hopkinson
- Investigation: Nelson
- Data Curation: Nelson
- Formal Analysis: Nelson, Chasmer (processed above-ground lidar data)
- Visualization: Nelson
- Writing – Original Draft Preparation: Nelson
- Writing – Review & Editing: Nelson, Chasmer, et al. (additional co-author review to come)
- Project Administration: Chasmer
- Supervision: Chasmer
- Resources: Chasmer, Hopkinson
- Funding Acquisition: Chasmer, Hopkinson, Nelson

Chapter 5: Disproportionate Soil Carbon Loss and Ecotone Sensitivity in Boreal Peatland Wildland Fires: Insights from Lidar and Field Data

Authors: Nelson, K., Thompson, D., Hopkinson, C., Petrone, R., Chasmer, L.

Publication status: Unpublished

Author contributions:

- Conceptualization: Nelson, Chasmer, Thompson, Hopkinson, Petrone
- Methodology: Nelson, Chasmer, Thompson, Hopkinson
- Investigation: Nelson

- Data Curation: Nelson
- Formal Analysis: Nelson
- Visualization: Nelson
- Writing – Original Draft Preparation: Nelson
- Writing – Review & Editing: Nelson, Chasmer, Thompson, Hopkinson, Petrone
- Project Administration: Chasmer
- Supervision: Chasmer
- Resources: Chasmer, Hopkinson
- Funding Acquisition: Chasmer, Hopkinson, Nelson

ACKNOWLEDGEMENTS

I have been fortunate throughout this Ph.D. to have had the support of exceptional supervisors, mentors, peers, family and friends. I am profoundly grateful for my supervisor, Dr. Laura Chasmer, who has guided and supported me with patience and kindness. She has an amazing ability to know exactly when to push, when to encourage, or when to step back, and I cannot imagine a better mentor. I am eternally grateful for the circumstances that landed me in her undergraduate classroom, which has led to many years of mentorship. I am also immensely thankful for my supervisory committee members, Dr. Chris Hopkinson, Dr. Daniel Thompson, Dr. Richard Petrone, and Dr. Koreen Millard. Their contributions to this thesis, and to my learning, have been invaluable. They have provided an incredible balance of challenging my thinking while being supportive, encouraging, and enthusiastic.

I have also had an incredible group of peers, in particular, Linda Flade and Emily Jones, who have helped with field work, talked through methodology, and most importantly, been endlessly supportive and encouraging. Finally, I am deeply grateful for my family and friends. I could not have done this without their support, balance, and perspective.

TABLE OF CONTENTS

LIST OF FIGURES

LIST OF TABLES

LIST OF EQUATIONS

LIST OF ABBREVIATIONS

AGB	Aboveground Biomass
AGFL	Aboveground Fuel Load
AR6	Sixth Assessment Report (IPCC)
AIC	Akaike Information Criterion
AOSR	Athabasca Oil Sands Region
BUI	Buildup Index
C	Carbon
CaMP	Canadian Model for Peatlands
cc	Cyclic Cubic Regression Spline
CFL	Canopy Fuel Load
CH_4	Methane
CI	Confidence Interval
CO_2	Carbon Dioxide
CO	Carbon Monoxide
CV	Cross Validation
DBH	Diameter at Breast Height
DC	Drought Code
DEM	Digital Elevation Model
DMC	Duff Moisture Code
dNBR	Differenced Normalized Burn Ratio
DOB	Depth of Burn
DTM	Digital Terrain Model
ESM	Earth System Model
FFMC	Fine Fuel Moisture Code
FWI	Fire Weather Index
GAM	Generalized Additive Model
GCBM	Generic Carbon Budget Model
GHG	Greenhouse Gas

GNSS	Global Navigation Satellite System
gp	Gaussian Process Smooth
IPCC	Intergovernmental Panel on Climate Change
ISI	Initial Spread Index
MNDWI	Modified Normalized Difference Water Index
NBR	Normalized Burn Ratio
NDMI	Normalized Difference Moisture Index
NDVI	Normalized Difference Vegetation Index
NIR	Near Infrared
NPP	Net Primary Productivity
PET	Potential Evapotranspiration
PPK	Post Processed Kinematic
R^2	Coefficient of determination
REML	Restricted Maximum Likelihood
RF	Random Forest
RMSE	Root Mean Square Error
SD	Standard Deviation
SHAP	Shapley Additive Explanations
SWIR	Shortwave Infrared
SR	Shorter Regeneration
te	Tensor Product Smooth
TIN	Triangulated Irregular Network
tp	Thin Plate Regression Spline
TPI	Topographic Position Index
TR	Taller Regeneration
TWI	Topographic Wetness Index
QQ	Quantile-Quantile (Plot)

CHAPTER 1: INTRODUCTION

1.1 Context

Boreal peatlands are a critical component of the global carbon-climate system, acting as long-term sinks for atmospheric carbon (C; Gorham, 1991; Yu, 2012) and storing a disproportionately large amount of the world's soil C relative to their area (Smith et al., 2007; Tarnocai, 2006). Globally, peatlands cover only ~2-3% of Earth's surface, yet store ~25-33% of the soil C (Gorham, 1991; Turetsky et al., 2015; Vitt & Short, 2020); comparable to that of the pre-industrial atmosphere (Turetsky et al., 2015). Over millennia, these ecosystems have accumulated vast C stocks as a result of high moisture levels limiting decomposition; however, this long-term C sink is becoming more vulnerable to C losses with climatic change (Yu, 2012; Yu et al., 2010). Increases in temperature and precipitation changes cause peatland drying, as well as increase the frequency, severity, and extent of wildland fires (Flannigan et al., 2009a; Hanes et al., 2019; Kohlenberg et al., 2018).

Within Canada, peatlands make up only ~12% of the land area, but store ~56% of the country's soil C (Tarnocai, 2006). Formed in cool, wet climates that are now becoming warmer and drier (Miller et al., 2015; Walker et al., 2015), Canada's western boreal peatlands exist in a delicate balance between evapotranspiration and precipitation (Brown et al., 2010). With annual potential evapotranspiration (PET) typically exceeding precipitation in many areas, these systems are especially vulnerable to climatic shifts (Elmes et al., 2018; Miller et al., 2015; Walker et al., 2015). Projected warming and drying in the region are likely to further increase the vulnerability of these peatlands to enhanced

C losses, reducing the stability of these long-term C sinks, which would have global implications for the C-climate feedback system.

1.1.1 Boreal Forest and Peatland Ecosystems

The boreal forest makes up approximately a third of the world's forested area (Brandt et al., 2013; Kellomäki, 2024). It is one of the largest terrestrial biomes, existing at high latitudes across North America and Eurasia (Gauthier et al., 2015). As such, it is an essential piece of the global C-climate cycle, regulating through C sequestration, energy exchanges, and moisture balances (Wieder et al., 2006; Steffen et al., 2015). The boreal forest holds at least 32% of the terrestrial C pool, most of which is stored below-ground (versus as vegetation; Bradshaw & Warkentin, 2015; Moen et al., 2014), and approximately one quarter of the world's boreal zone is covered by peatlands (Wieder et al., 2006). Boreal and subarctic peatlands are estimated to comprise ~87% of the peatlands, worldwide (Wieder et al., 2006).

Twenty-eight percent of the world's boreal forest is within Canada, where it extends from the northwest, in the Yukon, to the eastern coast of Newfoundland and Labrador (Pickell et al., 2016), and includes seven ecozones: Boreal Shield, Boreal Plains, Boreal Cordillera, Taiga Cordillera, Taiga Plains, Taiga Shield, and Hudson Plains (Ecological Stratification Working Group, 1996). Canada's boreal zone is a 552-million-hectare heterogeneous mosaic dominated by coniferous uplands, interspersed with wetlands, water bodies such as lakes and rivers, alpine zones, heathlands, and grasslands (Brandt et al., 2013). Dominant vegetation includes relatively cold-tolerant coniferous species such as *Picea glauca*, *Picea mariana*, *Larix laricina*, *Abies balsamea*, *Pinus banksiana*, *Pinus contorta*, *Abies lasiocarpa*, and *Picea engelmannii*, and deciduous species such as *Populus*

tremuloides, *Populus balsamifera*, and *Betula papyrifera* (Brandt, 2009). Geology of the boreal zone is dominated by sedimentary rock in the west, with intrusive and metamorphic rock in the east (Webster et al., 2015). The soils have developed since glaciation, with Luvisolic and Brunisolic soils developing in the western boreal, while the eastern zone is dominated by coarse, acidic Podzolic soils (Maynard et al., 2014). The climate is cool, with short summers, long winters, moderate precipitation, and large annual temperature fluctuations. Temperature and precipitation change on a north-south and an east-west gradient, where temperatures decrease to the north, and precipitation decreases to the west (Webster et al., 2015). Evapotranspiration is also greater in the western boreal than the eastern, resulting in increased drought potential in the west (Webster et al., 2015). On average, temperatures have been increasing over the last century –particularly in the northwestern boreal, where mean annual temperatures have increased by over 1.5°C since 1970 (Brandt et al., 2013). It is expected that temperatures in this region will continue to increase, and that despite projected increases in precipitation, the boreal region will become drier (Tarnocai, 2006). Natural drivers of ecosystem change are climate, wildland fire, insects, and disease; anthropogenic disturbances in this zone are predominantly related to forestry and energy resource extraction and development (Brandt et al., 2013).

Peatlands are a critical component of the Canadian boreal zone, storing over half the country's soil C. Developing in cool, water-saturated landscapes, peatlands are a sub-category of wetlands that have accumulated at least 40 cm of organic material (National Wetlands Working Group, 1997). Northern latitude peatlands have developed since the start of the Holocene, (~ 8000 to 9000 years BP; Halsey et al., 1998) on glacial landforms where high moisture supports peat-forming vegetation such as mosses and sedges. These

peatlands develop deep organic layers due to greater inputs from primary production than outputs from decomposition, disturbance, or leaching (Wieder et al., 2006; Vitt et al., 1995). Net primary productivity (NPP) is not necessarily high in peatlands, in fact, forested peatlands have similar NPP rates as forested uplands, but because of waterlogged, often anoxic conditions, decomposition is slowed, resulting in the accumulation of peat (Gorham, 1991; Gower et al., 2001). High water tables, subsequent dynamic of greater productivity than decomposition, and several negative feedback mechanisms, have allowed boreal peatlands to form vast, long term C sinks that have had a net cooling effect on the global climate throughout the Holocene (Frolking & Roulet, 2007).

Boreal peatlands consist of predominantly bogs and fens (e.g., Wieder & Vitt, 2006); however, swamps can also exist as peatlands (e.g., Locky et al., 2005; Zoltai et al., 1998), and are included as a peatland class, henceforth. Bogs are defined as ombrogenous peatlands – they are hydrologically isolated, receiving water only from precipitation, and therefore tend to be ombrotrophic – nutrient-poor. They are typically acidic, and are characterized by *Sphagnum* mosses, ericaceous shrubs, and if treed, *Picea mariana* (Warner & Asada, 2006; Wieder, 2006). Fens and swamps, on the other hand, are geogenous – they are hydrologically connected, receiving water from precipitation as well as the surrounding landscape, and tend to be more minerotrophic, or nutrient-rich, due to the transport of minerals via ground and surface water (Vitt, 2006; Zoltai & Vitt, 1995). Fens tend to be dominated more by herbaceous species, sedges, feather and brown mosses, and if treed, *Larix laricina* or *Picea mariana* (Warner & Asada, 2006; Wieder, 2006). Swamps are treed (*Thuja occidentalis*, *Picea mariana*, or small deciduous trees such as *Acer*, *Alnus*, or *Salix*), with an understory of herbaceous vegetation and bryophytes (Vitt,

2006). While peatlands exist across boreal ecozones, their prevalence, hydrology, and resiliency to climate change and disturbance varies.

The Boreal Plains ecozone, which extends from north-eastern British Columbia, through much of central and northern Alberta, through central Saskatchewan, and into south-western Manitoba, is heavily dominated by peatlands. Wetlands cover ~25-50% of the landscape, of which most are peatlands (Ferone & Devito, 2004; Ficken et al., 2019; National Wetlands Working Group, 1997). The surficial geology of the Boreal Plains consists of glacial and lacustrine deposits, which is underlain by sedimentary bedrock (Ireson et al., 2015), supporting high levels of interaction between surface and groundwater systems (Ferone & Devito, 2004). Uplands are characterized by luvisolic soils, with wet, lowland mineral soil predominantly gleysolic (Group SCW, 1998). Mean temperatures range from -10 to -22°C in the winter to 15 to 20°C in the summer (Ireson et al., 2015), and while peatlands are prevalent on the landscape, they exist at their climatic limit – on an annual basis, average PET exceeds precipitation, such that the landscape often exists in a water deficit (Devito et al., 2012; Petrone et al., 2007). As such, peatlands of the Boreal Plains are expected to be particularly vulnerable to climatic shifts due to increasing levels of water loss to the atmosphere associated with increased warming (Brown et al., 2010; Tarnocai, 2006). While it is predicted that precipitation will also increase with global climate change (Giorgi et al., 2019), Flannigan et al. (2016) calculated that for every one degree Celsius of warming, precipitation would need to increase by 15% to offset the temperature-induced drying. These peatland ecosystems may therefore be nearing a tipping point, where they could shift from C sinks to C sources – especially when considering wildland fire disturbances (e.g., Wilkinson et al., 2023; Zhao & Zhuang, 2023).

Understanding the geological, hydrological, and climatic conditions that shape peatland development and existence in the Boreal Plains provides important context for understanding their role in C sequestration and their vulnerability to climate change and disturbance, particularly fire, which can rapidly release long-stored C to the atmosphere via combustion.

1.1.2 Carbon Cycling and Peat Accumulation in Boreal Peatlands

Boreal peatlands function as globally significant C sinks due to the lack of balance between organic matter inputs via primary productivity, and organic matter outputs via decomposition, respiration and leaching that exist over millennia (Gorham, 1991; Wieder et al., 2006; Vitt et al., 1995). These ecosystems have been developing since the last major glacial recession and the early Holocene. In the boreal, peatlands can develop through four distinct processes (Vitt, 2006). They can build through paludification, where peat develops in previously dry, vegetated areas due to an increase in water table or shift in climate; they can form over unvegetated, wet mineral soils following glacial retreat; shallow bodies of water can fill in with vegetation through terrestrialization; or, peat can form in clay-lined basins that were previously lakes (Vitt, 2006). The cool, waterlogged nature of peatland soils limits decomposition, and facilitates the development of deep peat deposits.

Peatlands are composed of two primary layers – the acrotelm and the catotelm. The upper layer of peat, the acrotelm, may be periodically saturated due to fluctuations in water table depth, but is generally oxic and supports aerobic decomposition (Blodau, 2002; Clymo, 1984; Ingram, 1978). The lower layer of peat that exists between the acrotelm and the mineral soil, the catotelm, is permanently saturated and anoxic. Conditions in the catotelm promote anaerobic decomposition, which is very slow, supporting peat

accumulation (Clymo, 1984; Ingram, 1987). As organic matter enters the peat column, it decomposes in the acrotelm, releasing carbon to the atmosphere primarily as CO_2. The remaining organic matter (10-20%; Clymo, 1984) enters the catotelm, where it accumulates more rapidly than it can decompose, but where carbon emissions are predominantly CH_4 (Blodau, 2002; Gorham, 1991). Estimated C accumulation rates in boreal peatlands varies widely, but common findings estimate ranges from ~7 to 35 g C m^{-2} yr^{-1} (e.g., Holmquist et al., 2014; Ovenden, 1990; Robinson, 2006; Vitt et al., 2000).

As global temperatures increase, decomposition in the acrotelm is expected to increase, resulting in lower organic matter transfer to the catotelm, and therefore reduced C accumulation in peatlands (Allison & Treseder, 2011; Clymo et al., 1998). Further, projected drying, particularly in the western Canadian boreal, may lower water tables, reducing the catotelm depth and increasing aerobic decomposition (Moore & Basiliko, 2006). This may also result in a shift from predominantly *Sphagnum* species to vascular vegetation, further increasing decomposition (Fenner et al., 2007). Conversely, higher temperatures and reduced water tables may increase primary productivity, at least initially, offsetting some of the increased C emissions (Loisel & Yu, 2013). However, reduced levels of saturation would also increase the susceptibility of these C-rich ecosystems to combustion and associated C losses during wildland fire, potentially altering the long-term C balance.

1.1.3 Wildland Fire and Carbon Loss in Boreal Peatlands

Wildland fire is the dominant stand-replacing disturbance in the Boreal Plains (Stocks et al., 2002; Turetsky et al., 2004; Wieder et al., 2009). It is critical for forest health – regulating insects and disease, and shaping species and age composition, productivity, and

biodiversity (Weber & Flannigan, 1997). It also plays an important role in long-term C dynamics (Balshi et al., 2007). Due to their saturated nature, boreal peatlands are resistant to combustion, and much of the C stored is protected from combustion losses in permanently saturated zones (Magnan et al., 2020). However, this can be overcome through increases in fire severity, or decreases in peatland moisture content (Turetsky et al., 2002; Kettridge et al., 2015). During boreal peatland and forest fires, studies have estimated that ~70-90% of C losses during combustion are from the soil as opposed to above-ground vegetation (e.g. Rogers et al., 2014; Hokanson et al., 2016; Walker et al., 2018). The deep, C-rich organic soils of boreal peatlands are a source of potentially significant C loss during wildland fire due to their propensity for long-lasting smouldering burns (Van der Werf et al., 2010).

Peat provides ideal conditions for smouldering fires, which produce more C emissions than flaming fires (similar levels of CO_2, but significantly more CO and CH_4; French et al., 2002). Smouldering is a flameless type of combustion that occurs in low-oxygen environments (Rein et al., 2008), and dominates peatland fires (Frandsen et al., 1987; Turetsky et al., 2004; Zoltai et al., 1998). Smouldering is a low-temperature process (Rein et al., 2008), and smouldering fires can ignite in colder, wetter conditions than can flaming fires. Deep smouldering fires travel within peat layers, persisting through precipitation events (Rein et al., 2008), for months or even years – long after flaming combustion has ceased (Frandsen, 1997; Johnston et al., 2015), and can even re-establish flaming combustion long after it had originally ceased (Ohlemiller, 1990). The capacity of peat to undergo smouldering combustion is controlled by the hydrophysical properties of peat – specifically, volumetric water content and peat bulk density (Benscoter et al., 2011).

If the energy from combustion exceeds that needed to burn off moisture and increase peat temperatures to combustion temperatures (>300°C), smouldering can propagate vertically and laterally through the peat profile (Benscoter et al., 2011). If there is less soil moisture, the energy requirements for propagation are reduced, increasing rate of spread and increasing fuel consumption (Benscoter et al., 2011; Huang & Rein, 2014). However, peatlands can still undergo smouldering combustion under high moisture levels – moisture limits on smouldering combustion are typically ~100-125%, but may be upwards of 200% (Frandsen, 1987, 1997; Rein et al., 2008; Garlough & Keyes, 2011).

Currently, fire frequency in the boreal ranges from ~50-200 years, but it is expected that this will become more frequent with climate change (Flannigan et al., 2005). Concurrently, increased evapotranspiration, lowered water tables, and reduced soil moisture due to climate change is also likely to enhance risk of combustion (Flannigan et al., 2009b), undermining the resiliency of deep peat C stocks. With a change in fire regime and fuel, it is expected that peatlands will burn more deeply and more frequently, increasing C losses during combustion, potentially shifting broad regions of boreal peatlands from C sinks to C sources (Turetsky et al., 2004, 2011; Van der Werf et al., 2010). This increased loss of stored C then has a positive feedback effect, where the release of stored C to the atmosphere enhances climate change, which in turn disproportionately effects northern peatland through increased temperatures and drought, thereby further increasing their susceptibility to soil C loss from wildland fires (Nelson et al., 2021; Chapter 2). The potential implications of increased peatland soil C loss on the global C-climate cycle are notable due to the vast extent and volume of biomass of northern peatlands (Turetsky et al., 2011; Yu, 2012).

The depth of peat combustion, or depth of burn (DOB), and therefore C loss, is highly variable. Boreal peatland DOB can range from barely singed (0.01 m; e.g., Benscoter & Wieder, 2003), to full peat column combustion (>1 m; e.g., Lukenbach et al., 2015). Estimates of average C losses during peat combustion vary from ~0.6 to 2.5 kg C m^{-2} (Turetsky et al., 2011; Wilkinson et al., 2023), but can be upwards of ~16 to 19 kg C m^{-2} under drained or perched/isolated conditions and high intensity fire (e.g., Turetsky et al., 2011; Hokanson et al., 2016), resulting in the loss of thousands of years of C sequestration (Lukenbach et al., 2015). This highly variable DOB in peatlands, which is predominantly controlled by soil moisture and bulk density (Benscoter et al., 2011; Frandsen, 1997; Kohlenberg et al., 2018), is influenced by variability in the levels and stability of water tables (Sherwood et al., 2013; Lukenbach et al., 2015), hydrological connectivity and flow versus peatland fragmentation (Hokanson et al., 2016; Nelson et al., 2021; Chapter 2), vegetation composition and structure (Kettridge et al., 2013; Waddington et al., 2015; Wilkinson et al., 2018), microtopography and peatland-scale topographic position (Benscoter & Vitt, 2008; Hokanson et al., 2016), anthropogenic drainage (Turetsky et al., 2011; Wilkinson et al., 2018), and fire weather, including temperature, precipitation, and wind (Davies et al., 2016).

Apart from being a primary determinant of C loss during peat combustion, DOB also impacts post-fire ecosystem recovery (Nelson et al., 2021; Chapter 2). Low severity burns that combust only the upper centimeters of peat maintain or enhance peatland microtopography, retain seed banks, and allow peatlands to recover pre-fire vegetation and C conditions within the fire return interval (Benscoter & Vitt, 2008; Kettridge et al., 2015; Wieder et al., 2009). However, high severity burns that burn deeply into the peat can alter

hydrological flow, water table positions (Nelson et al., 2021; Chapter 2), peat structure (Granath et al., 2016; Waddington et al., 2015), and result in a shift in vegetation composition (Lukenbach et al., 2016; Lukenbach et al., 2017). These changes can further increase vulnerability to subsequent burns, increase C loss via decomposition, and contribute to a positive feedback cycle between peatlands, wildland fire, and C loss (Nelson et al., 2021; Chapter 2). Research suggests that climate change-induced drying and shifts in fire regimes will result in deeper burns and significantly greater C loss (Hokanson et al., 2016; Nelson et al., 2021; Chapter 2), shifting from C sink to a C source, resulting in a positive C-climate feedback cycle, and changing the role of boreal peatlands within the global C-climate system (Tarnocai, 2006; Thompson et al., 2017; Turetsky et al., 2011; Wieder et al., 2009).

1.1.4 Quantifying and Modelling Carbon Loss from Wildland Fire in Boreal Peatlands

Although peatlands cover a small fraction of land area, boreal peatland fires can release large quantities of C into the atmosphere. Of particular significance are below-ground C losses, which account for over 80% of total C losses during boreal forest and peatland fires (e.g., Rogers et al., 2014; Hokanson et al., 2016; Walker et al., 2018). However, despite their importance, there is significant uncertainty in DOB and associated C losses from boreal peatland fires (e.g., Alonzo et al., 2017; Frolking et al., 2009).

Quantifying below-ground C losses from boreal peatlands is challenging due to both methodological limitations (e.g., Sirin et al., 2021) and high spatial heterogeneity of peatlands. Peatland combustion is highly variable (e.g., Wilkinson et al., 2019), which makes it difficult to estimate C losses at the landscape scale, resulting in uncertain and often incomplete estimates of soil C loss included in models and reports (e.g., Loisel et al.,

2021). Field measurements of DOB are accurate, but sparse – limited by time and access, such that high spatial resolution data collection across multiple peatlands is not feasible (e.g., Hokanson et al., 2016; Thompson & Waddington, 2014). Laboratory experiments, while precise, lack generalizability to natural settings and real-world conditions due to their highly selective and controlled nature (Kohlenberg et al., 2018). Optical remote sensing data can provide important insights into peatland conditions and can be used as an indicator of biomass loss or ecosystem health through changes in pre- and post-fire spectral response (e.g., Chasmer et al., 2017) through indices such as the differenced Normalized Burn Ratio (dNBR) but cannot directly quantify biomass loss. In particular, optical sensors are limited in their ability to approximate below-ground combustion due to canopy occlusion (French et al., 2008) and the poor response of spectral indices in wet environments such as peatlands due to dampening of spectral responses (e.g., Lobell & Asner, 2002). Not only do methodological limitations reduce certainty of site-scale quantification of soil C loss, but because data on DOB, peat depth, soil moisture, bulk density, and other environmental controls are often sparse, it becomes challenging to accurately parameterize models (e.g., Mozafari et al., 2023; Tang et al., 2024). These challenges contribute to the large uncertainties in measured and modelled estimates of peat C losses during wildfire.

These challenges in quantifying DOB and C loss, and associated uncertainties, are reflected in a disconnect between the established understanding of peatlands as a potentially vast C sources and their lack of representation in large-area C budgets and models. Despite a broad consensus that boreal peatlands play a critical role in the global C-climate cycle (e.g., Loisel et al., 2021; Wilkinson et al., 2023), peatland C losses are poorly accounted for in global C and Earth System Models (ESMs; e.g., Lin et al., 2021;

Loisel et al., 2021), as well as GHG inventory reports (e.g., Bona et al., 2024). This has critical implications for global C budgets and climate change planning. For example, peatland processes and C within deep organic horizons were absent from many ESMs that were used in the development of the Intergovernmental Panel on Climate Change Sixth Assessment Report (IPCC AR6; Schuur et al., 2022). Loisel et al. (2021) highlight the need to incorporate peatland C stocks and fluxes in ESMs to quantify their contribution to the global C cycle.

Recent advances in modelling have started to address this disconnect. Peatland C fluxes have started to be included in global terrestrial models (Loisel et al., 2021), and operational C models such as Canada's Generic Carbon Budget Model (GCBM) have begun accounting for wildland fires in peatlands and associated soil C losses (e.g., Bona et al., 2020). The Canadian Model for Peatlands (CaMP), a peatland-specific module of the GCBM, is a semi-empirical model that estimates GHG emissions and removals from Canadian peatlands (Bona et al., 2024). However, there is need for improved, spatially explicit quantification of peatland C losses to improve model parameterizations, C inventories, global C-climate projections, and better understand vulnerabilities of peatlands to deep combustion.

Some of the uncertainties in DOB and associated soil C losses from peat combustion during wildland fire may be overcome by using high resolution lidar data. Airborne lidar data can be used to quantify vegetation structure (e.g., Coops et al., 2021; Hopkinson et al., 2005) and measure ground surface elevations (e.g., Chasmer et al., 2017) over broad spatial extents. Pre- and post-fire lidar data can be compared to estimate above- and below-ground changes in biomass, capturing spatial variability (Alonzo et al., 2017;

Chasmer et al., 2017; Reddy et al., 2015). This information can be used to better understand C loss, spatial variability, and conditions associated with DOB, improving estimates and understandings of how boreal peatlands contribute to atmospheric C.

1.2 Knowledge Gaps

The literature reviewed in section 1.1 highlights the fact that while DOB and associated C losses from boreal peatlands during wildland fire is becoming increasingly well-studied (e.g., Kohlenberg et al., 2018; Wilkinson et al., 2020; Lin et al., 2021; Morison et al., 2021), a lack of spatially continuous, landscape-scale data across a range of peatland types remains. This limits the full quantification and understanding of the role of boreal peatlands in the global C-climate system. Methodological constraints, changing fire regimes, and drying peatlands have resulted in uncertainties in the magnitude of C losses and the driving forces of combustion (Reddy et al., 2015; Turetsky et al., 2015). While the use of spatially coincident, pre- and post-fire lidar data may be used to overcome some of the methodological limitations, there are uncertainties associated with the utility of lidar for ground surface measurements, particularly during the classification stage (Aguilar & Mills, 2008).

Addressing these gaps to provide more accurate estimates and improved understanding of variability in soil C losses is essential for the improved parameterization of C models, more accurate C accounting and budgeting, and informing improved management and mitigation strategies in peatland areas to reduce the vulnerability of peatland C stocks to combustion.

1.3 Research Aims and Objectives

Based on the key themes and knowledge gaps identified in sections 1.1 and 1.2, this thesis has two primary aims. The first is to advance understanding of spatial variability in C combustion loss during wildland fires in boreal peatlands, and the second is to identify where peat combustion is greatest, and determine what ecological conditions drive this variability. These aims are addressed through the following objectives, which are addressed in thesis Chapters 2 through 5:

Synthesis and Conceptualization of Peatland-Fire Feedbacks (Chapter 2)

1. Synthesize existing research on peatland-fire feedbacks and mechanisms.
2. Identify feedbacks and ecological processes that function to increase or decrease burn severity.
3. Identify feedbacks and ecological mechanisms that occur post-fire that function to increase or decrease peatland resiliency to enhanced C loss and/or subsequent fires.
4. Develop conceptual models of pre- and post-fire peatland-fire feedbacks and processes related to wildland fire, hydro-climate, and ecosystem change.
5. Implement key findings from objectives 2 and 3 to conceptualize peatlands that are highly resilient to wildland fire and C losses, versus those that are most vulnerable.

Lidar Ground Elevation Accuracy and Parameterization Schemes for Post-Fire Peatland Ecosystems (Chapter 3)

6. Assess how post-fire vegetation regeneration impacts lidar surface elevation accuracy.
7. Examine how post-fire vegetation regeneration impacts classification parameterization of lidar data.
8. Identify optimal lidar ground classification parameters for unburned peatlands and burned peatlands in various stages of regeneration.
9. Compare ground classification parameters and lidar elevation accuracies between lidar emission wavelengths.
10. Validate post-fire lidar ground elevation accuracies.

Variability in, and Drivers of, Peat Combustion (Chapter 4)

11. Quantify the depth of peat burn across a range of peatland types and ecotones.
12. Identify antecedent conditions/drivers that explain variation in depth of peat burn.
13. Compare drivers of DOB between peatland types.
14. Identify the relative importance of top-down versus bottom-up controls on peat combustion.
15. Determine how well the drivers identified in obj. 12 explain spatial variability in DOB, versus what variability remains.
16. Propose management strategies to mitigate DOB and subsequent C losses.

Variability in Carbon Losses from Peat Combustion (Chapter 5).

17. Compare estimated C loss from above- versus below-ground C pools.
18. Examine how C losses differ between peatland types and ecotones.

19. Evaluate relationships between dNBR and lidar-derived C loss estimates across peatland types and ecotones.
20. Compare lidar-derived soil C loss estimates with modelled C losses from the Canadian Model for Peatlands (CaMP).

1.4 Study Area

The study area for this thesis is located within the Boreal Plains ecozone of western Canada, a flat to undulating region underlain by glacial deposits (Figure 1.1; Devito et al., 2012; Hokanson et al., 2016). The region is heavily treed (ESTR Secretariat, 2014) with a subhumid climate (Elmes et al., 2021), in which PET typically exceeds annual precipitation (Devito et al., 2012). Despite this moisture deficit, the landscape supports a high density of peatlands (Ferone & Devito, 2004; Ficken et al., 2019; National Wetlands Working Group, 1997), which exist near their ecohydrological limits and are therefore highly sensitive to warming, drying, and disturbance (Wilkinson et al., 2019; Devito et al., 2012).

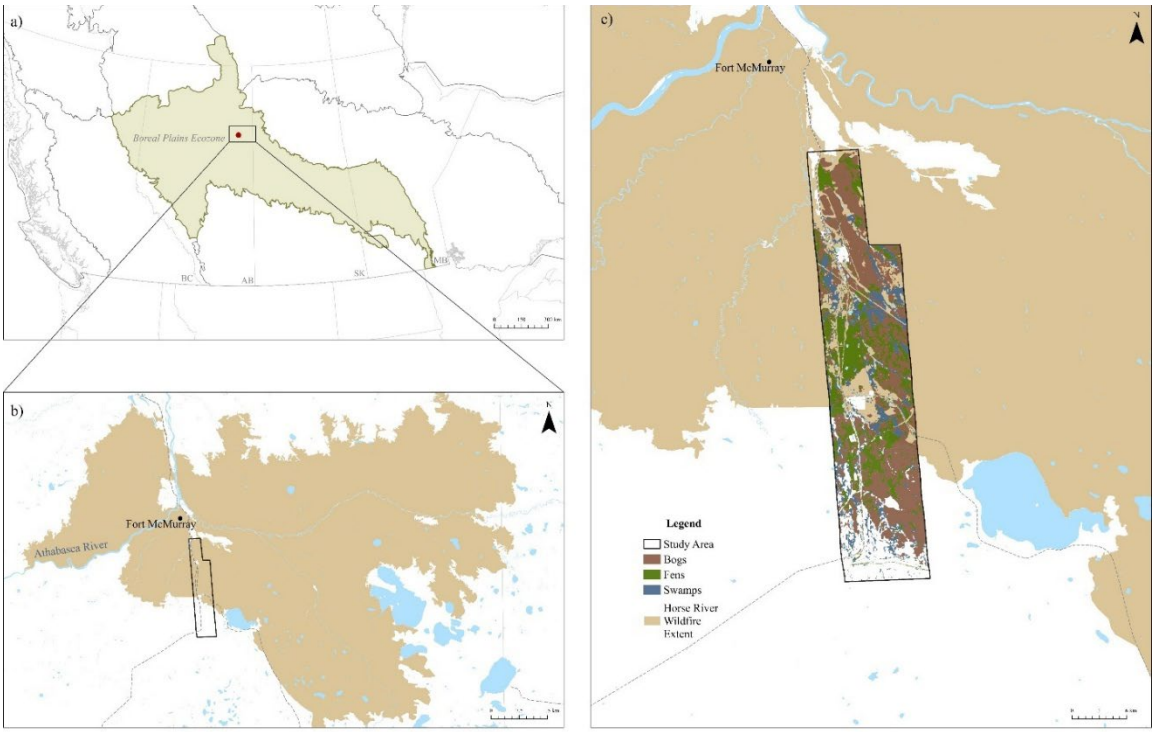

Figure 1.1. Study area overview. a) Extent of the Boreal Plains ecozone within Canada (study area is denoted in red). (b) The Horse River Wildfire and study area extent; and (c) Study area and peatland distribution (peatland types derived from Bourgeau-Chavez et al. (2017)).

Specifically, the research was conducted within an approximately 20,000 ha area in the Athabasca Oil Sands Region (AOSR; Elmes et al., 2021), in a peatland-dense zone in northeastern Alberta, just south of Fort McMurray (Figure 1.1). The area is heavily utilized for forestry and oil and gas exploration, and contains many access roads, seismic lines, cut lines, and well sites (e.g., Abib et al., 2019; Dabros et al., 2022).

The study area includes both burned and unburned peatlands and uplands, as it spans part of the southwestern burn perimeter of the 2016 Horse River Wildfire (Figure 1.1). The Horse River Wildfire ignited on May 1, 2016, burning over 589,000 ha (Natural Resources Canada, 2017). Hazardous fire weather conditions, including high temperatures, high winds, and low relative humidity (Alberta Agriculture and Forestry & MNP, 2017),

and dry spring conditions following the second warmest winter in 20 years (Elmes et al., 2018), led to rapid spread, and the costliest natural disaster in Canadian history (Kovacs et al., 2019). While the fire was declared under control approximately two months later (Alberta Agriculture and Forestry & MNP, 2017), smouldering combustion persisted through the winter, burning for approximately 15 months, extinguished August 2, 2017 (Kovacs et al., 2019).

The study area is within an area expected to be disproportionately impacted by climate change (e.g., Gauthier et al., 2014). It contains a range of peatland types with varying burn severities and levels of vegetative regeneration, providing an ideal opportunity to study both the high variability of DOB and C loss, as well as anthropogenic and environmental drivers that may influence this variability. The availability of existing pre-fire lidar coverage allowed for a unique opportunity to use high-resolution, pre- and post-fire lidar data to estimate peatland DOB and C losses.

1.5 Thesis Organization

The remainder of this thesis is organized into five chapters (2-6): four manuscript-style, research chapters, and a conclusion. Each chapter can be read as a stand-alone article, but each builds upon the preceding chapters in a logical progression, moving from a conceptual synthesis of fire ecology and C cycling, to methodological and accuracy assessment of lidar measurements in post-fire peatlands, to quantifying and modelling peat combustion, associated C losses, and their environmental drivers.

Chapter two synthesizes existing research to develop conceptual models of feedback mechanisms and ecological processes that impact peatland resiliency or

vulnerability to wildland fire. It explores the connections and mechanisms related to peat combustion, post-fire recovery, and the C-climate cycle, and highlights key peatland characteristics that promote ecosystem resiliency and C sequestration.

Chapter three evaluates lidar ground elevation accuracy in post-fire peatland environments across a range of vegetation recovery stages. It identifies optimal ground classification parameters and emission wavelength(s) for different levels of vegetation regeneration and provides the methodological foundation for lidar-based DOB analyses in subsequent chapters.

Chapter four quantifies the spatial variability in DOB across peatland types and ecotones using pre- and post-fire lidar data. Environmental drivers of peat combustion are explored using Generalized Additive Models (GAMs) and Random Forest models across peatland types.

Chapter five builds on the DOB analysis of Chapter four by integrating field-based soil C data and lidar-derived above-ground biomass to estimate above- and below-ground C losses across peatland types and ecotones. These estimates are compared with modelled outputs from the CaMP, and the relationships between optical burn severity indices (e.g., dNBR) and C losses are explored.

Finally, chapter six synthesizes the results of Chapters two through five to provide an integrated assessment of how boreal peatlands are impacted by wildland fire and what the implications are for the role of boreal peatlands in the global C-climate system.

In its whole, this thesis provides an advanced understanding of peatland-fire interactions, improves understanding of spatial variability in C loss during peat

combustion, and provides new insights into resiliency versus vulnerability of boreal peatlands to wildland fire in a changing climate.

1.6 References

Abib, T. H., Chasmer, L., Hopkinson, C., Mahoney, C., & Rodriguez, L. C. (2019). Seismic line impacts on proximal boreal forest and wetland environments in Alberta. Science of the Total Environment, 658, 1601-1613.

Aguilar, F. J., & Mills, J. P. (2008). Accuracy assessment of LiDAR-derived digital elevation models. *The Photogrammetric Record*, *23*(122), 148-169.

Alberta Agriculture and Forestry & MNP LLP. (2017). A review of the 2016 Horse River wildfire.

Allison, S. D., & Treseder, K. K. (2011). Climate change feedbacks to microbial decomposition in boreal soils. Fungal Ecology, 4(6), 362-374.

Alonzo, M., Morton, D. C., Cook, B. D., Andersen, H. E., Babcock, C., & Pattison, R. (2017). Patterns of canopy and surface layer consumption in a boreal forest fire from repeat airborne lidar. Environmental Research Letters, 12(6), 065004.

Balshi, M. S., McGuire, A. D., Zhuang, Q., Melillo, J., Kicklighter, D. W., Kasischke, E., Wirth, C., Flannigan, M., Harden, J., Clein, J. S., Burnside, T. J., & Shvidenko, A. (2007). The role of historical fire disturbance in the carbon dynamics of the pan-boreal region: A process-based analysis. *Journal of Geophysical Research: Biogeosciences*, *112*(G2).

Benscoter, B. W., Thompson, D. K., Waddington, J. M., Flannigan, M. D., Wotton, B. M., De Groot, W. J., & Turetsky, M. R. (2011). Interactive effects of vegetation, soil moisture and bulk density on depth of burning of thick organic soils. International Journal of Wildland Fire, 20(3), 418-429.

Benscoter, B. W., & Vitt, D. H. (2008). Spatial patterns and temporal trajectories of the bog ground layer along a post-fire chronosequence. Ecosystems, 11(7), 1054-1064. https://doi.org/10.1007/s10021-008-9178-4.

Benscoter, B. W., & Wieder, R. K. (2003). Variability in organic matter lost by combustion in a boreal bog during the 2001 Chisholm fire. Canadian Journal of Forest Research, 33(12), 2509-2513.

Blodau, C. (2002). Carbon cycling in peatlands A review of processes and controls. Environmental Reviews, 10(2), 111-134.

Bona, K. A., Shaw, C., Thompson, D. K., Hararuk, O., Webster, K., Zhang, G., Voicu, M., & Kurz, W. A. (2020). The Canadian model for peatlands (CaMP): A peatland carbon model for national greenhouse gas reporting. Ecological Modelling, 431, 109164.

Bona, K. A., Webster, K. L., Thompson, D. K., Hararuk, O., Zhang, G., & Kurz, W. A. (2024). Using the Canadian Model for Peatlands (CaMP) to examine greenhouse gas emissions and carbon sink strength in Canada's boreal and temperate peatlands. Ecological Modelling, 490, 110633.

Bradshaw, C. J., & Warkentin, I. G. (2015). Global estimates of boreal forest carbon stocks and flux. Global and Planetary Change, 128, 24-30.

Brandt, J. P. (2009). The extent of the North American boreal zone. Environmental Reviews, 17(NA), 101-161.

Brandt, J. P., Flannigan, M. D., Maynard, D. G., Thompson, I. D., & Volney, W. J. A. (2013). An introduction to Canada's boreal zone: ecosystem processes, health, sustainability, and environmental issues. Environmental Reviews, 21(4), 207-226.

Brown, S. M., Petrone, R. M., Mendoza, C., & Devito, K. J. (2010). Surface vegetation controls on evapotranspiration from a sub-humid Western Boreal Plain wetland. Hydrological Processes: An International Journal, 24(8), 1072-1085.

Chasmer, L. E., Hopkinson, C. D., Petrone, R. M., & Sitar, M. (2017). Using multitemporal and multispectral airborne lidar to assess depth of peat loss and correspondence with a new active normalized burn ratio for wildfires. Geophysical research letters, 44(23), 11-851.

Clymo, R. S. (1984). The limits to peat bog growth. Philosophical Transactions of the Royal Society of London. B, Biological Sciences, 303(1117), 605-654.

Clymo, R. S., Turunen, J., & Tolonen, K. (1998). Carbon accumulation in peatland. Oikos, 368-388.

Coops, N. C., Tompalski, P., Goodbody, T. R., Queinnec, M., Luther, J. E., Bolton, D. K., White, J. C., Wulder, M. A., van Lier, O. R., & Hermosilla, T. (2021). Modelling lidar-derived estimates of forest attributes over space and time: A review of approaches and future trends. Remote Sensing of Environment, 260, 112477.

Dabros, A., Higgins, K. L., & Pinzon, J. (2022). Seismic line edge effects on plants, lichens and their environmental conditions in boreal peatlands of Northwest Alberta (Canada). Restoration Ecology, 30(4), e13468.

Davies, G. M., Domènech, R., Gray, A., & Johnson, P. C. (2016). Vegetation structure and fire weather influence variation in burn severity and fuel consumption during peatland wildfires. *Biogeosciences*, *13*(2), 389-398.

Devito, K., Mendoza, C., & Qualizza, C. (2012). Conceptualizing water movement in the Boreal Plains. Implications for watershed reconstruction.

Ecological Stratification Working Group, 1996. A National Ecological Framework for Canada. Agriculture and Agri-Food Canada, Research Branch, Centre for Land and Biological Resources Research, and Environment Canada, State of the Environment Directorate, Ecozone Analysis Branch, Ottawa/Hull. Report and national map at 1:7,500,000 scale.

Elmes, M. C., Thompson, D. K., Sherwood, J. H., & Price, J. S. (2018). Hydrometeorological conditions preceding wildfire, and the subsequent burning of a fen watershed in Fort McMurray, Alberta, Canada. *Natural Hazards and Earth System Sciences*, *18*(1), 157-170.

Elmes, M. C., Davidson, S. J., & Price, J. S. (2021). Ecohydrological interactions in a boreal fen–swamp complex, Alberta, Canada. Ecohydrology, 14(7), e2335.

ESTR Secretariat. (2014). Boreal Plains Ecozone Evidence for Key Findings Summary. Canadian Biodiversity: Ecosystem Status and Trends 2010. Evidence for Key Findings Summary.

Fenner, N., Ostle, N. J., McNamara, N., Sparks, T., Harmens, H., Reynolds, B., & Freeman, C. (2007). Elevated CO2 effects on peatland plant community carbon dynamics and DOC production. Ecosystems, 10(4), 635-647.

Ferone, J. M., & Devito, K. J. (2004). Shallow groundwater–surface water interactions in pond–peatland complexes along a Boreal Plains topographic gradient. Journal of Hydrology, 292(1-4), 75-95.

Ficken, C. D., Cobbaert, D., & Rooney, R. C. (2019). Low extent but high impact of human land use on wetland flora across the boreal oil sands region. Science of the Total Environment, 693, 133647.

Flannigan, M. D., Krawchuk, M. A., de Groot, W. J., Wotton, B. M., & Gowman, L. M. (2009a). Implications of changing climate for global wildland fire. International journal of wildland fire, 18(5), 483-507.

Flannigan, Mike D., Kim A. Logan, Brian D. Amiro, Walter R. Skinner, and Brian J. Stocks. "Future area burned in Canada." Climatic change 72, no. 1 (2005): 1-16.

Flannigan, M., Stocks, B., Turetsky, M., & Wotton, M. (2009b). Impacts of climate change on fire activity and fire management in the circumboreal forest. Global change biology, 15(3), 549-560.

Flannigan, M. D., Wotton, B. M., Marshall, G. A., De Groot, W. J., Johnston, J., Jurko, N., & Cantin, A. S. (2016). Fuel moisture sensitivity to temperature and precipitation: climate change implications. Climatic Change, 134(1), 59-71.

Frandsen, W. H. (1987). The influence of moisture and mineral soil on the combustion limits of smoldering forest duff. Canadian Journal of Forest Research, 17(12), 1540-1544.

Frandsen, W. H. (1997). Ignition probability of organic soils. Canadian Journal of Forest Research, 27(9), 1471-1477.

French, N. H., Kasischke, E. S., Hall, R. J., Murphy, K. A., Verbyla, D. L., Hoy, E. E., & Allen, J. L. (2008). Using Landsat data to assess fire and burn severity in the North American boreal forest region: an overview and summary of results. *International Journal of Wildland Fire*, *17*(4), 443-462.

French, N. H., Kasischke, E. S., & Williams, D. G. (2002). Variability in the emission of carbon-based trace gases from wildfire in the Alaskan boreal forest. Journal of Geophysical Research: Atmospheres, 107(D1), FFR-7.

Frolking, S., & Roulet, N. T. (2007). Holocene radiative forcing impact of northern peatland carbon accumulation and methane emissions. Global Change Biology, 13(5), 1079-1088.

Frolking, S., Roulet, N., & Lawrence, D. (2009). Issues related to incorporating northern peatlands into global climate models. Carbon cycling in northern peatlands, 184, 19-35.

Garlough, E. C., & Keyes, C. R. (2011). Influences of moisture content, mineral content and bulk density on smouldering combustion of ponderosa pine duff mounds. International Journal of Wildland Fire, 20(4), 589-596.

Gauthier, S., Bernier, P., Burton, P. J., Edwards, J., Isaac, K., Isabel, N., Jayen, K., Le Goff, H., & Nelson, E. A. (2014). Climate change vulnerability and adaptation in the managed Canadian boreal forest. *Environmental Reviews*, *22*(3), 256-285.

Gauthier, S., Bernier, P., Kuuluvainen, T., Shvidenko, A. Z., & Schepaschenko, D. G. (2015). Boreal forest health and global change. Science, 349(6250), 819-822.

Giorgi, F., Raffaele, F., & Coppola, E. (2019). The response of precipitation characteristics to global warming from climate projections. Earth System Dynamics, 10(1), 73-89.

Gorham, E. (1991). Northern peatlands: role in the carbon cycle and probable responses to climatic warming. Ecological applications, 1(2), 182-195.

Gower, S. T., Krankina, O., Olson, R. J., Apps, M., Linder, S., & Wang, C. (2001). Net primary production and carbon allocation patterns of boreal forest ecosystems. Ecological applications, 11(5), 1395-1411.

Granath, G., Moore, P. A., Lukenbach, M. C., Waddington, J. M., & Sveriges, L. (2016). Mitigating wildfire carbon loss in managed northern peatlands through restoration. Scientific Reports, 6, 28498. https://doi.org/10.1038/srep28498.

Group SCW. The Canadian System of Soil Classification. Agriculture and Agri-Food Canada Publication 1646. 3rd ed. Ottawa: NRC Research Press; 1998.

Halsey, L. A., Vitt, D. H., & Bauer, I. E. (1998). Peatland initiation during the Holocene in continental western Canada. Climatic Change, 40(2), 315-342.

Hanes, C. C., Wang, X., Jain, P., Parisien, M. A., Little, J. M., & Flannigan, M. D. (2019). Fire-regime changes in Canada over the last half century. Canadian Journal of Forest Research, 49(3), 256-269.

Hokanson, K. J., Lukenbach, M. C., Devito, K. J., Kettridge, N., Petrone, R. M., & Waddington, J. M. (2016). Groundwater connectivity controls peat burn severity in the boreal plains. Ecohydrology, 9(4), 574-584.

Holmquist, J. R., MacDonald, G. M., & Gallego-Sala, A. (2014). Peatland initiation, carbon accumulation, and 2 ka depth in the James Bay Lowland and adjacent regions. Arctic, antarctic, and alpine research, 46(1), 19-39.

Hopkinson, C., Chasmer, L. E., Sass, G., Creed, I. F., Sitar, M., Kalbfleisch, W., & Treitz, P. (2005). Vegetation class dependent errors in lidar ground elevation and canopy height estimates in a boreal wetland environment. Canadian journal of remote sensing, 31(2), 191-206.

Huang, X., & Rein, G. (2014). Smouldering combustion of peat in wildfires: Inverse modelling of the drying and the thermal and oxidative decomposition kinetics. *Combustion and Flame*, *161*(6), 1633-1644.

Ingram, H. A. P. (1978). Soil layers in mires: function and terminology. Journal of Soil Science, 29(2), 224-227.

Ireson, A. M., Barr, A. G., Johnstone, J. F., Mamet, S. D., Van der Kamp, G., Whitfield, C. J., Michel, N. L., North, R. L., Westbrook, C. J., DeBeer, C., Chun, K. P., Nazemi, A., & Sagin, J. (2015). The changing water cycle: the Boreal Plains ecozone of Western Canada. Wiley Interdisciplinary Reviews: Water, 2(5), 505-521.

Johnston, D. C., Turetsky, M. R., Benscoter, B. W., & Wotton, B. M. (2015). Fuel load, structure, and potential fire behaviour in black spruce bogs. Canadian Journal of Forest Research, 45(7), 888-899.

Kellomäki, S. (2024). Global Forests, with a Focus on Boreal Forests. In Forest Management for Timber Production and Climate Change Mitigation: Linking Dynamics of Carbon Cycle in Ecosystem Management (pp. 9-29). Cham: Springer Nature Switzerland.

Kettridge, N., Thompson, D. K., Bombonato, L., Turetsky, M. R., Benscoter, B. W., & Waddington, J. M. (2013). The ecohydrology of forested peatlands: Simulating the effects of tree shading on moss evaporation and species composition. Journal of Geophysical Research: Biogeosciences, 118(2), 422-435.

Kettridge, N., Turetsky, M. R., Sherwood, J. H., Thompson, D. K., Miller, C. A., Benscoter, B. W., Flannigan, M. D., Wotton, B. M., & Waddington, J. M. (2015). Moderate drop in water table increases peatland vulnerability to post-fire regime shift. Scientific reports, 5(1), 8063.

Kohlenberg, A. J., Turetsky, M. R., Thompson, D. K., Branfireun, B. A., & Mitchell, C. P. (2018). Controls on boreal peat combustion and resulting emissions of carbon and mercury. Environmental Research Letters, 13(3), 035005.

Kovacs, P. J. E., McBean, G. A., McGillivray, R. G., & Pulsifer, K. (2019). Fort McMurray wildfire: Learning from Canada's costliest disaster. Zurich, Switzerland: Zurich Insurance Company Ltd.

Lin, S., Liu, Y., & Huang, X. (2021). Climate-induced Arctic-boreal peatland fire and carbon loss in the 21st century. Science of the Total Environment, 796, 148924.

Lobell, D. B., & Asner, G. P. (2002). Moisture effects on soil reflectance. Soil Science Society of America Journal, 66(3), 722-727.

Locky, D. A., Bayley, S. E., & Vitt, D. H. (2005). The vegetational ecology of black spruce swamps, fens, and bogs in southern boreal Manitoba, Canada. Wetlands, 25(3), 564-582.

Loisel, J., Gallego-Sala, A. V., Amesbury, M. J., Magnan, G., Anshari, G., Beilman, D. W., ... & Wu, J. (2021). Expert assessment of future vulnerability of the global peatland carbon sink. Nature climate change, 11(1), 70-77.

Loisel, J., & Yu, Z. (2013). Recent acceleration of carbon accumulation in a boreal peatland, south-central Alaska. Journal of Geophysical Research: Biogeosciences, 118(1), 41–53. https://doi.org/10.1029/2012JG001978.

Lukenbach, M. C., Devito, K. J., Kettridge, N., Petrone, R. M., & Waddington, J. M. (2016). Burn severity alters peatland moss water availability: Implications for post-fire recovery. Ecohydrology, 9(2), 341–353. https://doi.org/10.1002/eco.1639.

Lukenbach, M. C., Hokanson, K. J., Devito, K. J., Kettridge, N., Petrone, R. M., Mendoza, C. A., Granath, G., & Waddington, J. M. (2017). Post-fire ecohydrological conditions at peatland margins in different hydrogeological settings of the boreal plain. Journal of Hydrology, 548, 741–753. https://doi.org/10.1016/j.jhydrol.2017.03.034.

Lukenbach, M. C., Hokanson, K. J., Moore, P. A., Devito, K. J., Kettridge, N., Thompson, D. K., Wotton, B., M., Petrone, R. M., & Waddington, J. M. (2015). Hydrological controls on deep burning in a northern forested peatland. Hydrological Processes, 29(18), 4114-4124.

Magnan, G., Garneau, M., Le Stum-Boivin, É., Grondin, P., & Bergeron, Y. (2020). Long-term carbon sequestration in boreal forested peatlands in eastern Canada. *Ecosystems*, *23*(7), 1481-1493.

Maynard, D. G., Paré, D., Thiffault, E., Lafleur, B., Hogg, K. E., & Kishchuk, B. (2014). How do natural disturbances and human activities affect soils and tree nutrition and growth in the Canadian boreal forest?. Environmental Reviews, 22(2), 161-178.

Miller, C. A., Benscoter, B. W., & Turetsky, M. R. (2015). The effect of long-term drying associated with experimental drainage and road construction on vegetation composition and productivity in boreal fens. Wetlands ecology and management, 23(5), 845-854.

Moen, J., Rist, L., Bishop, K., Chapin III, F. S., Ellison, D., Kuuluvainen, T., Petersson, H., Puettman, K. J., Rayner, J., Warkentin, I. G., & Bradshaw, C. J. (2014). Eye on the taiga: removing global policy impediments to safeguard the boreal forest. Conservation Letters, 7(4), 408-418.

Moore, T., & Basiliko, N. (2006). Decomposition in boreal peatlands. In *Boreal peatland ecosystems* (pp. 125-143). Berlin, Heidelberg: Springer Berlin Heidelberg.

Morison, M., van Beest, C., Macrae, M., Nwaishi, F., & Petrone, R. (2021). Deeper burning in a boreal fen peatland 1-year post-wildfire accelerates recovery trajectory of carbon dioxide uptake. Ecohydrology, 14(3), e2277.

Mozafari, B., Bruen, M., Donohue, S., Renou-Wilson, F., & O'Loughlin, F. (2023). Peatland dynamics: A review of process-based models and approaches. *Science of The Total Environment*, *877*, 162890.

National Wetlands Working Group. 1997. The Canadian Wetland Classification System, 2nd Edition. Warner, B.G. and C.D.A. Rubec (eds.), Wetlands Research Centre, University of Waterloo, Waterloo, ON, Canada. 68 p.

Natural Resources Canada. (2017). The State of Canada's Forests—Annual Report 2017; Government of Canada: Ottawa, ON, Canada.

Nelson, K., Thompson, D., Hopkinson, C., Petrone, R., & Chasmer, L. (2021). Peatland-fire interactions: A review of wildland fire feedbacks and interactions in Canadian boreal peatlands. Science of the total environment, 769, 145212.

Ohlemiller, T. J. (1990). Forced smolder propagation and the transition to flaming in cellulosic insulation. *Combustion and flame*, *81*(3-4), 354-365.

Ovenden, L. (1990). Peat accumulation in northern wetlands. Quaternary research, 33(3), 377-386.

Petrone, R. M., Silins, U., & Devito, K. J. (2007). Dynamics of evapotranspiration from a riparian pond complex in the Western Boreal Forest, Alberta, Canada. Hydrological Processes: An International Journal, 21(11), 1391-1401.

Pickell, P. D., Coops, N. C., Gergel, S. E., Andison, D. W., & Marshall, P. L. (2016). Evolution of Canada's boreal forest spatial patterns as seen from space. PLoS One, 11(7), e0157736.

Reddy, A. D., Hawbaker, T. J., Wurster, F., Zhu, Z., Ward, S., Newcomb, D., & Murray, R. (2015). Quantifying soil carbon loss and uncertainty from a peatland wildfire using multi-temporal LiDAR. Remote Sensing of Environment, 170, 306-316.

Rein, G., Cleaver, N., Ashton, C., Pironi, P., & Torero, J. L. (2008). The severity of smouldering peat fires and damage to the forest soil. Catena, 74(3), 304-309.

Robinson, S. D. (2006). Carbon accumulation in peatlands, southwestern Northwest Territories, Canada. Canadian Journal of Soil Science, 86(Special Issue), 305-319.

Rogers, B. M., Veraverbeke, S., Azzari, G., Czimczik, C. I., Holden, S. R., Mouteva, G. O., Sedano, F., Treseder, K. K., & Randerson, J. T. (2014). Quantifying fire-wide carbon emissions in interior Alaska using field measurements and Landsat imagery. Journal of Geophysical Research: Biogeosciences, 119(8), 1608-1629.

Schuur, E. A., Abbott, B. W., Commane, R., Ernakovich, J., Euskirchen, E., Hugelius, G., Grosse, G., Jones, M., Koven, C., Leshyk, V., & Turetsky, M. (2022). Permafrost and climate change: carbon cycle feedbacks from the warming Arctic. Annual Review of Environment and Resources, 47(1), 343-371.

Sherwood, J. H., Kettridge, N., Thompson, D. K., Morris, P. J., Silins, U., & Waddington, J. M. (2013). Effect of drainage and wildfire on peat hydrophysical properties. Hydrological Processes, 27(13), 1866-1874.

Smith, K.B., C.E. Smith, S.F. Forest, and A.J. Richard. 2007. A Field Guide to the Wetlands of the Boreal Plains Ecozone of Canada. Ducks Unlimited Canada, Western Boreal Office: Edmonton, Alberta. 98 pp.

Steffen, W., Richardson, K., Rockström, J., Cornell, S. E., Fetzer, I., Bennett, E. M., ... & Sörlin, S. (2015). Planetary boundaries: Guiding human development on a changing planet. science, 347(6223), 1259855.

Stocks, B. J., Mason, J. A., Todd, J. B., Bosch, E. M., Wotton, B. M., Amiro, B. D., Flannigan, M. D., Hirsch, K. G., Logan, K. A., Martell, D. L., & Skinner, W. R. (2002). Large forest fires in Canada, 1959–1997. Journal of Geophysical Research: Atmospheres, 107(D1), FFR-5.

Tang, R., Jin, M., Mao, J., Ricciuto, D. M., Chen, A., & Zhang, Y. (2024). Quantifying wildfire drivers and predictability in boreal peatlands using a two-step error-correcting machine learning framework in TeFire v1. 0. *Geoscientific Model Development*, *17*(4), 1525-1542.

Tarnocai, C. (2006). The effect of climate change on carbon in Canadian peatlands. Global and planetary Change, 53(4), 222-232.

Thompson, D. K., Parisien, M. A., Morin, J., Millard, K., Larsen, C. P., & Simpson, B. N. (2017). Fuel accumulation in a high-frequency boreal wildfire regime: from wetland to upland. Canadian Journal of Forest Research, 47(7), 957-964.

Thompson, D. K., & Waddington, J. M. (2014). A Markov chain method for simulating bulk density profiles in boreal peatlands. *Geoderma*, *232*, 123-129.

Turetsky, M. R., Amiro, B. D., Bosch, E., & Bhatti, J. S. (2004). Historical burn area in western Canadian peatlands and its relationship to fire weather indices. Global Biogeochemical Cycles, 18(4).

Turetsky, M. R., Benscoter, B., Page, S., Rein, G., Van Der Werf, G. R., & Watts, A. (2015). Global vulnerability of peatlands to fire and carbon loss. Nature Geoscience, 8(1), 11-14.

Turetsky, M. R., Donahue, W., & Benscoter, B. W. (2011). Experimental drying intensifies burning and carbon losses in a northern peatland. Nature communications, 2(1), 514.

Turetsky, M., Wieder, K., Halsey, L., & Vitt, D. (2002). Current disturbance and the diminishing peatland carbon sink. Geophysical research letters, 29(11), 21-1.

Van der Werf, G. R., Randerson, J. T., Giglio, L., Collatz, G. J., Mu, M., Kasibhatla, P. S., Morton, D. C., DeFries, R, S., Jin, Y. V., & van Leeuwen, T. T. (2010). Global fire emissions and the contribution of deforestation, savanna, forest, agricultural, and peat fires (1997–2009). Atmospheric chemistry and physics, 10(23), 11707-11735.

Vitt, D. H. (2006). Functional characteristics and indicators of boreal peatlands. In Boreal peatland ecosystems (pp. 9-24). Berlin, Heidelberg: Springer Berlin Heidelberg.

Vitt, D. H., Halsey, L. A., Bauer, I. E., & Campbell, C. (2000). Spatial and temporal trends in carbon storage of peatlands of continental western Canada through the Holocene. Canadian Journal of Earth Sciences, 37(5), 683-693.

Vitt, D. H., Li, Y., & Belland, R. J. (1995). Patterns of bryophyte diversity in peatlands of continental western Canada. Bryologist, 218-227.

Vitt, D. H., & Short, P. (2020). Peatlands. In Wetlands and Habitats (pp. 27-36). CRC Press.

Waddington, J. M., Morris, P. J., Kettridge, N., Granath, G., Thompson, D. K., & Moore, P. A. (2015). Hydrological feedbacks in northern peatlands. Ecohydrology, 8(1), 113-127.

Walker, X. J., Rogers, B. M., Baltzer, J. L., Cumming, S. G., Day, N. J., Goetz, S. J., Johnstone, J. F., Schuur, E. A., Turetsky, M. R., & Mack, M. C. (2018). Cross-scale controls on carbon emissions from boreal forest megafires. Global Change Biology, 24(9), 4251-4265.

Walker, T. N., Ward, S. E., Ostle, N. J., & Bardgett, R. D. (2015). Contrasting growth responses of dominant peatland plants to warming and vegetation composition. Oecologia, 178(1), 141-151.

Warner, B. G., & Asada, T. (2006). Biological diversity of peatlands in Canada. Aquatic Sciences, 68, 240-253.

Weber, M. G., & Flannigan, M. D. (1997). Canadian boreal forest ecosystem structure and function in a changing climate: impact on fire regimes. Environmental Reviews, 5(3-4), 145-166.

Webster, K. L., Beall, F. D., Creed, I. F., & Kreutzweiser, D. P. (2015). Impacts and prognosis of natural resource development on water and wetlands in Canada's boreal zone. Environmental Reviews, 23(1), 78-131.

Wieder, R. K. (2006). Primary Production in Boreal Peatlands. In Boreal peatland ecosystems (pp. 9-24). Berlin, Heidelberg: Springer Berlin Heidelberg.

Wieder, R. K., Scott, K. D., Kamminga, K., Vile, M. A., Vitt, D. H., Bone, T., Xu, B. I. N., Benscoter, B. W., & Bhatti, J. S. (2009). Postfire carbon balance in boreal bogs of Alberta, Canada. Global Change Biology, 15(1), 63-81.

Wieder, R. K., & Vitt, D. H. (Eds.). (2006). Boreal peatland ecosystems (Vol. 188). Springer Science & Business Media.

Wieder, R. K., Vitt, D. H., & Benscoter, B. W. (2006). Peatlands and the boreal forest. In Boreal peatland ecosystems (pp. 1-8). Berlin, Heidelberg: Springer Berlin Heidelberg.

Wilkinson, S. L., Andersen, R., Moore, P. A., Davidson, S. J., Granath, G., & Waddington, J. M. (2023). Wildfire and degradation accelerate northern peatland carbon release. Nature Climate Change, 13(5), 456-461.

Wilkinson, S. L., Moore, P. A., Flannigan, M. D., Wotton, B. M., & Waddington, J. M. (2018). Did enhanced afforestation cause high severity peat burn in the Fort McMurray Horse River wildfire?. Environmental Research Letters, 13(1), 014018.

Wilkinson, S. L., Moore, P. A., & Waddington, J. M. (2019). Assessing drivers of cross-scale variability in peat smoldering combustion vulnerability in forested boreal peatlands. Frontiers in Forests and Global Change, 2, 84.

Wilkinson, S. L., Tekatch, A. M., Markle, C. E., Moore, P. A., & Waddington, J. M. (2020). Shallow peat is most vulnerable to high peat burn severity during wildfire. Environmental Research Letters, 15(10), 104032.

Yu, Z. C. (2012). Northern peatland carbon stocks and dynamics: a review. Biogeosciences, 9(10), 4071-4085.

Yu, Z., Loisel, J., Brosseau, D. P., Beilman, D. W., & Hunt, S. J. (2010). Global peatland dynamics since the Last Glacial Maximum. Geophysical research letters, 37(13).

Zhao, B., & Zhuang, Q. (2023). Peatlands and their carbon dynamics in northern high latitudes from 1990 to 2300: a process-based biogeochemistry model analysis. Biogeosciences, 20(1), 251-270.

Zoltai, S. C., Morrissey, L. A., Livingston, G. P., & Groot, W. D. (1998). Effects of fires on carbon cycling in North American boreal peatlands. Environmental Reviews, 6(1), 13-24.

Zoltai, S. C., & Vitt, D. H. (1995). Canadian wetlands: environmental gradients and classification. Vegetatio, 118(1), 131-137.

CHAPTER 2: PEATLAND-FIRE INTERACTIONS: A REVIEW OF WILDLAND FIRE FEEDBACKS AND INTERACTIONS IN CANADIAN BOREAL PEATLANDS

2.1 Abstract

Boreal peatlands store a disproportionately large quantity of soil carbon (C) and play a critical role within the global C-climate system; however, with climatic warming, these C stores are at risk. Increased wildfire frequency and severity are expected to increase C loss from boreal peatlands, contributing to a shift from C sink to source. Here, I provide a comprehensive review of pre- and post-fire hydrological and ecological interactions that affect the likelihood of peatland burning, address the connections between peatland fires and the C-climate cycle, and provide a conceptual model of peatland processes as they relate to wildland fire, hydro-climate, and ecosystem change. Despite negative ecohydrological feedback mechanisms that may compensate for increased C loss initially, the cumulative effects of climatic warming, anthropogenic peatland fragmentation, and subsequent peatland drying will increase C loss to the atmosphere, driving a positive C feedback cycle. However, the extent to which negative and positive feedbacks will compensate for one another and the timelines for each remains unclear. I suggest that a multi-disciplinary approach of combining process knowledge with remotely sensed data and ecohydrological and wildland fire models is essential for better understanding the role of boreal peatlands and wildland fire in the global climate system.

2.2 Introduction

Boreal and subarctic peatlands contain an estimated one-third of global soil carbon (C) stores, despite occupying only ~2–3% of the world's land cover (Gorham, 1991). Their C

stores are comparable to the amount of C in the atmosphere and exceed those in terrestrial vegetation (IPCC, 2013). Within Canada, boreal peatlands store over half the country's soil C, despite occupying only 12% of the land area (Tarnocai, 2006); however, recent modelling by Nichols and Peteet (2019) suggests that C stores may, in fact, be nearly twice that. North American boreal peatlands can be found in regions near climatic moisture deficits, where potential evapotranspiration exceeds precipitation (Petrone et al., 2006). These ecosystems may be especially vulnerable to climatic shifts due to water loss to the atmosphere associated with warming (Brown et al., 2010). Peatlands are considered a potentially critical tipping point of the global climate system (Lenton et al., 2008), and hydrological changes to peatlands could result in greater C losses due to microbial decomposition and wildland fire, offsetting peatlands as a long-term store of C (Wieder et al., 2009; Yu, 2012). It has been widely acknowledged that wildland fire regimes in the boreal are changing over time, increasing in extent, severity, and duration (e.g., Flannigan et al., 2009; Kohlenberg et al., 2018; Hanes et al., 2019), the results of which are likely to enhance C loss, impact air and water quality, and alter site hydrology and ecology. Though wildland fires are a natural part of ecosystem succession and regeneration, changes in fire regime could shift peatlands from a C sink to an expanding source through time (Turetsky et al., 2004, Turetsky et al., 2011; Wieder et al., 2009). Understanding processes associated with peatland wildland fire is essential for determining C combustion emissions and boreal peatlands' influence in the global C-climate cycle.

To understand peatland C losses during combustion and implications to climate, hydrology, and human health, I use burn severity as an indicator of the change in vegetation and soil as a result of wildland fire (Whitman et al., 2019). The following review examines

the relationship between wildland fire/burn severity (defined here as above- and below-ground fuel consumption; Keeley, 2009), boreal species, and the peat properties of the *acrotelm* (the top portion of peat, which is partially living and is periodically saturated due to a fluctuating water table) and the *catotelm* (the lower portion of peat, which is fully saturated and anaerobic; Ingram, 1978; Clymo, 1984). It synthesizes known peatland-fire-climate feedbacks that could increase burn severity and the propensity for peatland fires in the future, addressing current understanding and gaps in knowledge. To improve understanding of complex and interrelated feedbacks, I examine peatland feedbacks through the framework of those that occur a) prior to wildland fire to either increase or decrease burn severity; and b) in the years immediately following fire, which may either increase peatland resiliency or sensitivity, thereby altering future fire regimes. Finally, I discuss the implications of peatland-fire feedbacks to the climate system. I also present conceptual feedback diagrams of peatland processes related to wildland fire, hydro-climate, and ecosystem change, which may be incorporated into models of boreal peatland-fire-climate drivers and environmental characteristics that either maintain resilience or predispose peatlands to greater impacts from fire.

2.3 Pre-fire feedbacks affecting variability in burn severity

Burn severity varies both spatially and temporally as a result of any number of factors. Complex interactions related to burn severity include the weather at the time of fire: high wind speeds, prolonged warm conditions, and drying can spread fire rapidly through dry litter and understory vegetation to tree canopies (Bradshaw et al., 1984). Burn severity is also related to spatial variations in vegetation species and forest structural characteristics (e.g., Alonzo et al., 2017; Whitman et al., 2018), as well as surficial geology (Aldous et al.,

2015) and variations in local topography, which influence local moisture levels and the flammability of the soil organic layer. This is due, in part, to variations in energy receipt and water accumulation within soils (e.g., Lukenbach et al., 2017). Peat, a fuel source for wildland fire (Benscoter and Wieder, 2003), provides suitable conditions for smouldering fires, which produce similar carbon dioxide (CO_2) emissions but significantly more carbon monoxide (CO) and methane (CH_4) than flaming fires (French et al., 2002). Smouldering fires can also ignite in colder, wetter conditions, and persist for weeks to years, despite precipitation (Rein, 2013). Here, I describe peatland interactions and feedbacks that affect burn severity: a) soil properties; and, b) vegetation structures and species. These are critical for understanding how climate-mediated and other (e.g. anthropogenic) disturbances could alter peatland function and resiliency vs. sensitivity to fire in the future.

2.3.1 Soil properties: the relationship between hydrology, bulk density, and burn severity

Soil moisture is a primary control on the likelihood of peat ignition (Frandsen, 1997), as well as the depth and extent of burn (Rein et al., 2008; Figure 2.1). While vegetation, microtopography, and geology influence organic soil moisture locally (e.g., Benscoter and Wieder, 2003; Petrone et al., 2008; Wilkinson et al., 2018b), they do not appear to improve predictive models of depth of peat burn (Kohlenberg et al., 2018). Instead, the spatial variability of combustion and C losses results from variations in local hydrology and living/decomposed peat structural characteristics (e.g., Miyanishi and Johnson, 2002; Benscoter et al., 2011; Sherwood et al., 2013).

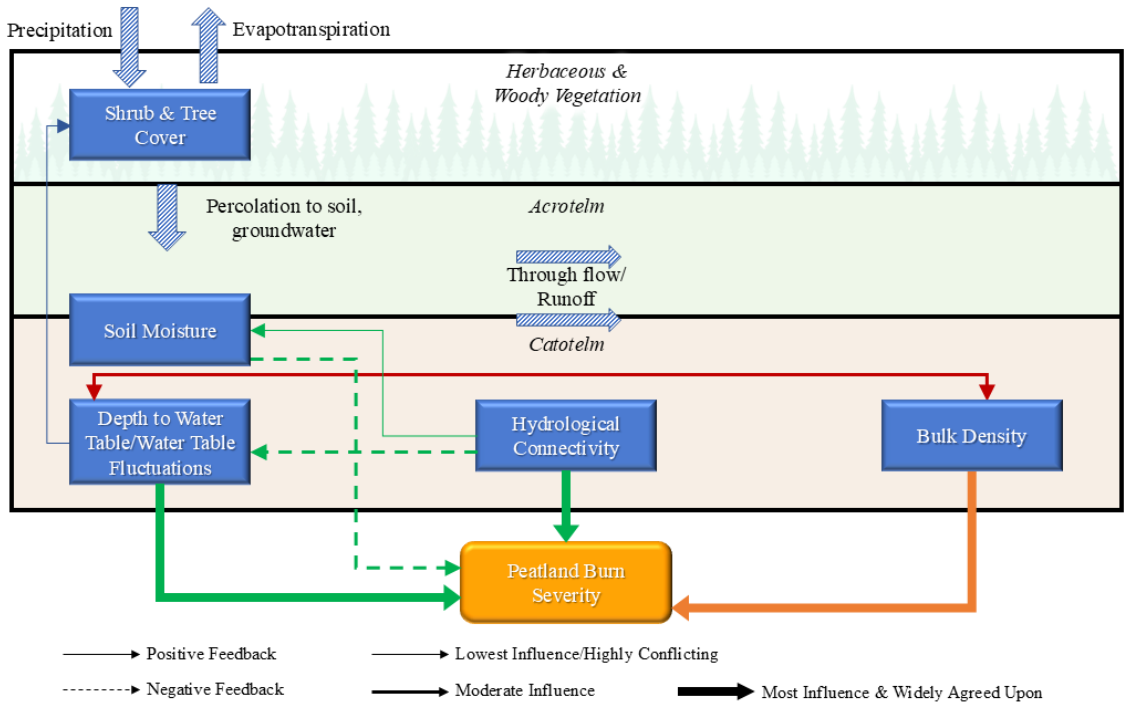

Figure 2.1. A conceptual diagram of positive and negative feedback mechanisms as they relate to peatland soil properties (hydrology and bulk density) and peat wildland fire. Major water fluxes are also included (wide, patterned arrows). Note that the diagram is not to scale and is not meant to represent horizontal spatial variations within a peatland.

Lowered water tables and increases in water table fluctuations increase depth of burn by reducing soil moisture, increasing bulk density ('red' positive feedback arrow, Figure 2.1), and improving conditions for tree and shrub growth (Sherwood et al., 2013; Lukenbach et al., 2015; 'blue' positive feedback arrow, Figure 2.1). An increase in depth to water table may increase soil tension, thereby reducing the soil's capacity to replace evaporated moisture (e.g., Lukenbach et al., 2015). Spatial variations in depth of burn are influenced by hydrological connectivity and groundwater movement or, alternatively, peatland fragmentation, which increases the edge to area ratio of peatlands, exposing them to greater proximal water use from surrounding forests ('green' positive and negative feedback arrows, Figure 2.1). For example, Hokanson et al. (2016) found that the

greatest depth of burn (50 cm, average) occurred along bog margins where the water table fluctuated substantially due to ephemeral groundwater connectivity to upland forests. Further, Lukenbach et al. (2015) found that depth of burn ranged from an average of 8 cm in peatland middles ($n = 580$) to an average of 42 cm in peatland margins ($n = 340$), illustrating the potential for greater depth of burn into peatlands with increased peatland fragmentation.

Variation in water table and soil moisture is enhanced by localised warming/drying of peatland soils. For example, Kohlenberg et al. (2018) found that within 0.012 m^{-3} samples, depth of burn more than tripled from field moisture levels to air-dried to oven-dried samples, while fuel consumption increased by ~61% in air-dried samples versus those left at field moisture. Oven-dried peat, which may be used as a proxy for hot, dry conditions, resulted in an average increase in total fuel consumption of 14.2%, emphasizing the importance of bulk density and hydrological conditions during peat fires. However, it is interesting to note that when controlling for other factors, the actual rate of downward spread in smouldering peat fires may increase at greater levels of soil moisture (Huang and Rein, 2017). Rein et al. (2008) found that for peat to ignite, soil gravimetric water content must be below 125 ± 10%, while Benscoter et al. (2011) found that the average surface gravimetric water content of samples in which ignition occurred was 61 ± 44%. Smouldering of over seven hours occurred in peat with up to 100% moisture content, regardless of bulk density, indicating that moisture content was the main control on the propagation of smouldering within soils containing variable amounts of organic matter. These studies' results are to be expected: reduction in soil moisture results in deeper peat burns, longer duration of peat burn, and peat that is more readily ignitable.

Depth of burn and subsequent soil C emissions are directly related to dry bulk density, defined as the weight of soil (dried) per given volume. Bulk density influences the maximum soil moisture at which combustion can occur (Benscoter et al., 2011; Kohlenberg et al., 2018), impacting both peatland hydrological conditions (Lukenbach et al., 2015) and depth of burn (Kohlenberg et al., 2018; Figure 2.1). Higher bulk densities can result in greater water table fluctuations (Lukenbach et al., 2015; 'red' positive feedback arrow, Figure 2.1), which are linked to greater depth of peat burn (Hokanson et al., 2016; 'orange' positive feedback arrow, Figure 2.1). Further, increased bulk density also provides an environment for combustion at higher moisture levels (Kohlenberg et al., 2018), as the increase in energy supplied by denser, and therefore added content of peat, results in greater burn severity (Benscoter et al., 2011). For example, Benscoter et al. (2011) found that combustion occurred at lower maximum gravimetric water content in peat with a bulk density of <40 kg m^{-3} than that with a bulk density of >40 kg m^{-3} (187% and 295%, respectively). While increased bulk densities may result in greater water table variability, temporal variations in hydrology may also lead to spatial variations in bulk density ('red' positive feedback arrow, Figure 2.2), and bulk density may also increase through compaction and increased aerobic decomposition (Waddington et al., 2015; Granath et al., 2016; Figure 2.1), which could alter fire propagation in peatlands. Conversely, Prat-Guitart et al. (2016) found that an increase in bulk density could slow lateral propagation of smouldering burn in peat blocks at 100% moisture or greater. While there was more energy produced in combustion as bulk density increases, the energy was less than that required to overcome high soil moisture levels. With the exception of these atypical findings, most studies demonstrate the potential for accelerated changes in bulk density, resulting from,

and causing further, water table fluctuations and moisture reduction (Lukenbach et al., 2015; Lukenbach et al., 2017), subsequently altering fire propagation patterns associated with anthropogenic and climate-mediated disturbance.

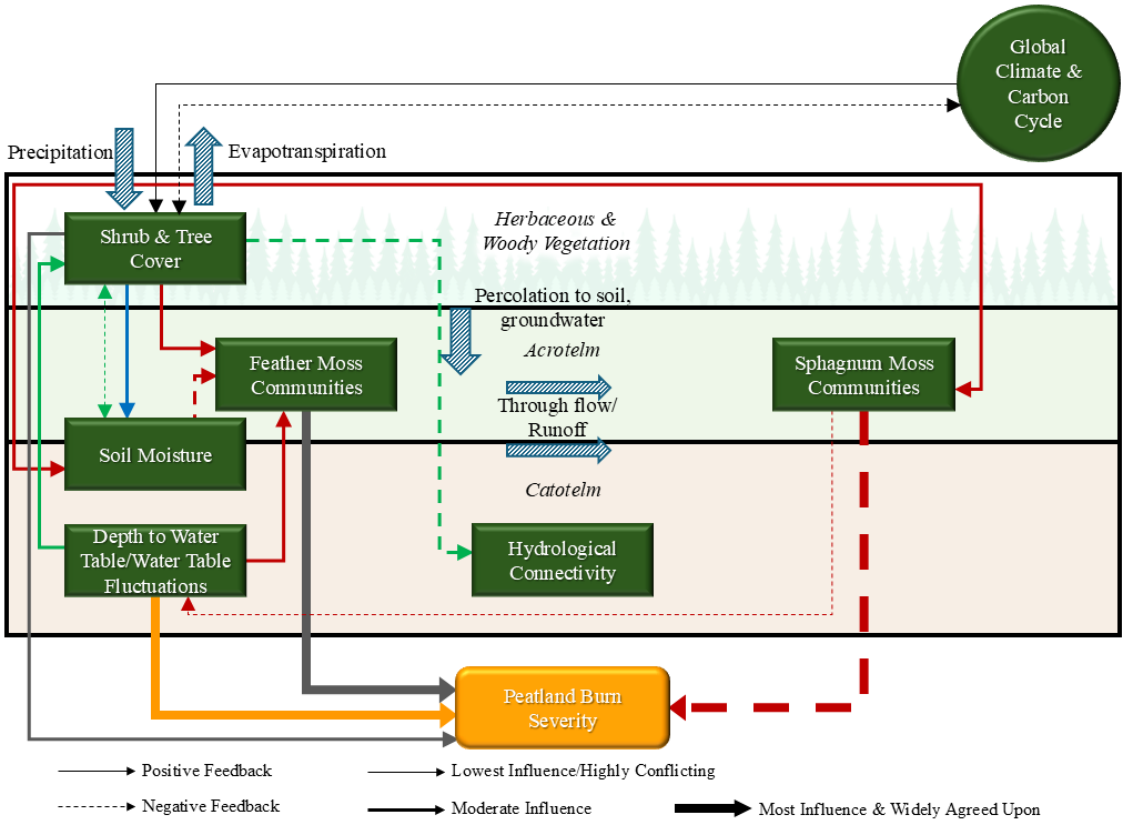

Figure 2.2. A conceptual diagram of positive and negative feedback mechanisms as they relate to vegetation distribution, structure, and peat wildland fire. Major water fluxes are also included (wide, patterned arrows). Note that the diagram is not to scale and is not meant to represent horizontal spatial variations within a peatland.

Natural peatlands that are artificially modified or drained may be analogous to future peatland conditions under climate change scenarios (Kettridge et al., 2015). Peatlands are commonly drained for forestry, road/infrastructure development, horticulture, and oil extraction, resulting in changes in peatland hydrological connectivity (Lieffers and Macdonald, 1990; Cleary et al., 2005; Rooney et al., 2012; Nieminen et al., 2018). Drained and/or disturbed peatlands are prone to greater

smouldering periods and increased depth of burn (Granath et al., 2016). For example, Wilkinson et al. (2018a) found that depth of burn was significantly greater in heavily drained areas (36.9 cm ± 29.6 cm) compared with moderately drained (6.4 cm ± 5.0 cm) and undrained (2.5 cm ± 3.5 cm) peatlands. Similar results were also found in Turetsky et al. (2011), who observed an almost three-fold increase in depth of burn from undisturbed to drained peatlands. Thus, deep peat fires found in drained peatland analogues illustrate the potential for significant impacts to the C-climate system and drying of peatlands in the future. Granath et al. (2016) estimated C losses of 21 kg m^{-2} from 30 cm deep burns (water table at 40 cm) to over 35–40 kg m^{-2} when water table is lowered to 80 cm. This is equivalent to 600–1000 years of C sequestration. Turetsky et al. (2011) found that wildland fire released 2.0 ± 0.5 kg C m^{-2} from undrained peatlands and 16.8 ± 0.2 kg C m^{-2} from drained peatlands. Similar to drained peatlands, deep burns resulting in large C emissions may be observed in undisturbed peatlands that are drying naturally (Granath et al., 2016). Lowered water tables expose deeper, compressed peat to smouldering, and consequently, higher C emissions per unit burned. Despite these results, many studies have not accounted for the variability of depth of burn and relation to C loss during combustion between peatland middles and margins, potentially underestimating C loss from boreal peatlands within the global C-climate cycle. This illustrates the importance of peatland hydrological connectivity and the implications of peatland fragmentation ('green' positive and negative feedback arrows, Figure 2.1).

2.3.2 Variability in vegetation distribution and structure: influences on burn severity

Ecological and vegetative processes controlling depth to water table in peatlands are non-linear, complex, and interacting (Waddington et al., 2015). Here, I examine vegetation-

related feedback mechanisms that directly and indirectly influence peatland fire severity within mature ecosystems. Vegetation feedback mechanisms associated with biomass losses from wildland fire include afforestation and shrubification, as well as changes to moss productivity and community over time (Figure 2.2).

Increased depth to water table associated with climate warming or other disturbances (Holmgren et al., 2015) can encourage the encroachment of shrubs ("shrubification") into peatlands (Weltzin et al., 2003), potentially resulting in afforestation (Waddington et al., 2015; 'green' positive feedback arrow, Figure 2.2). This may result in a positive soil drying feedback, where drying occurs due to transpiration ('green' negative feedback arrows, Figure 2.2), which further lowers the water table and enhances shrub/tree growth (Lieffers and Macdonald, 1990; Murphy et al., 2009; Waddington et al., 2015; 'green' positive feedback arrow, Figure 2.2). Alternatively, increased shading from trees may reduce evapotranspiration from the moss surface, partly mitigating increased interception and evapotranspiration fluxes associated with shrubification (Kettridge et al., 2013; 'blue' positive feedback arrow, Figure 2.2) and reducing burn severity. Changes to the structure of vegetation can increase wildland fire fuels and can alter the hydrological connectivity of the landscape (Thompson et al., 2019; 'grey' positive feedback arrows, Figure 2.2), thereby increasing fire risk and post-fire burn severity (e.g., Wilkinson et al., 2018a). Kettridge et al. (2015) suggest that ecological tipping points may exist when drying is significant enough that wildland fire results in deep burning (Wilkinson et al., 2018a; 'orange' positive feedback arrow, Figure 2.2). These processes have been observed in temperate peatlands in the U.K. (Davies et al., 2013). For example, Wilkinson et al. (2018a) examined the effects of peatland drainage on

afforestation and subsequent burn severity ('grey' positive feedback arrows, Figure 2.2). It was found that drainage significantly increased tree growth, contributing to the positive feedback mechanism between afforestation and water table reduction ('green' positive feedback arrow, Figure 2.2). Increased productivity also resulted in greater tree canopy cover (approximately 20% for undrained, 30% for moderately drained, and 70% for heavily drained peatlands). Wilkinson et al. (2018a) observed that tree cover further reduced the amount of precipitation that reached the peat surface ('blue' positive feedback arrow, Figure 2.2) and noted a threshold shift to a greater depth of burn during wildland fire. Variations in vegetation structures and foliage cover could have significant and complex implications for peatland maintenance vs. drying. Increased evapotranspiration due to shrubification and afforestation is enhanced by interception of precipitation, evaporation from leaves and branches, and reduced overall throughfall (Baisley, 2012; Thompson et al., 2014; Waddington et al., 2015). Not only does a reduction in precipitation reaching the peat surface affect burn severity via a decrease in soil moisture, but it may also result in increased burn severity by lessening the ability of precipitation to extinguish, or at least minimize the further spread of, smouldering in peat. The ability of rainfall to extinguish smouldering peat depends on intensity rather than only duration, and it must reach a threshold to have an impact (Lin et al., 2020). Low-intensity rain (<4 mm hr^{-1}) is unlikely to have any extinguishing impact (Lin et al., 2020); it is important to consider how greater canopy cover can reduce the intensity of rainfall.

While a general increase in shrubs or trees may result in further positive evapotranspiration-drying feedbacks, afforestation of an already shrubby peatland may counteract this if tree shading reduces shrub growth and maintenance (Waddington et al.,

2015), as, under some instances, evapotranspiration may be greater in shrubby peatlands than in treed peatlands (Strilesky and Humphreys, 2012). For example, treed peatlands dominated by black spruce (*Picea mariana*) will have lower evapotranspiration and gross ecosystem photosynthesis than open/shrubby peatlands, as *P. mariana* has lower transpiration and photosynthetic rates. *P mariana* has low stomatal conductance, which also decreases as vapour pressure deficit increases (Dang et al., 1997), so a transition from shrubs to trees may result in reduced evapotranspiration, reduced water loss, and improved peatland resilience to wildland fire.

Sphagnum mosses, particularly *Sphagnum fuscum*, which dominate peatland hummocks, retain moisture in dead hyaline cells and reduce soil temperature, thereby acting as a natural fire retardant in peatlands. When the depth to water table increases, hummock *Sphagnum* species increase hyaline cell area (Bu et al., 2013; Figure 2.2), increasing water storage capacity, maintaining surface moisture, and improving water storage capacity such that the potential for combustion is reduced ('red' positive and negative feedback arrows, Figure 2.2). Micro-topographic hollows are dominated by a diverse range of more flammable mosses, such as *Sphagnum angustifolium*, *Sphagnum magellanicum*, and feather moss (Kellner and Halldin, 2002; Benscoter et al., 2005). A decline in water table position or soil moisture, or increased shrubification and afforestation may result in a transition from *Sphagnum*-dominated moss communities to forest/upland species such as feathermoss (e.g., Bisbee et al., 2001; Breeuwer et al., 2009; Wilkinson et al., 2018a; 'red' positive and negative feedback arrows, Figure 2.2). Feathermoss species have lower moisture requirements than *Sphagnum* and thrive under shadier conditions (Bisbee et al., 2001). However, because feathermoss has a lower moisture content for the

same height above the water table, they tend to burn more severely (Wilkinson et al., 2018a; Figure 2.2). This could enhance future wildland fire burn severity within peatlands and surrounding transitional boundaries.

Figure 2.3 illustrates the combined feedbacks of the dominant pre-fire factors influencing the loss of biomass from C-rich peatland soils illustrated in Figure 2.1 and Figure 2.2 without highlighted feedbacks (used for the understanding of connections described above). Enhanced fragmentation of wetlands associated with drying, and also disturbance from natural resources extraction, will likely contribute to increased fire severity within peatlands in the future. This may occur as a result of reduced hydrological connectivity and a reduction of the ability of peatlands to maintain moisture conditions required for future fire resilience. Drying could enhance shrubification and positive feedbacks associated with water losses from evapotranspiration, resulting in a net increase of C fluxes to the atmosphere associated with combustion and microbial respiration.

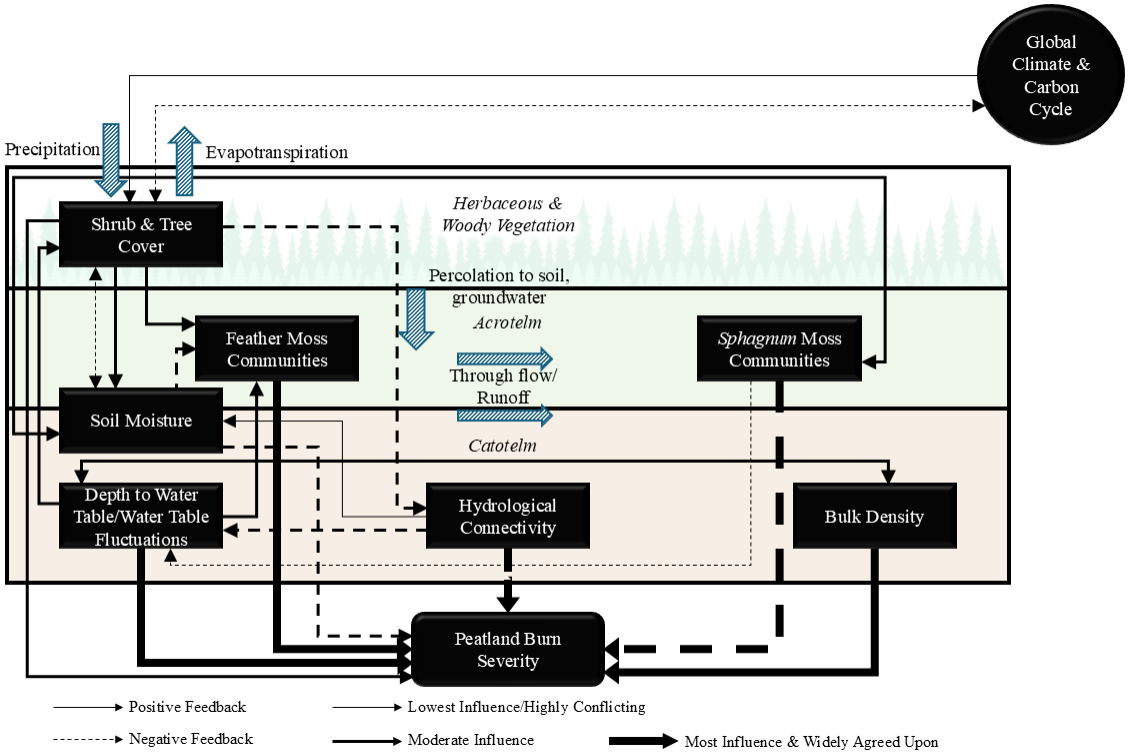

Figure 2.3. The combination of soil, hydrological, and vegetation influences (Figure 2.1, Figure 2.2) on pre-fire positive and negative feedback mechanisms and relationships affecting peatland burn severity. Major water fluxes are also included (wide, patterned arrows). Note that the diagram is not to scale and is not meant to represent horizontal spatial variations within a peatland.

2.4 Post-fire feedbacks and their influence on peatland ecosystem change

Wildland fire and burn severity in peatlands may critically impact feedback mechanisms, which, in the years immediately following fire, can enhance or diminish peatland resiliency to climate-mediated changes or future wildland fire regimes. Here I describe what is currently understood with regards to the immediate post-fire environment with regards to a) energy balance; b) soil properties, including bulk density and hydrological feedbacks; and c) vegetation regeneration.

2.4.1 Energy Balance

Boreal peatlands that have not recently burned have lower sensible heat fluxes, higher latent heat fluxes, and higher albedo (even through the growing season) than do boreal forests (Helbig et al., 2020). Boreal peatlands play an important role in local climates by cooling summer air temperatures by up to 1.7–2.5 °C (Helbig et al., 2020). As such, understanding how wildland fire impacts the energy balance of these peatlands in the years immediately following the fire is important in understanding energy partitioning into latent and sensible heat exchanges and interactions between evaporative losses, hydrology, and vegetative regeneration (Figure 2.4).

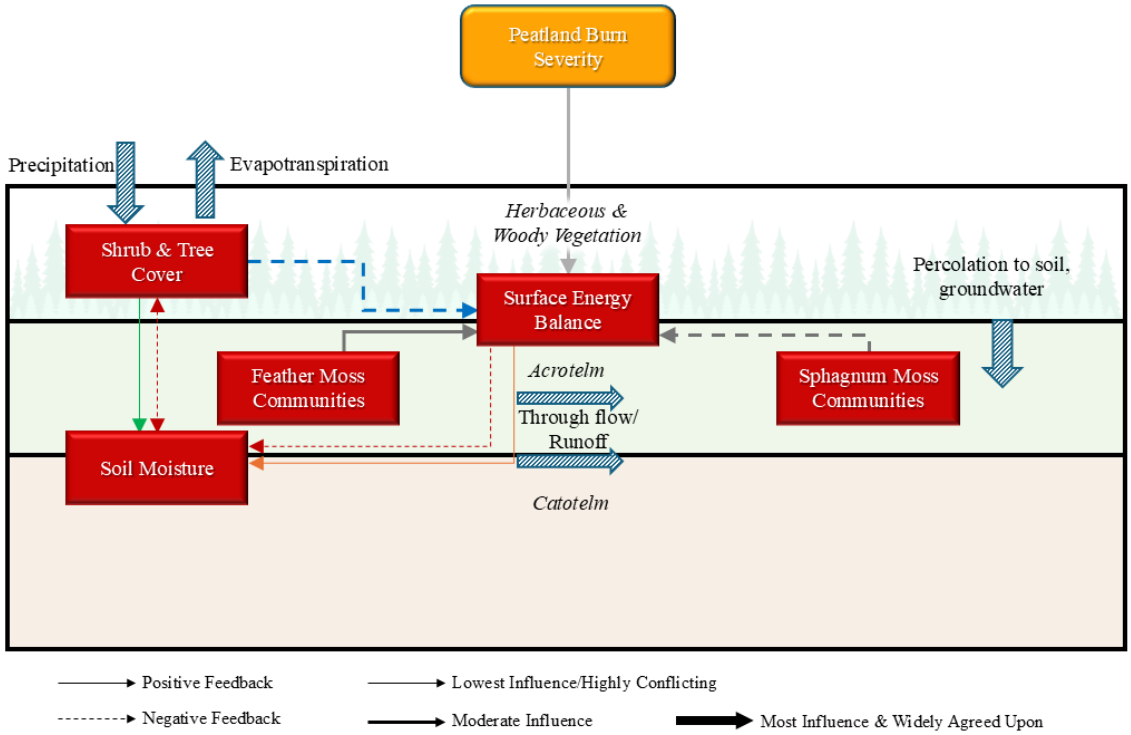

Figure 2.4. A conceptual diagram of positive and negative feedback mechanisms as they relate to energy balance in an immediately post-fire peatland. Major water fluxes are also included (wide, patterned arrows). Note that the diagram is not to scale and is not meant to represent horizontal spatial variations within a peatland.

In the period immediately following a moderate to severe fire, the ground surface receives increased incident shortwave radiation and reduced shading due to a loss of trees. This can result in a shift in the proportion of latent and sensible energy fluxes, which may result in significantly greater surface evaporation in burned peatlands than in unburned (~50%; Thompson et al., 2014; 'orange' positive feedback arrow, Figure 2.4). However, these positive feedbacks may be alleviated by negative feedback mechanisms such as reduced transpiration due to a loss of trees and changes in albedo associated with increased winter snow cover. While Thompson et al. (2014) found that evaporation increased from burned peatlands, once the reduction in transpiration due to a loss of trees was accounted for, the difference in evapotranspiration between burned and unburned peatlands was negligible. An increase in winter albedo and an increase in outgoing longwave radiation also mitigates increased shortwave radiation received by burned peatlands in the first few years post-fire ('red' negative feedback arrows Thompson et al., 2015). Further, rapid regrowth of shrubs within burned peatlands mitigated the impact of a loss of canopy on radiation at the moss surface ('blue' negative feedback arrow, Figure 2.4). Shrub growth likely reduces evaporation from the scorched ground surface as well as open water within small hummocks and ground cover vegetation, resulting in greater moisture retention (Kellner, 2001; 'green' positive feedback arrow, Figure 2.4).

Surface temperatures are also affected by moss species type and microtopography (Kettridge et al., 2012). *S. fuscum* hummocks maintain pre-fire temperatures ('grey' negative feedback arrow, Figure 2.4), and while the surface temperatures of hollows may be significantly greater than that of hummocks ('grey' positive feedback arrow, Figure 2.4), these differences are restricted to surface layers. Low

soil moisture and retention of sensible heat at the burned peat surface results in warming of the laminar surface temperature, while also insulating the sub-surface peat to a depth of ~1–2 cm. Kettridge et al. (2012) found that at approximately 1 m below the peat surface, burned and unburned peatland temperatures were similar. However, following wildland fire in sporadic permafrost environments, Gibson et al. (2018) found warmer soil thermal regimes and expansion of heat into the active layer (seasonally thawed soil). They hypothesize that the combined effects of deeper active layers, thermokarst bog expansion, and warmer soils will significantly increase rates of decomposition and C emissions, while thermokarst bog expansion could also result in net cooling, *Sphagnum* community enhancement, and possible net C sequestration. Further, during the period following fire, singed feather mosses may become hydrophobic, thereby reducing latent heat exchange (Kettridge et al., 2017; 'red' negative feedback, Figure 2.4).

2.4.2 Soil properties: hydrological and bulk density feedbacks

Combustion of peatlands may result in a positive or negative feedback response relative to the hydrological conditions of the peatland in the short-term post-fire, depending on environmental factors including pre-fire hydrology (e.g., Kettridge et al., 2015; Lukenbach et al., 2017), vegetation (e.g., Flannigan et al., 2009; Waddington et al., 2015) and burn severity (e.g., Lukenbach et al., 2016). Regarding hydrology, if peatlands are undrained (Kettridge et al., 2015) or are well-connected to groundwater sources (Lukenbach et al., 2017), post-fire water tables may remain at similar pre-fire levels and stability, enhancing recovery and moss regeneration. Alternatively, if peatlands are not well-connected to groundwater sources, or have been drained, increased depth of burn results in a lowered and more fluctuating water table in the years following the fire (Sherwood et al.,

2013; Thompson et al., 2014; Lukenbach et al., 2017; 'red' positive and negative feedback arrows, Figure 2.5). For example, peatlands that are poorly hydrologically connected may experience deeper, more severe burning, resulting in elevation loss ('red' positive and negative feedback arrows, Figure 2.5), exposure of high bulk density peat, and, subsequently, more dynamic hydrology ('grey' positive feedback arrows, Figure 2.5). Pre-fire surface peat with low bulk density has a high specific yield, which is important for moderating water table fluctuations (Thompson and Waddington, 2013a). Wildland fire results in the exposure of deeper peat with higher bulk density to the surface, especially in hollows. This denser peat has higher water retention and lower specific yield, which results in a less stable, "flashier" water table that fluctuates more readily with small weather changes (Thompson and Waddington, 2013a; 'grey' positive feedback arrows, Figure 2.5). Particularly when peatlands are poorly connected to groundwater and the surrounding peatland complex, this can result in increased flooding during wet conditions and greater water table draw-down during dry periods, in the years following wildland fire (Thompson et al., 2014).

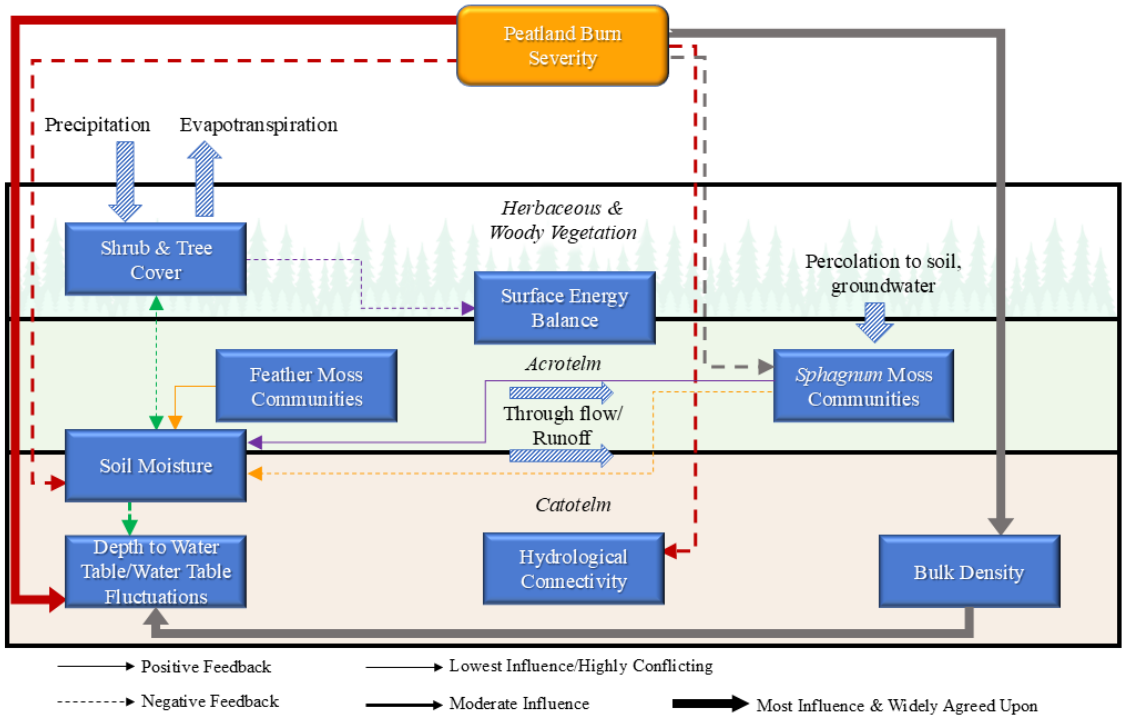

Figure 2.5. A conceptual diagram of positive and negative feedback mechanisms as they relate to post-fire burn severity and soil properties (hydrology and bulk density). Major water fluxes are also included (wide, patterned arrows). Note that the diagram is not to scale and is not meant to represent horizontal spatial variations within a peatland.

The importance of hydrological connectivity in post-wildland fire hydrological impacts is especially apparent when considering peatland margins. When comparing the post-fire hydrological conditions of poorly connected versus well-connected peatland margins, Lukenbach et al. (2017) found that poorly-connected peatlands had a less stable water table, whereas the well-connected peatlands' water table was moderated. Peatland margins that are well-connected within the peatland complex have lower depth of burn (like that of peatland middles). The deep burning in the margins of poorly connected peatlands not only result in a greater elevation loss, but enhance peat exposure to high bulk density and low specific yield.

Peatlands may have different hydrological responses following wildland fire, depending on their vegetation and/or microtopography and the severity of burn (e.g., Thompson and Waddington, 2013b). In peatlands dominated by *Sphagnum*, evapotranspiration may increase after a wildland fire, resulting in drier peatlands (Thompson et al., 2014) and an increased risk of recurring fire. Particularly in *S. fuscum*-dominated hummocks, there is a greater increase in pore-water pressure than in hollows, suggesting that despite the limited depth of burn, and the apparently low burn severity of hummocks relative to hollows, the hydrological impacts may be more severe. This is demonstrated by increased soil moisture losses post-fire ('orange' negative feedback arrow, Figure 2.5), increased moisture tension, limited *Sphagnum* growth, and reduced post-fire regeneration (Thompson and Waddington, 2013b).

However, changes to evapotranspiration may also result in negative hydrological feedbacks (Thompson and Waddington, 2013b). For example, lower severity burning resulting in residual feathermoss may become hydrophobic, increasing soil moisture retention (Wilkinson et al., 2020; 'orange' positive feedback arrow, Figure 2.5). As burn severity increases, hydrophobicity rises to a point where vegetation is thoroughly combusted, exposing the underlying peat (Wilkinson et al., 2020). This may reduce the risk of subsequent fires, the potential for vegetation regime shift, and/or the possibility of excess C release due to drying peat (Kettridge et al., 2014). Further, while other studies as described previously found that low severity burn of *Sphagnum* increases evapotranspiration, others have found that it may also increase the water repellency of *Sphagnum* (Kettridge et al., 2014), resulting in a negative feedback such that

evapotranspiration is reduced, water storage is increased, and propensity for future burn is reduced ('purple' positive feedback arrow and 'grey' negative feedback arrow, Figure 2.5).

Further mitigating potential increases in evapotranspiration from burned *Sphagnum* communities, post-combustion feathermoss evapotranspiration is much lower than that of *Sphagnum* and may be less than the evaporation from a non-vegetated environment (Kettridge et al., 2017). If treed peatlands are burned, the loss of trees and post-fire forb and shrub succession may result in a lower net loss of moisture in the post-fire peatland environment (Thompson et al., 2015; 'green' negative feedback arrows, Figure 2.5). A loss of canopy will also increase the amount of precipitation reaching the soil and will reduce the evaporation that occurs on the canopy before it reaches the peat surface (via interception). Fewer trees and shrubs will also reduce evapotranspiration (Baisley, 2012; Waddington et al., 2015; Wilkinson et al., 2018a; 'purple' negative feedback arrow, Figure 2.5). Because evapotranspiration is the dominant flux of water from boreal peatlands (Petrone et al., 2006), reduced transpiration is essential in maintaining peat moisture, and therefore reducing the susceptibility of peatlands from future wildland fire (Kettridge et al., 2017).

Regarding post-fire bulk density, Thompson and Waddington (2013a) found that surface bulk density was significantly greater in burned than in unburned peatlands (85 kg m^{-3} and 56 kg m^{-3}, respectively). Increased post-fire bulk density can result in enhanced water table variability, which in turn, can further increase bulk density and the probability of greater depth of burn in future fires (Waddington et al., 2015; Granath et al., 2016); 'grey' positive feedback arrows, Figure 2.5). Changes in post-fire bulk-density can also have significant implications for post-fire moisture by reducing saturated hydraulic

conductivity (Whittington and Price, 2006) and specific yield, which controls the rate of water table decline per unit of water loss (Price, 1997). Greater bulk density with depth, especially in post-fire peatlands, allows for increased water retention by peat found above the water table (Thompson and Waddington, 2013a). Finally, the positioning and bulk density within hollows vs. hummocks also varies following wildland fire. For example, Thompson and Waddington (2013a) found that post-fire bulk density was greater in hollows (where burn severity and loss of C-rich soils are often greater) than in hummocks (95 kg m^{-3} and 45 kg m^{-3}, respectively).

2.4.3 Shrubification and change to ground cover vegetation

The alteration of microtopography by wildland fire is an important determinant of post-fire vegetation regeneration and peatland resilience. Microtopography is a primary control of moss and lichen composition associated with variations in hydrology and energy balance (Vitt, 1990), which may result in a positive fire/species feedback response associated with different moisture levels and decomposition rates. Variations in ground cover species can also result in differences in peat bulk density, further enhancing variations in microtopography (Benscoter et al., 2015; 'red' positive and negative feedback arrows, Figure 2.6). Benscoter et al. (2015) found that the post-fire local microtopography elevation range between hummocks and hollows was nearly double that of pre-fire in a boreal peatland. Therefore, if wildland fire did not occasionally enhance local microtopograhical variations, peatlands would become more vertically homogeneous (Benscoter and Vitt, 2008; Rowe et al., 2017), resulting in successional changes and potentially lower diversity of vegetation species (Benscoter and Vitt, 2008). Following fire, hollows remain hollows; however, hummocks may be equally likely to become hollows as

they are to remain hummocks (Benscoter et al., 2005). Whether a microtopographic feature is changed or maintained is dependent on the local spatial variability of the depth of burn (burn severity). If burn severity is relatively low, hummocks may regenerate faster than hollows due to remaining *Sphagnum* fragments (Clymo and Duckett, 1986). However, if burn severity is high, hummocks can become hollows, and *Sphagnum* regeneration would be limited (Benscoter et al., 2005). This highlights the importance of fire severity and spatial variations in depth of burn for determining peatland succession and the overall form of boreal peatlands in the future (Figure 2.6).

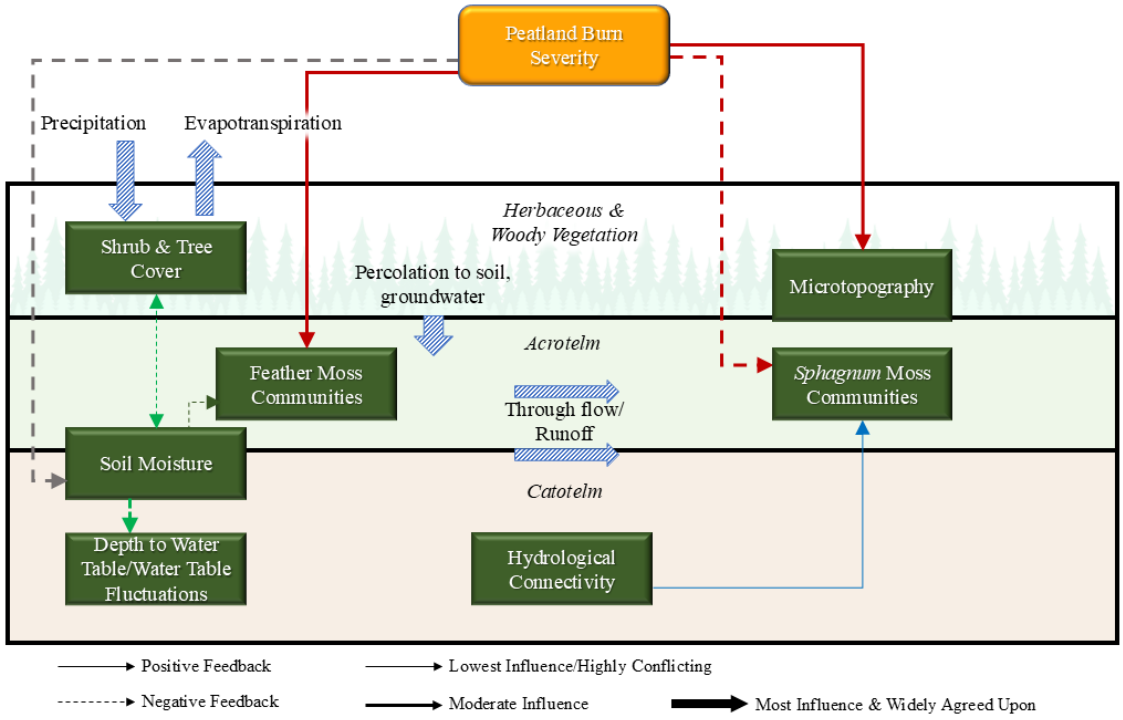

Figure 2.6. A conceptual diagram of positive and negative feedback mechanisms as they relate to post-fire burn severity and vegetative regeneration. Major water fluxes are also included (wide, patterned arrows). Note that the diagram is not to scale and is not meant to represent horizontal spatial variations within a peatland.

Regarding the influence of microtopography on post-fire vegetation communities, *S. fuscum* typically regenerates on hummocks, while hollows are often

characterised by a greater variety of post-fire species (Benscoter et al., 2005) due to greater variability of moisture conditions. *Sphagnum* regeneration on hummocks is supported if burn severity is low or if peatlands are hydrologically well-connected ('blue' positive feedback arrow, Figure 2.6); however, if burn severity increases, and/or peatlands are disconnected from groundwater and the surrounding peatland complex, the functionality of this negative feedback mechanism will be reduced. *Sphagnum* hummocks may not regenerate, resulting in the migration of feathermoss into hummocks (Lukenbach et al., 2016; Lukenbach et al., 2017) or the replacement of *Sphagnum* communities with upland species and, subsequently, enhanced peatland drying (e.g., Johnston et al., 2015; Miller et al., 2015; 'red' negative feedback arrow, Figure 2.6).

Post-fire water table variability within peatland margins may also promote a regeneration trajectory similar to that of uplands, as indicated by the growth of vegetation species such as aspen (*Populus tremuloides*; Lukenbach et al., 2017; Depante et al., 2019; 'green' negative feedback arrows, Figure 2.6). As these are not peat-forming species, they may affect the C sink capacity of the peatland and could increase transpiration. This may result in a positive feedback response in which increased drying results in further growth of upland vegetation and possible transition to an upland as opposed to a wetland ecosystem ('green' negative feedback arrows, Figure 2.6). The process feedbacks of post-fire peatland establishment associated with energy exchanges (Figure 2.4), burn severity, hydrological and topographical influences (Figure 2.5), and vegetation community establishment (Figure 2.6) are summarised in Figure 2.7.

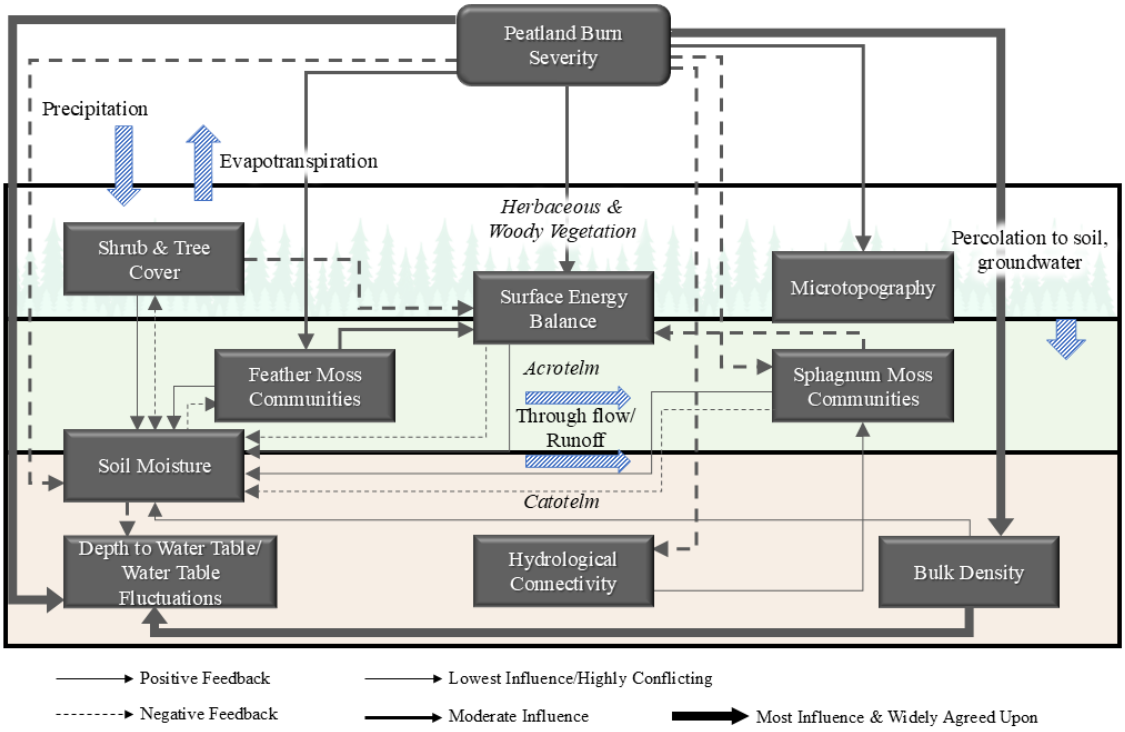

Figure 2.7. A conceptual feedback diagram with water fluxes summarizing post-fire positive and negative feedback mechanisms and relationships affected by peatland burn severity, hydrology, and vegetation described in Figure 2.4, Figure 2.5, Figure 2.6. Major water fluxes are also included (wide, patterned arrows). Note that the diagram is not to scale and is not meant to represent horizontal spatial variations within a peatland.

2.5 Peatland fire linkages to the climate system

Due to the vast C stores of northern peatlands, changes in hydrology and burn regimes will significantly influence peatland C cycling and implications to the global C cycle (Camill et al., 2009; Turetsky et al., 2011). Climatic warming and changes to the period of snow-cover in northern regions are causing major ecological shifts within boreal peatlands (e.g., Chasmer and Hopkinson, 2017 within the discontinuous permafrost zone), affecting both the directionality and strength of peatland-atmosphere C fluxes (Helbig et al., 2017). Further, C emissions from peatland fires are predicted to increase associated with projected climatic shifts (e.g., Kohlenberg et al., 2018; Wilkinson et al., 2018a; 'red' positive feedback arrow, Figure 2.8). Smouldering peat releases more C during peatland wildland

fire than does the burning of the forested overstory (Benscoter et al., 2011), while near equivalent amounts of C are released in the years following wildfire due to net balances of decreased gross primary production (Harden et al., 2000) and enhanced ecosystem decomposition/respiration (e.g., Auclair and Carter, 1993; Kasischke et al., 1995; O'Neill et al., 1997; Harden et al., 2000), exacerbating positive C-climate feedback cycle (Kasischke et al., 1995; Stocks et al., 1996; van der Werf et al., 2010; Figure 2.7). Such changes could shift peatlands from a gradual sink for atmospheric C to a source (Loisel and Yu, 2013).

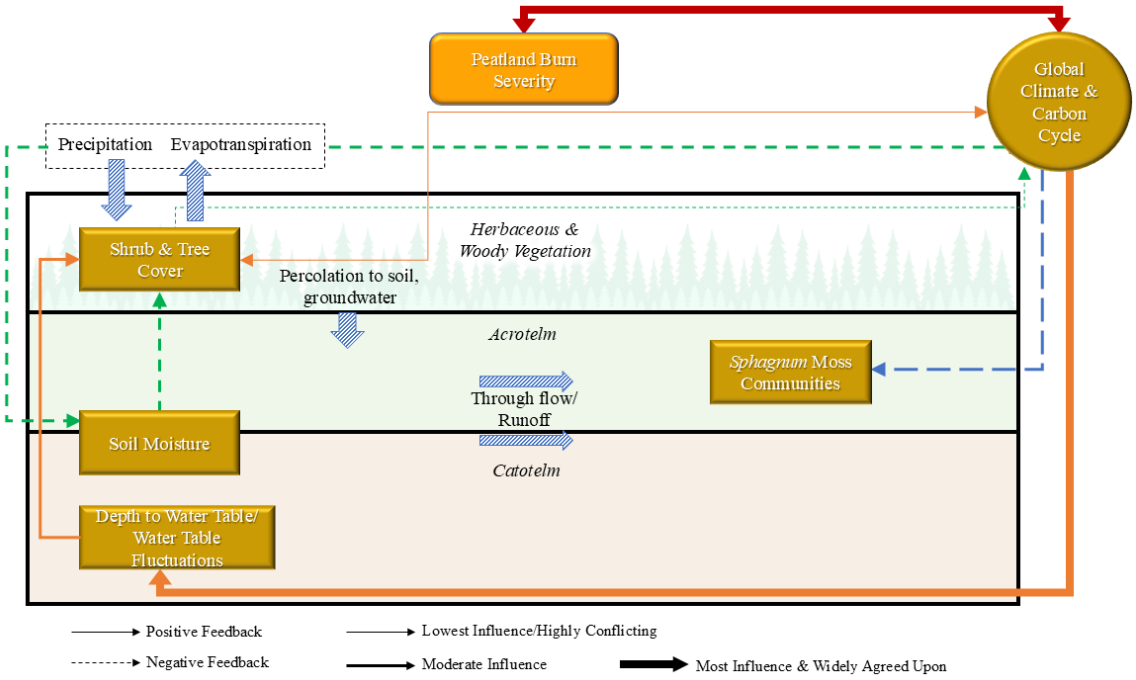

Figure 2.8. A conceptual diagram of positive and negative feedback mechanisms as they relate to the global C-climate cycle and peat wildland fire. Major water fluxes are also included (wide, patterned arrows). Note that the diagram is not to scale and is not meant to represent horizontal spatial variations within a peatland.

It is worth noting that while this chapter focuses on C emissions during peat combustion, which is mostly CO_2 (Hu et al., 2018), CO and CH_4 are also emitted in greater proportions than in flaming fires. In reviewing the literature, Hu et al. (2018) found that

average emissions factors in boreal and temperate peatland fires were 1133.8 g kg^{-1} CO_2, 179.4 g kg^{-1} CO, and 8.1 g kg^{-1} CH_4. The ratios of these C gasses will fluctuate depending on the soil's bulk density and moisture content (Kohlenberg et al., 2018). Dry peat results in an increase in flaming and greater CO_2 emissions, whereas wet peat emits more CO (Hu et al., 2019), which may be of concern when considering the negative impacts of CO on human health (Hinwood and Rodriguez, 2005). As the strength of combustion and oxidization declines with moisture content, the ratio of CO:CO_2 increases. While these are important metrics, especially when considering air quality, the loss of specific C gasses is not addressed in this chapter.

The extent to which North American boreal peatland fires affect global C and climate systems by re-introducing C sequestered over several millennia to the atmosphere, and the response of peatland C emissions to climatic warming, remains unclear. Because of the complexity of the combustion of organic peatland soils, spatial variations of depth of burn, and the large proportion of C emitted relative to other ecosystem components (Benscoter and Wieder, 2003), accurate quantification of C emissions can be challenging (van der Werf et al., 2010). This may result in the large variability in depth of burn, particularly between margins and middles, left unaccounted for (e.g., Thompson and Waddington, 2014; Kohlenberg et al., 2018). For example, Harden et al. (2000) found that the boreal ecosystem C losses from wildfire were three to ten times greater than those used in general circulation models. Wu et al. (2015) found that peatlands, in general, are not well represented within Earth systems models, and while they were incorporated into the Canadian Land Surface Scheme v3.6 and Canadian Terrestrial Ecosystem Model v2.0, wildland fire and its impacts of C loss were not represented. Other studies have modelled

C loss while assuming a maximum depth of peat burn of 15 cm (e.g. van der Werf et al., 2010), which underestimates depth of burn measurements identified using field sampling and airborne lidar data within boreal peatlands (e.g., Granath et al., 2016; Hokanson et al., 2016; Chasmer et al., 2017). If depth of burn is underestimated within C emissions models, then C losses from peatland fires are also significantly underestimated. The proportion of the landscape that is subject to such deep burning, however, remains unclear. Improved accuracy of C emissions estimations requires quantification of the proportion of deep to shallow burns associated with burn severity and a better understanding of the distribution of deep burns for statistical analyses and C budget modelling.

Peatland-climate feedback mechanisms are complex, and there are many uncertainties regarding the prediction of peatland fires in the future (e.g., Camill et al., 2009). It is possible that, while a warming climate may increase wildland fire frequency, severity, and/or extent (Flannigan et al., 2005), resulting in greater C emissions (Turetsky et al., 2011; 'orange' positive feedback arrows, Figure 2.8), the opposite could also occur. For example, increased shrubification of peatlands following fire will result in a pulse of increased net primary production (NPP), resulting in a negative C-climate feedback, potentially mitigating C emissions from peat combustion (Camill et al., 2009; Fan et al., 2013; Loisel and Yu, 2013; 'green' negative feedback arrows, Figure 2.8). Further, an increase in surface air temperature and length of growing season prolongs the period of C sequestration, resulting in net uptake (Fan et al., 2013; Loisel and Yu, 2013), while an increase in air temperature may also increase heterotrophic respiration. In some cases, a warming climate may also result in a transition from fen to bog within some boreal peatlands and an increase in *Sphagnum* production (Loisel and Yu, 2013; 'blue' negative

feedback arrow, Figure 2.8), both of which also promote increased C uptake. Finally, increased sequestration from historically wetter peatlands, such as fens, may offset C emissions of already-drier peatlands (Loisel and Yu, 2013). However, a shift from wetter to dryer peatlands may increase fire severity and the likelihood of ignition, further reducing fire return intervals. The long-term implications of increasing fire frequency are uncertain. If vegetation regeneration was not considered, the shortening of fire intervals by half could result in a net source of C from peatlands (Wieder et al., 2009); however, with more frequent fires, while deciduous trees may flourish, the quantity of conifers, surface organic material, and herbaceous plant species will likely decrease (Whitman et al., 2019). Shortened fire return intervals may not allow for regeneration of current stands, reducing fuel load (Johnstone et al., 2016), and possibly decreasing burn severity and C emissions from future wildland fires, despite their increased frequency.

The relationship between peatland vegetation communities in the post-fire ecosystem and impacts on C emissions may be mitigated by the regeneration of peatland mosses and vascular vegetation (Camill et al., 2009). Still, this enhanced regeneration could have other implications for peatland function and ecosystem services. For example, an increase in NPP or shifting vegetation communities could increase fire fuel sources, increasing the probability of ignition and spread. Further, Fan et al. (2013) suggest that peatland C sinks may transition to sources in the latter part of the 21st century as projected warming may increase respiration beyond what is sequestered through primary production, amplifying positive C-climate-fire feedback cycles (e.g., Kettridge et al., 2017).

2.6 Discussion of peatland feedbacks as related to resiliency and vulnerability to wildland fire

The processes and feedback mechanisms related to peatland fires and climatic change are complex and uncertain; however, the recent proliferation of research on these important topics helps to clarify our understanding of peatland-fire interactions. Here, I provide a summary of key characteristics and feedback mechanisms that affect the resiliency of peatlands to wildland fire (Figure 2.9a), as well as a comprehensive conceptual of all interactions discussed throughout the review (Figure 2.9b).

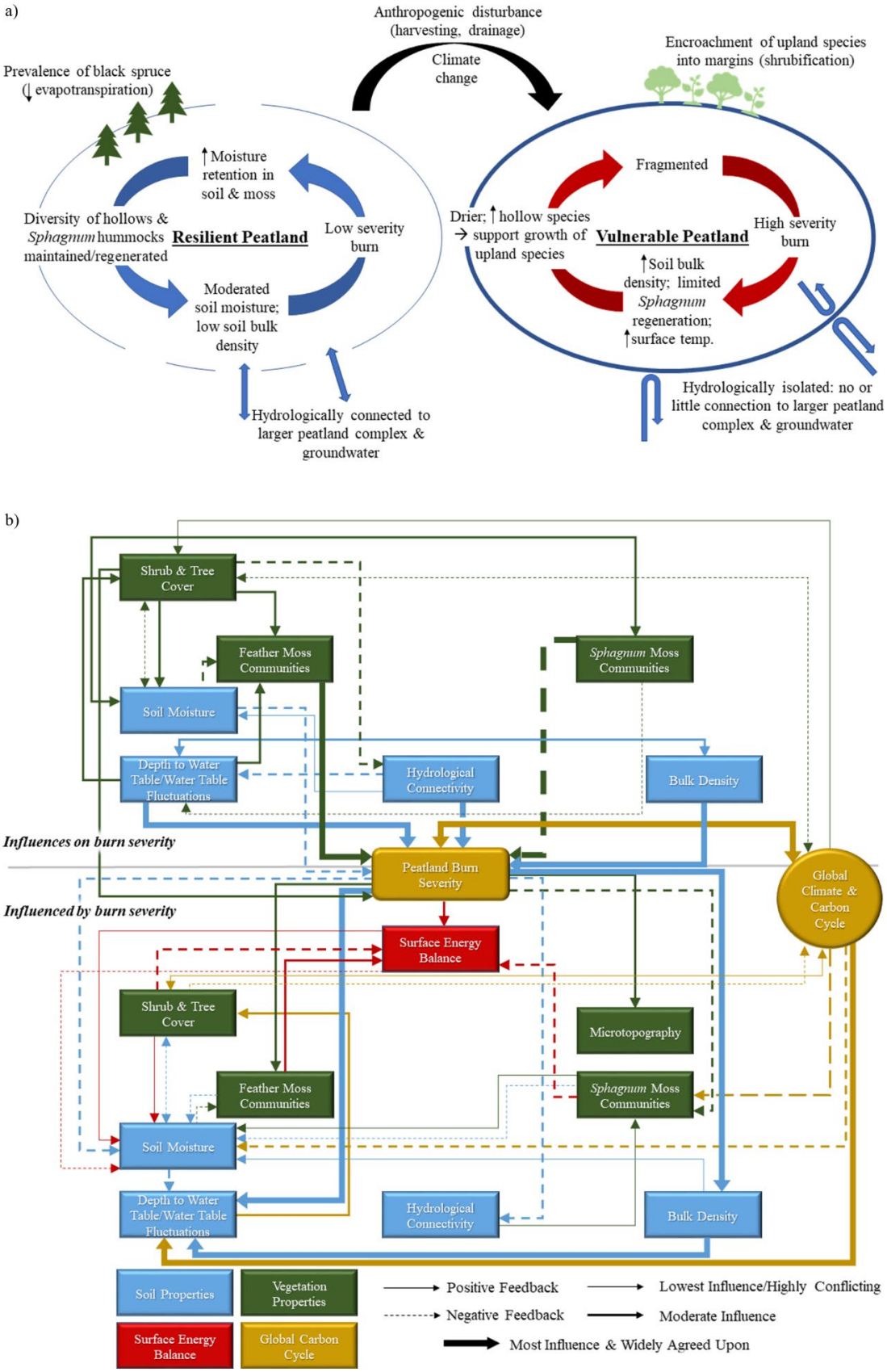
a)
Anthropogenic disturbance (harvesting, drainage)
Climate change
Encroachment of upland species into margins (shrubification)
Prevalence of black spruce (↓ evapotranspiration)
↑Moisture retention in soil & moss
Diversity of hollows & *Sphagnum* hummocks maintained/regenerated
Resilient Peatland
Low severity burn
Moderated soil moisture; low soil bulk density
Hydrologically connected to larger peatland complex & groundwater
Fragmented
Drier; ↑hollow species → support growth of upland species
Vulnerable Peatland
High severity burn
↑Soil bulk density; limited *Sphagnum* regeneration; ↑surface temp.
Hydrologically isolated: no or little connection to larger peatland complex & groundwater
b)
Shrub & Tree Cover
Feather Moss Communities
Sphagnum Moss Communities
Soil Moisture
Depth to Water Table/Water Table Fluctuations
Hydrological Connectivity
Bulk Density
Influences on burn severity
Peatland Burn Severity
Global Climate & Carbon Cycle
Influenced by burn severity
Surface Energy Balance
Shrub & Tree Cover
Microtopography
Feather Moss Communities
Sphagnum Moss Communities
Soil Moisture
Depth to Water Table/Water Table Fluctuations
Hydrological Connectivity
Bulk Density
Soil Properties
Vegetation Properties
Surface Energy Balance
Global Carbon Cycle
Positive Feedback
Negative Feedback
Most Influence & Widely Agreed Upon
Lowest Influence/Highly Conflicting
Moderate Influence

Figure 2.9. Conceptual models of a) feedbacks within resilient vs. sensitive peatlands; and b) cumulative positive and negative feedback mechanisms related to peatland-fire interactions and effects on the global C-climate cycle.

The most resilient peatlands are hydrologically well-connected to both the larger peatland complex and groundwater system, resulting in a moderated water table. They have not been anthropogenically altered (compacted, drained, or harvested), and therefore maintain stable soil moisture and low bulk density. They are not fragmented and have low margin:middle area ratios (e.g. Lukenbach et al., 2015). These peatlands have a thick surface layer of mosses, keeping surface bulk density low and moisture retention high, and a high proportion of hummock-dominating species, such as *Sphagnum fuscum*, which holds moisture even during drought, lowers surface temperatures, and limits encroachment of upland species (e.g. Kettridge et al., 2012; Bu et al., 2013). Highly resilient peatlands may have black spruce as a dominant tree species, as low stomatal conductance will help maintain peat moisture (Dang et al., 1997). Following fire, *Sphagnum* mosses prevalent in resilient peatlands will help mitigate the lowering of the water table and reduction of soil moisture.

The most vulnerable peatlands have been fragmented or disturbed and are more hydrologically isolated. Thus, their water tables are highly temporally variable, resulting in increased bulk density and conditions that support shrubification, particularly in the margins (e.g. Lukenbach et al., 2015; Hokanson et al., 2016). Aspens may dominate the margins, encroaching into the peatlands and promoting a transition to an upland ecosystem (e.g. Lukenbach et al., 2017; Depante et al., 2019). Fragmentation results in a high margin:middle area ratio, which increases the rate of shrubification, fuels for fire, and burn severity. These peatlands may have burned severely in the past, resulting in a loss of

hummocks and hummock-forming moss species. A transition from *S. fuscum* and other hummock-forming species to feathermoss and other hollow species due to either previous wildland fire or drying and afforestation may increase the risk of subsequent high severity fires (e.g. Bisbee et al., 2001; Breeuwer et al., 2009; Wilkinson et al., 2018a). Previous fires may have been severe, increasing bulk density, resulting in unstable water tables and increased risk of severe burns (e.g. Thompson and Waddington, 2013a; Waddington et al., 2015; Granath et al., 2016; Figure 2.9a).

2.7 Recommendations

Modelling and mapping peatlands based on the key attributes described in the previous section may allow for a better understanding of future wildland fire scenarios within the boreal and improved estimations of boreal peatlands' contribution to the global C-climate cycle. I also suggest that research focuses on improving estimates of wildland fire C emissions of the boreal region. By more accurately quantifying C emissions, the contribution of wildland fire to the global C-climate cycle can be better understood. I propose that better integration of process understanding and scaling of changes in peatlands through a combination of remotely sensed data and hydro-ecological and wildland fire models is necessary. In utilizing these multi-disciplinary approaches, I can better understand the coupling of boreal peatland-fire interactions and boreal peatlands' contribution to global climate change and climate forcing mechanisms.

2.8 Conclusion

In this review, I have synthesized knowledge of peatland-wildland fire feedback mechanisms and how they interact with the C-climate feedback cycle (Figure 2.9b). While this is by no means an exhaustive list, this review provides an overview of the dominant

processes and feedbacks and explanations as to their relative connections. It is clear that positive and negative feedbacks are numerous and complex and may act against one another, entirely or partially mitigating the effect of another, or may compound the effects, resulting in enhanced fire risk and C-climate forcing. The extent of the effects of these feedbacks also varies across peatlands, regions, and through time. However, we can conclude that over larger areas, climatic warming will result in greater fire frequency, extent, and severity in the boreal region, which will increase peatland C losses due to fire, as well as alter peatland condition and the ecosystem services that northern communities rely on. Initially, increased C emissions from wildland fire may be offset by increased NPP; however, this is temporary and may eventually result in further increases of C loss through enhanced decomposition and ecosystem respiration. Climatic warming and anthropogenic disturbance may also reduce peatland resiliency to wildland fire through reduced hydrological connectivity. While there are undoubtedly negative feedback mechanisms initiated following peatland fires, the dominant feedbacks are predominantly positive (Figure 2.1, Figure 2.2, Figure 2.3, Figure 2.4, Figure 2.5, Figure 2.6, Figure 2.7, Figure 2.8). It is clear that increases in wildland fire activity in boreal peatlands will result in greater C losses to the atmosphere, enhancing climate warming and resulting in a positive feedback mechanism.

2.9 Declaration of competing interest

The authors declare that they have no known competing financial interests or personal relationships that could have appeared to influence the work reported in this chapter.

2.10 Acknowledgements

The authors would like to acknowledge funding for this research from Natural Sciences and Engineering Research Council (NSERC) Discovery Grant and University of Lethbridge Start Up Funding to Dr. L. Chasmer. K. Nelson also acknowledges post-graduate support from NSERC and the University Of Lethbridge School Of Graduate Studies.

2.11 References

Aldous, A. R., Gannett, M. W., Mackenzie, K., & O'Connor, J. (2015). Geologic and geomorphic controls on the occurrence of fens in the Oregon Cascades and implications for vulnerability and conservation. Wetlands, 35(4), 757–767. https://doi.org/10.1007 /s13157-015-0667-x.

Alonzo, M., Morton, D. C., Cook, B. D., Andersen, H.-E., Babcock, C., & Pattison, R. (2017). Patterns of canopy and surface layer consumption in a boreal forest fire from repeat airborne lidar. Environmental Research Letters, 12(6), 065004.

Auclair, A. N. D., & Carter, T. B. (1993). Forest wildland fires as a recent source of CO_2 at northern latitudes. Canadian Journal of Forest Research, 23(8), 1528–1536. https: //doi.org/10.1139/x93-193

Benscoter, B. W., Greenacre, D., & Turetsky, M. R. (2015). Wildland fire as a key determinant of peatland microtopography. Canadian Journal of Forest Research, 45(8), 1132-1136. https://doi.org/10.1139/cjfr-2015-0028.

Benscoter, B. W., Kelman Wieder, R., & Vitt, D. H. (2005). Linking microtopography with post-fire succession in bogs. Journal of Vegetation Science, 16(4), 453-460. https://doi.org /10.1111/j.1654-1103.2005.tb02385.x.

Benscoter, B. W., Thompson, D. K., Waddington, J. M., Flannigan, M. D., Wotton, B. M., De Groot, W. J., & Turetsky, M. R. (2011). Interactive effects of vegetation, soil moisture and bulk density on depth of burning of thick organic soils. International Journal of Wildland Fire, 20(3), 418-429. https://doi.org/10.1071/WF08183.

Benscoter, B. W., & Vitt, D. H. (2008). Spatial patterns and temporal trajectories of the bog ground layer along a post-fire chronosequence. Ecosystems, 11(7), 1054-1064. https:
//doi.org/10.1007/s10021-008-9178-4.

Benscoter, B. W., & Wieder, R. K. (2003). Variability in organic matter lost by combustion in a boreal bog during the 2001 Chisholm fire. Canadian Journal of Forest Research, 33(12), 2509–2513. https://doi.org/10.1139/x03-162.

Bisbee, K. E., Gower, S. T., Norman, J. M., & Nordheim, E. V. (2001). Environmental controls on ground cover species composition and productivity in a boreal black spruce forest. Oecologia, 129(2), 261–270. https://doi.org/10.1007/s004420100719

Bradshaw, L. S., Deeming, J. E., Burgan, R. E., & Cohen, J. D. (1984). The 1978 National Fire-Danger Rating System: Technical documentation (General Technical Report INT-169). U.S. Department of Agriculture, Forest Service, Intermountain Forest and Range Experiment Station 44, pp. 169.

Breeuwer, A., Robroek, B. J., Limpens, J., Heijmans, M. M., Schouten, M. G., & Berendse, F. (2009). Decreased summer water table depth affects peatland vegetation. Basic and Applied Ecology, 10(4), 330–339. https://doi.org/10.1016/j.baae.2008.05.005.

Brown, S. M., Petrone, R. M., Mendoza, C., & Devito, K. J. (2010). Surface vegetation controls on evapotranspiration from a sub-humid Western Boreal Plain wetland. Hydrological Processes, 24(8), 1072–1085. https://doi.org/10.1002/hyp.7569.

Bu, Z.-J., Zheng, X.-X., Rydin, H., Moore, T., & Ma, J. (2013). Facilitation vs. competition: Does interspecific interaction affect drought responses in Sphagnum? Basic and Applied Ecology, 14(7), 574–584. https://doi.org/10.1016/j.baae.2013.08.002.

Camill, P., Barry, A., Williams, E., Andreassi, C., Limmer, J., & Solick, D. (2009). Climate-vegetation-fire interactions and their impact on long-term carbon dynamics in a boreal peatland landscape in northern Manitoba, Canada. Journal of Geophysical Research: Biogeosciences, 114, G04017. https://doi.org/10.1029/2009JG001071.

Chasmer, L., & Hopkinson, C. (2017). Threshold loss of discontinuous permafrost and landscape evolution. Global Change Biology, 23(7), 2672–2686.

Chasmer, L. E., Hopkinson, C. D., Petrone, R. M., & Sitar, M. (2017). Using multitemporal and multispectral airborne lidar to assess depth of peat loss and correspondence with a new active normalized burn ratio for wildfires. Geophysical Research Letters, 44(23), 11851–11859. https://doi.org/10.1002/2017GL075488.

Cleary, J., Roulet, N. T., & Moore, T. R. (2005). Greenhouse gas emissions from Canadian peat extraction, 1990–2000: A life-cycle analysis. AMBIO: A Journal of the Human Environment, 34(6), 456–462. https://doi.org/10.1579/0044-7447-34.6.456.

Clymo, R. S. (1984). The limits to peat bog growth. Philosophical Transactions of the Royal Society of London. B, Biological Sciences, 303(1117), 605–654.

Clymo, R. S., & Duckett, J. (1986). Regeneration of Sphagnum. New Phytologist, 102(4), 589–614. https://doi.org/10.1111/j.1469-8137.1986.tb00834.x.

Dang, Q. L., Margolis, H. A., Coyea, M. R., Sy, M., & Collatz, G. J. (1997). Regulation of branch-level gas exchange of boreal trees: Roles of shoot water potential and vapor pressure difference. Tree Physiology, 17(8–9), 521–535. https://doi.org/10.1093/treephys /17.8-9.521.

Davies, G. M., Gray, A., Rein, G., & Legg, C. J. (2013). Peat consumption and carbon loss due to smouldering wildfire in a temperate peatland. Forest Ecology and Management, 308, 169–177. https://doi.org/10.1016/j.foreco.2013.07.051.

Depante, M., Morison, M. Q., Petrone, R. M., Devito, K. J., Kettridge, N., & Waddington, J. M. (2019). Hydraulic redistribution and hydrological controls on aspen transpiration and establishment in peatlands following wildfire. Hydrological Processes, 33(21), 2714–2728. https://doi.org/10.1002/hyp.13522.

Fan, Z., McGuire, A. D., Turetsky, M. R., Harden, J. W., Waddington, J. M., & Kane, E. S. (2013). The response of soil organic carbon of a rich fen peatland in interior Alaska to projected climate change. Global Change Biology, 19(2), 604–620. https://doi.org /10.1111/gcb.12041.

Flannigan, M. D., Logan, K. A., Amiro, B. D., Skinner, W. R., & Stocks, B. J. (2005). Future area burned in Canada. Climatic Change, 72(1–2), 1–16. https://doi.org/10.1007/s10584-005-5935-y.

Flannigan, M., Stocks, B., Turetsky, M., & Wotton, M. (2009). Impacts of climate change on fire activity and fire management in the circumboreal forest. Global Change Biology, 15(3), 549–560. https://doi.org/10.1111/j.1365-2486.2008.01660.x.

Frandsen, W. H. (1997). Ignition probability of organic soils. Canadian Journal of Forest Research, 27, 1471–1477.

French, N. H., Kasischke, E. S., & Williams, D. G. (2002). Variability in the emission of carbon-based trace gases from wildfire in the Alaskan boreal forest. Journal of

Geophysical Research: Atmospheres, 107(D1), FFR-7. https://doi.org/10.1029/2001JD000480.

Gibson, C. M., Chasmer, L. E., Thompson, D. K., Quinton, W. L., Flannigan, M. D., & Olefeldt, D. (2018). Wildfire as a major driver of recent permafrost thaw in boreal peatlands. Nature Communications, 9, 3041. https://doi.org/10.1038/s41467-018-05457-1.

Gorham, E. (1991). Northern peatlands: Role in the carbon cycle and probable responses to climatic warming. Ecological Applications, 1(2), 182–195. https://doi.org/10.2307
/1941811.

Granath, G., Moore, P. A., Lukenbach, M. C., Waddington, J. M., & Sveriges, L. (2016). Mitigating wildfire carbon loss in managed northern peatlands through restoration. Scientific Reports, 6, 28498. https://doi.org/10.1038/srep28498.

Hanes, C. C., Wang, X., Jain, P., Parisien, M.-A., Little, J. M., & Flannigan, M. D. (2019). Fire-regime changes in Canada over the last half century. Canadian Journal of Forest Research, 49(3), 256–269. https://doi.org/10.1139/cjfr-2018-0293.

Harden, J., Trumbore, S. E., Stocks, B., Hirsch, A., Gower, S., O'Neill, K., & Kasischke, E. (2000). The role of fire in the boreal carbon budget. Global Change Biology, 6(S1), 174–184. https://doi.org/10.1046/j.1365-2486.2000.06019.x.

Helbig, M., Chasmer, L., Kljun, N., Quinton, W., Treat, C., & Sonnentag, O. (2017). The positive net radiative greenhouse gas forcing of increasing methane emissions from a thawing boreal forest-wetland landscape. Global Change Biology, 23(6), 2413–2427. https://doi.org/10.1111/gcb.13520.

Helbig, M., Waddington, J. M., Alekseychik, P., Amiro, B. D., Aurela, M., Barr, A. G., Black, T.A., Carey, S.K., Chen, J., Chi, J., Desai, A. R., Dunn, A., Euskirchen, E. S., Flanagan, L. B., Friborg, T., Garneau, M., Crelle, A., Harder, S., Heliasz, M., Humphreys, E. R., Ikawa, H., Isabelle, P., Iwata, H., Jassal, R., Korkiakoski, M., Kurbatova, J., Kutzbach, L., Lapshina, E., Lindroth, A. M., Löfvenius, M. O., Lohila, A., Mammarella, I., Marsh, P., Moore, P. A., Maximov, T., Nadeau, D. F., Nicholls, E. M., Nilsson, M. B., Ohta, T., Peichl, M., Petrone, R. M., Prokushkin, A., Quinton, W. L., Roulet, N., Runkle, B. R.K., Sonnentag, O., Strachan, I. B., Taillardat, P., Tuittila, E., Tuovinen, J., Turner, J., Ueyama, M., Varlagin A., Vesala, T., Wilmking, M., & Zyrianov, V. (2020). The biophysical climate mitigation potential of boreal peatlands during the growing season. Environmental Research Letters. https://doi.org/10.1088/1748-9326/abab34.

Hinwood, A. L., & Rodriguez, C. M. (2005). Potential health impacts associated with peat smoke: A review. Journal of the Royal Society of Western Australia, 88, 133–138.

Hokanson, K. J., Lukenbach, M. C., Devito, K. J., Kettridge, N., Petrone, R. M., & Waddington, J. M. (2016). Groundwater connectivity controls peat burn severity in the boreal plains. Ecohydrology, 9(4), 574–584. https://doi.org/10.1002/eco.1657.

Holmgren, M., Lin, C.-Y., Murillo, J. E., Nieuwenhuis, A., Penninkhof, J., Sanders, N., van Bart, T., van Veen, H., Vasander, H., Vollebregt, M. E., & Limpens, J. (2015). Positive shrub-tree interactions facilitate woody encroachment in boreal peatlands. Journal of Ecology, 103(1), 58–66. https://doi.org/10.1111/1365-2745.12331.

Hu, Y., Christensen, E. G., Amin, H. M. F., Smith, T. E. L., & Rein, G. (2019). Experimental study of moisture content effects on the transient gas and particle emissions from peat fires. Combustion and Flame, 209, 408–417. https://doi.org/10.1016 /j.combustflame.2019.07.046.

Hu, Y., Fernandez-Anez, N., Smith, T. E. L., & Rein, G. (2018). Review of emissions from smouldering peat fires and their contribution to regional haze episodes. International Journal of Wildland Fire, 27, 293–312. https://doi.org/10.1071/WF17084.

Huang, X., & Rein, G. (2017). Downward spread of smouldering peat fire: The role of moisture, density and oxygen supply. International Journal of Wildland Fire, 26(11), 907–918.

Ingram, H. A. P. (1978). Soil layers in mires: Function and terminology. Journal of Soil Science, 29(2), 224–227.

Intergovernmental Panel on Climate Change (IPCC). (2013). Climate change 2013: the physical science basis: Working Group I contribution to the Fifth assessment report of the Intergovernmental Panel on Climate Change. Cambridge University Press.

Johnston, D., Turetsky, M., Benscoter, B., & Wotton, B. (2015). Fuel load, structure, and potential fire behaviour in black spruce bogs. Canadian Journal of Forest Research, 45, 888–899. https://doi.org/10.1139/cjfr-2014-0334.

Johnstone, J. F., Allen, C. D., Franklin, J. F., Frelich, L. E., Harvey, B. J., Higuera, P. E., Mack, M. C., Meentemeyer, R. K., Metz, M. R., Perry, G. L., & Turner, M. G. (2016). Changing disturbance regimes, ecological memory, and forest resilience. Frontiers in Ecology and the Environment, 14(7), 369–378. https://doi.org/10.1002/fee.1311.

Kasischke, E. S., Christensen, N. L., & Stocks, B. J. (1995). Fire, global warming, and the carbon balance of boreal forests. Ecological Applications, 5, 437–451. https://doi.org/10.2307/1942034.

Keeley, J. E. (2009). Fire intensity, fire severity and burn severity: A brief review and suggested usage. International Journal of Wildland Fire, 18(1), 116–126. https://doi.org/10.1071/WF07049.

Kellner, E. (2001). Surface energy fluxes and control of evapotranspiration from a Swedish Sphagnum mire. Agricultural and Forest Meteorology, 110(2), 101–123. https://doi.org/10.1016/S0168-1923(01)00283-0.

Kellner, E., & Halldin, S. (2002). Water budget and surface-layer water storage in a Sphagnum bog in central Sweden. Hydrological Processes, 16(1), 87–103. https://doi.org/10.1002/hyp.286.

Kettridge, N., Humphrey, R. E., Smith, J. E., Lukenbach, M. C., Devito, K. J., Petrone, R. M., & Waddington, J. M. (2014). Burned and unburned peat water repellency: Implications for peatland evaporation following wildfire. Journal of Hydrology, 513, 335–341. https://doi.org/10.1016/j.jhydrol.2014.03.019.

Kettridge, N., Lukenbach, M. C., Hokanson, K. J., Hopkinson, C., Devito, K. J., Petrone, R. M., Mendoza, C. A., & Waddington, J. M. (2017). Low evapotranspiration enhances the resilience of peatland carbon stocks to fire. Geophysical Research Letters, 44(18), 9341–9349. https://doi.org/10.1002/2017GL074186.

Kettridge, N., Thompson, D. K., Bombonato, L., Turetsky, M. R., Benscoter, B. W., & Waddington, J. M. (2013). The ecohydrology of forested peatlands: Simulating the effects of tree shading on moss evaporation and species composition. Journal of Geophysical Research: Biogeosciences, 118, 1–14. https://doi.org/10.1002/jgrg.20043.

Kettridge, N., Thompson, D. K., & Waddington, J. M. (2012). Impact of wildfire on the thermal behavior of northern peatlands: Observations and model simulations. Journal of Geophysical Research: Biogeosciences, 117, G02014. https://doi.org/10.1029/2011JG001910.

Kettridge, N., Turetsky, M. R., Sherwood, J. H., Thompson, D. K., Miller, C. A., Benscoter, B. W., Flannigan, M. D., Wotton, B. M., & Waddington, J. M. (2015). Moderate drop in water table increases peatland vulnerability to post-fire regime shift. Scientific Reports, 5, 8063. https://doi.org/10.1038/srep08063.

Kohlenberg, A. J., Turetsky, M. R., Thompson, D. K., Branfireun, B. A., & Mitchell, C. P. (2018). Controls on boreal peat combustion and resulting emissions of carbon and mercury. Environmental Research Letters, 13(3), 035005.

Lenton, T. M., Held, H., Kriegler, E., Hall, J. W., Lucht, W., Rahmstorf, S., & Schellnhuber, H. J. (2008). Tipping elements in the Earth's climate system. Proceedings of the National Academy of Sciences of the United States of America, 105(6), 1786–1793. https://doi.org
/10.1073/pnas.0705414105.

Lieffers, V. J., & Macdonald, S. E. (1990). Growth and foliar nutrient status of black spruce and tamarack in relation to depth of water table in some Alberta peatlands. Canadian Journal of Forest Research, 20, 805–809. https://doi.org/10.1139/x90-106.

Lin, S., Cheung, Y. K., Xiao, Y., & Huang, X. (2020). Can rain suppress smoldering peat fire? Science of the Total Environment, 727, 138468.

Loisel, J., & Yu, Z. (2013). Recent acceleration of carbon accumulation in a boreal peatland, south-central Alaska. Journal of Geophysical Research: Biogeosciences, 118(1), 41–53. https://doi.org/10.1029/2012JG001978.

Lukenbach, M. C., Devito, K. J., Kettridge, N., Petrone, R. M., & Waddington, J. M. (2016). Burn severity alters peatland moss water availability: Implications for post-fire recovery. Ecohydrology, 9(2), 341–353. https://doi.org/10.1002/eco.1639.

Lukenbach, M. C., Hokanson, K. J., Devito, K. J., Kettridge, N., Petrone, R. M., Mendoza, C. A., Granath, G., & Waddington, J. M. (2017). Post-fire ecohydrological conditions at peatland margins in different hydrogeological settings of the boreal plain. Journal of Hydrology, 548, 741–753. https://doi.org/10.1016/j.jhydrol.2017.03.034.

Lukenbach, M. C., Hokanson, K. J., Moore, P. A., Devito, K. J., Kettridge, N., Thompson, D. K., Wotton, B. M., Petrone, R. M., & Waddington, J. M. (2015). Hydrological controls on deep burning in a northern forested peatland. Hydrological Processes, 29(18), 4114–4124. https://doi.org/10.1002/hyp.10440.

Miller, C. A., Benscoter, B. W., & Turetsky, M. R. (2015). The effect of long-term drying associated with experimental drainage and road construction on vegetation

composition and productivity in boreal fens. Wetlands Ecology and Management, 23(5), 845–854. https://doi.org/10.1007/s11273-015-9423-5.

Miyanishi, K., & Johnson, E. A. (2002). Process and patterns of duff consumption in the mixed-wood boreal forest. Canadian Journal of Forest Research, 32(7), 1285–1295. https:
//doi.org/10.1139/x02-051.

Murphy, M. T., Laiho, R., & Moore, T. R. (2009). Effects of water table draw-down on root production and aboveground biomass in a boreal bog. Ecosystems, 12, 1268–1282. https:
//doi.org/10.1007/s10021-009-9283-z.

Nichols, J. E., & Peteet, D. M. (2019). Rapid expansion of northern peatlands and doubled estimate of carbon storage. Nature Geoscience, 12(11), 917–921. https://doi.org/10.1038
/s41561-019-0454-z.

Nieminen, M., Palviainen, M., Sarkkola, S., Laurén, A., Marttila, H., & Finér, L. (2018). A synthesis of the impacts of ditch network maintenance on the quantity and quality of runoff from drained boreal peatland forests. Ambio, 47(5), 523–534. https://doi.org
/10.1007/s13280-017-0966-y.

O'Neill, K. P., Kasischke, E. S., & Richter, D. D. (1997). The effect of fire on biogenic carbon emissions from soils of interior Alaska. Eos, Transactions American Geophysical Union, 77, 46.

Petrone, R. M., Silins, U., & Devito, K. J. (2006). Dynamics of evapotranspiration from a riparian pond complex in the Western Boreal Forest, Alberta, Canada. Hydrological Processes, 21(11), 1391–1401. https://doi.org/10.1002/hyp.6298.

Petrone, R. M., Devito, K. J., Silins, U., Mendoza, C., Brown, S. C., Kaufman, S. C., & Price, J. S. (2008). Transient peat properties in two pond-peatland complexes in the sub-humid Western Boreal Plain, Canada. Mires and Peat, 3(5).

Prat-Guitart, N., Rein, G., Hadden, R. M., Belcher, C. M., & Yearsley, J. M. (2016). Propagation probability and spread rates of self-sustained smouldering fires under controlled moisture content and bulk density conditions. International Journal of Wildland Fire, 25(4), 456–465. https://doi.org/10.1071/WF15103

Price, J. S. (1997). Soil moisture, water tension, and water table relationships in a managed cutover bog. Journal of Hydrology, 202, 21–32. https://doi.org/10.1016/S0022-1694(97)00037-1.

Rein, G. (2013). Smouldering fires and natural fuels. In C. M. Belcher (Ed.), Fire phenomena and the Earth system: An interdisciplinary guide to fire science (pp. 15–34). Wiley. https: //doi.org/10.1002/9781118529539.

Rein, G., Cleaver, N., Ashton, C., Pironi, P., & Torero, J. L. (2008). The severity of smouldering peat fires and damage to the forest soil. Catena, 74, 304–309. https://doi.org/10.1016 /j.catena.2008.05.008.

Rooney, R. C., Bayley, S. E., & Schindler, D. W. (2012). Oil sands mining and reclamation cause massive loss of peatland and stored carbon. Proceedings of the National Academy of Sciences of the United States of America, 109(13), 4933–4937. https://doi.org/10.1073 /pnas.1117693108.

Rowe, E. R., D'Amato, A. W., Palik, B. J., & Almendinger, J. C. (2017). Early response of ground-layer plant communities to wildfire and harvesting disturbance in forested peatland ecosystems in northern Minnesota, U.S.A. Forest Ecology and Management, 398, 140–152. https://doi.org/10.1016/j.foreco.2017.05.012.

Sherwood, J. H., Kettridge, N., Thompson, D. K., Morris, P. J., Silins, U., & Waddington, J. M. (2013). Effect of drainage and wildfire on peat hydrophysical properties. Hydrological Processes, 27(13), 1866–1874. https://doi.org/10.1002/hyp.9820.

Stocks, B. J., Lee, B. S., & Martell, D. L. (1996). Some potential carbon budget implications of fire management in the boreal forest. In Forest ecosystems, forest management and the global carbon cycle (pp. 89–96). Springer.

Strilesky, S. L., & Humphreys, E. R. (2012). A comparison of the net ecosystem exchange of carbon dioxide and evapotranspiration for treed and open portions of a temperate peatland. Agricultural and Forest Meteorology, 153, 45–53. https://doi.org/10.1016 /j.agrformet.2011.06.006.

Tarnocai, C. (2006). The effect of climate change on carbon in Canadian peatlands. Global and Planetary Change, 53(4), 222–232. https://doi.org/10.1016/j.gloplacha.2006.03.012.

Thompson, D. K., Baisley, A. S., & Waddington, J. M. (2015). Seasonal variation in albedo and radiation exchange between a burned and unburned forested peatland: Implications for peatland evaporation. Hydrological Processes, 29(14), 3227–3235. https://doi.org /10.1002/hyp.10436.

Thompson, D. K., Benscoter, B. W., & Waddington, J. M. (2014). Water balance of a burned and unburned forested boreal peatland. Hydrological Processes, 28(24), 5954–5964. https://doi.org/10.1002/hyp.10074.

Thompson, D. K., Simpson, B. N., Whitman, E., Barber, Q. E., & Parisien, M. A. (2019). Peatland hydrological dynamics as a driver of landscape connectivity and fire activity in the boreal plain of Canada. Forests, 10(7), 534. https://doi.org/10.3390/f10070534.

Thompson, D. K., & Waddington, J. M. (2013a). Peat properties and water retention in boreal forested peatlands subject to wildfire. Water Resources Research, 49(6), 3651–3658. https://doi.org/10.1002/wrcr.20278.

Thompson, D. K., & Waddington, J. M. (2013b). Wildfire effects on vadose zone hydrology in forested boreal peatland microforms. Journal of Hydrology, 486, 48–56. https://doi.org/10.1016/j.jhydrol.2013.01.014.

Turetsky, M. R., Amiro, B. D., Bosch, E., & Bhatti, J. S. (2004). Historical burn area in western Canadian peatlands and its relationship to fire weather indices. Global Biogeochemical Cycles, 18(4). https://doi.org/10.1029/2004GB002222.

Turetsky, M., Donahue, W., & Benscoter, B. (2011). Experimental drying intensifies burning and carbon losses in a northern peatland. Nature Communications, 2, 514. https://doi.org/10.1038/ncomms1523

van der Werf, G. R., Randerson, J. T., Giglio, L., Collatz, G. J., Mu, M., Kasibhatla, P. S., Morton, D. C., DeFries, R. S., Jin, Y. V., & van Leeuwen, T. T. (2010). Global fire emissions and the contribution of deforestation, savanna, forest, agricultural, and peat fires (1997–2009). Atmospheric Chemistry and Physics, 10(23), 11707–11735. https://doi.org/10.5194/acp-10-11707-2010.

Vitt, D. H. (1990). Growth and production dynamics of boreal mosses over climatic, chemical and topographic gradients. Botanical Journal of the Linnean Society, 104(1–3), 35–59. https://doi.org/10.1111/j.1095-8339.1990.tb02210.x.

Waddington, J. M., Morris, P. J., Kettridge, N., Granath, G., Thompson, D. K., & Moore, P. A. (2015). Hydrological feedbacks in northern peatlands. Ecohydrology, 8, 113–127. https://doi.org/10.1002/eco.1493.

Weltzin, J. F., Bridgham, S. D., Pastor, J., Chen, J., & Harth, C. (2003). Potential effects of warming and drying on peatland plant community composition. Global Change Biology, 9, 141–151. https://doi.org/10.1046/j.1365-2486.2003.00571.x.

Whitman, E., Parisien, M.-A., Thompson, D. K., & Flannigan, M. D. (2019). Short-interval wildfire and drought overwhelm boreal forest resilience. Scientific Reports, 9(1). https:
//doi.org/10.1038/s41598-019-55036-7.

Whitman, E., Parisien, M. A., Thompson, D. K., Hall, R. J., Skakun, R. S., & Flannigan, M. D. (2018). Variability and drivers of burn severity in the northwestern Canadian boreal forest. Ecosphere, 9(2), e02128.

Whittington, P. N., & Price, J. S. (2006). The effects of water table draw-down (as a surrogate for climate change) on the hydrology of a fen peatland, Canada. Hydrological Processes, 20, 3589–3600. https://doi.org/10.1002/hyp.6376.

Wieder, R. K., Scott, K. D., Kamminga, K., Vile, M. A., Vitt, D. H., Bone, T., Xu, B., Benscoter, B. W., & Bhatti, J. S. (2009). Post-fire carbon balance in boreal bogs of Alberta, Canada. Global Change Biology, 15, 63–81. https://doi.org/10.1111/j.1365-2486.2008.01756.x.

Wilkinson, S. L., Moore, P. A., Flannigan, M. D., Wotton, B. M., & Waddington, J. M. (2018a). Did enhanced afforestation cause high severity peat burn in the Fort McMurray Horse River wildfire? Environmental Research Letters, 13(1), 014018.

Wilkinson, S. L., Moore, P. A., Thompson, D. K., Wotton, B. M., Hvenegaard, S., Schroeder, D., & Waddington, J. M. (2018b). The effects of black spruce fuel management on surface fuel condition and peat burn severity in an experimental fire. Canadian Journal of Forest Research, 48(12), 1433–1440. https://doi.org/10.1139/cjfr-2018-0217.

Wilkinson, S. L., Verkaik, G. J., Moore, P. A., & Waddington, J. M. (2020). Threshold peat burn severity breaks evaporation-limiting feedback. Ecohydrology, 13(1), e2168. https:
//doi.org/10.1002/eco.2168.

Wu, Y., Verseghy, D. L., & Melton, J. R. (2015). Integrating peatlands into the coupled Canadian Land Surface Scheme (CLASS) v3.6 and the Canadian Terrestrial Ecosystem Model (CTEM) v2.0. Geoscientific Model Development Discussions, 8(11), 10089–10143.

Yu, Z. C. (2012). Northern peatland carbon stocks and dynamics: A review. Biogeosciences, 9(10), 4071–4085. https://doi.org/10.5194/bg-9-4071-2012.

CHAPTER 3: QUANTIFYING LIDAR ELEVATION ACCURACY: PARAMETERIZATION AND WAVELENGTH SELECTION FOR OPTIMAL GROUND CLASSIFICATIONS BASED ON TIME SINCE FIRE/DISTURBANCE

3.1 Abstract

Pre- and post-fire airborne lidar data provide an opportunity to determine peat combustion/loss across broad spatial extents. However, lidar measurements of ground surface elevation are prone to uncertainties. Errors may be introduced in several ways, particularly associated with the timing of data collection and the classification of ground points. Ground elevation data must be accurate and precise when estimating relatively small elevation changes due to combustion and subsequent carbon losses. This study identifies the impact of post-fire vegetation regeneration on ground classification parameterizations for optimal accuracy using TerraScan and LAStools with airborne lidar data collected in three wavelengths: 532 nm, 1064 nm, and 1550 nm in low relief boreal peatland environments. While the focus of the study is on elevation accuracy and losses from fire, the research is also highly pertinent to hydrological modelling, forestry, geomorphological change, etc. The study area includes burned and unburned boreal peatlands south of Fort McMurray, Alberta. Lidar and field validation data were collected in July 2018, following the 2016 Horse River Wildfire. An iterative ground classification analysis was conducted whereby validation points were compared with lidar ground-classified data in five environments: road, unburned, burned with shorter vegetative regeneration (SR), burned with taller vegetative regeneration (TR), and cumulative burned (both SR and TR areas) in each of the three laser emission wavelengths individually, as well as combinations of 1550 nm and 1064 nm and 1550 nm, 1064 nm, and 532 nm. I find

an optimal average elevational offset of ~0.00 m in SR areas with a range (RMSE) of ~0.09 m using 532 nm data. Average accuracy remains the same in cumulative burned and TR areas, but RMSE increased to ~0.13 m and ~0.16 m, respectively, using 1550 nm and 1064 nm combined data. Finally, data averages ~0.01 m above the field-measured ground surface in unburned boreal peatland and transition areas (RMSE of ~0.19 m) using all wavelengths combined. I conclude that the 'best' offset for depth of burn within boreal peatlands is expected to be ~0.01 m, with single point measurement uncertainties upwards of ~0.25 m (RMSE) in areas of tall, dense vegetation regeneration. The importance of classification parameterization identified in this study also highlights the need for more intelligent adaptative classification routines, which can be used in other environments.

3.2 Introduction

Boreal peatlands contain considerable carbon (C) stores and have acted as a long-term sink for atmospheric C since the Holocene (Frolking & Roulet, 2007; Yu, 2012). However, with climate change, many of these peatland regions are drying and becoming more vulnerable to wildland fire (Flannigan et al., 2013; Miller et al., 2015; Walker et al., 2015), which are increasing in both frequency and severity (Kohlenberg et al., 2018; Miller et al., 2015). There is interest in quantifying the contribution of peat combustion to atmospheric C (Chasmer et al., 2017; Thompson et al., 2014; Van der Werf et al., 2010). Improving estimations of C loss during wildland fire is especially critical in boreal environments, where soil combustion can account for up to ~90% of C loss (Van der Werf et al., 2010).

In recent years, several studies (Kohlenberg et al., 2018; Lin et al., 2021; Mickler et al., 2017; Morison et al., 2021) have described the loss of C from wildland fire in peatlands; however, there are methodological limitations for estimating C loss across a

broad range of peatland and boreal ecosystems. Fieldwork is labor-intensive and time-consuming and cannot survey the full range of environmental variations that influence the loss of C from fire in peatland landscapes (Aguilar & Mills, 2008; Hokanson et al., 2016; Thompson et al., 2014). Optical remote sensing is often utilized to estimate burn severity and is particularly useful in its ability to cover broad spatial extents (e.g., Aguilar & Mills, 2008; Whitman et al., 2020); however, optical remote sensing of the understory and ground surface is occluded by the pre-fire vegetation canopy and any remaining post-forest canopy—a limitation in assessing burn severity as well as pre-fire conditions (Aguilar & Mills, 2008; Hudak et al., 2007; Thompson et al., 2014). Therefore, these sensing techniques cannot easily measure ground surface elevation and cannot measure depth of burn, an essential component of biomass loss (Chasmer et al., 2017).

Airborne and Unpiloted Aerial Vehicle (UAV) lidar provide an opportunity to resolve both the lack of spatial coverage of field data and reduced ability to determine ground elevation from high spatial resolution optical remote sensing due to occlusion. Lidar is useful for measuring ground surface elevations and vegetation structural characteristics across a range of land cover types, including boreal peatlands (e.g., Ekhtari et al., 2018; Hopkinson et al., 2005; Moudrý et al., 2020). This capability allows for not only the quantification of pre-fire fuels and post-fire ecosystem regeneration in the study of wildland fire (e.g., Andersen et al., 2005; Chasmer et al., 2017; McCarley et al., 2020), but also in forestry (e.g., Chen et al., 2017; Moudrý et al., 2020), urban planning and road design (e.g., Aguilar & Mills, 2008), hydrological modelling (e.g., O'Neil et al., 2019), mapping and modelling of land cover distribution (i.e., wetlands) (e.g., Millard & Richardson, 2013; O'Neil et al., 2018), monitoring of permafrost thaw (e.g., Chasmer &

Hopkinson, 2017), soil erosion (e.g., Neugirg et al., 2015) and flooding (e.g., Escobar Villanueva et al., 2019). A benefit of the use of lidar is the ability to measure both canopy structure, understory, and ground surface elevation (Aguilar & Mills, 2008). Multi-temporal, pre- and post-fire lidar data also enable quantification of biomass losses from fire and post-fire vegetation regeneration (e.g., Campbell et al., 2021). As laser pulse returns can measure ground surface elevation, the technology is particularly useful for determining surface elevation changes, such as depth of burn during wildland fire, quantification of erosion, and impacts of permafrost slaw if pre- and post-disturbance lidar data are available. However, despite its utility, questions arise on the accuracy of lidar data for determining elevation (and therefore depth of burn, C losses, etc.) associated with different ground classification routines and also, the efficacy of lidar-based observations as time since fire increases. Aguilar & Mills (2008) suggest that most error is introduced during the classification stage; however, custom, environment-specific ground classification parameterization can improve DEM accuracy (Moudrý et al., 2020; Schmid et al., 2011). Due to the need for accurate ground surface data when quantifying relatively small changes in elevation from combustion, erosion, slumping, permafrost thaw, and anthropogenic disturbance, the quantification of ground classification routines specific to land cover and vegetation growth that result in the least error is required. There is also an urgent need for more accurate measurements of soil combustion and overall C losses from boreal peatlands and their potential influence on the global climate system (Lin et al., 2021; Nelson et al., 2021; Chapter 2).

Based on the necessity for accurate ground elevation data for estimating depth of peatland burn in pre- and post-fire lidar data, this study aims to: (a) identify how post-fire

vegetation regeneration impacts optimal ground classification configurations using industry-standard software: TerraScan (Terrasolid, Helsinki, Finland) and LAStools (RapidLasso, Gilching, Germany, GmbH); and (b) compare multispectral lidar emission wavelength(s) (532 nm (green); 1064 nm (near infrared); 1550 nm (shortwave infrared); 1064 and 1550 nm combined; and, 532, 1064, and 1550 nm combined) in burned and unburned boreal peatlands and transition zones in western Canada. The overall goal is to provide recommendations for ground classification of lidar data across a range of vegetation regeneration required for quantifying subtle changes in elevation, including depth of burn from fire (in bi-temporal, pre- and post-fire lidar data). While this research focuses on wildland fire, recommendations will also be useful for hydrological modelling, forestry applications, and land surface engineering/mining/cut-fill operations.

3.3 Materials and Methods

3.3.1 Study Area

The study area is located about 30 km south of Fort McMurray, Alberta (centre: 12N 482464E 6260554N) in the Boreal Plains ecozone of Canada (Figure 3.1; Downing & Pettapiece, 2006). The region is characterized by flat to slightly undulating terrain with some hummocky zones. It is dominated by bog and fen peatlands (dominant wetland classes in Alberta; Alberta ESRD, 2015), aspen (*Populus tremuloides*) uplands, and black spruce (*Picea mariana*) lowlands/transition zones (Downing & Pettapiece, 2006). Extensive forestry and oil exploration and extraction occur within the region, as do subsistence and commercial hunting and fishing and minor agricultural practices (Downing & Pettapiece, 2006).

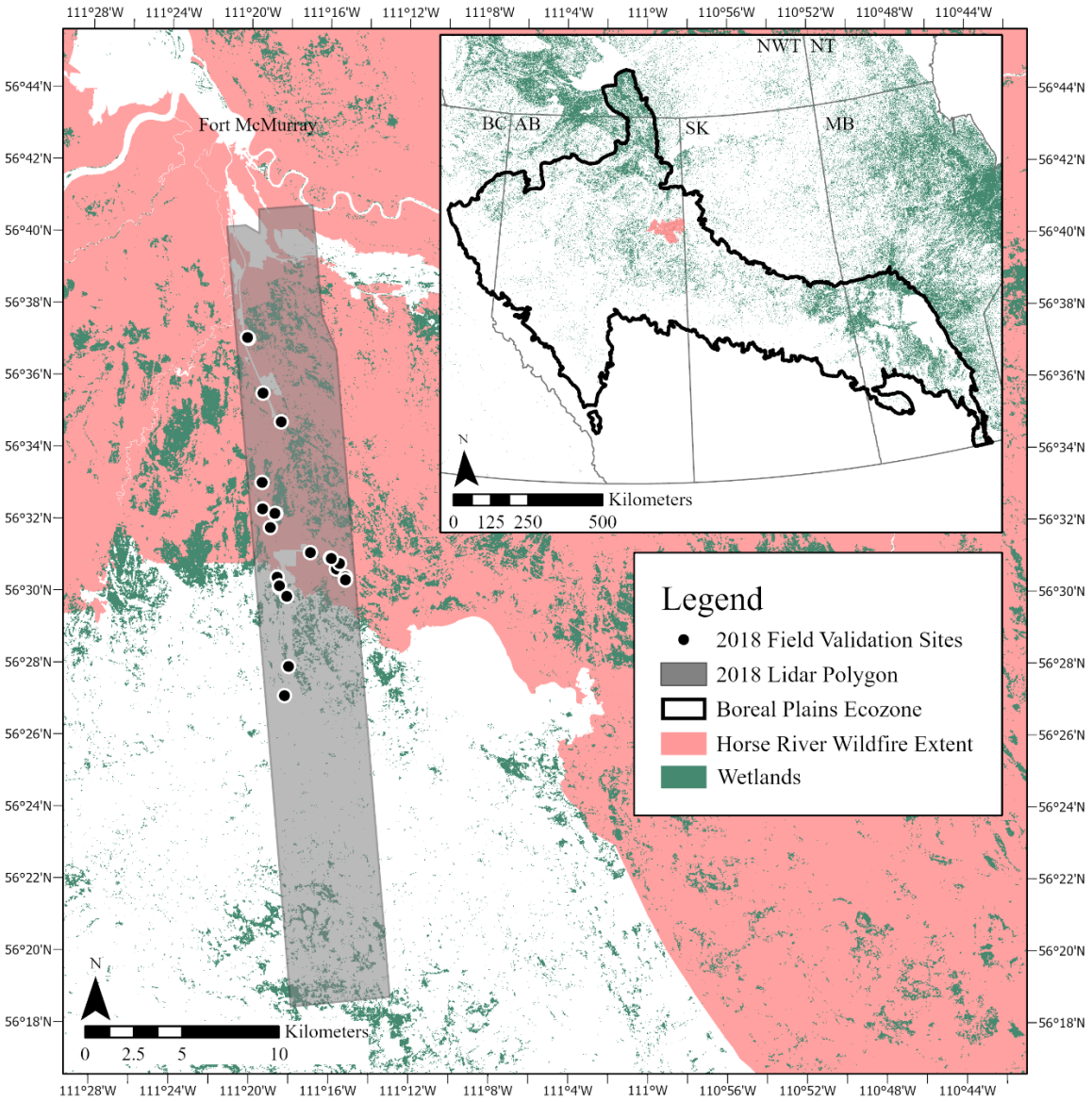

Figure 3.1. Map illustrating the extent of the Horse River Wildfire within the Boreal Plains Ecozone (inset), which extends across Canada from northern British Columbia (BC) and into Alberta (AB), Saskatchewan (SK), and Manitoba (MB) and the study area, including lidar survey polygon and field validation transects/plots.

The study covers a 20,441-ha area south of Fort McMurray, extending beyond the area burned by the Horse River Wildfire in 2016 (Figure 3.1). The Horse River Wildfire, covering approximately 600,000 ha, ignited 7 km outside Fort McMurray on 1 May 2016, under hazardous conditions—uncharacteristically hot (~35 °C), dry, and windy (~43 km hr^{-1}) weather. The fire was declared under control on 4 July 2016; however, smoldering

peat burn continued for approximately 15 months before being extinguished (Institute for Catastrophic Loss Reduction, 2019; MNP LLP, 2017). The burned region includes a variety of burn severities and levels of vegetative regeneration since the fire, from little to no regeneration to significant vegetation growth (Figure 3.2). This allows for the opportunity to compare laser pulse interactions and ground elevation accuracies across a range of conditions akin to timing of lidar data collection following fire.

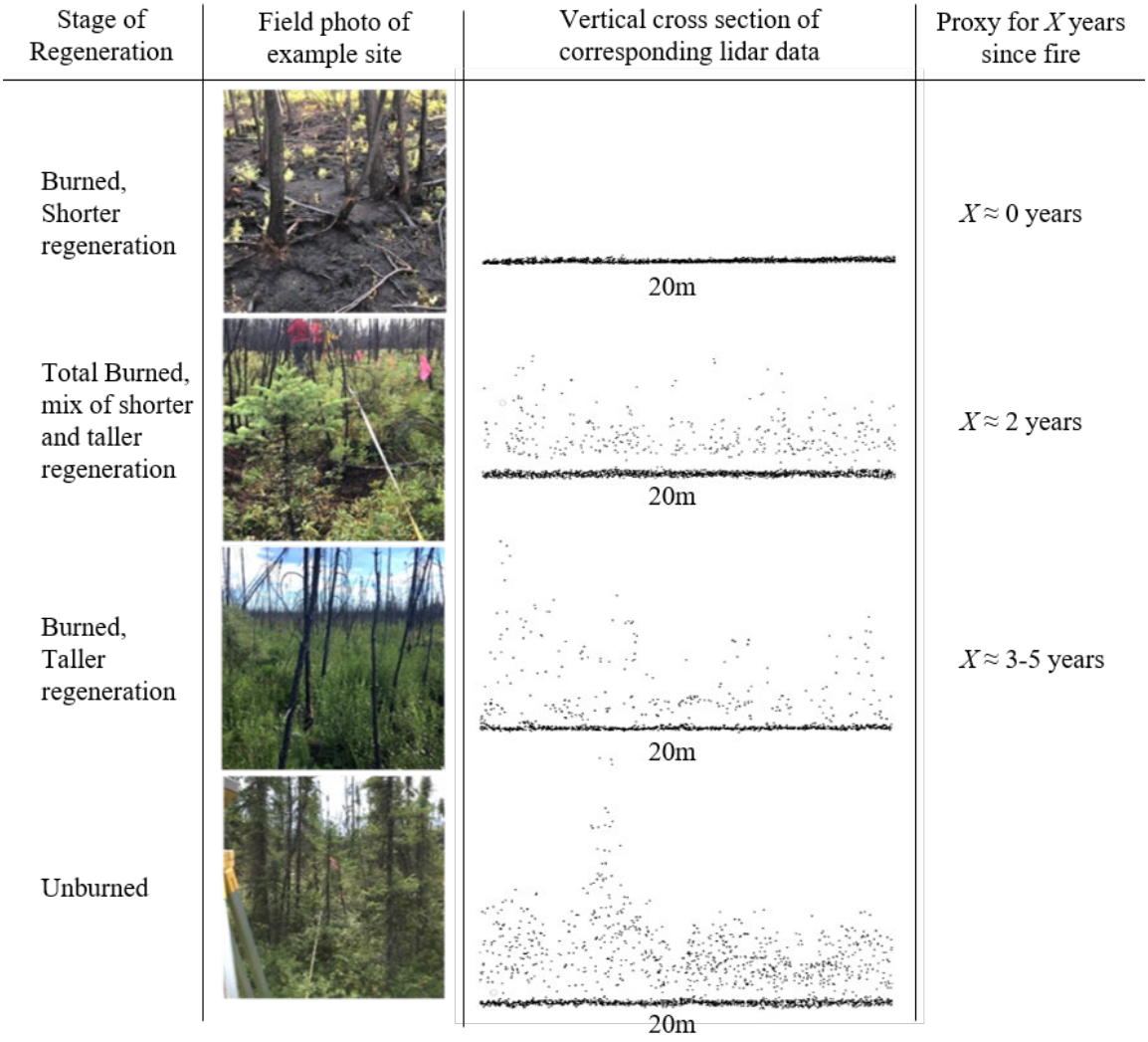

Figure 3.2. Four vegetation categories used to represent time since fire with field photos and lidar point clouds.

In sites with shorter regeneration (SR), post-fire vegetation heights averaged 0.20–0.35 m (Figure 3.2). Dominant vegetation was primarily *Sphagnum* spp. And feathermoss (*Pleurozium* spp.), with subdominant vegetation consisting of mosses, herbs, and low-lying herb species such as Labrador tea (*Rhododendron groenlandicum*), reindeer lichen (*Cladonia rangiferina*), bog cranberry (*Vaccinium oxycoccos*), cloudberry (*Rubus chamaemorus*), and horsetail (*Equisetum fluviatile*). In sites with taller post-fire vegetative regeneration (TR), above-surface vegetation heights averaged 0.40–1.00 m (Figure 3.2). While dominant vegetation included some similar species as the SR sites such as feathermoss and *Sphagnum* spp., sites were also dominated by more woody vegetation and tall shrubs, such as willow (*Salix* spp.), bog, shrub, and paper birch (*Betula pumila*, *glandulosa*, and *papyrifera*), black spruce (*Picea mariana*), fireweed (*Chamaenerion angustifolium*), horsetail (*Equisetum* spp.), rose (*Rosa acicularis*), trembling aspen (*Populus tremuloides*), and raspberry (*Rubus idaeus*).

3.3.2 Data Acquisition

Airborne lidar data were collected in July 2018, two years following the Horse River Wildfire, using a Titan multispectral lidar (Teledyne Optech, Inc., Vaughan, ON, Canada). The Titan collects data using three laser emission wavelengths (channels): 1550 nm (shortwave infrared (SWIR); channel 1), which is 3.5° forward of nadir; 1064 nm (near-infrared (NIR); channel 2), which is emitted at nadir; and 532 nm (green; channel 3) which is 7° forward of nadir (Figure 3.3a; Ekhtari et al., 2018). The survey was flown at ~1000 m above ground, with scan angles of ±25 degrees, a pulse repetition frequency of 100 kHz per channel (300 kHz total), and a 50% flightline overlap. This survey configuration resulted in average point densities of 4.8 pts m^{-2}, 4.2 pts m^{-2}, and 2.1 pts m^{-2} for channels

1, 2, and 3, respectively. As laser scan lines are not spatially coincident, the 50% overlap reduces gaps, especially prevalent along scan line edges, such that validation points do not exist within one or two channels, introducing bias (Figure 3.3b).

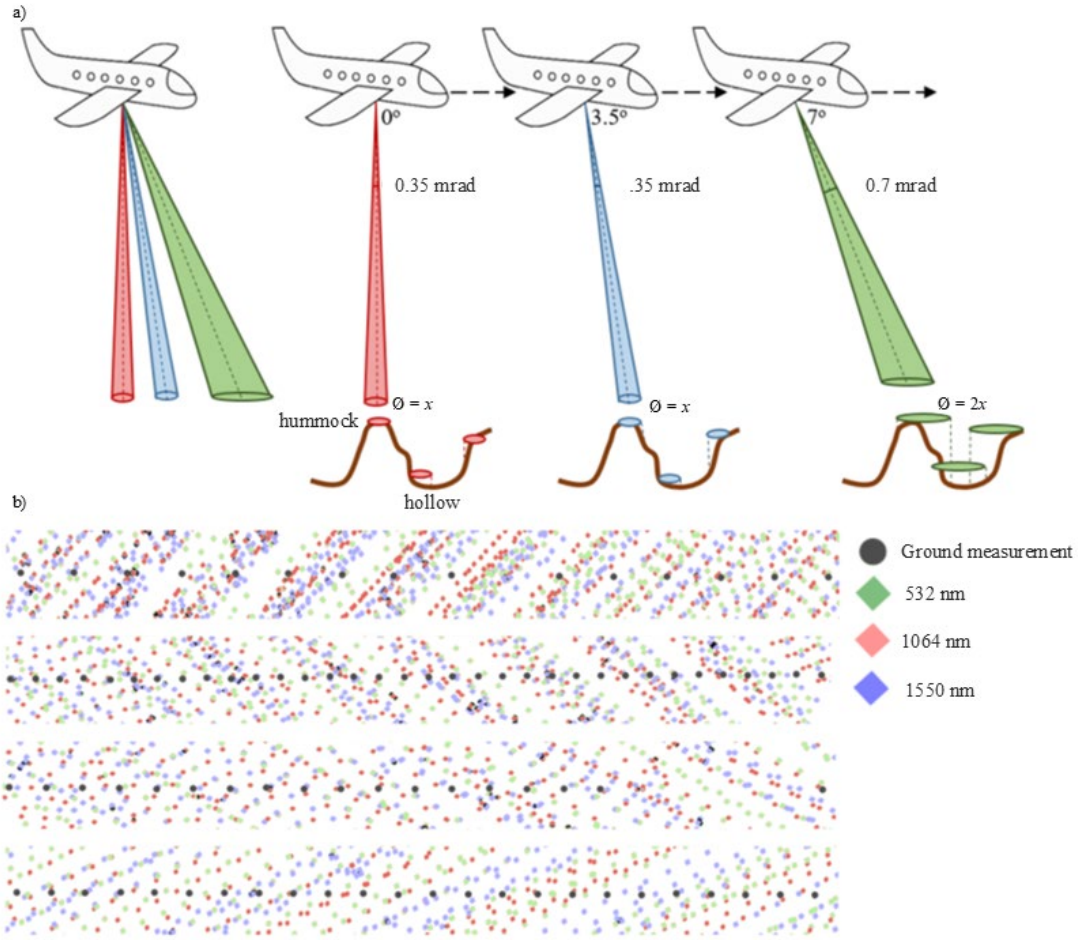

Figure 3.3. a) Illustration of lidar laser beam angles, beam divergence, and impact on footprint diameter (Ø) in peatlands with variable microtopography (hollows and hummocks); b) Samples of validation transects and lidar data demonstrating spatial distribution of validation points throughout the three channels. Note: microtopography in a) has been exaggerated for demonstration purposes.

Field data were collected coincident with the 2018 lidar data collection for the calibration and validation of lidar data. To select sample sites, the study area was first stratified into scales of influence: (a) burned versus non-burned areas within and proximal

to the Horse River wildfire; (b) within burned areas, different classes of burn severity (minimum, medium, and severe) determined visually from optical remote sensing imagery as well as through on-the-ground assessments at the time of field data collection; and, (c) peatland type (treed and open bogs; rich and poor fens) determined from optical remote sensing imagery and on-the-ground assessments. Data were collected along ~30 m transects in 18 burned and 6 unburned peatland sites. Transects intersected upland-peatland transition zones and peatlands. Global Navigation Satellite System (GNSS) ground elevation validation points were collected in burned and unburned landscapes. To validate post-fire ground surface elevations (Chasmer et al., 2017), GNSS stations were placed at the beginning and end of each transect and were left to run for the duration of sampling (>1 h for centimeter accuracy). Precise Point Positioning (PPP) was used to process these end points. A level was used at one- (burned sites) or two- (unburned sites) meter intervals to determine ground elevation relative to the GNSS base stations. A total of 708 ground elevations were measured: 130 in unburned and 578 in burned peatlands with variable rates of vegetation regeneration. Post Processed Kinematic (PPK) GNSS elevation locations were also collected along two road surfaces (n = 2655) to ensure the elevational accuracy of airborne lidar data in areas of flat terrain without any overstory canopy influences on ground surface elevation (Csanyi & Toth, 2007; Hopkinson et al., 2005).

3.3.3 Data Processing

Lidar returns from road surfaces were compared with PPK GNSS survey points and vertically batch-shifted to ensure the average offset between lidar data and calibration points was zero (Csanyi & Toth, 2007) using Bentley Microstation TerraSolid Terrascan software version 021.011 (Terrasolid, Helsinki, Finland; Axelsson, 2000). Isolated or

outlier points were removed, and an iterative ground classification analysis was then conducted through which ground vs. non-ground returns were classified. The five ground cover types (road, unburned, short vegetation regeneration (SR), and tall vegetation regeneration (TR), and cumulative burned (all regeneration stages)) were analyzed separately to identify optimal ground return classifications for each type, optimized for relatively flat to slightly undulating boreal peatland and transitional environments with micro-topographic hummocks and hollows.

3.3.3.1 TerraScan

Within TerraScan, six ground classification parameters can be readily modified: (a) 'max building size', which sets the grid size for seed ground point selection; (b) 'terrain angle', which is the maximum slope between a seed point and a candidate point; (c) 'iteration angle', which is the maximum angle that a point can be added to the ground classification; (d) 'iteration distance', which is the maximum distance that a point can be added to the ground classification; (e) 'reduce iteration angle', a binary choice which reduces the number of unnecessary points added to the surface in areas of high point density by reducing the number of points that are added to the surface if edge length is longer than all triangle edges; and (f) 'stop triangulation', another binary choice which reduces the number of unnecessary points added to the surface by not processing points within a triangle if edge length is longer than all triangle edges (Table 3.1; GeoCue Group, 2020; Terrasolid Ltd., 2021). Adjusting each ground classification parameter results in morphological differences in the resultant ground-classified data.

Table 3.1. TerraScan ground classification parameter modifications used in ground classification iteration analysis

Ground Classification	Max Building Size	Terrain Angle	Iteration Angle	Iteration Distance	Reduce Iteration Angle When Edge Length <	Stop Triangulation When Edge Length <
1	60	50	6	1.4	5	-
2	60	55	6	1.4	5	-
3	60	60	6	1.4	5	-
4	60	65	6	1.4	5	-
5	60	70	6	1.4	5	-
6	60	75	6	1.4	5	-
7	60	80	6	1.4	5	-
8	60	88	6	1.4	5	-
9	60	88	2	1.4	5	-
10	60	88	2	0.5	5	-
11	60	88	2	1	5	-
12	60	88	2	1.5	5	-
13	60	88	2	2	5	-
14	60	88	5	1.4	5	-
15	60	88	5	0.5	5	-
16	60	88	5	1	5	-
17	60	88	5	1.5	5	-
18	60	88	5	2	5	-
19	60	88	10	1.4	5	-
20	60	88	10	0.5	5	-
21	60	88	10	1	5	-
22	60	88	10	1.5	5	-
23	60	88	10	2	5	-
24	60	88	15	1.4	5	-
25	60	88	15	0.5	5	-
26	60	88	15	1	5	-
27	60	88	15	1.5	5	-
28	60	88	15	2	5	-
29	60	88	15	1.5	-	-
30	60	88	15	1.5	1	-
31	60	88	15	1.5	2	-
32	60	88	15	1.5	10	-
33	60	88	15	1.5	5	0.5
34	60	88	15	1.5	5	2
35	60	88	15	1.5	5	5
36	60	88	15	1.5	5	0.25

Thirty-six different ground classification parameterizations were developed by making adjustments to TerraScan's classification parameters (Table 3.1). Classifications 1–28 were produced by iterating through adjustments to the four primary parameters: 'Max Building Size', 'Terrain Angle', 'Iteration Angle', and 'Iteration Distance'. Classifications 29–36 were developed by refining an optimal classification (27) using 'Reduce Iteration Angle When Edge Length<' and 'Stop Triangulation When Edge Length <' (Table 3.1). Each of the classification parameterizations was used to produce ground surfaces in the channels and channel combinations tested, resulting in 180 distinct ground surfaces. Each surface output was compared to ground elevation field validation data (elevation collected along the road, unburned peatlands, TR peatlands, SR peatlands, and total burned peatlands) using TerraScan's control report function (see Section 3.3.4) for a total of 740 ground classification tests.

3.3.3.2 LAStools

LASground, from LAStools (RapidLasso GmbH, Gilching, Germany), offers five defined ground classifications that, like TerraScan, use an adaptive TIN algorithm to classify ground points. Two were tested (excluding urban settings): 'nature' and 'wilderness'. These settings differ in their step size (cell size within which lowest point becomes initial ground point) and 'bulge' (height allowance for TIN to "bulge" above planar surface). These can be refined using the options 'default', 'fine', 'extra', 'ultra', and 'hyper', resulting in ten different readily accessible ground classification parameterizations (lettered A–J; Table 3.2). Using refining options intensifies the search for seed ground points—this is often most useful for ground surfaces with steep hills (Rapidlasso GmbH, 2021). Each of the ten different classification parameterizations was used to produce ground surfaces in the

channels and channel combinations tested, resulting in 50 distinct ground surfaces. These were brought into TerraScan for the quantification of control point statistics. Like the TerraScan analysis, each ground surface was compared with field elevation measurements from road, unburned peatlands, TR peatlands, SR peatlands, and burned peatlands cumulatively, for a total of 250 ground classification tests.

Table 3.2. LAStools ground classification parameter modifications used in ground classification iteration analysis.

	Ground Classification	Refinement	Bulge (m)	Step Size (m)	Subgrid for Initial Ground Points
A	Nature	Default	0.5	5	= step size
B	Nature	Fine	0.5	5	Default granularity*4
C	Nature	Extra Fine	0.5	5	Fine granularity*4
D	Nature	Ultra-Fine	0.5	5	Extra Fine granularity*4
E	Nature	Hyper Fine	0.5	5	Ultra-Fine granularity*4
F	Wilderness	Default	0.3	3	=step size
G	Wilderness	Fine	0.3	3	Default granularity*4
H	Wilderness	Extra Fine	0.3	3	Fine granularity*4
I	Wilderness	Ultra-Fine	0.3	3	Extra Fine granularity*4
J	Wilderness	Hyper Fine	0.3	3	Ultra-Fine granularity*4

3.3.4 Vertical Accuracy Assessment

Ground classification outputs performed using TerraScan (n = 36) and LAStools software (n = 10) in each of the three available laser emission wavelengths and wavelength combinations were compared with field-measured elevations from road (n = 2655), unburned peatlands (n = 130), burned peatlands (n = 578), TR peatlands (n = 267), and SR peatlands (n = 269). Validation data were segregated into TR vs. SR vegetative regeneration based on average measured vegetation height and dominant species per plot (1 m × 1 m with three elevation measures through the center of each plot, perpendicular to the transect; Figure 3.2). The separation of peatlands based on vegetation provides an opportunity to quantify elevation accuracy from lidar across a range of environmental

characteristics, including unburned with a full understory, burned with no or shorter regeneration (SR; a proxy for lidar data collected immediately post-fire), and burned with tall regeneration (TR; a proxy for data collection several years post-fire). Validation data were distributed throughout the study area, and the number of validation elevations measured in the field exceeded the minimum (n = 20) and the recommended (n = 30) suggested for each vegetation cover type by the American Society for Photogrammetry and Remote Sensing (Aguilar & Mills, 2008; ASPRS, 2004; Pourali et al., 2014). All ground-classified data were examined in TerraScan, where validation point elevations were compared with lidar point elevations, a standard methodology for lidar vertical accuracy assessments (Maune et al., 2007; Pourali et al., 2014). Through TerraScan's control report function, lidar points were used to interpolate a surface using a Triangulated Irregular Network (TIN). As it is unlikely that a lidar point exists at the same x, y location as a validation point, validation points were compared to their x, y location on the TIN surface (GeoCue Group, 2017; Goulden et al., 2016). Control point statistics, including the difference in elevation between control points and lidar ground returns (*dz*; average, maximum, and minimum), standard deviation, and root mean square error (RMSE), were quantified via TerraScan's control report function (GeoCue Group, 2017).

To identify the optimal ground classification for each vegetation cover type, classified outputs were assessed based on RMSE (commonly used to determine accuracy; Carlisle, 2005; Goulden & Hopkinson, 2010; Pourali et al., 2014) and by absolute average *dz* (||), while also being mindful of point density. Optimal ground classification statistics (and standard deviation (SD)) were then used to determine total error (± SD) when using multitemporal lidar data to assess ground surface elevation changes (pre- and

post-fire). The uncertainties associated with multi-temporal surface elevation measurements are independent of one another, so the propagated error (SD) was calculated through quadrature, (Equation (3.1)), where Q is the average over- or under-estimation of surface elevation change, $\in a$ is cumulative SD, (b) and (c) are the average deviations of lidar classified ground surface from the measured ground surface at times b and c, and $\in b$ and $\in c$ are the SDs of ground surface measurements at two points in time (i.e., pre- and post-fire). Note that the average deviation () is used, and not absolute average deviation (||).

3.4 Results

The results demonstrate wavelength dependencies and optimal ground classification parameterizations for each vegetation cover type tested within TerraScan and LAStools.

3.4.1 Differences between Ground-Surveyed Road Elevations and Lidar-Measured Road Ground Classifications

The optimal ground return classification aims to observe the lowest differences in ground surface elevations between field validation and nearby laser returns in each wavelength. Based on the flat, non-vegetated road surface GNSS measurements, I found that neither classification parameter choice (Table 3.1 and Table 3.2), nor wavelength, significantly impacted the quality of the ground classification along road surfaces (Figure 3.4 and Figure 3.5; Table S3.1). Using both TerraScan and LAStools, the || from the measured elevations ranged from 0.00 to 0.02 m, and RMSE from 0.04 m to 0.05 m.

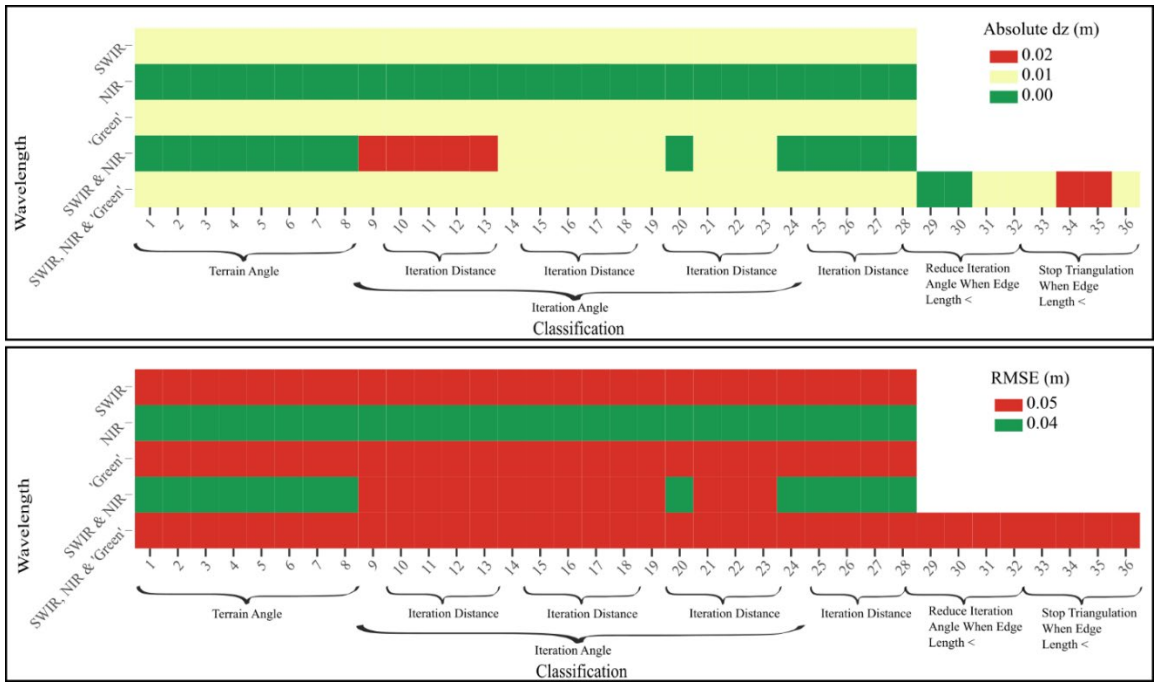

Figure 3.4. Ground classification results (|| and RMSE) along a flat road surface for baseline comparisons using parameterization methods in Table 3.1. Classifications were conducted in TerraScan.

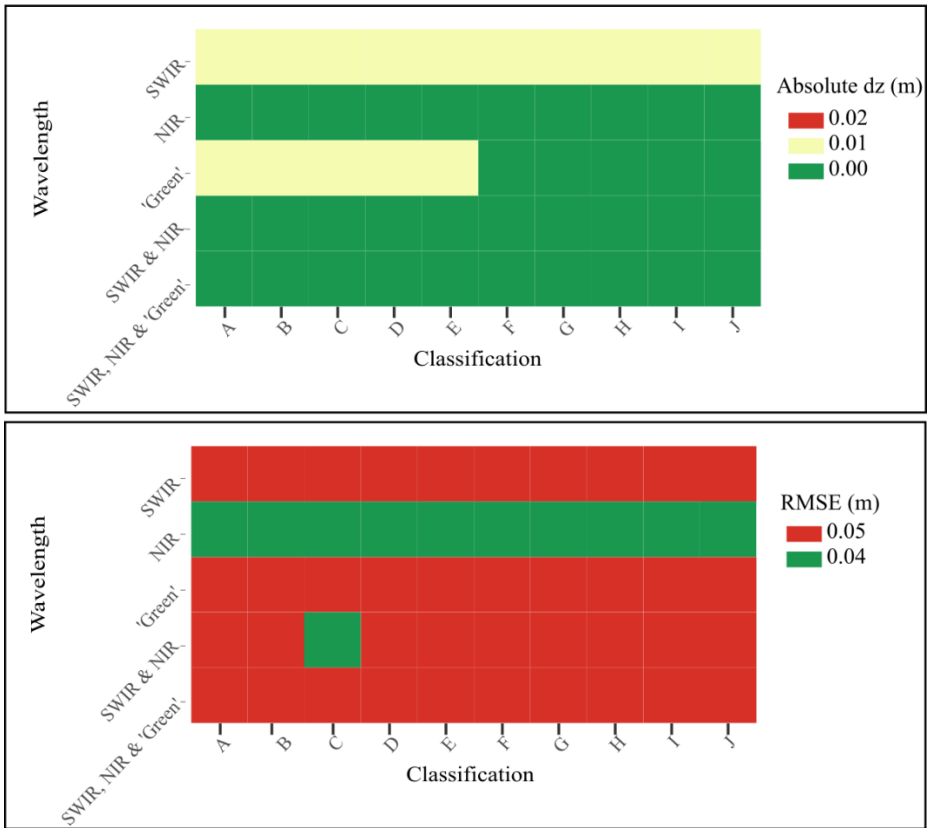

Figure 3.5. Ground classification results (|| and RMSE) along a flat road surface for baseline comparisons using parameterization methods in Table 3.2. Classifications were conducted in LAStools.

This provides a baseline for comparisons to ground classifications in varying vegetation regeneration stages and demonstrates that any changes observed in ground classification accuracies result from different parameterizations responding differently to variable vegetation regeneration.

3.4.2 Differences between Field-Measured Elevation and Lidar Return Ground Classification in Shorter Vegetative Regeneration Peatlands

In SR peatlands and transitional areas (representing characteristics that are similar to peatlands that have been surveyed soon after a fire), I found that the ground classifications that produced the most accurate results in TerraScan were classifications 14 through 18 (a

slight reduction in iteration angle from six to five as compared to default) with laser pulse emission at 532 nm (Figure 3.6 and Table 3.1). These all produced a lidar-derived ground-classified elevation with an || = 0.00 m (RMSE = 0.09 m). However, the point density was below 1 point m^{-2}; (0.86 points m^{-2}; Table S3.1). If a higher point density were required, using all three laser pulse emissions (IR, NIR and Visible) and increasing iteration angle from 6 to 15, as well as reducing iteration angle when edge length < 1.0, 2.0, or turned off (classifications 29–31) produce nearly-as-accurate ground surfaces with || = 0.01 m (RMSE = 0.09 m) and 4.06, 3.94, and 3.32 points m^{-2}, respectively (Figure 3.6; Table 3.1 and Table S3.1). In more typically used lidar systems that collect data at 1064 nm (NIR), the optimal classifications were 24–28 (iteration angle increased from 6 to 15°; Table 3.1), which resulted in ||s slightly elevated above the true ground surface (|| = 0.03 m; RMSE = 0.10 m; 1.03 points m^{-2}; Figure 3.6 and Table S3.1).The poorest ground classifications for SR areas were those within which iteration angle was narrowed to 2°.

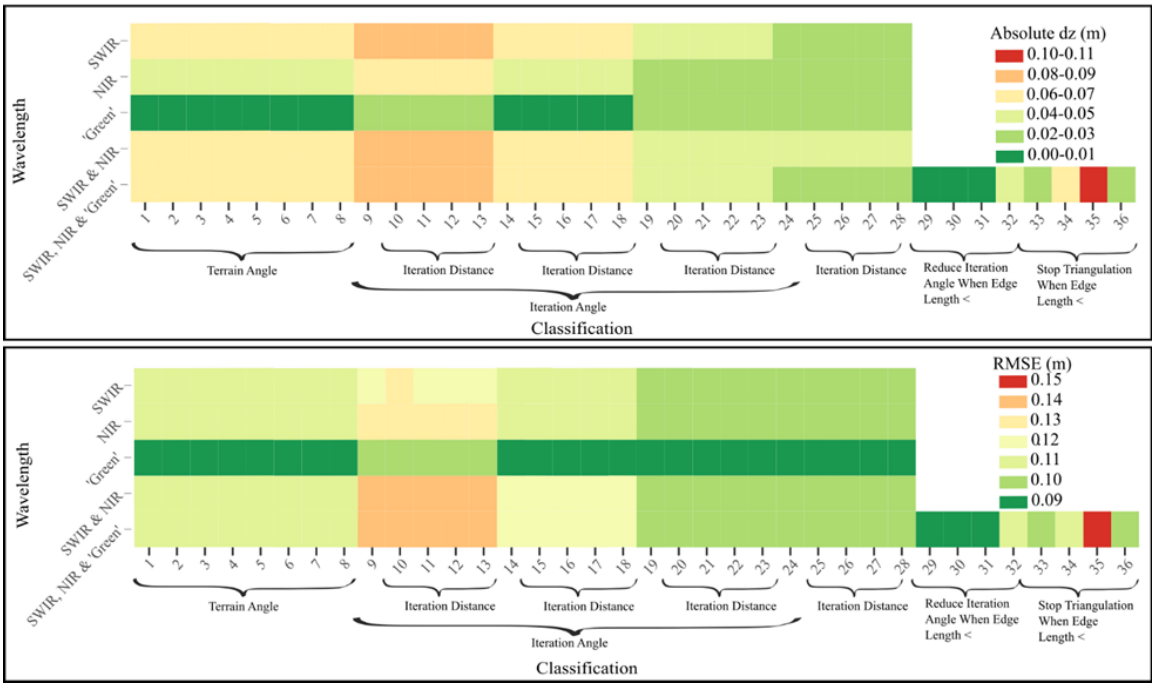

Figure 3.6. Ground classification results (|| and RMSE) in burned peatlands with low vegetation regeneration two years post-fire (as a proxy for immediately post-fire). Classifications were conducted in TerraScan.

Using LAStools, ground classifications F–J using lidar data collected at all three wavelengths were optimal (Figure 3.7 and Table 3.2). These classifications produced lidar-measured ground elevations that did not, on average, deviate from the true ground surface (|| = 0.00 m; RMSE = 0.09 m; 3.70–3.72 points m^{-2}; Figure 3.7 and Table S3.1). In this case, where all channels were used, refinement did not impact the ground-classified surface's accuracy or point density (m^{-2}). In a lidar system that collects data in the 1064 nm wavelength, optimal classifications were G–J, which produced lidar-measured ground classifications with || = 0.01 m (RMSE = 0.09 m; 1.3–1.31 points m^{-2}; Figure 3.7 and Table 3.2). However, in this landscape, when using LAStools, the most significant difference in classification accuracy was due to the channel with which the data were collected; changes within a channel were negligible (i.e., within the 1064 nm data: || remained at 0.01 m regardless of classification, RMSE only varied by 0.01 m (0.09–0.10 m), and point density varied from 1.24–1.31 points m^{-2} (Figure 3.7 and Table S3.1). While the optimal classifications from TerraScan and LAStools were comparable, the poorest classifications from each were notably different. The classifications produced in LAStools had an || ranging from 0.00–0.03 m and an RMSE ranging from 0.09–0.10 m, whereas TerraScan classifications had an || ranging from 0.00–0.09 m and an RMSE ranging from 0.09–0.15 m (Figure 3.5 and Figure 3.6).

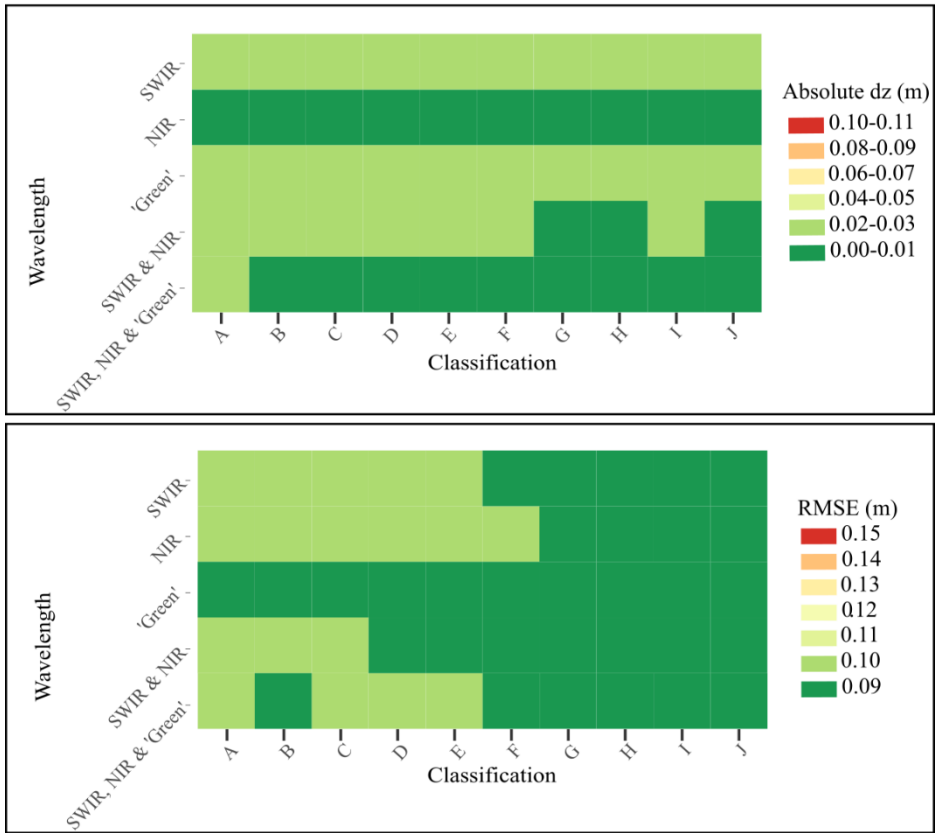

Figure 3.7. Ground classification results (|| and RMSE) in burned peatlands with low vegetation regeneration two years post-fire (as a proxy for immediately post-fire). Classifications were conducted in LAStools.

In summary, for a well-calibrated and locally controlled (e.g., over a nearby highway surface) airborne lidar survey we can expect a spatially averaged difference in elevation of <0.01 m with a range of ~0.09 m in areas of burned ground surface with no to low vegetation regeneration using optimal classifications in both TerraScan and LAStools. However, appropriate parameterization in TerraScan is dependent on the channel(s) available and required point density (Table 3.1 and Table S3.1).

3.4.3 Differences between Field-Measured Elevation and Lidar Ground Classification across All Burned Peatlands (Cumulative Shorter Vegetative Regeneration and Taller Vegetative Regeneration Sites)

As vegetation growth increases in the two years following wildland fire, and vegetation regeneration varies from low (as in SR sites) to high (as in TR sites), optimal ground classification parameters change. In TerraScan, the greatest similarity (and lowest error) when comparing lidar ground-classified returns with the surveyed ground elevation in all burned sites combined (a proxy for ~2 years post-fire) was found when the iteration angle was increased from 6 to 15, but iteration distance was reduced to 0.5 or 1.0 from 1.4 default (parametrization methods 25 or 26) using both 1550 nm and 1064 nm data (Figure 3.8; Table 3.1 and Table S3.1). These classifications produced lidar-measured ground elevations with an || = 0.00 m (RMSE = 0.13 m; 1.88 points m^{-2}). For a typical 1064 nm laser emission wavelength system, classifications 20 through 23 produced optimal results (iteration angle increased from six to ten), also producing ground elevations with an || = 0.00 m but with a slightly higher RMSE and lower point density (RMSE = 0.14 m; 1.03 points m^{-2}; Figure 3.8 and Table 3.1). As with SR areas, the ground classifications with the lowest accuracy in cumulative burned areas were those whose iteration angle was narrowed to 2.

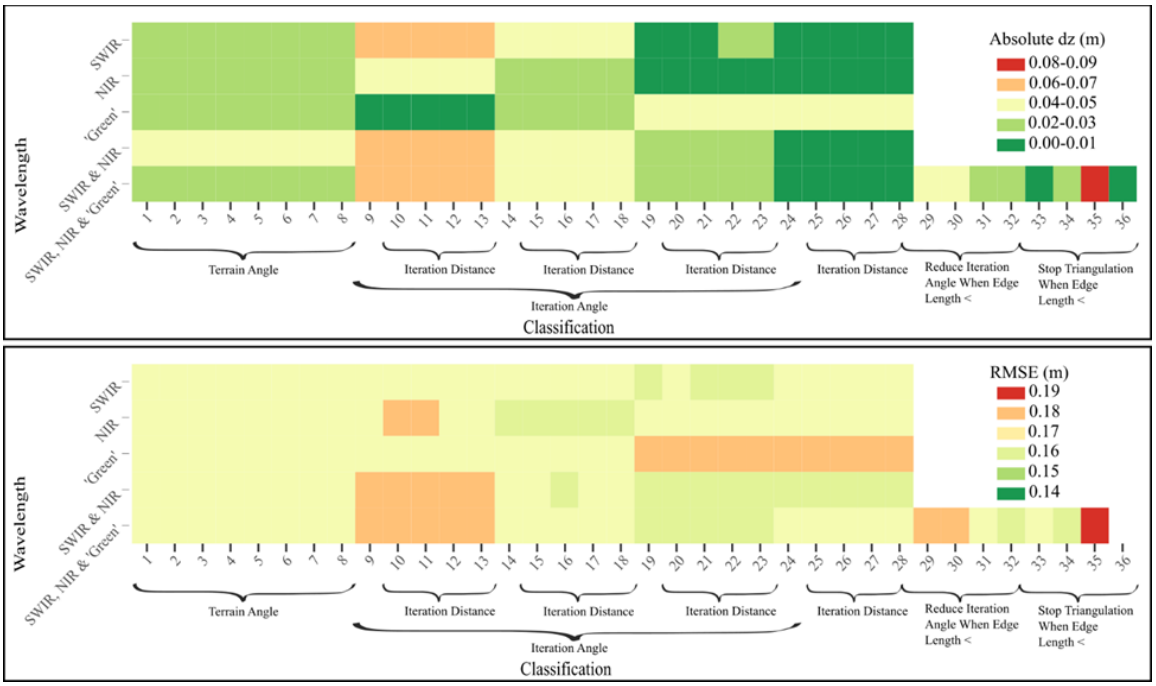

Figure 3.8. Ground classification results (|| and RMSE) in burned peatlands unsegregated based on vegetation regeneration two years post-fire (true representation of two years post-fire). Classifications were conducted in TerraScan.

When compared with optimal ground classification for laser returns in SR landscapes, the optimal ground classification used for total burned areas provides results with comparable ||, but slightly higher uncertainty (SR RMSE = 0.09 m), as would be expected with an increase in vegetation height and height variability.

As in SR areas, classification of returns to ground and elevation accuracy in areas representative of vegetation two years post-fire (cumulative burn areas) depended more on laser pulse emission wavelength than on classification parameters applied in LAStools; however, channel optimization differed. The ground classifications that produced the most accurate results for burned surfaces compared with measured elevations were A through C, E, G, and J (Table 3.2), using 1550 nm data (|| = 0.00; RMSE = 0.14; point density = 1.27–1.34 points m^{-2}; Figure 3.9; Table 3.2); however, within a given wavelength, all

parameterizations produced similar results (for example, using 1550 nm data, || = 0.00–0.01 m; RMSE = 0.14–0.15 m; points m^{-2} = 1.27–1.34). By using combined 1550 nm and 1064 nm data, similar results are produced (|| = 0.01–0.02 m; RMSE = 0.14) but point density increases to 2.4–2.61 points m^{-2}. Similarly to SR landscapes, optimal classifications from TerraScan and LAStools were negligibly different; however, the poorest classification from LAStools was more accurate than that of TerraScan (|| = 0.06 m; RMSE = 0.15 m and || = 0.09 m; RMSE = 0.16 m, respectively; Figure 3.7 and Figure 3.8).

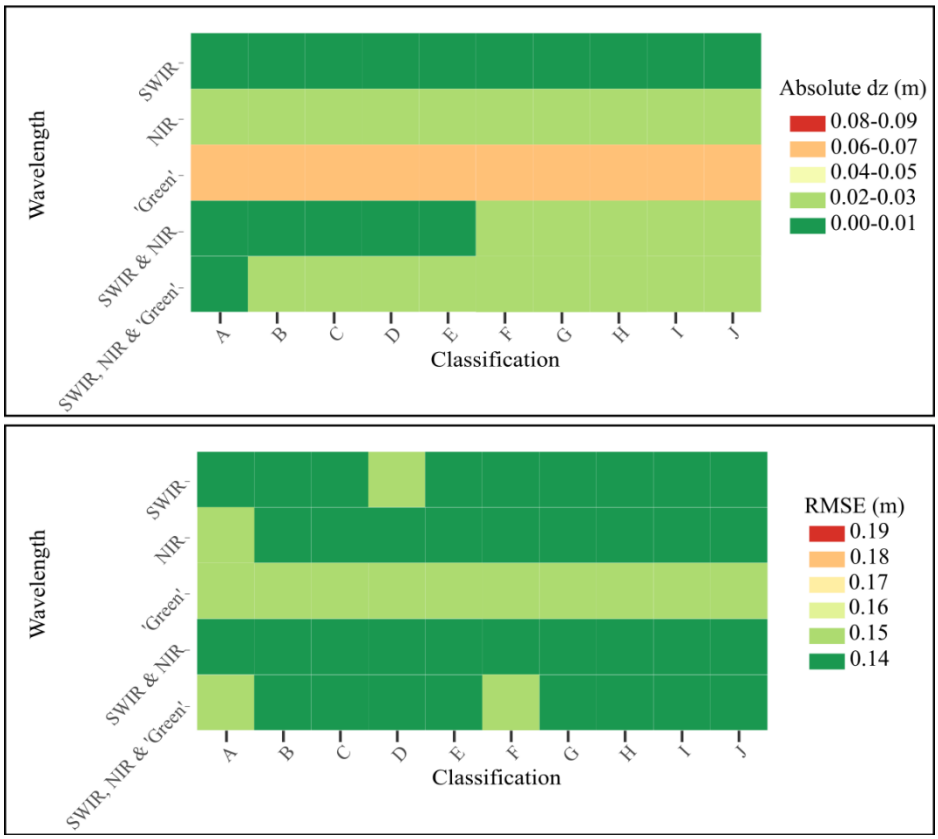

Figure 3.9. Ground classification results (|| and RMSE) in burned peatlands unsegregated based on vegetation regeneration two years post-fire (true representation of two years post-fire). Classifications were conducted in LASTools.

In the case of more typical 1064 nm lidar systems, classifications B through J produced ground elevations with an || of 0.02 m, an RMSE of 0.14 m, and 1.24–1.31 points m^{-2} compared with field-measured; however, even the "poorest" classification (greatest difference from measured) produced from 1064 nm data showed nearly identical results (|| = 0.02; RMSE = 0.15; Figure 3.9 and Table 3.2), emphasizing the importance of channel selection during data collection over classification parameterization choice when using LAStools.

In summary, two years post-fire, we can expect an average elevational accuracy of ~0.00 m with a range of ~0.13 m using combined 1550 nm and 1064 nm data with TerraScan. Using LAStools, spatially averaged elevational accuracy is comparable at ~0.00 m but with a slightly higher range of ~0.14 m when measured at 1550 nm.

3.4.4 Differences between Field-Measured Elevation and Lidar Return Ground Classification in Taller Vegetative Regeneration Peatlands

In areas with the greatest vegetation growth since fire (proxies for >2 years post-burn), the most accurate ground classification in TerraScan was classification 20, using combined 1550 nm and 1640 nm data (Figure 3.10; Table 3.1 and Table S3.1). For this classification, the iteration angle was increased from six to ten, and the iteration distance was reduced from 1.4 m to 0.5 m when compared with default parameters. This resulted in a lidar ground classification output with a ground classification accuracy of || = 0.00 m (RMSE = 0.16 m; 1.54 points m^{-2}). In the case of more typical airborne lidar emitting laser pulses at 1064 nm, this classification still resulted in the most optimal ground surface (with a point density of >1 point m^2); however, the lidar-measured ground surface sat ~0.03 m above measured (|| = 0.03 m; RMSE = 0.17 m; 1.03 points m^{-2}). More accurate classification schemes were

identified, with fewer (in this case, 0.75) points m^{-2} (classifications 14 through 18; || = 0.00 m; RMSE = 0.17 m; Figure 3.10; Table 3.1). Generally, the least accurate results were similar to those for cumulative burned areas—those within which the iteration angle was reduced to two; however, in TR areas, emission wavelength made the most difference to accuracy, with the lowest accuracy classifications produced by 532 nm data.

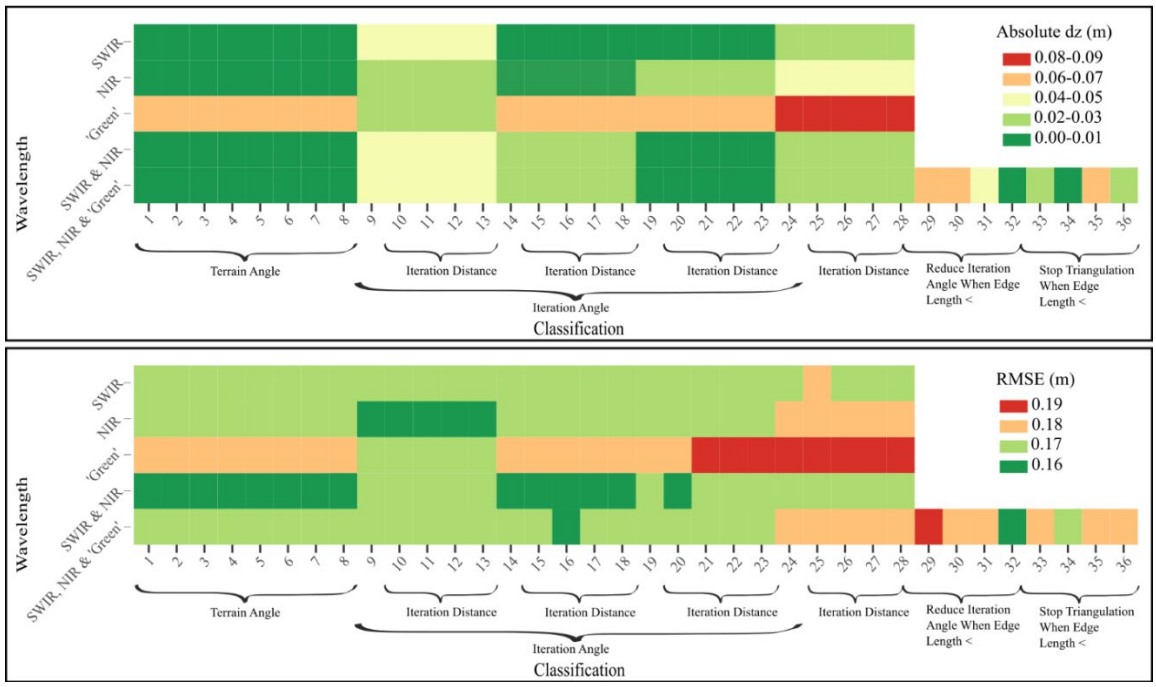

Figure 3.10. Ground classification results (|| and RMSE) in burned peatlands with tall vegetation regeneration two years post-fire (as a proxy for 3+ years post-fire). Classifications were conducted in TerraScan.

Using LAStools, the optimal ground classifications were A through E ('Nature' classifications with any level of refinement) using combined 1550 nm and 1064 nm data (Figure 3.11; Table 3.2 and Table S3.1). The lidar-measured ground classified returns had an || = 0.03 m from field-measured (RMSE = 0.18 m; 2.40–2.42 points m^{-2}). Comparable results were achieved using only 1550 nm data, but point density was reduced to 1.27–1.34 points m^{-2}. As with earlier vegetation regeneration stages, classification accuracy depended

more on the wavelength than on classification parameters with LAStools. For systems using only 1064 nm emission wavelengths, the lidar-measured ground surface sits slightly above the measured ground (|| = 0.04–0.05 m; RMSE = 0.18 m; 1.24–1.31 points m^{-2}). Similar to TerraScan results, the poorest classifications were those produced with 532 nm data.

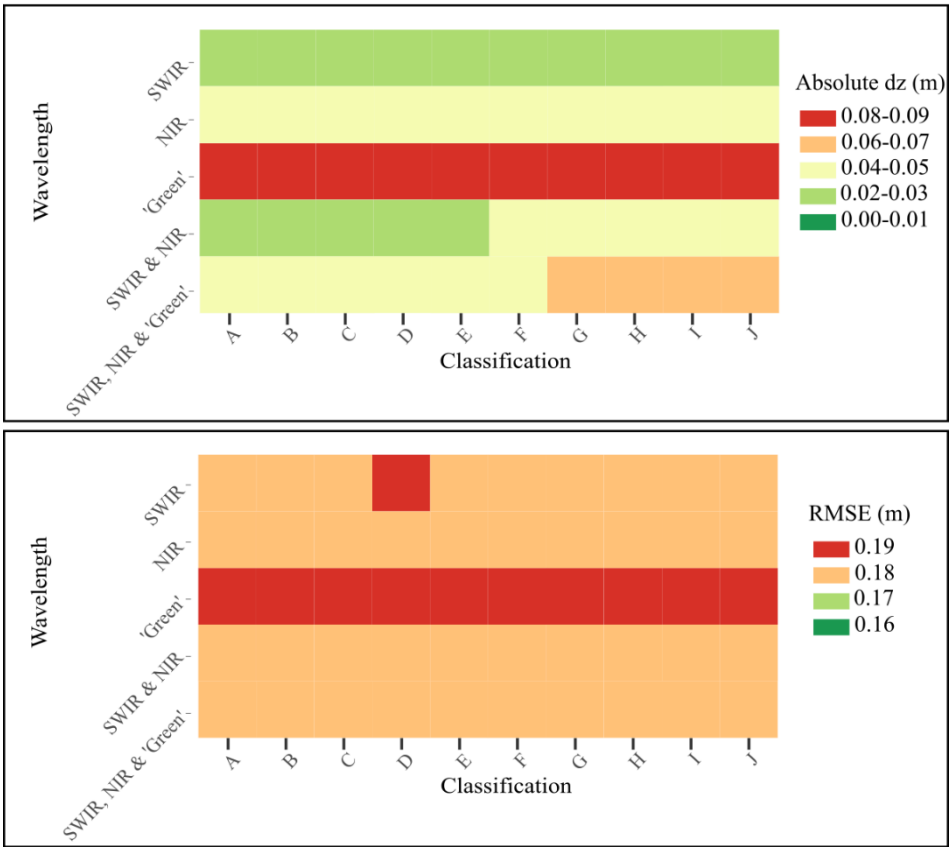

Figure 3.11. Ground classification results (|| and RMSE) in burned peatlands with tall vegetation regeneration two years post-fire (as a proxy for 3+ years post-fire). Classifications were conducted in LAStools.

In summary, unlike areas with lower vegetation regeneration, in TR areas, the optimal classifications from TerraScan and LAStools differed, with TerraScan classifications generally performing better (Figure 3.10 and Figure 3.11). Using TerraScan we can still expect an average elevation accuracy of ~0.00 m; however, the accuracy at a

given point is expected to have a range of ~0.16 m using combined 1550 nm and 1640 nm data with TerraScan. Using the same lidar data but with LAStools, the average elevational accuracy is slightly lower at ~0.03 m, with a slightly increased RMSE of ~0.18 m.

3.4.5 Differences between Field-Measured Elevation and Lidar Return Ground Classification in Unburned Peatlands

Finally, in unburned areas (or areas that have fully regenerated post-fire), the optimal ground classifications were 9 through 13 using all wavelengths combined (Figure 3.12; Table 3.1 and Table S3.1). By reducing the iteration angle to two, these classifications resulted in an || = 0.01 m and an RMSE = 0.19 m; however, point density was relatively low for this particular survey (0.64 points m^{-2}). When a threshold of 1.0 points m^{-2} is set, the optimal ground classifications shifted to 14 through 18, with their iteration angles set to 5° (Table S3.1). These classifications have a point density of 1.16 points m^{-2}, but an || = 0.05 m (Figure 3.12; Table 3.1). In the case of a lidar emitting at 1064 nm, the optimal classifications are the same as those when all wavelengths are combined (9 through 13); however, classification accuracies notably decline with a threshold of 1.0 points m^{-2}. Classifications 19 through 23 provide the best outputs, in this case, with an || = 0.09 m (RMSE = 0.22 m; 1.03 points m^{-2}). The least accurate classifications are those produced using lidar data collected at 532 nm, where the iteration angle is 15 (widest angle tested).

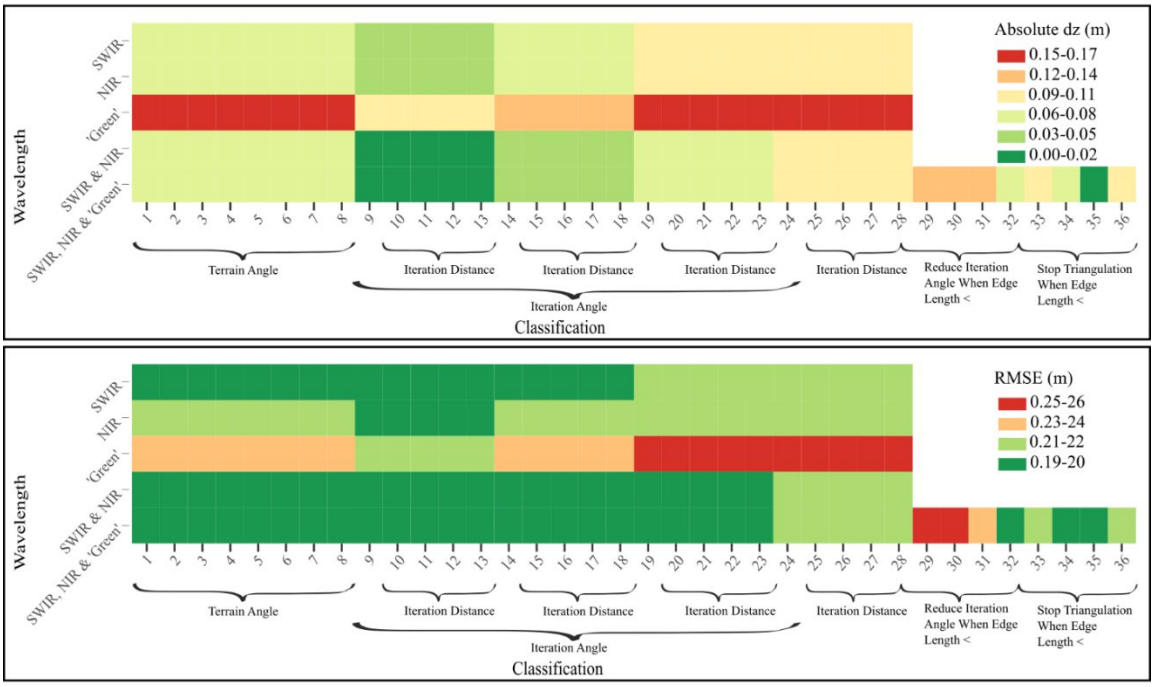

Figure 3.12. Ground classification results (|| and RMSE) in unburned peatlands. Classifications were conducted in TerraScan.

Unlike in burned landscapes, where classification was not the dominant control on accuracy compared with emission wavelength in LAStools, there was a distinction between classifications in unburned areas. In these zones, classification B using data collected at 1064 nm was optimal (Figure 3.13 and Table 3.2), resulting in the lowest difference between field-measured and ground classified returns. This classification resulted in an || = 0.09 m (RMSE = 0.21 m; 1.24 points m^{-2}). As with other vegetation regeneration stages, data collected at 532 nm resulted in the least accurate ground classifications, regardless of parameterization, followed by use of all channels combined.

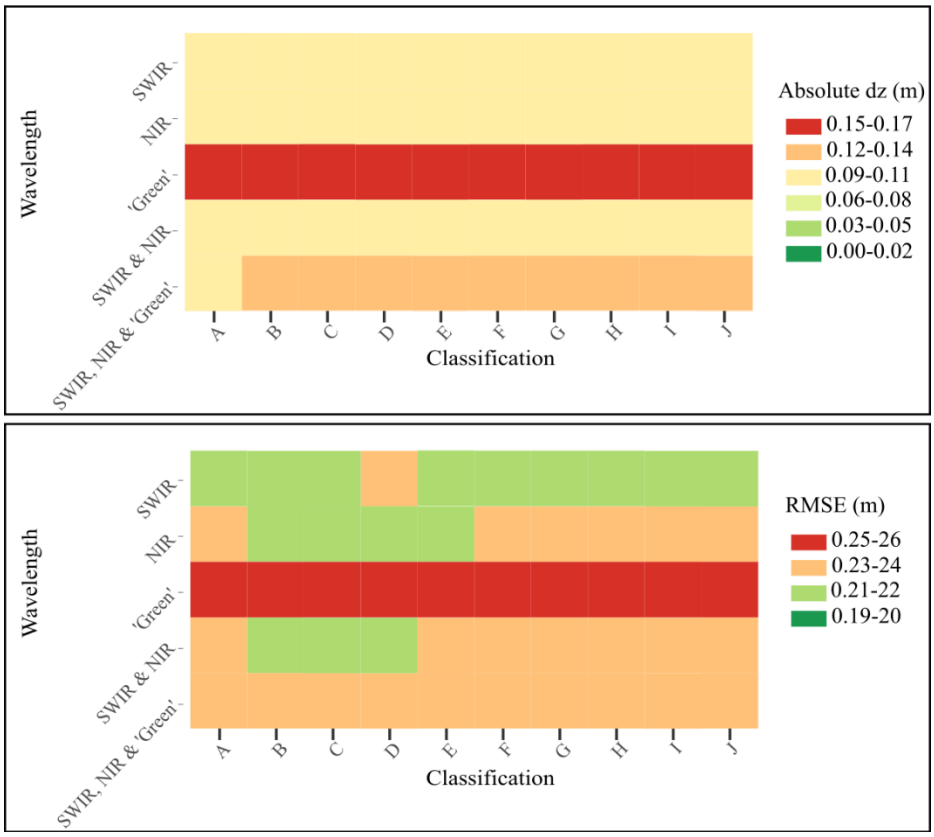

Figure 3.13. Ground classification results (|| and RMSE) in unburned peatlands. Classifications were conducted in LAStools.

In summary, as with TR areas, the optimal classifications from TerraScan and LAStools differed in unburned boreal peatlands. We can expect a spatially averaged elevation accuracy of ~0.01 m (or ~0.05 m with a threshold of point density > 1 point m^{-2}) with an accuracy at a given point within an RMSE of ~0.19 m when using all channels combined, processed in TerraScan (Figure 3.12). Using LAStools, accuracy was poorer, with an average elevation accuracy of ~0.09 m with an RMSE of ~0.21 m at 1064 nm (Figure 3.13).

3.4.6 Expected Ground Surface Elevation Accuracies of Lidar Data in the Years following Wildland Fire

By isolating taller versus shorter vegetative regeneration regions and using these as proxies for time since fire, we can estimate the elevation accuracy of lidar data collection in the years following wildland fire. Within the first year since fire (which I assume is the 'SR' category), lidar-measured ground elevation accuracies would be expected to be approximately 0.00 ± 0.09 m (± standard deviation (SD); Figure 3.14a and Table S3.1). For this classification, as well as the others used, below, SD was equal to RMSE. Approximately two years post-fire (at the time of this lidar data collection, assumed to include burned area surveyed–SR and TR), we would expect to see ground elevation accuracy of approximately 0.00 ± 0.13 m (Figure 3.14a and Table S3.1). As vegetation growth continues beyond the third year post-fire ('TR' category), the elevation accuracy of the lidar-measured ground classified points would be reduced to approximately 0.00 ± 0.16 m (Figure 3.14a and Table S3.1). In unburned areas, elevation accuracy would be approximately 0.01 ± 0.19 m (Figure 3.14a and Table S3.1).

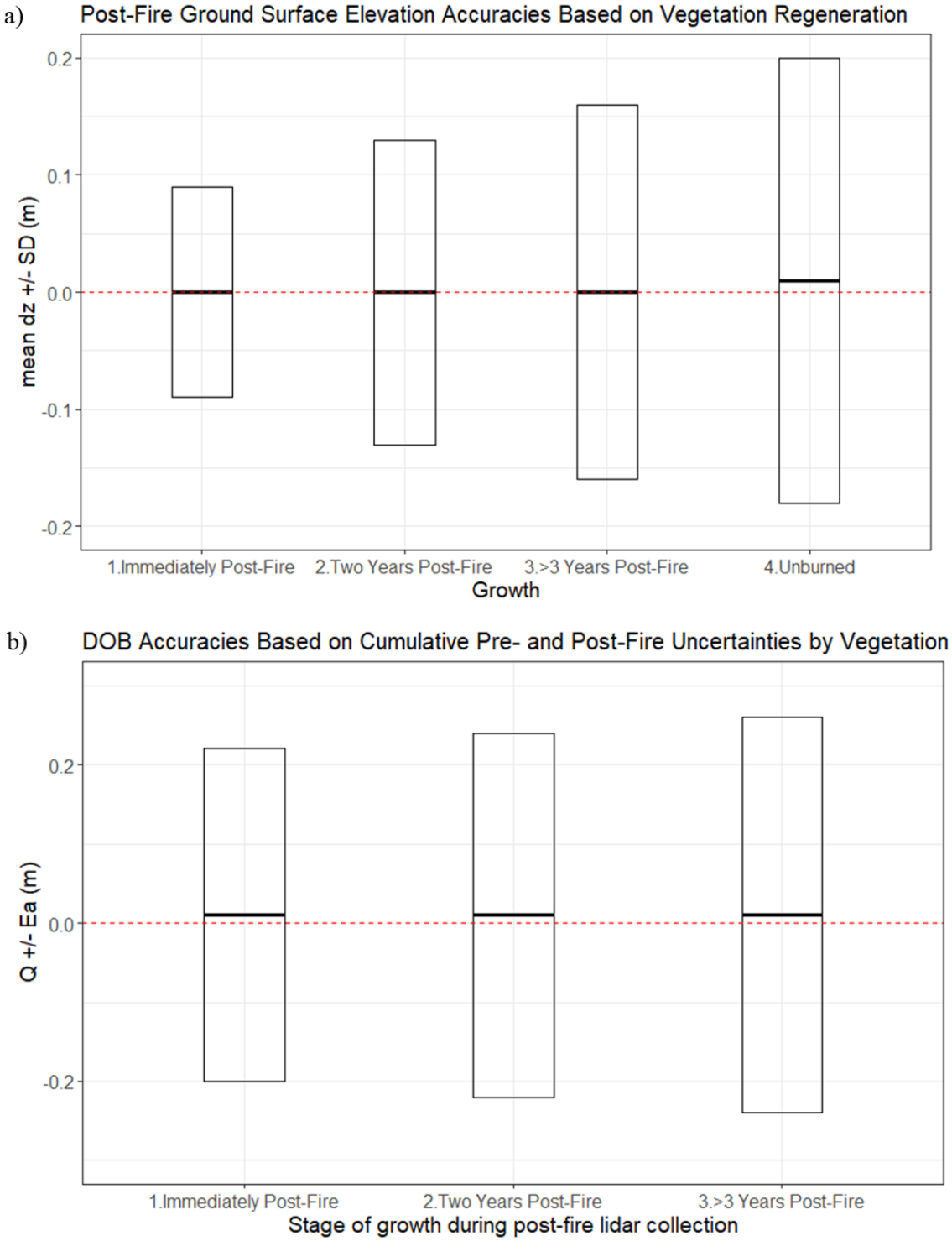

Figure 3.14. a) Expected ground elevation accuracies of lidar data in the years following wildland fire in boreal peatlands; b) Expected depth of burn (DOB) accuracies of lidar data in the years following wildland fire in boreal peatlands, assuming pre-fire lidar data were collected in "unburned conditions", where Q = average over- or under-estimation of

surface elevation change, and Ea is cumulative error (SD). Note: for all measurements used, SD was equal to RMSE.

As the highest uncertainty (SD) was associated with unburned (pre-fire) areas, the RMSEs associated with surface elevation changes were minimally different depending on the stage of post-fire vegetation regeneration (Figure 3.14b). By using optimal ground classification schemes, the post-fire s were consistently 0.00 m, and pre-fire was ~0.01 m (Figure 3.4, Figure 3.5, Figure 3.6, Figure 3.7, Figure 3.8, Figure 3.9, Figure 3.10, Figure 3.11, Figure 3.12 and Figure 3.13; Table S3.1). As such, the standard offset for elevation change was ~0.01 m, on average, regardless of vegetation regeneration. I found that if lidar data were collected immediately post-fire (i.e., SR areas), SD of the elevation change (depth of burn) was 0.21 m (Figure 3.14b). If data were collected ~ two years post-fire (i.e., cumulative burned areas), SD was 0.23 m (Figure 3.14b). Furthermore, if lidar data were collected three or more years post-fire (i.e., TR areas), SD was 0.25 m (Figure 3.14b).

3.4.7 Wavelength Dependency of Ground Classification Accuracy as Varies by Vegetation Regeneration

By optimizing parameterizations, highly accurate ground classifications in low relief environments are possible for any wavelength or combination used. However, regardless of processing software, local vegetation characteristics still influence which wavelength produces optimal ground classification results. When applying the TerraScan ground classification parameterizations to road surfaces, optimal ground classification parameterizations derived from 1064 nm data had the lowest error compared with ground control measurements. However, wavelength-associated differences in ground surface elevation were negligible: ||s ranged from 0.00 to 0.02 m (on average for all combination

of wavelengths) and RMSEs from 0.04 to 0.05 m (Figure 3.3.15a and Table S3.1). In unburned and TR areas, the combination of 1550 nm and 1064 nm wavelengths resulted in the most accurate ground classifications, with the least variability based on parameterization optimizations (Figure 3.15e,c). The least wavelength-dependent vegetation regeneration stage was that of cumulative burned areas with variable regeneration heights (a proxy for ~2 years post-fire; Figure 3.15d). While 1064 nm data resulted in the most accurate ground classifications with the least variability based on the parameterization scheme, the use of any wavelength individually resulted in similar levels of accuracy. However, the accuracy of ground classifications became more variable when wavelengths were combined (either 1550 nm and 1064 nm; or, 1550 nm, 1064 nm, and 532 nm). In SR zones, lidar-based ground elevations measured at 532 nm were the most accurate, with the lowest variability based on parameterizations (Figure 3.15b).

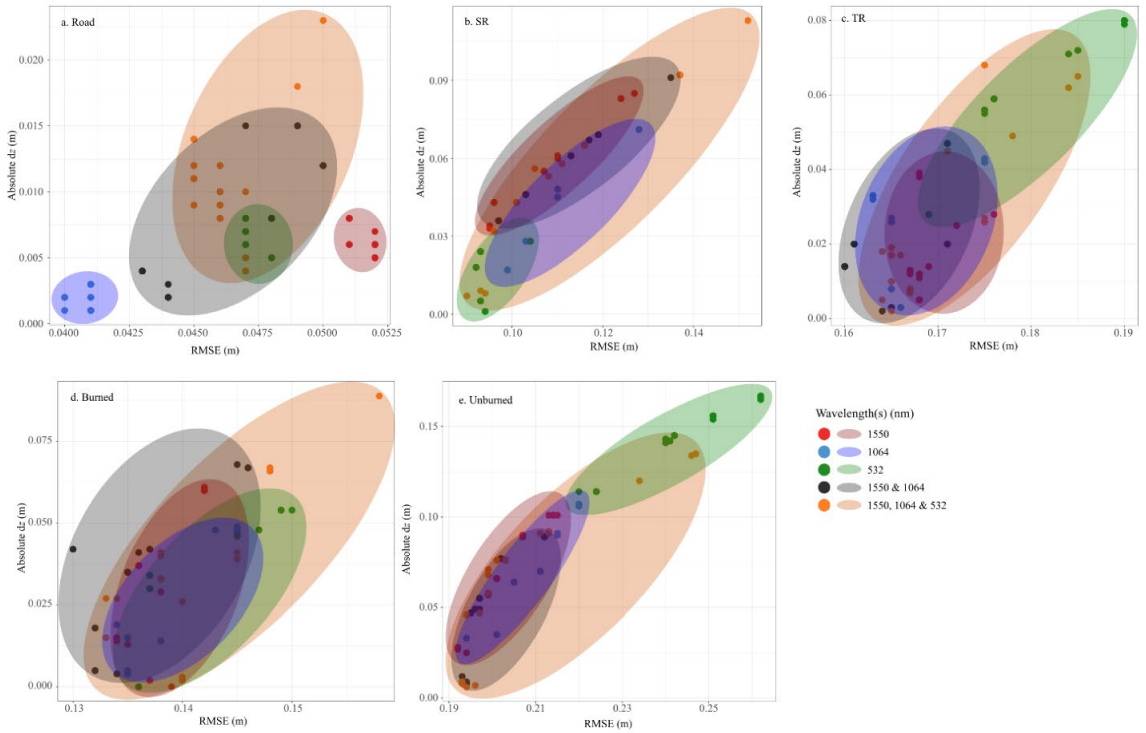

Figure 3.15. Ground classification results by wavelength along/in: (a) roads, (b) burned peatlands with short regeneration, (c) burned peatlands with tall regeneration, (d) all burned peatlands, and (e) unburned peatlands two years post-fire. Results were identified using TerraScan as determined by lidar channel. Each point represents an iterative parameter set. Note: axis range varies by plot.

In LAStools, wavelength selection impacted ground classification accuracy more than in TerraScan (Figure 3.15 and Figure 3.16). Interestingly, processing software affects wavelength dependency for a given regeneration stage, particularly in SR areas (Figure 3.15b and Figure 3.16b). Along road surfaces, the use of data collected at 1064 nm, or both 1550 nm and 1064 nm, resulted in slightly lower RMSEs; however, || differences were negligible, and RMSEs varied by only ~0.01 m (Figure 3.16a). In unburned areas, 1064 nm data resulted in ground classifications with the lowest ||s and RMSEs (Figure 3.16e). Data collected using the 1550 nm wavelength provided the most accurate classifications in both cumulative burned and TR areas (Figure 3.16d,c). In SR areas, all wavelengths combined provided the most accurate ground classifications (Figure 3.16b).

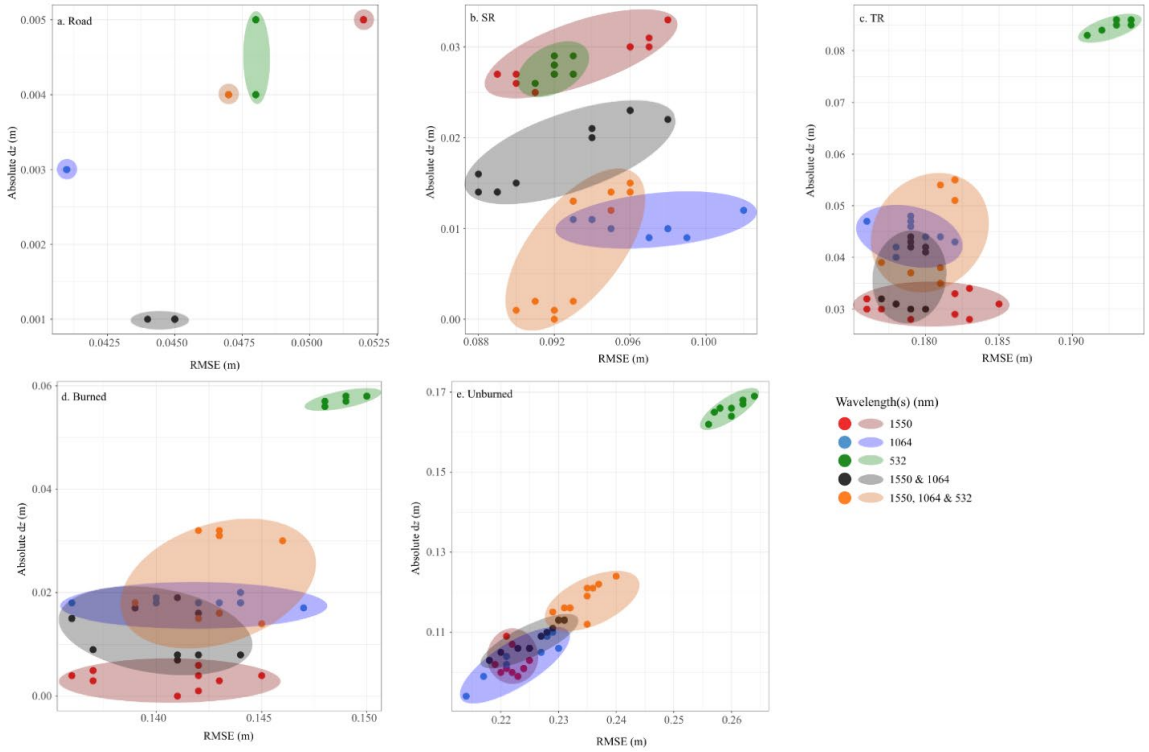

Figure 3.16. Ground classification results by wavelength along/in: (a) roads, (b) burned peatlands with short regeneration, (c) burned peatlands with tall regeneration, (d) all burned peatlands, and (e) unburned peatlands two years post-fire. Results were identified using LAStools as determined by lidar channel. Each point represents an iterative parameter set. Note: axis range varies by plot.

3.5 Discussion

Despite the utility of lidar data for measuring ground surface elevation, time-series lidar data pre- and immediately post-fire is relatively rare but is increasing in availability with the application of lidar for understanding the impacts of wildland fire on ecosystems. This study provides an opportunity to assess the potential for error during the classification of lidar returns as "ground" and the accuracy of ground elevations for use in DEMs. It also identifies the ground classification errors associated with scorched patches/new vegetation regeneration (SR) and early post-fire regeneration stages, indicating time since disturbance.

Previous studies have found that errors in ground classification most often occur as a result of steep terrain (Goulden & Hopkinson, 2014; Moudrý et al., 2020; Pourali et al., 2014) or dense vegetation (Hopkinson et al., 2004; Moudrý et al., 2020; Schmid et al., 2011). Here, the study area is relatively flat, and so the potential for error that results from sloped terrain is greatly reduced (e.g., Moudrý et al., 2020). However, where vegetation has regenerated post-fire, stems and foliage can be relatively dense. Further, burned peatland surfaces can have significant microtopographical variability (hummocks and hollows) that may be difficult for the lidar ground classification to differentiate from short, dense vegetation (e.g., Brubaker et al., 2013). Our results show that within a given vegetation height range, the accuracies of lidar ground classifications (provided the parameters are set logically) do not deviate greatly from the most to least accurate ground classification of laser returns compared with ground control (Table S3.1). For example, within SR zones, using the least accurate classification scheme/wavelength combination results in classified returns that were, on average, 0.11 m below measured ground elevation, with a RMSE of 0.15 m. For many applications, such as canopy height measurements in forested environments, this may be sufficient (e.g., Tinkham et al., 2012); however, it is important to achieve the best accuracy possible when determining ground surface elevations for applications including combustion from wildland fire (e.g., using pre- and post-fire datasets) and hydrological modelling (e.g., Moudrý et al., 2020). This is due to the need for accurate quantification of slight differences in the elevation surface from pre-post fire or spatial changes in local surface topography.

We found that as vegetation regenerates post-fire, both optimal parameterizations and the wavelength used for lidar data collection differ at varying growth stages. In SR

areas, or immediately post-fire, laser pulse emissions at 532 nm or using all wavelengths combined (532 nm, 1064 nm, and 1550 nm) provide the most accurate ground classifications compared with measured (Figure 3.4, Figure 3.5, Figure 3.15 and Figure 3.16; Table S3.1). In these areas where vegetation regeneration was minimal, laser pulses emitted at 532 nm better characterized the ground surface due to the dominance of moss cover in measurement plots with little overlying vegetation in these peatland environments. It should be noted that channel dependencies are likely a result of both wavelength as well as pulse geometry (beam angle and footprint). Pulses emitted at 532 nm have lower energy receipt, a wider footprint, and a tendency to reflect from green vegetation above the ground surface (Figure 3.3a; Hopkinson et al., 2016; Okhrimenko et al., 2019). As such, ground classified returns at 532 nm were the least accurate in unburned and TR areas (Figure 3.15 and Figure 3.16).

As vegetation heights increased, the data from 1064 nm, 1550 nm, or both wavelengths combined, produced the most accurate elevations, noting that the addition of the 532 nm wavelength reduced accuracy even when combined with the other two (Figure 3.15 and Figure 3.16). In cumulative burned areas, the use of 1550 nm provided the most optimal ground classifications, while in TR areas, either using 1550 nm data or combined 1064 nm and 1550 nm data had the least error and variability based on parameterizations (Figure 3.15 and Figure 3.16). In cumulative burn areas where ground classification was conducted over regions of highly variable vegetation heights and densities, classifications that used 1064 nm data resulted in vegetation misclassified as ground (Hopkinson et al., 2005; Reddy et al., 2015). Typical lidar systems with 1064 nm laser wavelength emission have greater reflectance from short vegetation and mosses (Gerrand et al., 2021).

Therefore, in areas with low, dense vegetation, there may be energy transmission losses as the laser pulse intercepts and reflects from vegetation instead of the ground surface (Chasmer et al., 2017; Hopkinson et al., 2004; Hopkinson et al., 2005; Reddy et al., 2015). This was also observed in (Moudrý et al., 2020) who found that low, dense vegetation was more commonly misclassified as ground, such that the classification was less accurate than in areas with tall overstory vegetation and reduced understory, e.g., in some forests. This phenomenon can be seen in the classifications of unburned peatlands, where 1064 nm data were optimal for ground classifications as this resulted in the lowest error (Figure 3.15 and Figure 3.16). Here, it is likely that lidar was penetrating through canopies to low-lying understory vegetation (ground dominated by mosses) and the ground surface.

As with channel selection, the parameterization settings that optimized ground classifications depended on the dominant and sub-dominant vegetation heights found within plots. In TerraScan, I found that changes to three parameters impacted ground classifications: iteration angle, iteration distance, and the ability to reduce iteration angle when edge length exceeds a set distance (Table 3.1 and Table S3.1). In burned landscapes with little vegetation regeneration (SR), adjustments made to the iteration angle improved the accuracy of the lidar-measured ground elevations compared with field-measured (Table 3.1 and Table S3.1). Using 532 nm wavelength data (most accurate but low point density), the iteration angle was slightly reduced from six to five degrees in the optimal classification. Using all wavelengths combined, or only the 1064 nm wavelength data, the iteration angle was increased to 15 and 10 degrees, respectively (Table S3.1). The classifications using 532 nm data were more optimal using a smaller iteration angle (best for flat landscapes), likely due to the large pulse footprint. However, by increasing the

iteration angle when using all wavelengths or 1064 nm data, the classification was better able to retain the steep transitions between hummocks and hollows, which would be most significant in areas with low regeneration, resulting in higher accuracy ground classification. A larger iteration angle allows the ground classification routine to adhere to surface elevation variability (Terrasolid Ltd., 2021) by including returns that follow the microtopographic morphology of the hummocks and hollows. Despite the general topography of peatlands and transitions into forests being relatively flat, we are able to optimize the classification to account for highly localized topographic variability by setting the iteration angle to a greater angle within a confined area (Mickler et al., 2017; Terrasolid Ltd., 2021).

As vegetation heights increased (cumulative burned and TR areas), maintaining a high iteration angle but reducing iteration distance improved results. Iteration distance, which is the maximum height at which a point will be added to the ground classification (Terrasolid Ltd., 2021), may be optimized at a longer distance in landscapes with little vegetation (e.g., for lidar surveys in the months following a fire). This will better account for the discrepancies in *dz* from returns from hummocks vs. hollows. However, in areas with greater vegetation regeneration and fewer scorched gaps between vegetation patches, a larger iteration distance of 1.4 m (vs. 0.5 m) may result in some returns from short vegetation being included in the ground classification. This increases the lidar ground classified elevation surface above the measured ground surface elevation, thereby increasing the inaccuracy of the DEM (Table 3.1 and Table S3.1). Optimal parameterizations change notably in unburned areas or in areas with complete vegetation regeneration, post-fire. Interestingly, the optimal classifications in these regions had a

reduced iteration angle of two degrees, which was the iteration angle that resulted in the poorest classifications in all post-burn analyses, even in TR areas. As peat combustion can enhance elevation differences between hummocks and hollows in peatlands (Benscoter et al., 2015), unburned peatlands often have less undulating moss ground surfaces. Further, reducing the iteration angle in unburned areas reduces the likelihood of including low herbaceous or shrubby vegetation in the ground classification. However, by reducing the iteration angle, the tendency to add more points into the ground class is also reduced, thereby reducing the point density. I found that by increasing the iteration angle to 5°, point density was increased to >1 point m^{-2}; however, this increased the as the routine included low-lying vegetation as ground.

When using LAStools, I found that classification parameters were less important than the channel (laser pulse emission/reception wavelength as well as pulse geometry) with which data were collected. In SR and TR areas, ground elevation classifications were slightly improved when step size was set to 5 ('Nature' setting) instead of 3 ('Wilderness' setting) but were not impacted by the level of refinement. The ground classification was slightly better in unburned landscapes when step size was five and refinement was set to 'Fine', where the initial ground point search grid is four times more refined than the step size (Table 3.2 and Table S3.1).

The results of this study demonstrate that not only do optimal classification parameters differ based on vegetation structures and environmental conditions within these low-relief ecosystems, but also that the same ground classification parameters can be optimal for specific environmental conditions (e.g., burned, low, moderate vegetation regeneration), but far less accurate for a different set of environmental conditions. For

example, in TerraScan, classifications 8 through 13 provided the most accurate classifications in unburned landscapes but were the least accurate in cumulative burned and SR areas. There may be more variable ground topography in a burned landscape, which is not optimally parameterized using the same classification. With reduced iteration angle, areas with highly variable microtopography result in underestimation of ground surface elevation because returns from hummocks are excluded from the classification because the angular differences between returns in hollows vs. hummocks is too great. Steep angular classification of returns from the tops of the *Sphagnum* hummocks resulted in points being added to short vegetation instead of the ground class. This emphasizes the need to classify returns not only by land cover type but also by vegetation characteristics within those land covers for the most optimal/accurate classification parameterization. For example, classification to wetland class, burned and unburned, and within the burned class, high versus low regeneration (which can be determined based on the lidar data derivatives).

3.6 Conclusions

This study demonstrates the importance of optimizing classification parameters from default settings and optimizing parameters for different land cover types and vegetation structural characteristics. While it is important to iterate/optimize methods with any new data set, the results here provide parameters that can be used in burned and unburned boreal peatland environments and as a starting point for parameterization in similar environments. I provide optimal parameterization for boreal peatlands along a post-fire regeneration trajectory, with “SR” representing peatlands soon after burn, unsegmented burned land cover representing two years post-fire, “TR” representing several years post-fire, and unburned vegetation covers representing land cover later in the regeneration trajectory.

However, I suggest that there is a need for the development of accessible adaptative classification procedures, which can be used to (a) filter the landscape by attributes and (b) identify optimal parameterizations.

From this study, I conclude an expected 'best' average accuracy for depth of burn (pre-fire elevation minus post-fire elevation) within peatlands will have a spatially averaged error (dz) of ~0.01 m, indicating that soil organic matter loss (determined most simply as a change in elevation) would be over-estimated by an average of 0.01 m. Using the adventitious roots method, the average uncertainty is 0.004 m to 0.04 m (e.g., Boby et al., 2010; Gerrand et al., 2021; Kasischke et al., 2005) at the tree base. However, airborne lidar methods provide an opportunity to quantify spatially continuous elevational variability between trees and across a broad range of peatlands and environmental characteristics. In addition, I demonstrate that lidar surveys completed in the years following combustion do not become significantly less accurate for quantifying depth of burn overall (offset at ~0.01 m and RMSEs ranging from ~0.21 m to ~0.25 m in SR to TR areas; Figure 14). I suggest that lidar data collected up to three years post-fire can be utilized for depth of burn analyses without significant differences in cumulative errors associated with laser pulse interactions in the understory.

3.7 Author Contributions

Conceptualization, K.N., L.C. and C.H.; methodology, K.N., L.C. and C.H.; formal analysis, K.N.; investigation, K.N.; resources, L.C. and C.H.; data curation, K.N.; writing—original draft preparation, K.N.; writing—review and editing, K.N., L.C. and C.H.; visualization, K.N.; supervision, L.C.; project administration, L.C.; funding

acquisition, L.C., C.H. and K.N. All authors have read and agreed to the published version of the manuscript.

3.8 Funding

This research was funded by the Natural Sciences and Engineering Research Council (NSERC) Discovery Grant and University of Lethbridge Start-Up Funding to L. Chasmer. The Teledyne Optech Inc. Titan multispectral lidar was purchased using Western Economic Diversification Canada funding to C. Hopkinson. GNSS equipment was purchased using Canadian Foundation for Innovation funds provided to C. Hopkinson. Research was also funded by post-graduate support of K. Nelson, including the NSERC Canada Graduate Scholarship–Doctoral (CGS D), the Alberta Innovates Graduate Student Scholarship, the Nexen Fellowship in Water Research, and the University Of Lethbridge School Of Graduate Studies, as well as funding from Canada Wildfire (NSERC SPG-N).

3.9 Acknowledgements

The authors would like to thank Linda Flade, Emily Jones, Craig Mahoney, and Maxim Okhrimenko for their field and lidar data collection/processing assistance.

3.10 Conflicts of Interest

The authors declare no conflict of interest.

3.11 References

Aguilar, F. J., & Mills, J. P. (2008). Accuracy assessment of LiDAR-derived digital elevation models. Photogrammetric Record, 23(122), 148–169.

Alberta Environment and Sustainable Resource Development (ESRD). (2015). Alberta wetland classification system. Water Policy Branch, Policy and Planning Division: Edmonton, AB, Canada.

Andersen, H. E., McGaughey, R. J., & Reutebuch, S. E. (2005). Estimating forest canopy fuel parameters using LiDAR data. Remote Sensing of Environment, 94(4), 441–449.

ASPRS. (2004). ASPRS guidelines: Vertical accuracy reporting for lidar data (Version 1.0). American Society for Photogrammetry and Remote Sensing Lidar Committee (PAD): Baton Rouge, LA, USA.

Axelsson, P. (2000). DEM generation from laser scanner data using adaptive TIN models. International Archives of Photogrammetry and Remote Sensing, 33(B4), 110–117.

Benscoter, B. W., Greenacre, D., & Turetsky, M. R. (2015). Wildland fire as a key determinant of peatland microtopography. Canadian Journal of Forest Research, 45(8), 1132–1136.

Boby, L. A., Schuur, E. A., Mack, M. C., Verbyla, D., & Johnstone, J. F. (2010). Quantifying fire severity, carbon, and nitrogen emissions in Alaska's boreal forest. Ecological Applications, 20(6), 1633–1647.

Brubaker, K. M., Myers, W. L., Drohan, P. J., Miller, D. A., & Boyer, E. W. (2013). The use of LiDAR terrain data in characterizing surface roughness and microtopography. Applied and Environmental Soil Science, 2013, 891534.

Campbell, M. J., Dennison, P. E., Kerr, K. L., Brewer, S. C., & Anderegg, W. R. (2021). Scaled biomass estimation in woodland ecosystems: Testing the individual and combined capacities of satellite multispectral and lidar data. Remote Sensing of Environment, 262, 112511.

Carlisle, B. H. (2005). Modelling the spatial distribution of DEM error. Transactions in GIS, 9(4), 521–540.

Chasmer, L., & Hopkinson, C. (2017). Threshold loss of discontinuous permafrost and landscape evolution. Global change biology, 23(7), 2672-2686.

Chasmer, L. E., Hopkinson, C. D., Petrone, R. M., & Sitar, M. (2017). Using multitemporal and multispectral airborne lidar to assess depth of peat loss and correspondence with a new active normalized burn ratio for wildfires. Geophysical Research Letters, 44(23), 11851–11859.

Chen, Y., Zhu, X., Yebra, S., & Harris, N. (2017). Development of a predictive model for estimating forest surface fuel load in Australian eucalypt forests with LiDAR data. Environmental Modelling & Software, 97, 61–71.

Csanyi, N., & Toth, C. K. (2007). Improvement of lidar data accuracy using lidar-specific ground targets. Photogrammetric Engineering & Remote Sensing, 73(4), 385–396.

Downing, D. J., & Pettapiece, W. W. (2006). Natural regions and subregions of Alberta (Pub. No. T/852). Government of Alberta Publishing: Edmonton, AB, Canada.

Ekhtari, N., Glennie, C., & Fernandez-Diaz, J. C. (2018). Classification of airborne multispectral lidar point clouds for land cover mapping. IEEE Journal of Selected Topics in Applied Earth Observations and Remote Sensing, 11(6), 2068–2078.

Escobar Villanueva, J. R., Iglesias Martínez, L., & Pérez Montiel, J. I. (2019). DEM generation from fixed-wing UAV imaging and LiDAR-derived ground control points for flood estimations. Sensors, 19(14), 3205.

Flannigan, M., Cantin, A. S., De Groot, W. J., Wotton, M., Newbery, A., & Gowman, L. M. (2013). Global wildland fire season severity in the 21st century. Forest Ecology and Management, 294, 54–61.

Frolking, S., & Roulet, N. T. (2007). Holocene radiative forcing impact of northern peatland carbon accumulation and methane emissions. Global Change Biology, 13(5), 1079–1088.

GeoCue Group. (2017). Control point statistics in TerraScan: TerraScan, versions 002.001 and above. https://support.geocue.com/wp-content/uploads/2017/03/Control-Point-Statistics-in-TerraScan.pdf.

GeoCue Group. (2020). TerraScan ground parameters. https://support.geocue.com/terrascan-ground-filter-parameters/.

Gerrand, S., Aspinall, J., Jensen, T., Hopkinson, C., Collingwood, A., & Chasmer, L. (2021). Partitioning carbon losses from fire combustion in a montane valley, Alberta, Canada. Forest Ecology and Management, 496, 119435.

Goulden, T., & Hopkinson, C. (2010). The forward propagation of integrated system component errors within airborne lidar data. Photogrammetric Engineering & Remote Sensing, 76(5), 589–601.

Goulden, T., & Hopkinson, C. (2014). Mapping simulated error due to terrain slope in airborne lidar observations. International Journal of Remote Sensing, 35(19), 7099–7117.

Goulden, T., Hopkinson, C., Jamieson, R., & Sterling, S. (2016). Sensitivity of DEM, slope, aspect and watershed attributes to LiDAR measurement uncertainty. Remote Sensing of Environment, 179, 23–35.

Hokanson, K. J., Lukenbach, M. C., Devito, K. J., Kettridge, N., Petrone, R. M., & Waddington, J. M. (2016). Groundwater connectivity controls peat burn severity in the boreal plains. Ecohydrology, 9(4), 574–584.

Hopkinson, C., Chasmer, L., Zsigovics, G., Creed, I. F., Sitar, M., Treitz, P., & Maher, R. V. (2004). Errors in lidar ground elevations and wetland vegetation height estimates. International Archives of Photogrammetry, Remote Sensing and Spatial Information Sciences, 36(8), 108–113.

Hopkinson, C., Chasmer, L., Sass, G., Creed, I., Sitar, M., Kalbfleisch, W., & Treitz, P. (2005). Vegetation class dependent errors in lidar ground elevation and canopy height estimates in a boreal wetland environment. Canadian Journal of Remote Sensing, 31(2), 191–206.

Hopkinson, C., Chasmer, L., Gynan, C., Mahoney, C., & Sitar, M. (2016). Multisensor and multispectral lidar characterization and classification of a forest environment. Canadian Journal of Remote Sensing, 42(6), 501–520.

Hudak, A. T., Morgan, P., Bobbitt, M. J., Smith, A. M. S., Lewis, S. A., Lentile, L. B., Robichaud, P. R., Clark, J. T., & McKinley, R. A. (2007). The relationship of multispectral satellite imagery to immediate fire effects. Fire Ecology, 3(1), 64–90.

Institute for Catastrophic Loss Reduction. (2019). Fort McMurray wildfire: Learning from Canada's costliest disaster. Toronto, ON, Canada. https://www.zurichcanada.com/-/media/project/zwp/canada/docs/english/weather/fort-mcmurray-report_canada.pdf

Kasischke, E. S., & Johnstone, J. F. (2005). Variation in postfire organic layer thickness in a black spruce forest complex in interior Alaska and its effects on soil temperature and moisture. Canadian Journal of Forest Research, 35(9), 2164–2177.

Kohlenberg, A. J., Turetsky, M. R., Thompson, D. K., Branfireun, B. A., & Mitchell, C. P. (2018). Controls on boreal peat combustion and resulting emissions of carbon and mercury. Environmental Research Letters, 13(3), 035005.

Lin, S., Liu, Y., & Huang, X. (2021). Climate-induced Arctic-boreal peatland fire and carbon loss in the 21st century. Science of the Total Environment, 796, 148924.

Maune, D., Black, T., & Constance, E. (2007). DEM user requirements. In D. Maune (Ed.), Digital elevation model technologies and applications: The DEM users manual (2nd ed., pp. 449–473). American Society for Photogrammetry and Remote Sensing: Bethesda, MD, USA.

McCarley, T. R., Hudak, A. T., Sparks, A. M., Vaillant, N. M., Meddens, A. J., Trader, L., Francisco, M., Kreitler, J., & Boschetti, L. (2020). Estimating wildfire fuel consumption with multitemporal airborne laser scanning data and demonstrating linkage with MODIS-derived fire radiative energy. Remote Sensing of Environment, 251, 112114.

Mickler, R. A., Welch, D. P., & Bailey, A. D. (2017). Carbon emissions during wildland fire on a North American temperate peatland. Fire Ecology, 13(1), 34–57.

Millard, K., & Richardson, M. (2013). Wetland mapping with LiDAR derivatives, SAR polarimetric decompositions, and LiDAR–SAR fusion using a random forest classifier. Canadian Journal of Remote Sensing, 39(4), 290–307.

Miller, C. A., Benscoter, B. W., & Turetsky, M. R. (2015). The effect of long-term drying associated with experimental drainage and road construction on vegetation composition and productivity in boreal fens. Wetlands Ecology and Management, 23(5), 845–854.

MNP LLP. (2017). A review of the 2016 Horse River wildfire. Forestry Division, Alberta Agriculture and Forestry: Edmonton, AB, Canada. https://www.alberta.ca/assets/documents/Wildfire-MNP-Report.pdf

Morison, M., van Beest, C., Macrae, M., Nwaishi, F., & Petrone, R. (2021). Deeper burning in a boreal fen peatland 1 year post-wildfire accelerates recovery trajectory of carbon dioxide uptake. Ecohydrology, 14(4), e2277.

Moudrý, V., Klápště, P., Fogl, M., Gdulová, K., Barták, V., & Urban, R. (2020). Assessment of LiDAR ground filtering algorithms for determining ground surface of non-natural terrain overgrown with forest and steppe vegetation. Measurement, 150, 107047.

Nelson, K., Thompson, D., Hopkinson, C., Petrone, R., & Chasmer, L. (2021). Peatland–fire interactions: A review of wildland fire feedbacks and interactions in Canadian boreal peatlands. Science of the Total Environment, 769, 145212.

Neugirg, F., Kaiser, A., Schmidt, J., Becht, M., & Haas, F. (2015). Quantification, analysis and modelling of soil erosion on steep slopes using LiDAR and UAV photographs. Proceedings of the International Association of Hydrological Sciences, 367, 51–58.

O'Neil, G. L., Goodall, J. L., & Watson, L. T. (2018). Evaluating the potential for site-specific modification of LiDAR DEM derivatives to improve environmental planning-scale wetland identification using Random Forest classification. Journal of Hydrology, 559, 192–208.

O'Neil, G. L., Saby, L., Band, L. E., & Goodall, J. L. (2019). Effects of LiDAR DEM smoothing and conditioning techniques on a topography-based wetland identification model. Water Resources Research, 55(5), 4343–4363.

Okhrimenko, M., Coburn, C., & Hopkinson, C. (2019). Multispectral lidar: Radiometric calibration, canopy spectral reflectance, and vegetation vertical SVI profiles. Remote Sensing, 11(13), 1556.

Pourali, S., Arrowsmith, C., Chrisman, N., & Matkan, A. (2014). Vertical accuracy assessment of LiDAR ground points using minimum distance approach. In Proceedings of Research Locate 14 (pp. 1–8). Canberra, Australia.

Rapidlasso GmbH. (2021). Lasground_new README. https://lastools.github.io/download /lasground_new_README.txt

Reddy, A. D., Hawbaker, T. J., Wurster, F., Zhu, Z., Ward, S., Newcomb, D., & Murray, R. (2015). Quantifying soil carbon loss and uncertainty from peatland wildfire using multi-temporal LiDAR. Remote Sensing of Environment, 170, 306–316.

Schmid, K. A., Hadley, B. C., & Wijekoon, N. (2011). Vertical accuracy and use of topographic LiDAR data in coastal marshes. Journal of Coastal Research, 27(6A), 116–132.

Terrasolid Ltd. (2021). TerraScan user guide: Batch processing reference > classification routines > points > ground. https://terrasolid.com/guides/tscan/crground.html

Thompson, D. K., & Waddington, J. M. (2014). A Markov chain method for simulating bulk density profiles in boreal peatlands. Geoderma, 232–234, 123–129.

Tinkham, W. T., Smith, A. M., Hoffman, C., Hudak, A. T., Falkowski, M. J., Swanson, M. E., & Gessler, P. E. (2012). Investigating the influence of LiDAR ground surface errors on the utility of derived forest inventories. Canadian Journal of Forest Research, 42(3), 413–422.

Van der Werf, G. R., Randerson, J. T., Giglio, L., Collatz, G. J., Mu, M., Kasibhatla, P. S., Morton, D. C., DeFries, R. S., Jin, Y., & van Leeuwen, T. T. (2010). Global fire

emissions and the contribution of deforestation, savanna, forest, agricultural, and peat fires (1997–2009). Atmospheric Chemistry and Physics, 10(23), 11707–11735.

Walker, X. J., Mack, M. C., & Johnstone, J. F. (2015). Stable carbon isotope analysis reveals widespread drought stress in boreal black spruce forests. Global Change Biology, 21(8), 3102–3113.

Whitman, E., Parisien, M. A., Holsinger, L. M., Park, J., & Parks, S. A. (2020). A method for creating a burn severity atlas: An example from Alberta, Canada. International Journal of Wildland Fire, 29(11), 995–1008.

Yu, Z. C. (2012). Northern peatland carbon stocks and dynamics: A review. Biogeosciences, 9(10), 4071–4085.

CHAPTER 4: PATTERNS AND PREDICTORS OF PEAT COMBUSTION AS INDICATORS OF CARBON LOSS AND FIRE RESILIENCE IN BOREAL PEATLANDS

4.1 Abstract

Canadian boreal peatlands are globally important carbon (C) sinks. However, warming, drying, and changing fire regimes due to climate change threaten the resiliency of these ecosystems, and there is potential for these vast C stores to shift to C sources, releasing C stored over millennia to the atmosphere. During wildland fires in peatlands, the majority of the C loss is from the soil (~80-90%). As such, quantifying depth of peat combustion (depth of burn; DOB) as well as environmental factors that influence this combustion, and thus improving estimates of soil C loss, is essential. However, peatland DOB is still highly uncertain, due to the complex, heterogeneous nature of peatland ecosystems, and a lack of high-resolution spatial DOB data.

In this chapter, pre- and post-fire lidar data are used to quantify spatial variability in DOB across bog, fen, and swamp peatlands and their ecotones that burned during the

2016 Horse River wildfire. DOB averaged 8.1 ± 6.2 cm across the study area, with the greatest burn depths occurring in bog ecotones (9.3 ± 7.3 cm). Fen ecotones exhibited the largest variability in DOB, with small areas of deep combustion. Generalized Additive Models (GAMs) and Random Forest (RF) models were used to identify remotely measurable predictors associated with peat combustion. Model convergence identified the most influential predictors within each peatland type. In bogs, topographic and morphological variables showed the strongest associations with combustion depth; in fens, vegetation and anthropogenic disturbance were most influential; and swamps, peat combustion was predominantly associated with hydrological variables.

4.2 Introduction

Wildland fire is the dominant stand-renewing disturbance and determinant of carbon balance across Canada's boreal (e.g., Stocks et al., 2002; Turetsky et al., 2002; Bond-Lamberty et al., 2007). Boreal peatlands are a critical component of the C sink, storing a disproportionate amount of C in their soils (Gorham, 1991; Turetsky et al., 2015; Vitt & Short, 2020). Peatlands, typically defined as a type of wetland with >40 cm of peat (National Wetlands Working Group, 1997), are optimally structured for C storage. The waterlogged, anaerobic conditions limit decomposition of organic material, allowing it to accumulate as peat (Gorham, 1991; Gower et al., 2001).

Due to climate change and associated warming temperatures, wildland fires in Canada's boreal region have been, and are expected to continue to, increase in size, frequency, and severity (e.g., Flannigan et al., 2009; de Groot et al., 2013; Hanes et al., 2019). Concurrently, peatland ecosystems are experiencing fragmentation (e.g., Vitt & Wieder, 2006), drying and water table declines (Waddington et al., 2012), and increasingly intensive anthropogenic disturbances (Chasmer et al., 2021). Some regions in Canada, such as the Boreal Plains, also exist in a water deficit most years, where potential evapotranspiration exceeds precipitation (Devito et al., 2012), resulting in increased vulnerability of peatlands in this region to projected warming and drying (e.g., Brown et al., 2010). With an increase in fire activity and enhanced susceptibility to drying, there is strong potential for an increase in peat combustion, and subsequently, an increase in soil C loss (e.g., Turetsky et al., 2015). Deep combustion results in the loss of C that has been stored for centuries, potentially resulting in a shift from C sink to source (e.g., Turetsky et al., 2004; Turetsky et al., 2011; Wieder et al., 2009).

The vast majority of C loss from peatlands during wildland fire is from the soil, as opposed to aboveground biomass (e.g., van der Werf et al., 2010) so quantifying the volume of soil combusted, as well as identifying influencing factors, is essential for understanding the fire and climate change resiliency of boreal peatlands, particularly as fire behaviour is influenced by interacting top-down and bottom-up controls that have direct implications for land management and combustion mitigation. However, depth of peat combustion (depth of burn; DOB) is highly variable – ranging from sub-cm singeing to peat profile consumption of over a metre (e.g., Benscoter & Wieder, 2003; Lukenbach et al., 2015) – and driven by numerous, complex and interrelated factors, such as the spatial and temporal distribution of fuel and moisture, and how these vary with geology and topography (e.g., Benscoter & Vitt, 2008; Lukenbach et al., 2015; Nelson et al., 2021; Wilkinson et al., 2018; Chapter 2).

While the variability in depth of peat combustion during wildland fire is an increasing area of study (e.g., Kohlenberg et al., 2018; Wilkinson et al., 2020; Lin et al., 2021; Morison et al., 2021), there is still a lack of high-resolution, spatially continuous data on peatland DOB. Many studies have used field measurements, such as adventitious roots or residual peat depth, to approximate DOB (e.g., Hokanson et al., 2016). While these measurements may be quite accurate at the measurement location, they cannot capture the variability in DOB that occurs between measured trees (surfaces are interpolated), and they are too labour intensive to be spatially continuous, and therefore cannot be representative of a continuum of peatland conditions and burn severities (e.g., Aguilar & Mills, 2008; Thompson & Waddington, 2014; Hokanson et al., 2016). Pre- and post-fire lidar data can be used to generate high-resolution, spatially continuous estimates of DOB across large

extents and across different peatland types (e.g., Chasmer et al., 2017; Nelson et al., 2022; Chapter 3). Measuring DOB across peatland types (bogs, fens, and swamps) and their ecotones is essential for assessing spatial variability in peat combustion. Because peatland types differ in hydrology, vegetation, and topographic morphology, their burn depth distributions are also likely to differ. Insights into variability of DOB can subsequently be utilized to identify environmental drivers of smouldering potential.

Understanding the drivers of DOB is extremely complex (Chapter 2). It is widely recognized that moisture content, water table depth and fluctuations, and bulk density are key determinants of DOB (e.g., Benscoter et al., 2011; Chapter 2), but the influence of each is impacted by complex interacting positive and negative feedbacks associated with other factors. These can be grouped as top-down variables that influence the ecosystem, such as fire weather and atmospheric conditions, or bottom-up variables, that are characteristics of the ecosystem itself, such as peat bulk density, hydrologic connectivity, vegetation structure, and microtopography (e.g., Nelson et al., 2021; Chapter 2). Bulk density, water table depth, and soil moisture content are also typically field-measured variables and are not available across large spatial scales or timeframes, making them impractical for assessing combustion potential across a landscape. In contrast, remotely measured variables such as lidar-derived vegetation structural metrics, optical vegetation and moisture indices, and DEM-derived topographic and hydrological layers can be used as spatially continuous proxies for underlying ecohydrological conditions. Consequently, identifying readily measurable, spatially continuous variables such as topographic indices, canopy structure, and vegetation health, which may be indicative of underlying

environmental processes, can be explored as direct or indirect influencing factors on the hydrophysical properties of peat.

This study utilizes pre- and post-fire airborne lidar data from the 2016 Horse River Wildfire in the Boreal Plains ecozone to quantify spatial variability in depth of peat combustion across bogs, fens, swamps, and their ecozones. It uses statistical modelling techniques (Generalized Additive Models (GAMs) and Random Forest (RF) models) to improve understanding of relationships between environmental conditions and DOB. Specifically, this study addresses the following questions:

1) What is the average depth of peat combustion in bogs, fens, swamps, and their ecotones, and how does this vary within, and between, peatland types?
2) Which remotely measurable (non-field based) variables are most strongly associated with variation in depth of peat burn, after accounting for covariation among predictors, and are these variables similarly important across bogs, fens, and swamps?
3) What is the relative importance of top-down (e.g., fire weather indices) versus bottom-up (e.g., hydrology, topography, vegetation) variables associated with peat combustion within the study area?
4) How much of the spatial variability in depth of burn is explained by the predictive variables identified in (2)?

4.3 Methods

4.3.1 Study Area

This study was conducted within a 5 x 25 km area ~30 km south of Fort McMurray, AB (Figure 4.1), in the Boreal Plains ecozone. Average annual temperature in the area is ~1°C (Elmes & Price, 2019). The climate is subhumid, with potential evapotranspiration (PET) frequently exceeding precipitation, leading to moisture deficits most years (Marshall et al., 1999; Devito et al., 2005). The western region of the Boreal Plains are underlain by thick glacial deposits (Ireson et al., 2015) and soils are predominantly gray luvisols, gleysols or organic in the uplands, and organic in the lowlands with peat depths >40 cm in peatlands (Bourgeau-Chavez et al., 2020; Jean et al., 2020). Uplands are dominated by jack pine (*Pinus banksiana*), black spruce (*Picea mariana*), white spruce (*Picea glauca*) and trembling aspen (*Populus tremuloides*), interspersed with eastern larch (*Larix laricina*; e.g., Lee & Boutin, 2004) with black spruce and tamarack dominating the lowlands (Wilkinson et al., 2019; Bourgeau-Chavez et al., 2020). Fire disturbance is common in the region, historically recurring on average every ~40 to 100 years depending on stand species dominance (Larsen, 1997). The region contains extensive roads, seismic lines, cutlines, and industrial infrastructure such as oil and gas well sites and extensive open pit mines north of the city (Abib et al., 2019; Dabros et al., 2022).

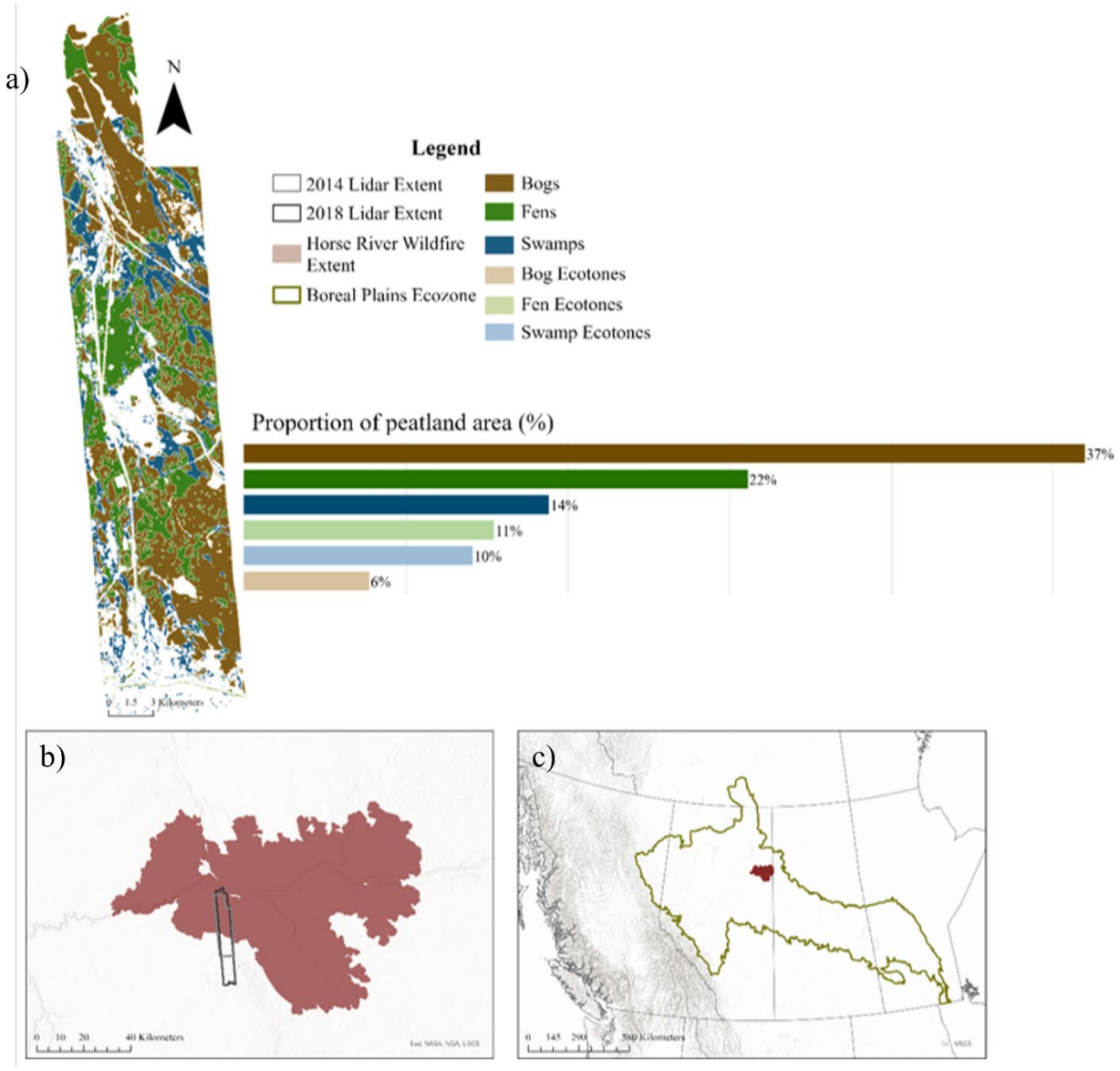

Figure 4.1. Study area location (a) within the Horse River Wildfire extent (b) in the Boreal Plains ecozone (c). The main panel shows the study area with classified peatland extents derived from Bourgeau-Chavez et al. (2017), the proportion of which (peatland/ecotone type of total peatland area) are summarized in the bar chart.

Approximately 38% of Alberta's boreal is made up of wetlands, with some areas upwards of 85-95%; 56% of these are peatlands (Ducks Unlimited, 2017). Within the study area, approximately 43% of the peatlands are bogs, 33% are fens, and 24% are swamps. Bogs are considered ombrogenous and ombrotrophic, hydrologically isolated from surrounding ground water, receiving water exclusively from precipitation (Vitt, 2006).

They tend to be poor in nutrients and highly acidic (Vitt, 2006). Fens and swamps, on the other hand, are geogenous and minerotrophic, and are connected to the surrounding ground and surface water, typically increasing their nutrients and pH (Locky et al., 2005; Vitt, 2006). While swamps may exist as mineral wetlands or peatlands, they were included as a peatland class, as they are known to support peat accumulation. DOB analyses were applied only to areas with detectable organic layer combustion, such that mineral swamps did not contribute to findings.

On May 1, 2016, the Horse River Wildfire ignited ~7 km southwest of Fort McMurray and burned for over a year as smouldering combustion (Kovacs et al., 2019), burning over 589,000 hectares (Natural Resources Canada, 2017). Prior to ignition, high air temperatures (>25°C), low relative humidity (<20%), and high wind speeds provided ideal conditions for fire ignition and spread (Elmes et al., 2018; Alberta Agriculture and Forestry & MNP, 2017). Initial spread was rapid, with temperatures and wind speeds rising, relative humidity decreasing, and dry vegetation that had yet to flush (Kochtubajda et al., 2017). The study area itself burned from May 4 to May 16 (Alberta Agriculture and Forestry & MNP, 2017).

4.3.2 Data Acquisition

4.3.2.1 Field Data

Field data were collected coincident to post-fire airborne lidar data collection (described in section 2.2.2), in July 2018 for calibration and validation purposes. To select sample sites, the study area was first stratified into scales of influence: a) burned versus non-burned areas within and proximal to the Horse River wildfire; b) within burned areas, different

classes of burn severity (minimum, medium, and severe) determined from optical remote sensing imagery and on-the-ground assessments; and, c) peatland type (treed and open bogs; rich and poor fens) determined from pre-fire, optical remote sensing imagery and on-the-ground assessments. Sample sites included 18 burned and six unburned peatlands. Transects ~30 m in length were placed such that they ran from transition zone into the peatland middles, with Global Navigation Satellite System (GNSS) stations at the beginning and end of each transect left to run for >1 hr. Plots were placed along the transect at one-and two-meter intervals in burned and unburned sites, respectively. To validate ground surface elevations along the transect, level measurements were taken at each plot location and later referenced to the GNSS station elevations. This resulted in 708 ground surface elevation measurements to be used for the validation of lidar data. Two road surfaces were also used for the calibration and validation of lidar data, along which Post Processed Kinematic (PPK) GNSS elevation measurements were collected (n=2655) to ensure the elevational accuracy of airborne lidar data in areas of flat terrain without any overstory canopy influences on ground surface elevation (Hopkinson et al., 2005; Csanyi & Toth, 2007).

4.3.2.2 Lidar Data

Pre-fire lidar data was acquired from Airborne Imaging Inc. (Canada). It was collected using a Leica ALS70 (Leica Geosystems, Switzerland) in May of 2014 at a flying height of 1550 m. Flightline overlap was 50%, scan angles were ±25 degrees, and pulse repetition frequency was 300 kHz, producing data with a point density of 7.2 points m^{-2}. Post-fire lidar data were collected by the University of Lethbridge ARTeMiS Lab with a Titan multispectral lidar (Teledyne Optech Inc., Canada). Flights were conducted in July of 2018

at a flying height of 1000 m. Flightline overlap was 50%, scan angles were ±25 degrees, and pulse repetition frequency was 300 kHz. The Titan collects multispectral data at three emission wavelengths: 532 nm, 1064 nm, and 1550 nm. The resulting point density was 11.1 points m^{-2}. Total overlapping coverage was ~123 km^2.

4.3.2.3 Other Geospatial Data

Peatlands were mapped using the classification from Bourgeau-Chavez et al. (2017), which segregates land cover into wetland classes: bog, open fen, treed fen, swamp, and marsh; upland classes: deciduous forest and coniferous forest; and other classes: water, barren/logged, and recently-burned, with 93% overall accuracy. Using this classification as a base, bogs, fens, and swamp edges were manually adjusted to smooth boundaries and eliminate obvious classification errors (i.e. over a road or a single pixel of classified fen within a large bog region), etc. Ecotones were delineated around each peatland boundary using the changes in tree height and surface elevation as distance from peatland increased (Jones et al. 2024).

Anthropogenic landscape features including cutlines (Alberta Geospatial Services, 2021) and roads (Natural Resources Canada, 2016) were added to the map, and missing cutlines, roads, industrial infrastructure, industrial water features, and large seismic lines were manually delineated. Spatially explicit fire weather data (described in detail in section 2.3.3), including day of flaming front, Fire Weather Index (FWI), Fine Fuel Moisture Code (FFMC), Duff Moisture Code (DMC), Drought Code (DC), Initial Spread Index (ISI), and Buildup index (BUI), were provided by Natural Resources Canada, using weather estimated from ERA5-Land. Pre-fire Landsat 8 OLI scenes from April, 2016 were downloaded in red, green, near-infrared (NIR), and shortwave infrared (SWIR; Landsat-8

data courtesy of the U.S. Geological Survey) for the calculation of vegetation and wetness indices. A 25 m, hydrologically corrected DEM (Government of Alberta, 2018) was used to calculate topographic wetness index and flow accumulation. This was selected instead of the higher resolution lidar elevation data to avoid edge effects within the study area that could drastically alter hydrological flows if broader watershed context is lacking.

4.3.3 Data Processing & Analysis

4.3.3.1 Lidar Data Processing

Using Bentley Microstation TerraSolid Terrascan software version 021.011 (Terrasolid, Helsinki, Finland; Axelsson, 2000), pre- and post-fire lidar datasets were co-registered to the road surface as measured with the PPK GNSS survey, such that there was no mean offset between either lidar data set with the calibration points (Csanyi & Toth, 2007), minimizing potential bias. Isolated points were removed, and points were classified into ground or non-ground (vegetation) using the optimal wavelengths (2018 data only) and classification parameters that Chapter 3 (Nelson et al., 2022) identified as producing the most accurate ground classifications.

Pre- and post-fire digital terrain models (DTMs) at 1 m resolution were created from ground points using las2dem from LAStools (RapidLasso GmbH, Germany). Pre-fire canopy closure and vegetation structure metrics (section 2.3.3) were created using lascanopy from LAStools, at resolutions of 1 m (closure) and 20 m (height metrics). Vegetation structure metrics were processed at a lower resolution to ensure enough laser returns within a pixel to calculate height metrics such as skew, kurtosis, and percentiles.

4.3.3.2 GIS Analyses

All spatial analyses were conducted in ArcGIS Pro (Esri, California, U.S.). Depth of peat burn was determined by differencing the pre- and post-fire DTMs to generate an elevation change raster at 1 m resolution. To reduce inherent, fine-scale noise in the lidar data, this raster was aggregated by the mean to 5 m pixels (25 m^2). This approach will result in a conservative estimate of depth of burn, as pixels with positive elevation differences (whether due to noise or post-fire peat expansion) pull the aggregated mean elevation difference upwards towards zero. This will reduce the influence of any potential very small (<25 m^2), deep areas of combustion; however, it produces a more reliable estimate of elevation difference by reducing the likelihood that lidar elevation noise is amplified and misinterpreted as depth of burn. Following data aggregation, any pixel with an elevation change greater than zero (reflecting elevation increase/surface growth) was set to "no data," such that areas that did not burn were not included in the depth of burn analysis. A second layer was created in which any pixel within the fire perimeter with an elevation change greater than zero was set to zero, to be used in driver analysis. These are important to include for the examination of drivers of depth of burn, as it allowed for the analysis of factors that impacted why a pixel did not burn.

Vegetation canopy closure metrics were also aggregated to a 5 m pixel resolution. Landsat-8 data were used to calculate the Normalized Difference Vegetation Index (NDVI; eq. 4.1), the Normalized Difference Moisture Index (NDMI; eq. 4.2), and the Modified Normalized Difference Water Index (MNDWI; eq. 4.3). The 2014 DTM was used to determine three topographic metrics: slope, aspect, and Topographic Position Index (TPI).

TWI and flow accumulation were calculated using the 25 m resolution DEM from the Government of Alberta (2018).

(4.1)

(4.2)

(4.3)

Random points were distributed using a clustered, stratified random sampling design within each peatland class: bogs (n=2906), fens (n=3552), and swamps (n=3216). Five points were dispersed within each peatland to ensure point density to test for the influence of individual peatland on depth of burn. To improve spatial distribution, additional 1000 points per peatland class were randomly dispersed across all peatlands within that class. Distances were calculated from each point to: edge of the peatland, nearest road, nearest seismic line, nearest cutline, nearest source of industrial water, nearest industrial landmark, nearest hydrological linear feature, and Gregoire Lake (the nearest natural water body) to determine the influence of linear anthropogenic features and natural water bodies on peat combustion. Depth of burn, vegetation canopy and height metrics, vegetation and water indices, fire weather metrics, and topographic metrics were also extracted at each point.

4.3.3.3 Variable Selection and Extraction

Eighty-four potential predictive variables for depth of peat burn were examined (Table 4.1). Canopy cover and vegetation structural characteristics were assessed, as these may influence peat combustion in several different ways, including impacting hydrology (e.g.,

Nelson et al., 2021; Waddington et al., 2015; Chapter 2), ground cover vegetation (i.e. Sphagnum vs. feathermoss; e.g., Nelson et al., 2021; Wilkinson et al., 2018; Chapter 2), and how fire moves through a landscape (e.g., Hakkenberg et al., 2024). Topographic attributes at various scales were considered in the model, including aspect; slope; TWI, an index representing slope and upstream area (e.g., Sörensen et al., 2006); TPI, a representation of relative elevation; and flow accumulation, a value weighted based on upslope area (Esri, n.d.). These metrics can also influence vegetation composition and structure (Moeslund et al., 2013), hydrology (e.g., Chen & Kumar, 2001), and local energy balance (e.g., Arnold et al., 2006). Landsat NDVI indicates vegetation density, understory in open canopies, and vegetation health (e.g., Mehmood et al., 2024); NDWI is indicative of vegetation moisture content (Gao, 1996), and MNDWI can be used to identify wet areas (e.g., Ali et al., 2019), all of which are factors in fire behaviour. Distance to anthropogenic features, including roads, cutlines, seismic lines, and industrial sites, as well as distance to water bodies, were included, as these can alter hydrologic flows (e.g., Petrone et al., 2008; Lovitt et al., 2018), energy balance (e.g., Groot et al., 1997), and vegetation (e.g., Ficken et al., 2019; Chasmer et al., 2021). Distance from peatland edge, peatland area, and peatland edge length were included, as peatland edges, as well as smaller, more segmented peatlands may burn more deeply than peatland middles and large peatland complexes (e.g., Hokanson et al., 2016). Several fire weather indices were included, representing conditions on the day that each pixel burned. Day of burn was explored as a random effect, to determine whether there were differences in depth of burn by day that were not captured by fire weather indices. The Drought Code (DC), Duff Moisture Code (DMC), and Fine Fuel Moisture Code (FFMC) are all soil moisture content ratings – the FFMC represents

the moisture content of litter and fine surface fuels, the DMC the moisture content of upper, looser soil immediately below the surface litter (~7 cm depth), and the DC that of the more compact, deeper soil (~18 cm depth; Van Wagner, 1987; de Groot et al., 2009). Although developed for upland soils, these indices are likely to function well for peatlands (Waddington et al., 2012). The Initial Spread Index (ISI) estimates fire spread based on wind speed and fuel moisture, and the Buildup Index (BUI) estimates the fuel available for combustion (Van Wagner, 1987). The Fire Weather Index (FWI) is based on these components and rates the likely intensity of the fire (Van Wagner, 1987; Lawson & Armitage, 2008). Latitude and longitude were included to absorb residual spatial autocorrelation of other covariates (see 4.3.3.4 and 4.3.3.5), but were not considered as ecological predictors in final models.

Table 4.1. Variables included in initial depth of burn models. All continuous variables were treated as floating-point numbers in modelling workflows.

Category	Variables	Scales/height thresholds (m)
Canopy cover (lidar; 5 m)	Canopy cover	Min. height cutoffs: 1.37 (DBH), 5, 10
Vegetation structure distribution (lidar; 20 m)	Mean height, max height, P25–P95, skewness, kurtosis, SD	Min. height cutoffs: 0.2, 0.5, 1.37, 5
Topography (lidar DEM; 5 m)	Slope, aspect, TPI	Scales: 5–500 m (varies by metric)
Hydrology (AB DEM; 25 m)	Flow accumulation, TWI	Scales: 25–250 m
Landscape positioning	Distance to nearest: peatland edge, road, seismic line, cut line, industrial site, industrial water source, linear hydrological feature, Gregoire Lake	—
Peatland morphology	Area, perimeter length, length:area ratio	—
Fire weather indices	FWI, FFMC, DMC, DC, BUI, ISI, Day of Burn	Scale: 90 m
Vegetation & moisture indices	NDVI, NDMI, MNDWI	Scale: 30 m

4.3.3.4 GAM Analysis

To examine potential environmental conditions associated with peatland depth of burn, Generalized Additive Models (GAMs; mgcv package in R v4.4.2; Wood, 2024; R Core Team, 2025) were fit separately for bogs, fens, and swamps. GAMs are widely used in ecological modelling to understand the nonlinear relationships between predictive and response variables using smooth functions, without the criteria of linearity (e.g., Wood, 2017; Pedersen et al., 2019). Models were developed using a Tweedie distribution with a log link, which functions well for modelling positive, continuous data with a large proportion of zeros (Dunn & Smyth, 2005), such as biomass data (e.g., Lecomte et al.,

2013; Dons et al., 2016). This allowed for the use of a single likelihood model that identifies covariate effects that influence both occurrence and magnitude of DOB, as opposed to a two-part model. Smoothing parameters were selected using restricted maximum likelihood (REML) to avoid undersmoothing (Pedersen et al., 2019; Wood, 2022). Predictive variables were modelled using predominantly thin plate regression splines (tp) but using cyclic cubic splines (cc) for aspect, Gaussian process smooths (gp) that assume increased correlation with closer proximity for spatial coordinates, and tensor product smooths (te) for interaction terms (Wood, 2017). Continuous predictive variables were log-transformed or rescaled when highly skewed or were orders of magnitude larger than other predictors.

Variable selection was performed using an initial shrinkage approach that adds an extra penalty to each term, effectively selecting smooths with negligible influence out of the model (Marra & Wood, 2011). This was applied to all 84 potential drivers (Table S4.1), followed by iterative backwards selection. Following the shrinkage approach, variables with negligible effective degrees of freedom (< 0.001) were removed from the model, after which variables were removed iteratively based on low effective degrees of freedom, high p-values, and flat (null) smooth functions when visualized using the mgcv draw() function (Marra & Wood, 2011; Wood, 2022). When multiple variables showed similar candidacy for removal, all options were evaluated, and backwards selection was outlined by deviance explained and Akaike information criterion (AIC). In cases where removal produced only minimal reductions in model performance, that variable was occasionally removed to simplify model structure and highlight the most influential predictive variables. Concurvity was assessed using the concurvity() function, and highly concurved variables (>0.7) were

selected out of the model to improve stability (Wood, 2017). Once core variables were identified, plausible interactions were tested and were added to the model if significant and if they improved the deviance explained and reduced AIC. Latitude and longitude were retained throughout variable selection to account for residual spatial autocorrelation (Wood, 2017) and reduce the likelihood of spatial proxy variables being retained. Suitability of basis dimensions was assessed using gam.check(), and final drivers included in the model were determined based on R^2, deviance explained, and AIC. Full model evaluation details are provided in section 4.3.3.6.

4.3.3.5 Random Forest & SHAP Value Analysis

To increase the robustness in identifying environmental conditions associated with peat depth of burn, Random Forest (RF) regression models were fitted in addition to the GAMs using Python scikit-learn v1.3.0 (Pedregosa et al., 2011). RF regression can model nonlinear relationships and interactions between variables to relate numerous predictive variables to a response variable (e.g., Breiman, 2001). To assess the relative importance of predictors, variable importance was quantified using SHAP (SHapley Additive exPlanations) values (SHAP Python package v0.48.0; e.g., Lundberg & Lee, 2017). SHAP estimates the individual variable contribution of each explanatory variable to a model output based on cooperative game theory. Using the absolute average Shapley values per variable provides a ranking of variable contribution (Molnar, 2022). These were computed using TreeSHAP, a path-dependent SHAP implementation for tree-based machine learning models (Lundberg et al., 2019; Molnar, 2022). A flow diagram illustrating variable selection for final bog, fen, and swamp RF models is shown in Figure 4.2.

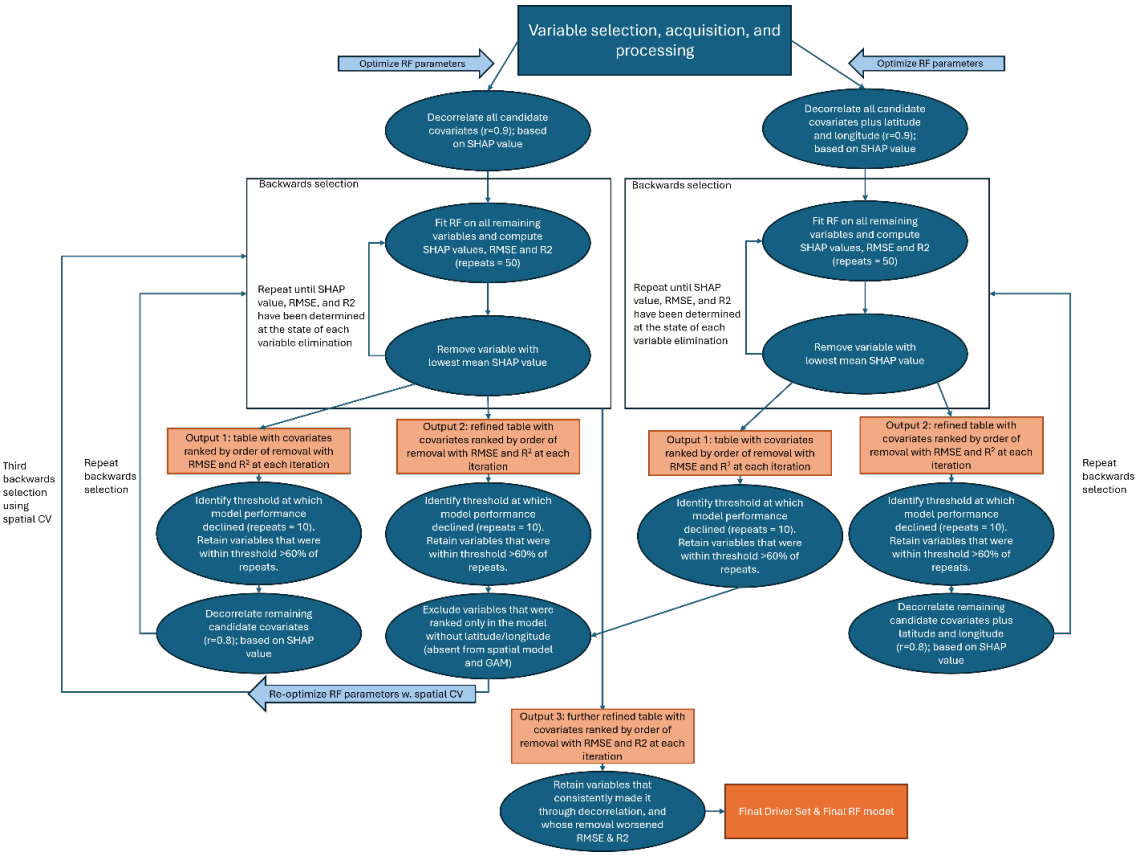

Figure 4.2. Flow diagram illustrating variable selection for final RF model as described in section 2.3.5. Processes are indicated in blue ovals and outputs are indicated with orange rectangles. This process was repeated for each peatland type: bogs, fens, and swamps.

Initial RF parameters were optimized using RandomizedSearchCV on 80:20 split training data with 5-fold cross-validation (Table S4.3). Thirty combinations were evaluated, and optimal parameters were selected – first based on the lowest RMSE, and second, based on the highest R^2. While RF is generally robust to correlation between predictors (e.g., Albertini et al., 2024), highly correlated variables may split their importance or become unstable in rankings (e.g., Nicodemus, 2011). To minimize this, an initial decorrelation was performed at r = 0.9, with the metric with a higher SHAP value of each pair retained.

RF models were fit using the decorrelated predictors, and absolute mean SHAP values were computed for each variable. An iterative backward selection followed, in which the variable with the lowest mean SHAP value was removed, RF was re-trained, and the process was repeated. To improve stability, RF models were trained 50 times at each step of feature elimination (five grouped 80:20 splits across ten base seeds) to determine average SHAP value, RMSE, and R^2. This process was repeated until all variables were removed, allowing changes in RMSE and R^2 to be tracked sequentially with each variable removal. These analyses were conducted twice, once including the latitude and longitude of sample points and once excluding them, to identify spatial proxy variables. A survival table approach was used to identify the threshold at which the removal of variables began to reduce model performance across the ten base seeds. Variables that were included below the "elbow" at least 60% of the time were retained. Datasets including and excluding latitude/longitude were assessed independently.

A second round of backwards selection was conducted using the reduced-variable model following the same procedure as round one, but with a stricter decorrelation threshold ($r = 0.8$). Survival tables were again used to retain top variables, ranked based on SHAP values, and to compare variable rankings between the models that included latitude/longitude and those that excluded them. Variables that were highly ranked only in the model without latitude/longitude but were absent from both the model including latitude/longitude, as well as the final GAM, were identified as spatial proxies and removed.

Once the predictor set was reduced and identified spatial proxies were removed, spatial cross-validation was implemented in place of random cross-validation to reduce

spatial correlation and prevent overly optimistic model performance metrics (e.g., Schratz et al., 2019; Ploton et al., 2020; Risk & James, 2022). RF parameters were re-tuned using the reduced predictor set following the second round of feature elimination (Table S4.3). Parameters were optimized using RandomizedSearchCV with spatial cross-validation (GroupKFold; k=5; e.g., Schratz et al., 2019). In total, 120 combinations across three independent base seeds were evaluated and ranked by mean cross-validated RMSE (see Table S4.4 for final parameterizations). A final variable elimination run was performed (again, 50 times across ten base seeds), on only non-spatial models with a decorrelation threshold of r=0.8 and using spatial CV to compute performance metrics. Variables that rarely made it through decorrelation, or whose elimination negligibly or minimally worsened RMSE and R^2, were removed. The remaining variables were identified as the predictors most strongly associated with depth of burn and were included in the final model.

4.3.3.6 Statistical Analyses and Model Evaluations

To identify patterns in DOB with and between peatlands, significant differences between peatland types were determined via a Kruskal-Wallis test, which compares medians between groups, and post-hoc Dunn's tests to identify possible pairwise differences. Because of the skewed data structure, to better understand significant differences in means between peatland types, bootstrapped confidence intervals of means were used to determine significant differences at the 95% confidence level. To test for significant variability within a peatland or ecotone type, Fligner-Killeen tests, which compare variances between sample groups, were performed.

To evaluate the reliability of lidar-derived DOB measurements, total elevation change (positive and negative) was calculated within the fire perimeter and in unburned peatlands outside the fire perimeter. Average changes in elevation in known unburned peatlands were used as a basis for approximating expected elevation changes in unburned pixels within the fire perimeter. The proportions of burned and unburned pixels within the fire perimeter were determined based on DOB > 0 cm and were used as weights to calculate the expected weighted average of change in elevation within the fire perimeter. Comparing the expected change in elevation based on weighted averages of burned pixels and unburned pixels from outside the fire with observed mean elevation changes across all pixels (burned and unburned) within the fire perimeter provided a confidence assessment of lidar-derived DOB estimates.

GAM variable importance was calculated based on hierarchical partitioning of deviance with the gam.hp() package in R (Lai et al., 2024). RF variable importance was based on absolute average SHAP values run on the entire model over ten seeds. Variables were summarized based on ecological categories, and variables and variable ranks were compared a) between peatland types within each model framework, and b) between models to identify the most robust drivers. By using GAMs as the primary framework for variable selection and interpretation, and RF as a complementary method for filling gaps and providing an independent validation of the GAM findings, predictive variables most strongly associated with DOB were more confidently identified.

While the aim of this study was not to develop a predictive model, model performance was evaluated to understand the strength of the identified drivers. GAM performance was determined for two models per peatland type – one that included a spatial

smooth (section 2.3.4) and one without. Performance was based on deviance explained and adjusted R^2, which are computed by the summary() function of mgcv (Wood, 2017). RF model performance was evaluated using an 80:20 blocked train/test split with 50 m blocks. While this block size does not eliminate spatial autocorrelation, it reduces immediate neighbourhood effects while retaining fine-scale ecological gradients and variability within the limited study area. Given the small area, clustered samples, zero inflation, and non-linear link relationships, large blocks were not feasible and likely over-pessimistic (Roberts et al., 2017). R^2, Root Mean Square Error (RMSE), and variable importance rank were derived, and the process was repeated 100 times (10 times per base seed) to ensure stability in performance metrics and rank. To ensure variable importance rank was not due to local proximity, a compatible variable rank analysis was performed using 200 m blocks with one seed and compared.

Within each model, predictive variables were compared between peatland types. For a fairer comparison, variables that were tested at multiple scales were divided into local (<50 m), stand (<300 m), and landscape scales (300-500 m) – for example, TPI at 10 m, 20 m and 30 m were considered a shared, local predictor if one of the three was present. Predictive variables were also categorized as related to anthropogenic disturbance, climate/fuel moisture, fuel structure (lidar), hydrology, peatland morphology, topography, or vegetation (spectral). These categories were used to assess dominant, broad patterns in the variables associated with DOB across peatland types. Both individual predictors and predictor categories were compared between models.

4.4 Results

4.4.1 Depth of Burn Across Peatland and Ecotone Types

Average DOB across all peatland types was 8.1 ± 6.2 cm (n = 6813), with bog ecotones showing the greatest mean DOB (9.3 ± 7.3 cm) and fens the lowest (7.0 ± 5.2 cm; Figure 4.3; Figure 4.4; Table 4.2). A Kruskal-Wallis test revealed significant differences between groups (H = 109.24, p < 0.001). Post-hoc Dunn's tests showed that bog cores and bog ecotones differed significantly from fen and swamp cores and ecotones (p <0.05; Table 4.2).

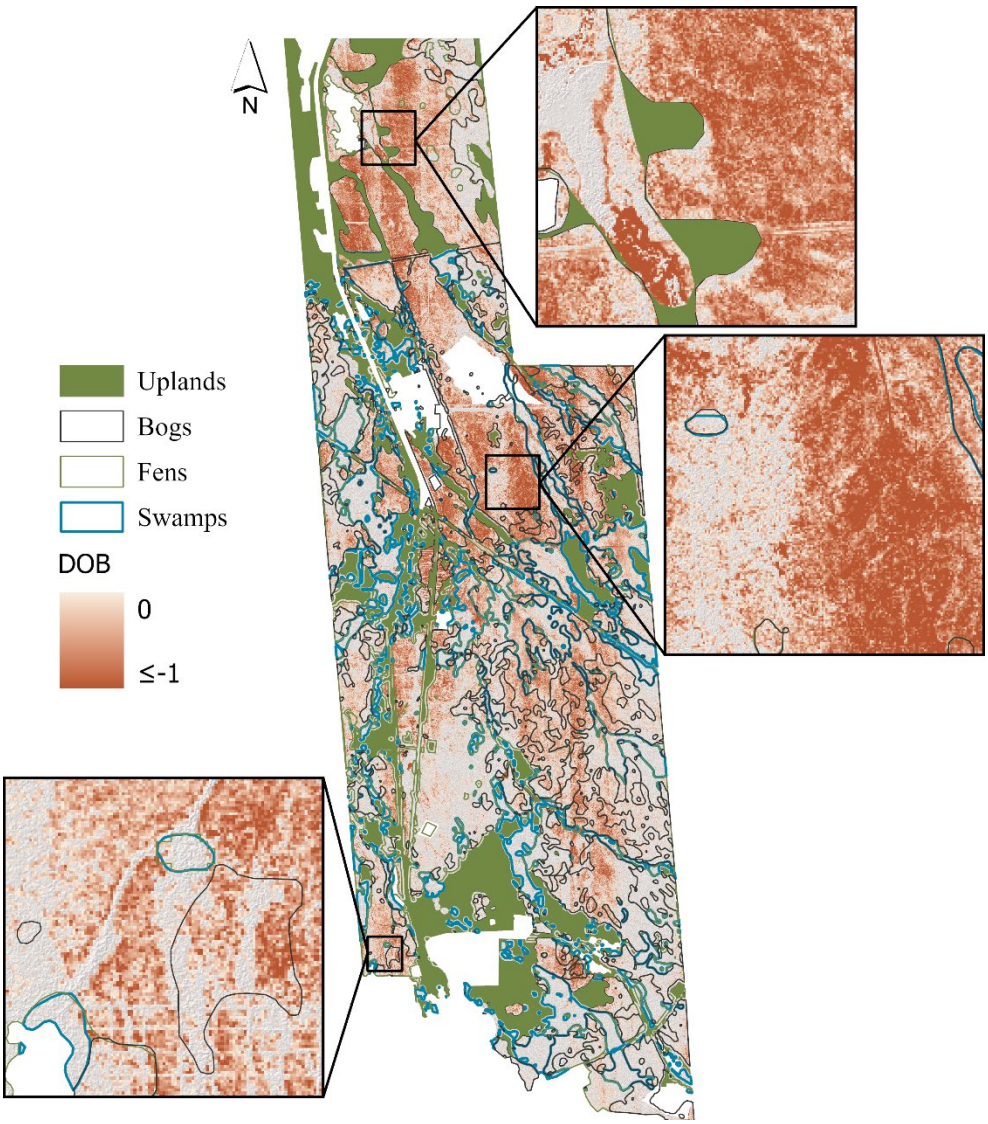

Figure 4.3. Lidar-derived depth of peat burn across the study area with peatlands delineated by type.

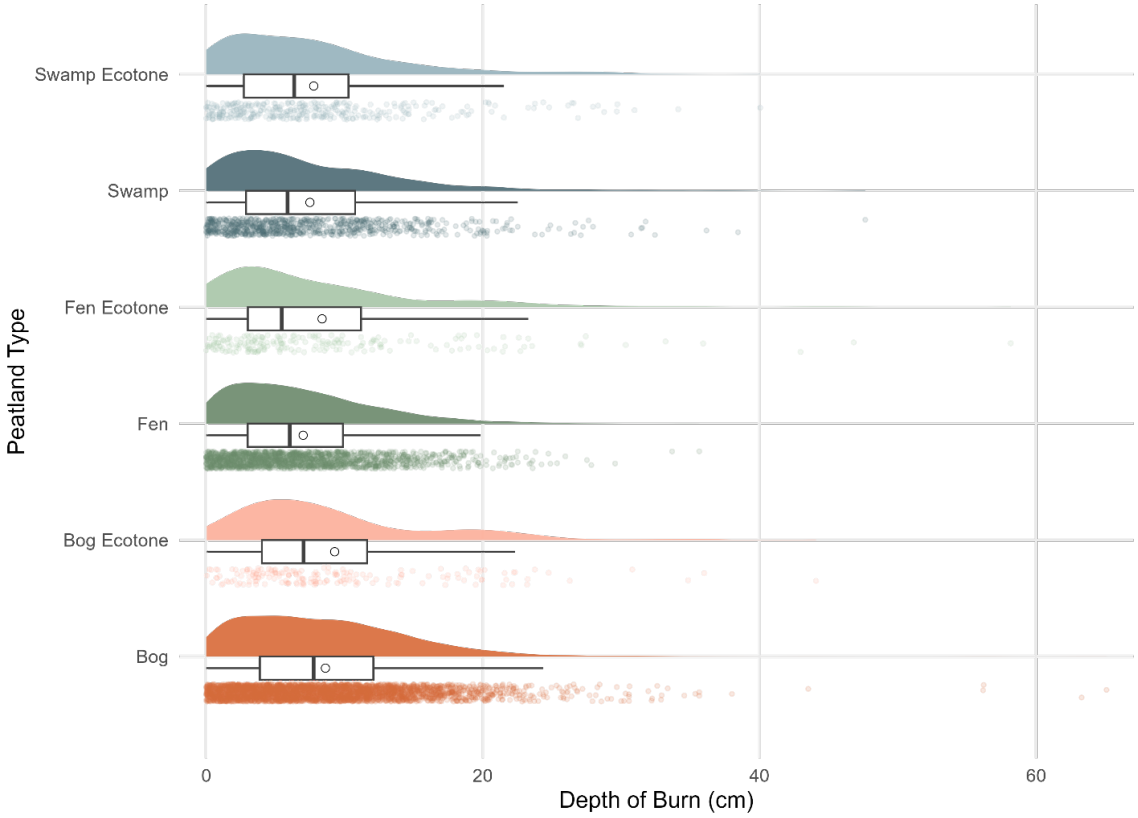

Figure 4.4. Raincloud plots showing depth of burn distributions across peatland types and their ecotones (n=184 to 3581). Half violins show kernel density estimates; boxplots represent the interquartile range and median with whiskers to the 5th and 95th percentiles, and circles denoting the mean; points illustrate sample density distribution.

Table 4.2. Mean, median, and standard deviation of depth of peat burn (cm) across peatland and ecotone types. Connecting lines indicate significantly different ($p < 0.05$) depths of burn based on Dunn's tests (median) or bootstrapping (mean).

Peatland Type	Mean	Median	Standard Deviation
Bog	8.6	7.8	6.2
Bog Ecotone	9.3	7.0	7.3
Fen	7.0	6.0	5.2
Fen Ecotone	8.4	5.5	8.6
Swamp	7.5	5.9	6.3
Swamp Ecotone	7.8	6.4	6.7

Because observed means diverged from the medians (Figure 4.4), bootstrapped confidence intervals of the means were used to identify significant differences in mean DOB. Outcomes were mostly aligned, with two differences: they identified significant

differences in mean DOB between fens and fen ecotones, and no significant difference between bogs and fen ecotones (95% confidence interval; Table 4.2). These differences highlight the influence of deep burning in a small proportion of fen ecotone samples, increasing the mean, despite a lower median (Table 4.2). This high variability in fen ecotones was confirmed by significant variance when compared to fen cores (Fligner-Killeen, med $\chi^2 = 10.7$, $p < 0.01$); bog and swamp core-ecotone pairs did not differ significantly in variance ($p > 0.05$). While observed DOB values were greater in ecotones than corresponding cores, they were non-significant in bogs and swamps ($p > 0.05$).

Proportions of peatland burned (based on lidar-derived DOB) were used as weights to determine the expected difference in elevation (*dz*) of peatlands within the fire perimeter. Lidar-derived mean elevation changes within the burn perimeter aligned well with what would be expected based on weighted averages using offsets from unburned peatlands outside the burn perimeter as controlled "no combustion" pixels (Table 4.3). Average elevation changes within the burned perimeter deviated from expected based on weighted averages by 0.2 cm in bogs, 0.1 cm in fens, and 1.2 cm in swamps. When simply subtracted without accounting for proportions of burned vs unburned area, elevation changes within the burned perimeter were lower than may be expected by 2.3 cm in bogs, 1.2 cm in fens, and 2.0 cm in swamps (Table 4.3).

Table 4.3. Comparison of observed versus expected elevation changes (cm) based on mean elevation changes inside and outside the fire perimeter.

	Obs. DOB (neg. *dz* only)	Weight (burned pixels)	Obs. net *dz* outside fire perimeter	Weight (unburned pixels)	Obs. net *dz* within fire perimeter	Expected net *dz* based on weighted averages	Weighted difference (Straight subtraction)
Bog	-8.6	0.62	9.3	0.38	-1.6	-1.8	+0.2 (+2.3)
Fen	-7.0	0.45	11.1	0.55	2.9	3.0	+0.1 (+1.2)
Swamp	-7.5	0.34	17.0	0.66	7.5	8.7	+1.2 (+2.0)

4.4.2 GAMs: Top Predictive Variables Associated with Depth of Peat Burn and Model Performance

4.4.2.1 Bogs

The covariates selected via backwards selection for the bog GAM included slope at 10 and 100 m resolutions, TPI (100 m), aspect (100 m), distance to peatland edge, distance to industrial water, vegetation structure (p50, p25 and standard deviation), peatland area (m^2), peatland perimeter length (m), and DMC. Two significant interactions were identified: distance to peatland edge and peatland area, and TPI and distance to linear hydrological features. Complete model structure and parameters are included in Supplementary Data. Diagnostic checks from gam.check() showed no systematic biases. A QQ plot showed residuals closely followed expected quantiles, with only slight deviations at the tails, and a residuals vs. linear predictor plot showed even scatter, indicating that the data structure is captured well by the smooth terms in the model (Figure S4.3).

Most variables included in the model were highly significant ($p < 0.001$), with the exception of distance to peatland edge (m), which was significant at $p < 0.01$; distance to industrial water (m) and peatland area (m^2), which were moderately significant ($p < 0.05$); and peatland perimeter length (m), which was non-significant ($p > 0.05$), but still improved model performance based on R^2, deviance explained, and AIC. When a spatial smooth was included in the model, essential for preventing spatial autocorrelation from influencing variable importance, the bog model resulted in 39% deviance explained and an adjusted R^2 of 0.36. When the spatial smooth is excluded from the model, deviance explained drops to 24.3% with an adjusted R^2 of 0.23.

Three covariates accounted for over 50% of the model's explanatory power (Figure 4.5; Table S4.4): slope (100 m resolution), distance to peatland edge (m), and peatland area (m^2). Together with aspect (100 m) and median height of above-ground lidar returns(p50), these top five variables explain ~75% of the variation in depth of burn captured by this model. Topography and peatland morphology covariates were the most influential predictors of DOB in bogs (Figure 4.5).

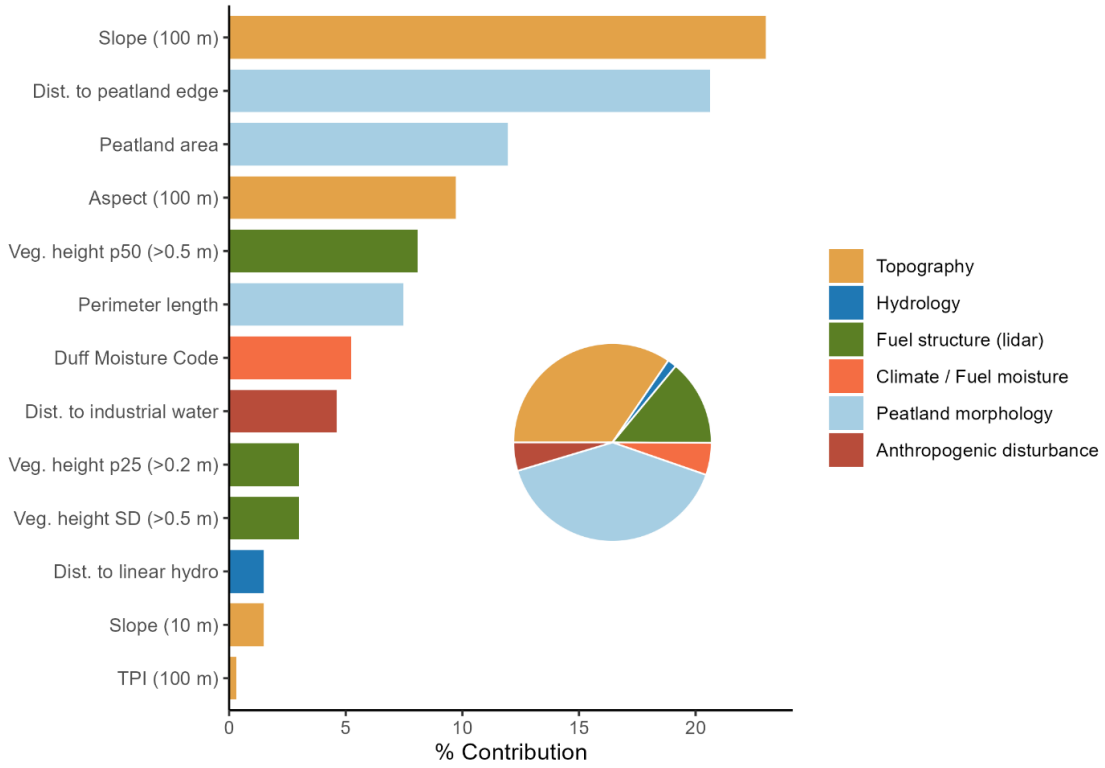

Figure 4.5. Percent contribution of covariates to the final bog GAM. Colours correspond to the category of predictive variable. Bars represent individual variables and are ranked in order of predictor performance. The pie chart summarizes the proportional contribution of each category to the bog GAM.

Figure 4.6 illustrates the partial effects of the top nine covariates from the bog model, as well as a key interaction term between distance to peatland edge (m) and peatland area (m^2). A negative, linear relationship was identified between slope and DOB, with

steeper slopes associated with reduced burn depths (Figure 4.6A). DOB increased with distance from the peatland edge (Figure 4.6B); however, there was a notable interaction between distance from peatland edge and peatland area that provided a nuanced explanation (Figure 4.6J). The deepest burns occurred along the edges of large bogs, while moderate burn depths were identified towards the interior of mid-sized bogs. The lowest burn depths corresponded to peatland centres as well as the edges of small- to mid-sized bogs. Peatland area on its own was negatively associated with DOB (Figure 4.6C), indicating that in general, larger bogs burned less deeply. Greater DOB was associated with south to southeast-facing aspects (Figure 4.6D), and peatlands with low-stature vegetation were found to burn more deeply, with DOB decreasing as the median of the lidar return height (p50 >0.5 m) increased (Figure 4.6E).

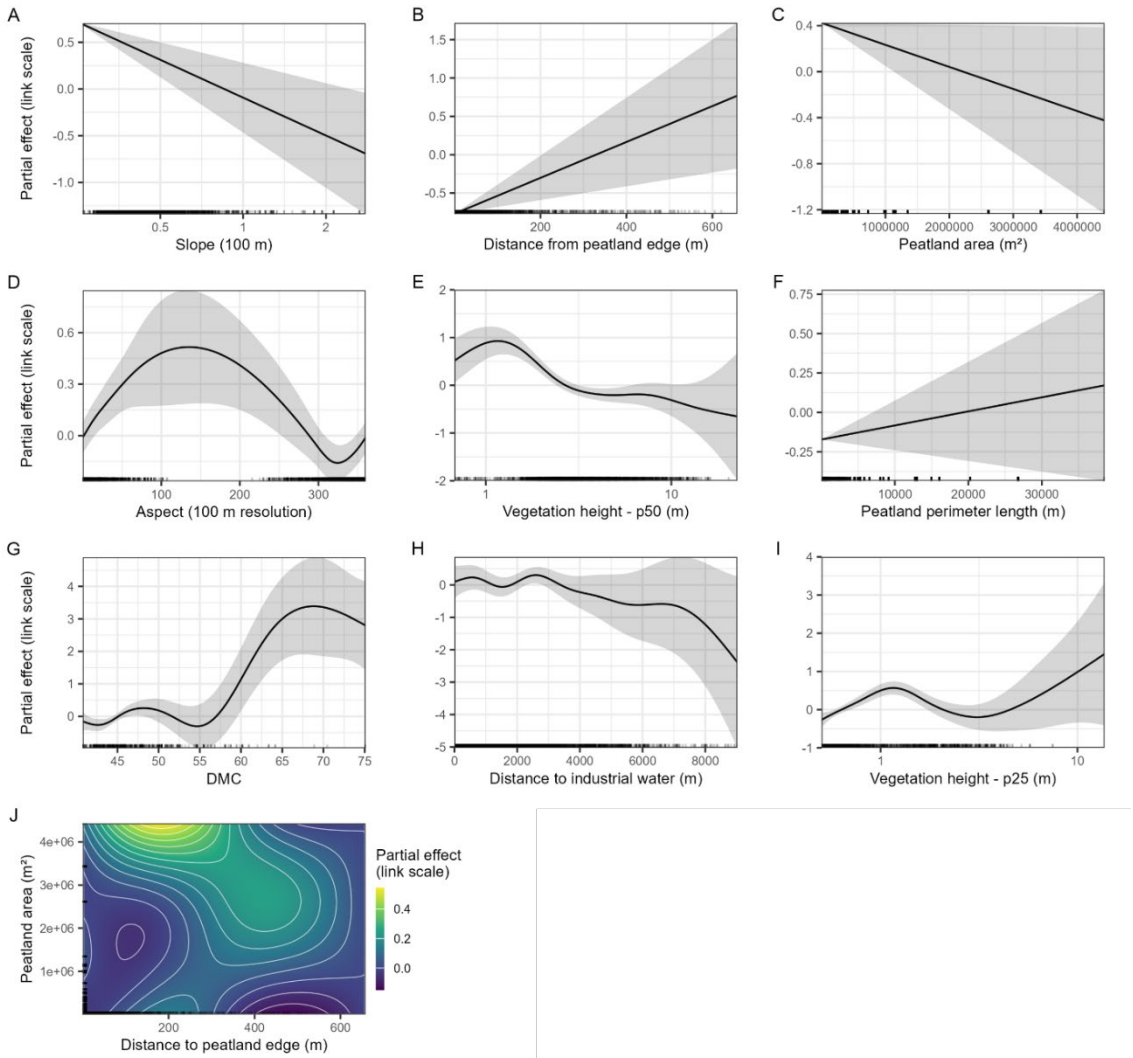

Figure 4.6. Partial effects plots of the top nine covariates, in order of importance, plus a key interaction term (distance to peatland edge and peatland area) from the bog GAM. The y-axis of each smooth plot represents the partial effect on the link scale and shaded zones represent 95% confidence intervals. Plots of all covariates, interactions, and a spatial smooth, are shown in Figures S4.1 and S4.2.

Covariates ranked 6-9 (Figure 4.5; Figure 4.6) contributed less to the model's explanatory power but still showed interesting trends. DOB increased with peatland perimeter length (Figure 4.6F) and with Duff Moisture Code (DMC), particularly once DMC exceeded ~60 (Figure 4.6G). As bogs became further removed from industrial water sources, DOB decreased (Figure 4.6H). Lower canopy (p25 >0.2 m) showed divergent

trends to mid-canopy (p50 >0.5) heights, where increases in p25 were associated with an increase in DOB (Figure 4.6J). The four remaining, weaker covariates and the second interaction term are plotted in Supplemental Figures S4.1 and S4.2.

4.4.2.2 Fens

The final fen GAM covariates included NDVI and NDMI; distance to nearest seismic lines, roads, and cutlines; height of median lidar returns (p50); aspect (100 m); peatland length:area ratio; FFMC; flow accumulation (250 m); and TPI (30 m). Two notable interactions were identified for fens – one between TPI and flow accumulation and another between NDVI and NDMI. See Supplementary Material for complete model structure. Diagnostic checks (Figure S4.6) revealed that the model was correctly specified, but behaviour in the upper tail of the QQ plot showed extreme positive residuals, indicating that the model was unable to capture some of the extremely deep burns. A residuals vs. linear predictor plot showed fairly even scatter clustered around zero, with some fanning demonstrating heteroscedasticity, but without a strong, systematic bias.

Unlike in the bog GAM, no linear associations were identified. Most covariates were highly significant ($p < 0.001$), except for aspect (100 m), which was significant at $p < 0.01$, NDMI, which was moderately significant at $p < 0.05$, and FFMC and length:area ratio, which were non-significant ($p > 0.05$), but still important to model performance. The fen GAM had better explanatory power than the bog GAM, with a deviance explained of 45.1% (non-spatial: 29.1%) and an adjusted R^2 of 0.44 (non-spatial: 0.31).

NDVI, the top ranked covariate, accounted for nearly 50% of the fen model's explanatory power (Figure 4.7; Table S4.5). Together with the second ranked covariate,

distance to nearest seismic line, nearly 70% of the variation in DOB captured by the model is accounted for. These, plus median height of above-ground lidar returns (p50 >0.05 m), aspect (100 m), length:area ratio, and NDMI, account for over 90% of the model's power in explaining DOB. It is clear from Figure 4.7 that variability in depth of peat burn in fens is most strongly associated with vegetation properties and anthropogenic disturbances – patterns that differ from those observed in bogs.

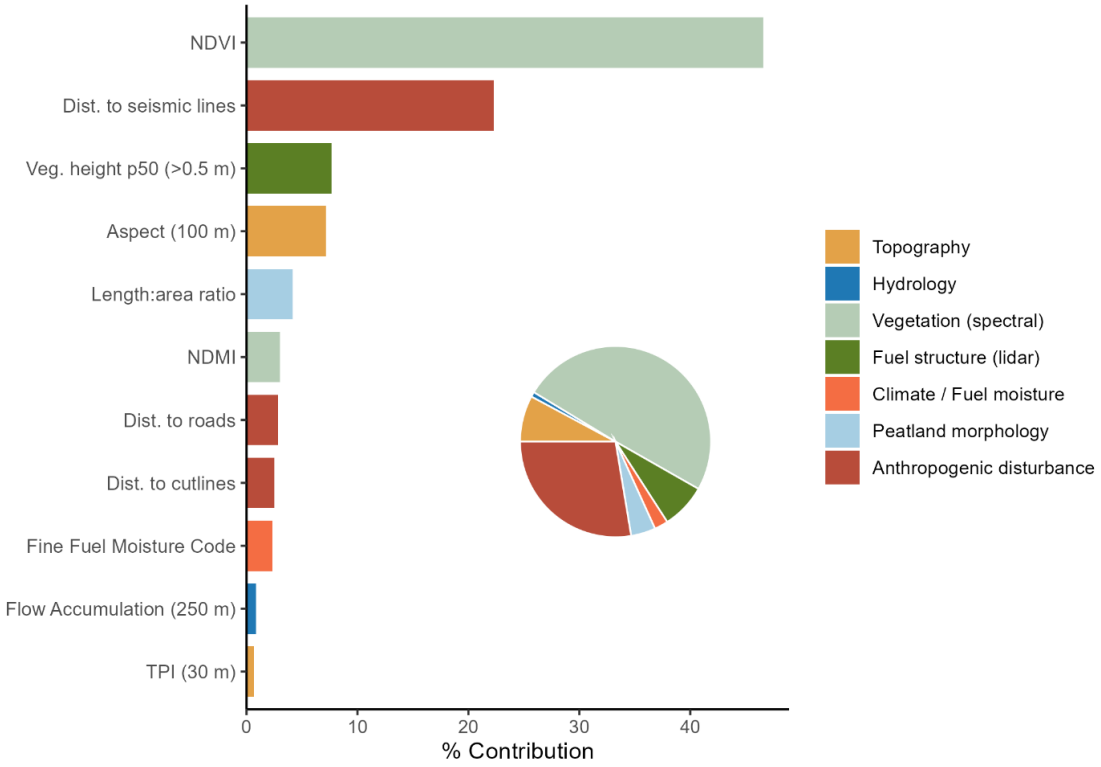

Figure 4.7. Percent contribution of covariates to the final fen GAM. Colours correspond to the category of predictive variable. Bars represent individual variables and are ranked in order of predictor performance. The pie chart summarizes the proportional contribution of each category to the fen GAM.

The top nine covariates of the fen GAM are illustrated in Figure 4.8. NDVI, the top predictive variable in the GAM, shows a curved relationship with DOB, where DOB is lower in areas with low NDVI (~0.1-0.2). Areas with very low NDVI (NDVI <0.1) show

the strongest positive association with greater DOB, with moderate NDVI values (~0.2-0.25) also showing a positive association (Figure 4.8A). While there was some irregularity in the smooth, distance from seismic lines was negatively associated with DOB. Points within ~2500 m of a seismic line show enhanced burn depths, with stronger associations closer to lines. Beyond this threshold, the greater distances correspond with reduced DOB (Figure 4.8B). Where the median height of lidar returns was low (p50 < ~3 m), there was a minimal, slightly positive relationship with DOB. Burn depth is lower where median canopy height increases (p50 > ~3 m) but increases again at high p50 values (>~15 m; Figure 4.8C). Contrary to patterns identified in bogs, south to southwest aspects are associated with lower DOB, while north-facing slopes experienced greater DOB (Figure 4.8D). As length:area ratio increases, DOB declines, suggesting that longer, more narrow peatlands experienced reduced burn depths (Figure 4.8E). NDMI has a negligible impact on DOB, with its effect hovering near zero, until it reaches a threshold of ~0.25, after which an increase in NDMI is associated with a reduction in burn depth (Figure 4.8F). Distance to the nearest road had a negative association with DOB, with a clear threshold: within ~2000 m of a road, DOB is slightly higher with closer proximity; beyond this, however, an increased distance from roads is related to an extremely strong reduction in DOB (Figure 4.8G). Distance to nearest cutlines, however, had the opposite effect, where increased proximity to cutlines is associated with a reduced DOB (Figure 4.8H). Lastly, FFMC shows a positive, nearly linear relationship with DOB: values below ~90 have a negative relationship (reduced DOB), whereas FFMC values above ~90 are associated with an increasingly enhanced DOB (Figure 4.8I). The two remaining, weaker covariates and the two interaction terms are plotted in Supplemental Figures S4.4 and S4.5.

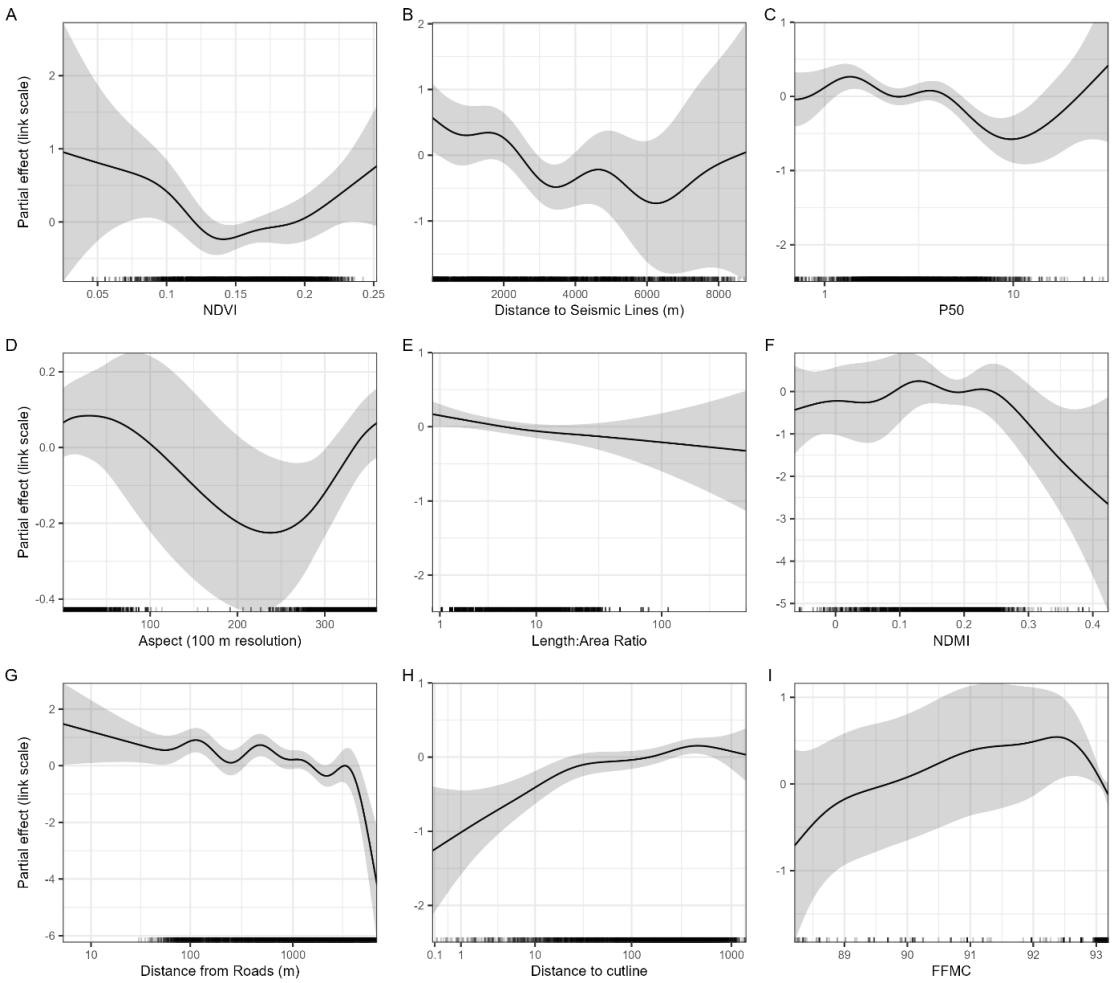

Figure 4.8. Partial effects plots of the top 9 covariates, in order of importance from the fen GAM. The y-axis of each smooth plot represents the partial effect on the link scale and shaded zones represent 95% confidence intervals. Plots of all covariates, interactions, and a spatial smooth, are shown in Figures S4.4 and S4.5.

4.4.2.3 Swamps

The top covariates, and those included in the final swamp GAM, were MNDWI; the 25th percentile of above-ground lidar returns (p25 >0.5 m); distances to nearest roads, seismic lines, cutlines, and linear hydrological features; TPI at 10, 20, and 500 m resolutions; slope (10 m resolution); and peatland area and length:area ratio. There were two interaction terms identified: between TPI (20 m) and distance to the nearest linear hydrological feature, and between slope (10 m) and distance to the nearest road. Complete model structure and

parameters are provided in Supplementary Material. Diagnostic checks using gam.check() (Figure S4.9) showed that the residual distribution was approximately normal, with minor deviance in the upper tail. The residuals vs. linear predictor plot showed the expected fan-shaped pattern, indicating heteroscedasticity, as would be expected for heavily skewed DOB data. Based on the QQ plot and effective degrees of freedom checks, the pattern is not indicative of poor model fit.

Approximately half the covariates included in the final swamp GAM were highly significant ($p < 0.001$): 25th percentile lidar return height (p25), distance to nearest seismic line, TPI (10 m), peatland area, and both interaction terms. Distance to nearest road and MNDWI were significant at $p < 0.01$, and length:area ratio was moderately significant at $p < 0.05$). Slope (10 m), distance to cutline, and distance to linear hydrological features were non-significant ($p > 0.05$), but still improved the model based on R^2, deviance explained, and AIC. Interestingly, peatland area only remained a useful model variable when peatland shape (length:area ratio) was included – suggesting that peatland size only mattered once the effect of shape was accounted for. While deviance explained by the swamp GAM fell between those of the bog and fen GAMs at 43.2% (non-spatial: 27.1%) the adjusted R^2 was the weakest of the three models at 0.34 (non-spatial: 0.19).

The strongest variables identified in the swamp GAM – MNDWI and 25th percentile of above-ground lidar returns – accounted for over 50% of the model's explanatory power (Figure 4.9; Table S4.6). When the third through fifth highest ranked covariates are accounted for – distance to nearest road, TPI (10 m), and distance to nearest seismic line – the top five variables drive over 80% of the model's power. Variable categories that contribute most to modelled variation were again different for swamps than

for bogs or fens (Figure 4.9). Hydrology and fuel structure were the highest ranked predictor categories, followed by topography and anthropogenic disturbance.

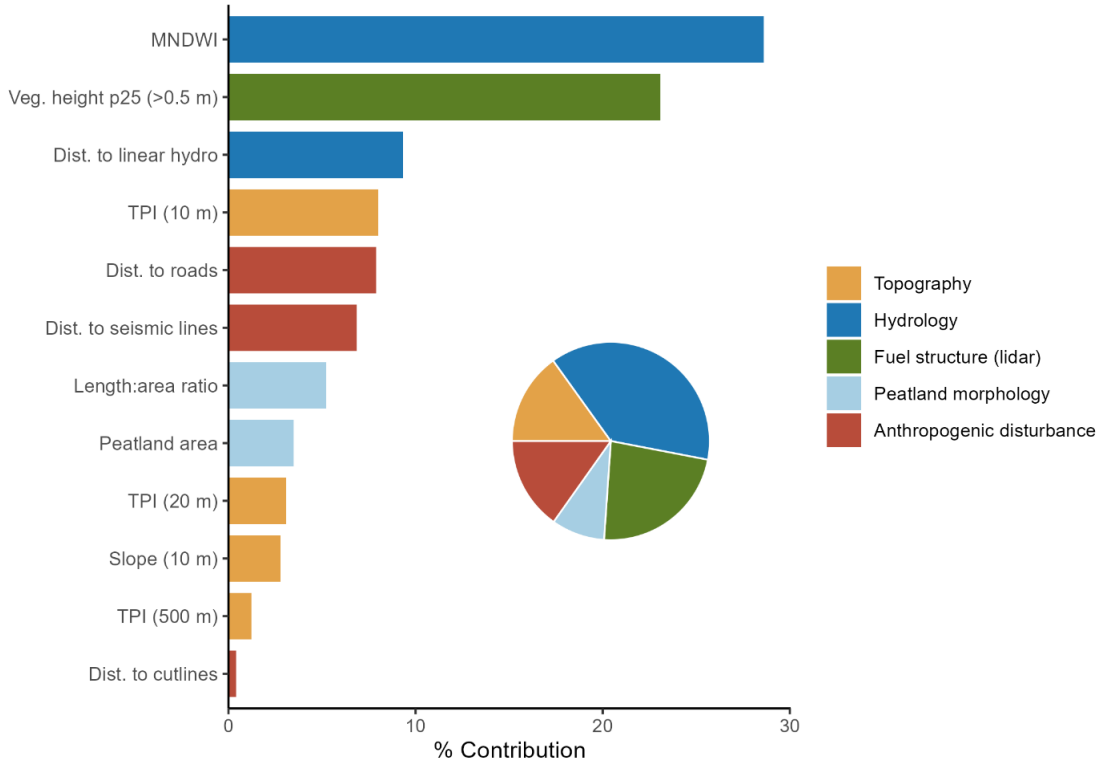

Figure 4.9. Percent contribution of covariates to the final swamp GAM. Colours correspond to the category of predictive variable. Bars represent individual variables and are ranked in order of predictor performance. The pie chart summarizes the proportional contribution of each category to the swamp GAM.

Figure 4.10 illustrates the smooths, or relationships, between depth of burn and the top six predictive variables identified through the swamp GAM. A negative, linear relationship was identified between MNDWI and burn depth (Figure 4.10A), where values below ~0.08 were associated with enhanced DOB. The 25th percentile height of above-ground lidar returns (p25 >0.5 m) had a generally negative relationship with DOB, where greater p25 was associated with a lower DOB (there was a shift to a positive influence at p25 values over ~9 m, but there is extremely sparse data with a highly uncertain confidence

interval; Figure 4.10B). As proximity to linear hydrological features increased, DOB was reduced (Figure 4.10C); the same effect was seen with proximity to seismic lines (Figure 4.10F) – the opposite effect as was seen in fens (Figure 4.8B). An increase in TPI was related to an increase in DOB, with TPI over ~0 (convex features) associated with an enhanced DOB, and TPI below 0 (concave features) associated with a dampening pattern (Figure 4.10D).

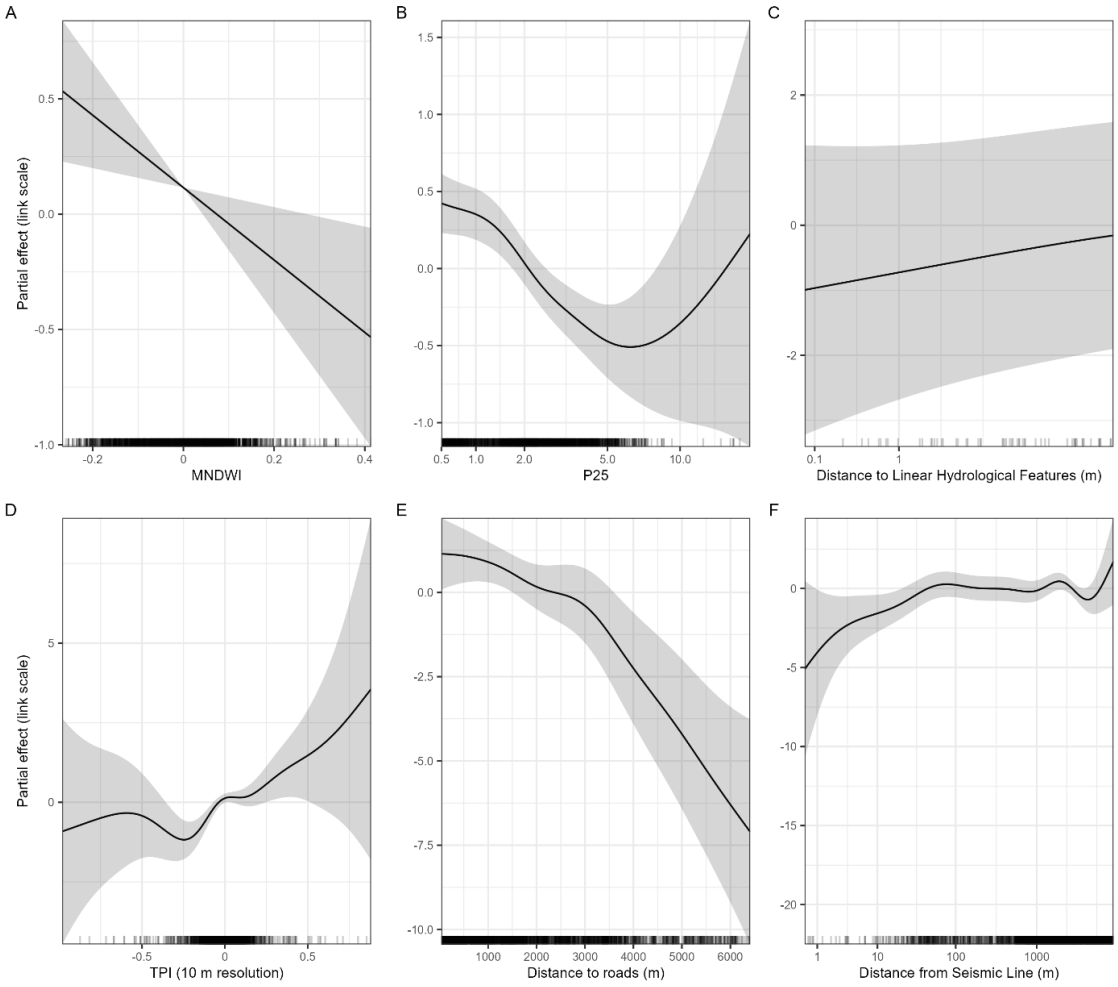

Figure 4.10. Partial effects plots of the top 6 covariates, in order of importance, from the swamp GAM. The y-axis of each smooth plot represents the partial effect on the link scale and shaded zones represent 95% confidence intervals. Plots of all covariates, interactions, and a spatial smooth, are shown in Figures S4.7 and S4.8.

4.4.2.4 Common Versus Wetland-Specific Environmental Conditions

Multiple predictive variables were common between peatland types – particularly between fens and swamps; however, there were no top variables identified that were common to all three (Figure 4.11). Area was a common predictor in both bogs and swamps, but was more important in bogs (Figures 4.5, 4.7). Median height of above-ground lidar returns (p50) and aspect (stand scale) were both similarly ranked predictive variables in bogs and fens. However, the influence of aspect was nearly inverse between the two peatland types (Figures 4.6, 4.8).

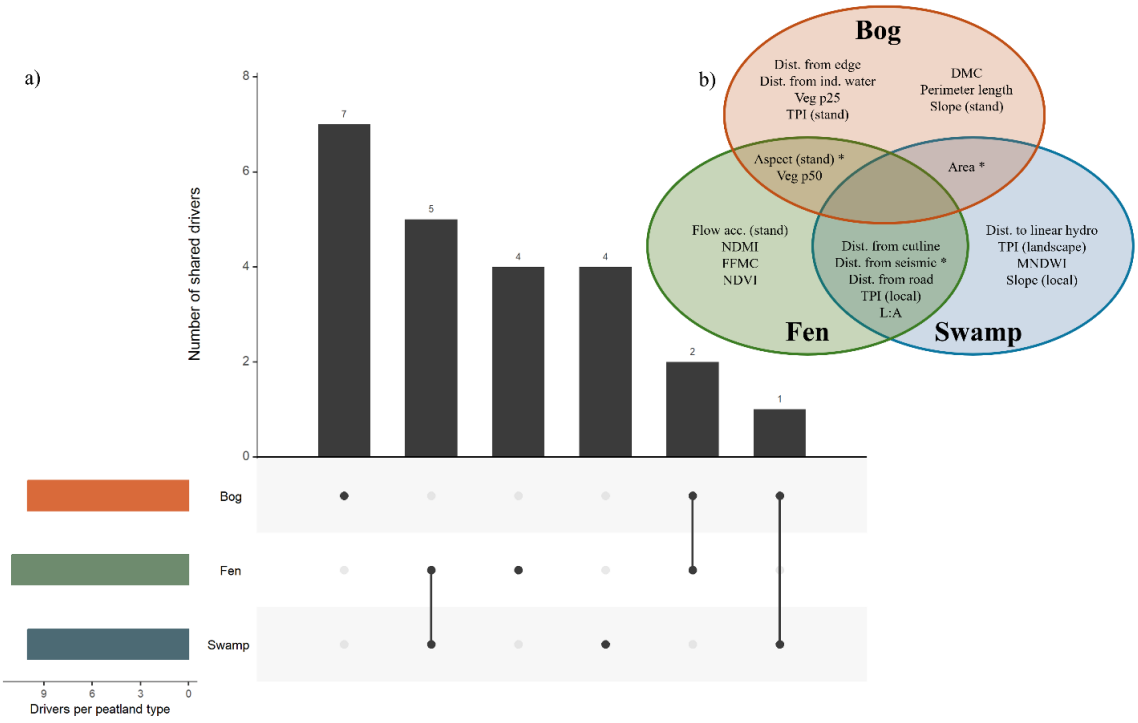

Figure 4.11. Shared vs. unique predictive variables of depth of burn across bogs, fens, and swamps identified via GAM analysis. The UpSet plot (a) illustrates the number of predictors shared between, or unique to, each peatland. The Venn diagram (b) lists these predictive variables. Asterisks denote shared variables but with notably different influences.

Fens and swamps shared five common predictive variables – distance from cutline, distance from seismic line, distance from the nearest road, TPI (local scale), and length:area ratio (Figure 4.11). TPI was much more important in swamps, however, than in fens (Figures 4.7, 4.9), and distance from the nearest seismic line had opposite relationship with DOB – associated with an increase in DOB with proximity to fens (Figure 4.8) and reduced DOB with proximity to swamps (Figure 4.10).

4.4.3 Random Forest: Top Predictive Variables Associated with Depth of Peat Burn and Model Performance

4.4.3.1 Bogs

The top predictive variables associated with depth of peat burn in bogs, identified via RF and SHAP backwards selection, were DC, TPI at 50 and 15 m resolutions, distances to nearest seismic line and to nearest industrial water source (m), 25th percentile height of lidar returns (p25 >1.37 m), distance to peatland edge (m), length:area ratio, flow accumulation at 250 m resolution, and peatland area (Figure 4.12). Explanatory power was more evenly distributed between variables in the RF model than the GAM (Figure 4.5), with the top 4 variables (Drought Code, TPI at 50 m resolution, distance to nearest seismic line, and p25) providing just over 50% of the model's power. While Drought Code, a climate/fuel moisture variable, contributed the most of any single variable to the model, the predictor categories of topography and peatland morphology were the categories with the greatest contribution (Figure 4.12). These match those identified as top predictive categories in the GAM (Figure 4.5).

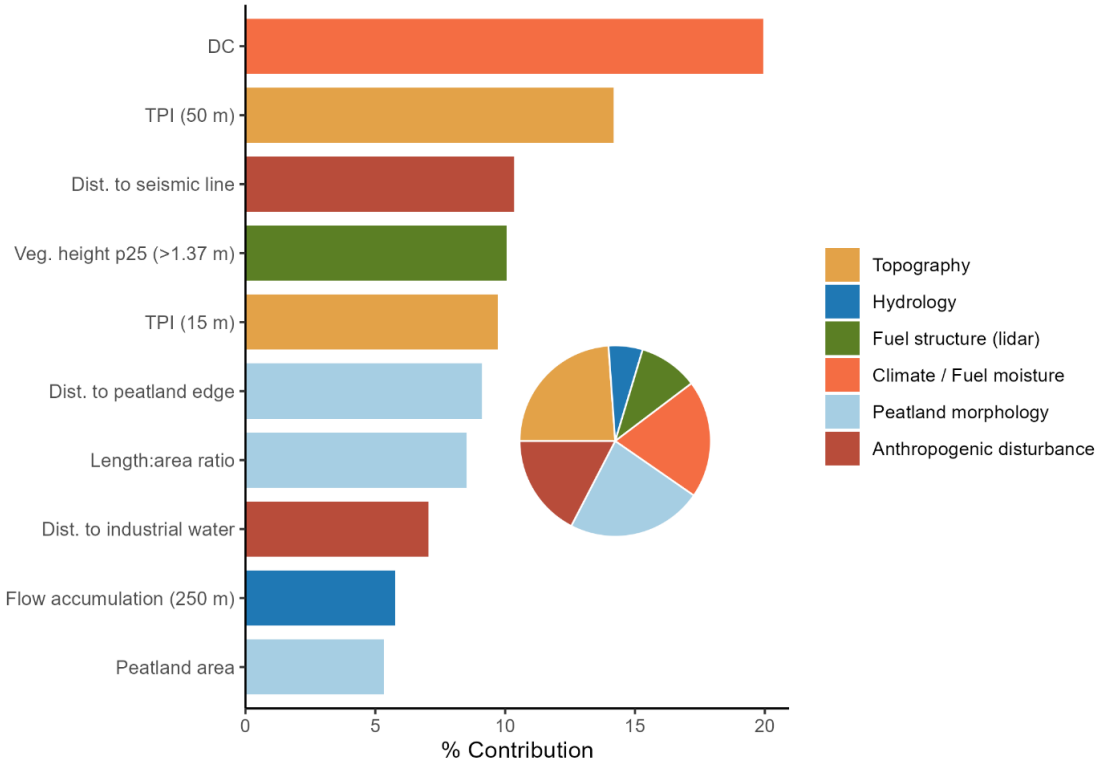

Figure 4.12. Percent contribution of covariates to the final bog RF model. Colours correspond to the category of predictive variable. Bars represent individual variables and are ranked in order of predictor performance. The pie chart summarizes the proportional contribution of each category to the bog RF model.

Model R^2 was 0.30 ± 0.03 with an RMSE of 4.76 ± 0.35. Variable ranks remained consistent when checked with a larger spatial block. Variables with the highest and lowest percent contribution remained stable throughout model runs, though variables four through six – veg. height p25, TPI (15 m), and distance to peatland edge (m) varied between these ranks to the extent that one should not be considered of higher importance than the others.

4.4.3.2 Fens

The top predictive variables associated with depth of peat burn in fens, identified via RF and SHAP backwards selection, were TPI at 50 and 10 m resolutions, NDVI, distance to nearest seismic line and to nearest industrial zone (m), 25th percentile height of lidar returns

(p25 >1.37 m) and skew (>0.5 m), slope at 100 m resolution, FWI and DMC, and flow accumulation at 250 m resolution. The top three covariates contributed nearly 50% of the fen RF model's explanatory power (Figure 4.13). As a category, topography dominated the predictive variables associated with DOB (not identified as a top predictive category in the fen GAM; Figure 4.6), followed by vegetation and anthropogenic disturbance (the top categories from the fen GAM).

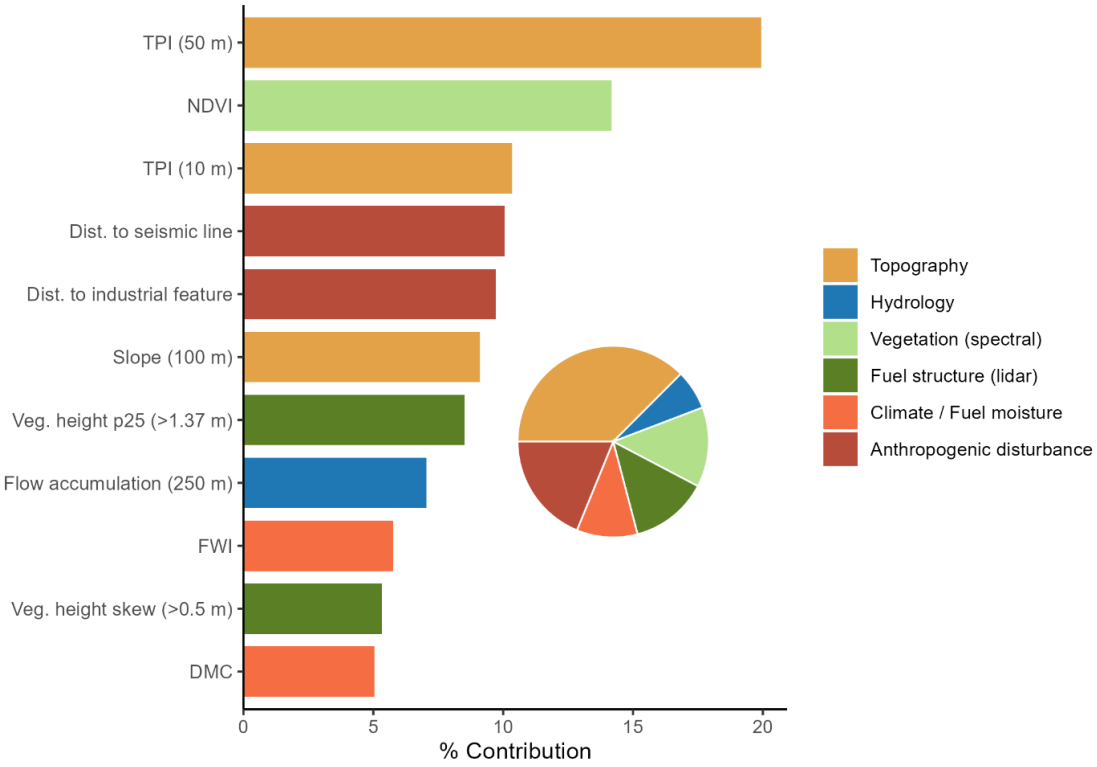

Figure 4.13. Percent contribution of covariates to the final fen RF model. Colours correspond to the category of predictive variable. Bars represent individual variables and are ranked in order of predictor performance. The pie chart summarizes the proportional contribution of each category to the fen RF model.

The fen RF model performance metrics were weaker than those of bogs, with an R^2 of 0.24 ± 0.04 and an RMSE of 4.85 ± 0.55. Variable ranks, however, remained consistent in model runs using larger spatial blocks. The top five variables, TPI (50 m), NDVI, TPI

(10 m), distance to nearest seismic line (m), and distance to nearest industrial feature (m), were stable in their rankings, as was the weakest contributor, DMC. Covariates ranked here as six through ten, however, were variable in their ranks. Slope (100 m) and p25 fluctuated between 6th and 7th and flow accumulation, FWI, and the skewness of the vertical distribution of lidar returns fluctuated between 8th and 10th.

4.4.3.3 Swamps

The top predictive variables associated with depth of peat burn in swamps, identified via RF and SHAP backwards selection, were MNDWI, distance to nearest seismic line, distance to nearest road, distance to nearest linear hydrological feature (m), 25th percentile height of lidar returns (p25 >0.5 m), TPI at 30 m resolution, DC, aspect at 100 m resolution, perimeter length (m), and flow accumulation at 250 m resolution. Among the categories, anthropogenic disturbance and hydrology had the strongest relationship with DOB in swamps, closely followed by topography and fuel structure (Figure 4.14). GAMs also identified these categories as the most influential predictors, though in different proportions (Figure 4.9).

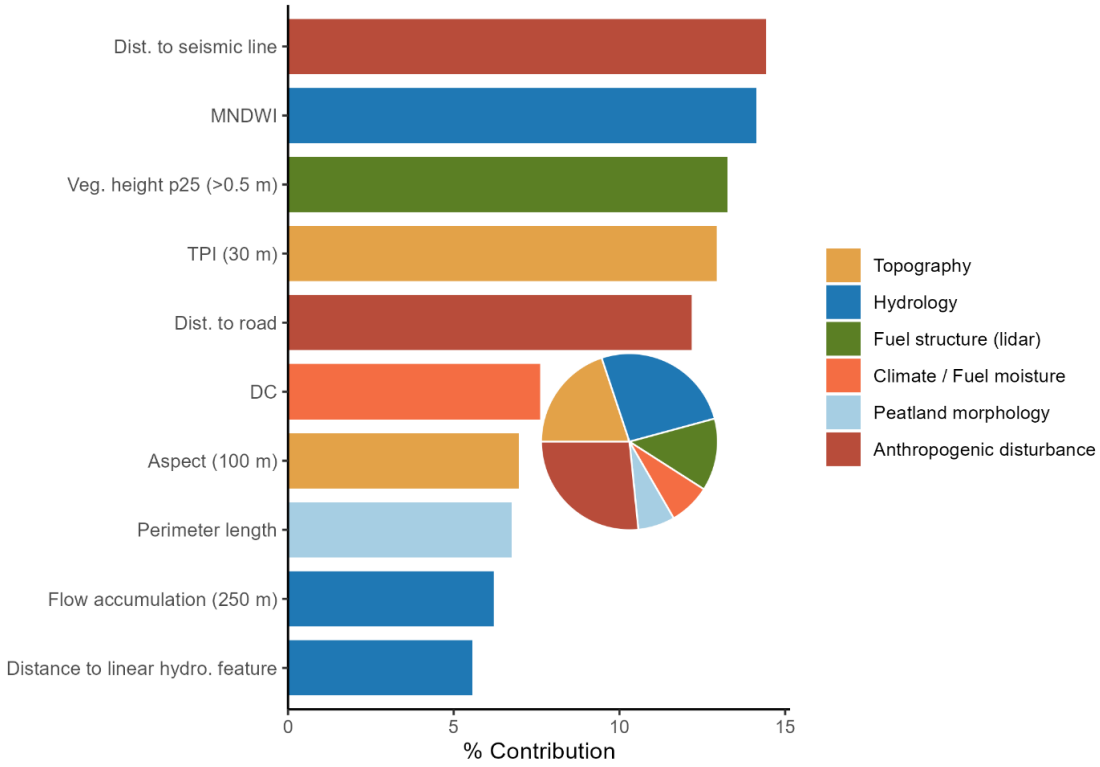

Figure 4.14. Percent contribution of covariates to the final swamp RF model. Colours correspond to the category of predictive variable. Bars represent individual variables and are ranked in order of predictor performance. The pie chart summarizes the proportional contribution of each category to the swamp RF model.

The strength of the swamp RF model performance metrics fell between those of bog and fen models, with an R^2 of 0.27 ± 0.05 and an RMSE of 4.45 ± 0.38. Variable ranks remained consistent in model runs using larger spatial blocks. Driver ranks were less stable in the swamp model than those of bogs and fens. The top two variables, distance to seismic lines and MNDWI, fluctuated between 1st and 2nd throughout the model runs. P25 and TPI shifted between 3rd and 4th rank, and aspect, perimeter length, and flow accumulation fluctuated between one another (7th through 9th). Distance to linear hydrological features was consistently ranked last (Figure 4.14).

4.4.3.4 Common Versus Wetland-Specific Environmental Conditions

RF models identified four variables as being common across all three peatland types – TPI (local scale), distance from seismic lines, p25, and flow accumulation (stand scale; Figure 4.15). Distance from seismic lines was of greater importance in swamp models than bog or fen (Figures 4.12-4.14). TPI (stand scale) was shared as a highly ranked variable in both bogs and fens (Figures 4.12, 4.13) and Drought Code was a common variable for both bogs and swamps, though was identified as a top predictive variable in bogs, and mid-rank in swamps (Figures 4.12, 4.14, 4.15).

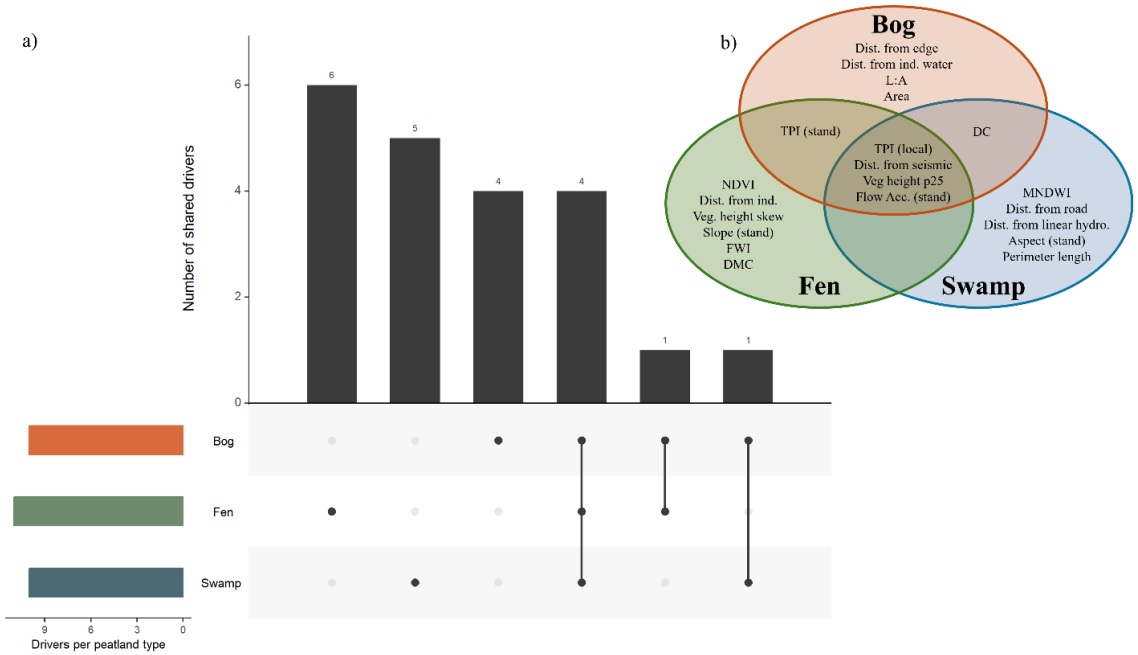

Figure 4.15. Shared vs. unique predictive variables associated with depth of burn among bogs, fens, and swamps identified via RF & SHAP. The UpSet plot (a) illustrates the number of variables shared between, or unique to, each peatland. The Venn diagram (b) lists these predictive variables. Asterisks denote shared predictors but with notably different influences.

4.5 Discussion

4.5.1 Variability in Depth of Burn Across Peatland and Ecotone Types

Depth of peat combustion averaged ~8 cm across the burned area, with bogs and bog ecotones exhibiting the greatest DOB, fens the lowest DOB, and fen ecotones experiencing the greatest variability in DOB (Figure 4.4). Due to their ombrogenous nature, bogs may experience greater water table fluctuations and increased drawdown of soil moisture (e.g., Waddington et al., 2015). This can subsequently increase soil bulk density, optimizing the conditions for deeper combustion (Lukenbach et al., 2015; Lukenbach et al., 2017). Zoltai et al. (1998) found that bogs were more likely to have low soil moisture contents that supported ignition as compared to fens. Bog ecotones, which often transition between upland forests and bog peatlands, are especially susceptible to these conditions. High bulk densities can promote greater fluctuations in water tables (Lukenbach et al., 2015), and the greater proportion of shrubby or upland-typical vegetation typical in ecotones can enhance evapotranspiration (e.g., Markle et al., 2020), further reducing soil moisture. The low snowpack and high early-spring temperatures preceding the Horse River Wildfire (Elmes et al., 2018) likely exacerbated the drier conditions in bogs and promoted deeper combustion. Fens and swamps experienced significantly lower soil combustion (Table 4.2), consistent with their hydrogeological settings. As geogenous peatlands, fens and swamps hydrological connectivity likely allows them to maintain higher water tables (Ferone et al., 2004).

The high variability in DOB within fen ecotones likely reflects ecotonal characteristics such as variable vegetation and peat properties, where vegetation and soil characteristics of both peatland and upland overlap (e.g., Hartshorn et al., 2003).

Correspondingly, hydrological connectivity was likely variable, with some zones recharged by fens and others drained into adjacent uplands – a pattern likely enhanced by the low snowpack and warm spring temperatures preceding the fire (Elmes et al., 2018). Additionally, fens may have linear hydraulic flow paths, which could increase their sensitivity to anthropogenic disturbances that alter the patterns of surface water flow (e.g. Elmes et al., 2022). Results from the driver analysis were consistent with this – distance to nearest seismic line was identified as an important driver of DOB (Figure 4.7). The deep burns in bog and bog ecotones, as well as the localized deep burns in fen ecotones, highlight areas with high potential to contribute disproportionately to C losses during peatland fires. This is particularly notable in ecotones, where bulk density, and therefore C density, is often highest (Lukenbach et al., 2015).

Validation of lidar-derived DOB measurements enhanced confidence in the reliability of these estimates. Mean elevation changes within the fire perimeter matched closely to those estimated based on weighted averages incorporating elevation offsets measured in unburned peatlands outside the fire perimeter. Small offsets (≤1.2 cm) were well within the lidar's vertical accuracy and had minimal impact on average DOB estimates. When burned area was unaccounted for and elevation changes within the fire perimeter were simply subtracted from those outside the fire perimeter, these offsets increased but remained small (≤ 2.3 cm). Both methods indicate that DOB estimates provided in this chapter are likely slightly conservative.

4.5.2 Robust Predictors of Peat Burn: Convergence of GAMs and RF

Although individual predictors varied somewhat between GAMs and RF models, both approaches converged on the finding that depth of peat combustion in bogs was most

strongly associated with topographic and morphological factors (Figures 4.5, 4.12). Bottom-up predictive variables accounted for substantially greater model variability of DOB than top-down, accounting for 80 to 95% of model explanatory power (RF and GAM, respectively). This aligns with the ombrogenous nature of bogs, as smaller differences in elevation, slope, and shape would likely have direct control on movement of surface water and soil moisture and the depth to water table.

Both GAMs and RF identified distance to peatland edge, peatland area, distance to the nearest industrial water feature, either perimeter length (GAM) or length:area ratio (RF), and vertical forest structure (p25 in both; p50 and sd in GAM only), as top predictive variables. These showed that DOB was greater in smaller bogs (Figure 4.6C). These also indicated that DOB increased with distance from peatland edge – counterintuitive to what is understood about deep burning in edges, or ecotones, and opposing what the DOB results demonstrated. However, this pattern only existed once area, perimeter length, slope, etc., were accounted for. These smooths (Figure 4.6A-I), along with the interaction between peatland area and distance to the edge (Figure 4.6J), suggest that large bogs burned most deeply at their edges, while smaller bogs, which are more prone to drying, burned more deeply towards the middle.

Drought Code was the top variable identified via. RF, while it was not included in the GAM. Instead, Duff Moisture Code was highlighted as a predictor, though it contributed substantially less to the GAM than DC did to the RF model. While DC represents longer-term, deep peat drought and DMC shorter-term responses in the upper peat (e.g., Miller, 2020; Wotton, 2005), they are likely both representative of similar effects of fire weather and drought. Topographic variables, though important in both, were not

consistent between models, with slope and aspect showing the strongest associations in the GAM, while TPI emerged as most influential in the RF model. These discrepancies likely reflect differences in how the models handle assumptions in correlation vs. concurvity, as opposed to true disagreement about the importance of predictors. As GAMs penalize complexity in smooths (Wood, 2017), it is also possible that variables such as DMC, slope, and aspect had less complex relationships with DOB than RF's corresponding DC and TPI.

In fens, vegetation and anthropogenic disturbances were the top predictive categories that both the GAM and the RF model agreed upon, though topography ranked highest in the RF model (Figures 4.7, 4.13). Again, bottom-up variables accounted for the majority of the modelled variation in depth of burn, explaining ~89 to 98% of the model's explanatory power. This highlights the essential role of vegetation in shaping fire severity in fens and reiterates the impact of linear anthropogenic disturbances on the linear flow of fens.

Both models identified NDVI, distance to seismic lines, flow accumulation, local-scale TPI, and vertical vegetation structure (p25 in RF and p50 in GAM) as variables associated with DOB in fens. This convergence strengthens the likelihood that these predictors are robust environmental conditions associated with DOB. NDVI was associated with deeper burns at both very low and moderate responses, with low NDVI associated with the lowest DOB (Figure 4.8A), indicating that non-photosynthetic surfaces (i.e. bare shrub stems, exposed peat, etc.) and areas with denser fuels (cured preceding the fire) enhanced smouldering conditions. Flow accumulation had a logical relationship, with greater accumulation associated reduced DOB (Figure S4.4I). Both convex and concave shapes at local scales were associated with reduced DOB (Figure S4.4C).

Notable divergences between the GAM and RF models were the inclusion of aspect and length:area ratio in GAM, but not in RF, and the selection of different fire weather indices – RF included FWI and DMC, while GAM highlights FFMC. The implications are not that these variables are not ecologically relavent, but instead support the use of two distinct approaches – GAMs likely included aspect in bogs and fens, as they were treated as circular variables using cyclic cubic splines. Fire weather indices are highly related, and differences in models are likely reflective of modelling approaches rather than contradictory evidence.

Hydrology was the primary, model-agreed-upon, predictor of variability in DOB in swamps (Figures 4.9, 4.14), followed by fuel structure (GAMs), and anthropogenic disturbance (RF). As in bogs and fens, bottom-up predictive categories accounted for the vast majority of modelled variation in swamps, accounting for 92 to 100% of explanatory power RF and GAMs, respectively. The predominance of hydrology in the models is consistent with the hydrogeological setting of swamps. Geogenous peatlands, swamps often exist in transitional zones, adjacent to uplands, or along riparian zones (Locky et al., 2005). They typically have shallower peat, increasing sensitivity to fluctuations in moisture (e.g., Zoltai & Vitt, 1995). Swamps may be seasonally inundated by standing water (National Wetlands Working Group, 1997), so indices such as MNDWI are able to capture the dampening effect of increased moisture on DOB (e.g., Frandsen, 1987; Benscoter et al., 2011).

Other converging variables included 25th percentile height of lidar returns (p25), distance to the nearest road, distance to the nearest seismic line, distance to the nearest linear hydrological feature, TPI (local scale), and perimeter length (RF) and length:area

ratio (GAM). While proximity to the nearest seismic line was associated with increased DOB in fens, underscoring a drainage effect of anthropogenic disturbance, swamps showed the opposite pattern, with lower DOB in closer proximity to seismic lines (Figure 4.10F). One possibility is that these linear disturbances interrupt natural flows (e.g., Braverman & Quinton, 2016), flooding swamps that are either nearby or that cutlines intersect. An increased distance from roads was strongly associated with lower DOB in swamps (Figure 4.10E), and proximity to hydrological features was associated with lower DOB, a pattern that might be expected based the importance of water table and soil moisture on peat combustion(Figure 4.10C). Key divergences between models were the inclusion of distance to the nearest cutline in the GAM and inclusion of DC in the RF model.

The final GAMs explained 39 to 45% of the deviance in DOB (non-spatial: 24 to 29%) with adjusted R^2 values of 0.34 to 0.44 (non-spatial: 0.19 to 0.31), while RF models had R^2 of 0.24 to 0.30. While these values are in line with results of comparable studies, though these are very few (e.g., R^2 of 0.206 in black spruce forests, de Groot et al., 2008), and indicate that the variables identified are meaningful in their contribution to DOB variability, there is significant, unexplained variability, emphasizing the highly variable and unpredictable nature of peatland combustion. The remaining variability is likely a result of numerous environmental factors and fire behaviour influences that are unable to be captured with proxy, remotely sensed variables such as hydrological processes and bulk densities, as well as lidar measurement noise. Importantly, the objective was not to develop a predictive model, but to identify robust, readily measured environmental conditions associated with peat combustion. To enhance interpretability, the methodology focused on using clear, directly interpretable predictors – avoiding methods such as principal

component analysis (PCA), variable reduction beyond optimized RMSE, and strategies to minimize the effects of spatial autocorrelation.

4.5.3 Management Implications

The findings of this study have important land use management implications for risk reduction of deep peat combustion. The differences in depth of peat burn between peatland types and ecotones emphasize the importance of differentiating peatland types and ecotones in C accounting and modelling. Particularly, the high variability in fen ecotone DOB suggests potential risks of disproportionately deep combustion under enhanced fragmentation – as a result of either climate change-induced drought and shifts in vegetation (Weltzin et al., 2003) or increases in linear anthropogenic disturbances such as seismic lines and roads (Turetsky & St. Louis, 2006).

Delineation of peatland types should be a critical first step in assessing areas most at risk of deep combustion and in developing actionable management strategies. For example, the increased vulnerability of small and irregular bogs, as well as the edges of large bogs, should be prioritized areas for monitoring, potential restoration, and fire management. In fen-heavy regions, on the other hand, reducing or restoring anthropogenic linear disturbances may mitigate risk. In swamps, maintaining hydrological connectivity is likely essential to risk reduction. Integrating peatland-specific risk assessments into fire management protocols and land use planning would likely enhance the resiliency of these peatland ecosystems to deep combustion and subsequently large C losses.

4.5.4 Limitations and Future Direction

While the results of this study have important implications, there are also limitations and uncertainties that must be considered. Inherently variable lidar data was aggregated to smooth noise and mitigate risks of over-estimating DOB, resulting in a loss of potentially fine-scale deep burn patterns. The limited spatial extent of the study area and the scope of a single fire study provides insights into context-specific patterns associated with peat combustion, but these may partially reflect local environmental conditions, and transferability to unique peatland areas is uncertain. Because of the limited area, the spatial distribution of samples, and the zero-inflated nature of the data, spatial CV blocks were limited. This was further mitigated by the inclusion of spatial covariates to eliminate proxy variables but is still a factor limiting spatial extrapolation.

While fire weather indices were included as initial covariates, these were represented by day-of combustion indices tied to each pixel, as opposed to a consideration of fire progression or residence time. As a result, variation in fire behaviour and duration of combustion may not be fully captured. While latitude and longitude were included to absorb residual spatial structure, this does not explicitly represent fire trajectory, which is likely an important mechanism. Further work that incorporates fire progression, including trajectory and residence time, could improve understanding of the interaction between fire behaviour and peatland DOB.

There was substantial unexplained variability in DOB, which is expected in highly variable ecological data, but highlights opportunities for further investigation into unmeasured processes and expanded datasets. Future research should expand a comparable analysis across larger spatial and temporal gradients, which would allow for the exploration

of predictive variables at broader scales, such as time of year, topography and hydrological variables at landscape scales, ecoregions, and vegetation type. This would also improve confidence in the transferability of conclusions.

4.6 Conclusion

There were notable patterns in depth of peat combustion between peatland types, with bog and bog ecotones experiencing significantly greater burn depths than any other peatland or ecotone type. While fens experienced the lowest average DOB, fen ecotones experienced significantly greater DOB, and notably large variability in DOB. Distributions indicated that small, deep burning pockets can disproportionately increase average DOB, subsequently enhancing average C loss. This emphasizes the importance of accounting for both peatland type and core-ecotone separation in DOB and C loss analyses.

Model convergence between the GAM and RF models increases confidence in identifying of the predictors most strongly associated with DOB – particularly those that are consistently highly ranked. Agreements in predictor categories between models further supports confidence in these associations. Broadly, topography, hydrology, and linear anthropogenic disturbances emerged as predictor categories with the strongest associations with DOB; however, the relative importance of these categories differed among peatland types, underscoring the importance of assessing and mitigating combustion risk differently depending on peatland type. DOB in bogs was most strongly associated with topographic and morphological variables, which emphasized the sensitivity of small bogs, and bog edges, to deep combustion. In fens and swamps, however, where groundwater connectivity reduces the impact of small variations in topography on water table position, other predictive variables such as vegetation, hydrology, and anthropogenic disturbance had the strongest associations with variability in DOB. These patterns are crucial for understanding vulnerabilities of peatlands to enhanced C losses, and for generating mitigation and risk-management plans.

4.7 Acknowledgements

Thank you to Dr. Linda Flade, Emily Jones, and Dr. Craig Mahoney for assistance with field data collection and to Maxim Okhrimenko for lidar data collection and processing assistance. Fire weather and day-of-burn data was provided by Quinn Barber (Natural Resources Canada). This research was supported by funding from several sources. Dr. Laura Chasmer's funding from Natural Sciences and Engineering Research Council (NSERC) Discovery Grant, the Canada Wildfire NSERC SPG-N, and University of Lethbridge Start-Up Funding. Dr. Chris Hopkinson's funding from the Western Economic Diversification Canada Funding and a Canadian Foundation for Innovation grant. Kailyn Nelson received funding from an NSERC Canada Graduate Scholarship, Alberta Innovates Graduate Student Scholarship, the Nexen Fellowship in Water Research, Canada Wildfire (NSERC SPG-N), and the University of Lethbridge School of Graduate Studies.

4.8 References

Abib, T. H., Chasmer, L., Hopkinson, C., Mahoney, C., & Rodriguez, L. C. (2019). Seismic line impacts on proximal boreal forest and wetland environments in Alberta. Science of the Total Environment, 658, 1601-1613.

Aguilar, F. J., & Mills, J. P. (2008). Accuracy assessment of LiDAR-derived digital elevation models. The Photogrammetric Record, 23(122), 148-169.

Alberta Agriculture and Forestry & MNP LLP. (2017). A review of the 2016 Horse River wildfire.

Alberta Geospatial Services (2021). Cutline (ID:30). Shapefile. Available at: https://geospatial.alberta.ca/titan/rest/services/utility/access/MapServer/30. (Accessed December 2022).

Albertini, C., Gioia, A., Iacobellis, V., Petropoulos, G. P., & Manfreda, S. (2024). Assessing multi-source random forest classification and robustness of predictor variables in flooded areas mapping. Remote Sensing Applications: Society and Environment, 35, 101239.

Ali, M. I., Dirawan, G. D., Hasim, A. H., & Abidin, M. R. (2019). Detection of changes in surface water bodies urban area with NDWI and MNDWI methods. International Journal on Advanced Science Engineering Information Technology, 9(3), 946-951.

Arnold, N. S., Rees, W. G., Hodson, A. J., & Kohler, J. (2006). Topographic controls on the surface energy balance of a high Arctic valley glacier. Journal of Geophysical Research: Earth Surface, 111(F2).

Axelsson, P. (2000). DEM generation from laser scanner data using adaptive TIN models. In International Archives of Photogrammetry and Remote Sensing, Proceedings of the ISPRS, Amsterdam, The Netherlands, 16–23 July 2000; Volume 33, Part B4/1, pp. 110–117.

Benscoter, B. W., Thompson, D. K., Waddington, J. M., Flannigan, M. D., Wotton, B. M., de Groot, W. J., & Turetsky, M. R. (2011). Interactive effects of vegetation, soil moisture and bulk density on depth of burning of thick organic soils. International Journal of Wildland Fire, 20(3), 418-429.

Benscoter, B. W., & Vitt, D. H. (2008). Spatial patterns and temporal trajectories of the bog ground layer along a post-fire chronosequence. Ecosystems, 11(7), 1054-1064. https://doi.org/10.1007/s10021-008-9178-4.

Benscoter, B. W., & Wieder, R. K. (2003). Variability in organic matter lost by combustion in a boreal bog during the 2001 Chisholm fire. Canadian Journal of Forest Research, 33(12), 2509-2513.

Bond-Lamberty, B., Peckham, S. D., Ahl, D. E., & Gower, S. T. (2007). Fire as the dominant driver of central Canadian boreal forest carbon balance. Nature, 450(7166), 89-92.

Bourgeau-Chavez, L. L., Endres, S., Powell, R., Battaglia, M. J., Benscoter, B., Turetsky, M., ... & Banda, E. (2017). Mapping boreal peatland ecosystem types from multitemporal radar and optical satellite imagery. Canadian Journal of Forest Research, 47(4), 545-559.

Bourgeau-Chavez, L. L., Grelik, S. L., Billmire, M., Jenkins, L. K., Kasischke, E. S., & Turetsky, M. R. (2020). Assessing boreal peat fire severity and vulnerability of peatlands to early season wildland fire. Frontiers in Forests and Global Change, 3, 20.

Brandt, J. P., Flannigan, M. D., Maynard, D. G., Thompson, I. D., & Volney, W. J. A. (2013). An introduction to Canada's boreal zone: ecosystem processes, health, sustainability, and environmental issues. Environmental Reviews, 21(4), 207-226.

Braverman, M., & Quinton, W. L. (2016). Hydrological impacts of seismic lines in the wetland-dominated zone of thawing, discontinuous permafrost, Northwest Territories, Canada. Hydrological Processes, 30(15), 2617-2627.

Breiman, L. (2001). Random forests. Machine learning, 45(1), 5-32.

Brown, S. M., Petrone, R. M., Mendoza, C., & Devito, K. J. (2010). Surface vegetation controls on evapotranspiration from a sub-humid Western Boreal Plain wetland. Hydrological Processes: An International Journal, 24(8), 1072-1085.

Chasmer, L. E., Hopkinson, C. D., Petrone, R. M., & Sitar, M. (2017). Using multitemporal and multispectral airborne lidar to assess depth of peat loss and correspondence with a new active normalized burn ratio for wildfires. Geophysical Research Letters, 44(23), 11-851.

Chasmer, L., Lima, E. M., Mahoney, C., Hopkinson, C., Montgomery, J., & Cobbaert, D. (2021). Shrub changes with proximity to anthropogenic disturbance in boreal wetlands determined using bi-temporal airborne lidar in the Oil Sands Region, Alberta Canada. Science of the Total Environment, 780, 146638.

Chen, J., & Kumar, P. (2001). Topographic influence on the seasonal and interannual variation of water and energy balance of basins in North America. Journal of Climate, 14(9), 1989-2014.

Csanyi, N., & Toth, C.K. (2007). Improvement of lidar data accuracy using lidar-specific ground targets. Photogramm. Eng. Remote Sens., 73, 385–396.

de Groot, W. J., Flannigan, M. D., & Cantin, A. S. (2013). Climate change impacts on future boreal fire regimes. Forest Ecology and Management, 294, 35-44.

Dabros, A., Higgins, K. L., & Pinzon, J. (2022). Seismic line edge effects on plants, lichens and their environmental conditions in boreal peatlands of Northwest Alberta (Canada). Restoration Ecology, 30(4), e13468.

Devito, K., Mendoza, C., & Qualizza, C. (2012). Conceptualizing water movement in the Boreal Plains. Implications for watershed reconstruction.

Dons, K., Bhattarai, S., Meilby, H., Smith-Hall, C., & Panduro, T. E. (2016). Indirect approach for estimation of forest degradation in non-intact dry forest: modelling biomass loss with Tweedie distributions. Carbon balance and management, 11(1), 14.

Ducks Unlimited Canada & Alberta North American Waterfowl Management Plan. (2017, March 15). Boreal Wetlands and Climate Change: Alberta Science Summary [PDF]. AB NAWMP. https://abnawmp.ca/wp-content/uploads/2020/09/Boreal-Science-Summary-Final_web.pdf

Dunn PK, Smyth GK (2005). "Series evaluation of Tweedie exponential dispersion models." Statistics and Computing, **15**(4), 267-280.

Elmes, M. C., & Price, J. S. (2019). Hydrologic function of a moderate-rich fen watershed in the Athabasca Oil Sands Region of the Western Boreal Plain, northern Alberta. Journal of Hydrology, 570, 692-704.

Elmes, M. C., Thompson, D. K., Sherwood, J. H., & Price, J. S. (2018). Hydrometeorological conditions preceding wildfire, and the 10 subsequent burning of a fen watershed in Fort McMurray, Alberta, Canada.

Elmes, M. C., Davidson, S. J., & Price, J. S. (2021). Ecohydrological interactions in a boreal fen–swamp complex, Alberta, Canada. Ecohydrology, 14(7), e2335.

Elmes, M. C., Petrone, R. M., Volik, O., & Price, J. S. (2022). Changes to the hydrology of a boreal fen following the placement of an access road and below ground pipeline. Journal of Hydrology: Regional Studies, 40, 101031.

Esri. (n.d.). Flow Accumulation (Spatial Analyst). In ArcGIS Pro documentation. Retrieved from https://pro.arcgis.com/en/pro-app/3.3/tool-reference/spatial-analyst/flow-accumulation.htm.

Ferone, J. M., & Devito, K. J. (2004). Shallow groundwater–surface water interactions in pond–peatland complexes along a Boreal Plains topographic gradient. Journal of Hydrology, 292(1-4), 75-95.

Ficken, C. D., Cobbaert, D., Rooney, R.C. (2019). Low extent but high impact of human land use on wetland flora across the boreal oil sands region. Sci. Total Environ. 693, 133647.

Flannigan, M., Stocks, B., Turetsky, M., & Wotton, M. (2009). Impacts of climate change on fire activity and fire management in the circumboreal forest. Global change biology, 15(3), 549-560.

Frandsen, W. H. (1987). The influence of moisture and mineral soil on the combustion limits of smoldering forest duff. Canadian Journal of Forest Research, 17(12), 1540-1544.

Gao, B. C. (1996). NDWI—A normalized difference water index for remote sensing of vegetation liquid water from space. Remote sensing of environment, 58(3), 257-266.

Gorham, E. "Northern peatlands: role in the carbon cycle and probable responses to climatic warming." Ecological applications 1.2 (1991): 182-195.

Gower, S. T., Krankina, O., Olson, R. J., Apps, M., Linder, S., & Wang, C. (2001). Net primary production and carbon allocation patterns of boreal forest ecosystems. Ecological applications, 11(5), 1395-1411.

Government of Alberta. (2018). Base Watersheds [Data set]. Open Government – Government of Alberta. Retrieved April 11, 2025, from https://open.alberta.ca/opendata/gda-87c2f32f-cd0b-4250-8142-e49391512c64

Groot, A., Carlson, D.W., Fleming, R.L., Wood, J.E., 1997. Small openings in trembling aspen forest: microclimate and regeneration of white spruce and trembling aspen. NODA/NFP Technical Report TR-47 31 pgs. (ISBN 0-662-25461-9)

Hakkenberg, C. R., Clark, M. L., Bailey, T., Burns, P., & Goetz, S. J. (2024). Ladder fuels rather than canopy volumes consistently predict wildfire severity even in extreme topographic-weather conditions. Communications Earth & Environment, 5(1), 721.

Hanes, C. C., Wang, X., Jain, P., Parisien, M. A., Little, J. M., & Flannigan, M. D. (2019). Fire-regime changes in Canada over the last half century. Canadian Journal of Forest Research, 49(3), 256-269.

Hartshorn, A. S., Southard, R. J., & Bledsoe, C. S. (2003). Structure and function of peatland-forest ecotones in southeastern Alaska. Soil Science Society of America Journal, 67(5), 1572-1581.

Hokanson, K. J., Lukenbach, M. C., Devito, K. J., Kettridge, N., Petrone, R. M., & Waddington, J. M. (2016). Groundwater connectivity controls peat burn severity in the boreal plains. Ecohydrology, 9(4), 574-584.

Hopkinson, C., Chasmer, L. E., Sass, G., Creed, I. F., Sitar, M., Kalbfleisch, W., & Treitz, P. (2005). Vegetation class dependent errors in lidar ground elevation and canopy height estimates in a boreal wetland environment. Canadian journal of remote sensing, 31(2), 191-206.

Ireson, A. M., Barr, A. G., Johnstone, J. F., Mamet, S. D., Van der Kamp, G., Whitfield, C. J., Michel, N. L., North, R. L., Westbrook, C. J., DeBeer, C., Chun, K. P., Nazemi, A., & Sagin, J. (2015). The changing water cycle: the Boreal Plains ecozone of Western Canada. Wiley Interdisciplinary Reviews: Water, 2(5), 505-521.

Jean, S. A., Pinno, B. D., & Nielsen, S. E. (2020). Early regeneration dynamics of pure black spruce and aspen forests after wildfire in boreal Alberta, Canada. Forests, 11(3), 333.

Jiangshan Lai, Jing Tang, Tingyuan Li, Aiying Zhan, Lingfeng Mao. 2024. Evaluating the relative importance of predictors in Generalized Additive Models using the gam.hp R package. Plant Diversity, 46(4): 542-546.

Jones, E. A., Chasmer, L. E., Devito, K. J., & Hopkinson, C. D. (2024). Shortening fire return interval predisposes west-central Canadian boreal peatlands to more rapid vegetation growth and transition to forest cover. Global Change Biology, 30(2), e17185.

Kochtubajda, B.; Brimelow, J.; Flannigan, M.; Morrow, B.; Greenhough, M.D. The extreme 2016 wildfire in Fort McMurray, Alberta, Canada. Bull. Am. Meteorol. Soc. 2017, 7, 176–177.

Kohlenberg, A. J., Turetsky, M. R., Thompson, D. K., Branfireun, B. A., & Mitchell, C. P. (2018). Controls on boreal peat combustion and resulting emissions of carbon and mercury. Environmental Research Letters, 13(3), 035005.

Kovacs, P. J. E., McBean, G. A., McGillivray, R. G., & Pulsifer, K. (2019). Fort McMurray wildfire: Learning from Canada's costliest disaster. Zurich, Switzerland: Zurich Insurance Company Ltd.

Larsen, C. P. (1997). Spatial and temporal variations in boreal forest fire frequency in northern Alberta. Journal of Biogeography, 24(5), 663-673.

Lawson B. D. & Armitage O. B. (2008). Weather Guide for the Canadian Forest Fire Danger Rating System. Natural Resources Canada, Canadian Forest Service, Northern Forestry Centre, Edmonton, Alberta. 84 p. Available at: http://cfs.nrcan.gc.ca/pubwarehouse/pdfs/29152.pdf. (Accessed January 2023).

Lecomte, J. B., Benoît, H. P., Etienne, M. P., Bel, L., & Parent, E. (2013). Modeling the habitat associations and spatial distribution of benthic macroinvertebrates: A hierarchical Bayesian model for zero-inflated biomass data. Ecological Modelling, 265, 74-84.

Lee, P., Smyth, C., & Boutin, S. (2004). Quantitative review of riparian buffer width guidelines from Canada and the United States. Journal of environmental management, 70(2), 165-180.

Lin, S., Liu, Y., & Huang, X. (2021). Climate-induced Arctic-boreal peatland fire and carbon loss in the 21st century. Science of the Total Environment, 796, 148924.

Locky, D. A., Bayley, S. E., & Vitt, D. H. (2005). The vegetational ecology of black spruce swamps, fens, and bogs in southern boreal Manitoba, Canada. Wetlands, 25(3), 564-582.

Lovitt, J., Rahman, M.M., Saraswati, S., McDermid, G.J., Strack, M., Xu, B. (2018). UAV remote sensing can reveal the effects of low-impact seismic lines on surface morphology, hydrology, and methane (CH4) release in a boreal treed bog. J. Geophys. Res. Biogeosci. 123, 1117–1129.

Lukenbach, M. C., Hokanson, K. J., Moore, P. A., Devito, K. J., Kettridge, N., Thompson, D. K., Wotton, B. M., Petrone, R. M., & Waddington, J. M. (2015). Hydrological controls on deep burning in a northern forested peatland. Hydrological Processes, 29(18), 4114-4124.

Lukenbach, M. C., Hokanson, K. J., Devito, K. J., Kettridge, N., Petrone, R. M., Mendoza, C. A., Granath, G., & Waddington, J. M. (2017). Post-fire ecohydrological conditions at peatland margins in different hydrogeological settings of the Boreal Plain. Journal of Hydrology, 548, 741-753.

Lundberg, S. M., & Lee, S. I. (2017). A unified approach to interpreting model predictions. Advances in neural information processing systems, 30.

Lundberg, Scott M., Gabriel G. Erion, and Su-In Lee. 2019. "Consistent Individualized Feature Attribution for Tree Ensembles." arXiv. https://doi.org/10.48550/arXiv.1802.03888.

Markle, C. E., North, T. D., Harris, L. I., Moore, P. A., & Waddington, J. M. (2020). Spatial heterogeneity of surface topography in peatlands: Assessing overwintering habitat availability for the eastern massasauga rattlesnake. Wetlands, 40(6), 2337-2349.

Marra, G., & Wood, S. (2011). Practical variable selection for generalized additive models. Computational Statistics & Data Analysis, 55, 2372–2387.

Marshall, I. B., Schut, P., & Ballard, M. (1999). A national ecological framework for Canada: Attribute data. Environmental Quality Branch, Ecosystems Science Directorate, Environment Canada and Research Branch, Agriculture and Agri-Food Canada, Ottawa/Hull. http://sis. agr.gc.ca/cansis/nsdb/ecostrat/1999report/index.html (Accessed February 2023).

Mehmood, K., Anees, S. A., Muhammad, S., Hussain, K., Shahzad, F., Liu, Q., Ansari, M. J., & Khan, W. R. (2024). Analyzing vegetation health dynamics across seasons and regions through NDVI and climatic variables. Scientific Reports, 14(1), 11775.

Miller, E. A. (2020). A conceptual interpretation of the drought code of the Canadian forest fire weather index system. Fire, 3(2), 23.

Moeslund, J. E., Arge, L., Bøcher, P. K., Dalgaard, T., & Svenning, J. C. (2013). Topography as a driver of local terrestrial vascular plant diversity patterns. Nordic Journal of Botany, 31(2), 129-144.

Molnar, C. (2025). Interpretable Machine Learning: A Guide for Making Black Box Models Explainable (2nd ed.).

Morison, M., van Beest, C., Macrae, M., Nwaishi, F., & Petrone, R. (2021). Deeper burning in a boreal fen peatland 1-year post-wildfire accelerates recovery trajectory of carbon dioxide uptake. Ecohydrology, 14(3), e2277.

National Wetlands Working Group. 1997. The Canadian Wetland Classification System, 2nd Edition. Warner, B.G. and C.D.A. Rubec (eds.), Wetlands Research Centre, University of Waterloo, Waterloo, ON, Canada. 68 p.

Natural Resources Canada. (2016). National Road Network (NRN) – AB, Alberta. Shapefile. Available at: https://open.alberta.ca/opendata/gda-6aa3584c-e1c1-4d9e-879c-082686587608#summary. (Accessed December 2022).

Natural Resources Canada. (2017). The State of Canada's Forests—Annual Report 2017; Government of Canada: Ottawa, ON, Canada.

Nelson, K., Thompson, D., Hopkinson, C., Petrone, R., & Chasmer, L. (2021). Peatland-fire interactions: A review of wildland fire feedbacks and interactions in Canadian boreal peatlands. Science of the total environment, 769, 145212.

Nelson, K., Chasmer, L., & Hopkinson, C. (2022). Quantifying Lidar Elevation Accuracy: Parameterization and Wavelength Selection for Optimal Ground Classifications Based on Time since Fire/Disturbance. Remote Sensing, 14(20), 5080.

Nichols, J. E., & Peteet, D. M. (2019). Rapid expansion of northern peatlands and doubled estimate of carbon storage. Nature Geoscience, 12(11), 917-921.

Nicodemus, K. K. (2011). On the stability and ranking of predictors from random forest variable importance measures. Briefings in bioinformatics, 12(4), 369-373.

Pedersen, E. J., Miller, D. L., Simpson, G. L., & Ross, N. (2019). Hierarchical generalized additive models in ecology: an introduction with mgcv. PeerJ, 7, e6876.

Pedregosa, F., Varoquaux, G., Gramfort, A., Michel, V., Thirion, B., Grisel, O., Blondel, M., Prettenhofer, P., Weiss, R., Dubourg, V., Vanderplas, J., Passos, A., Cournapeau, D., Brucher, M., Perrot, M., & Duchesnay, É. (2011). Scikit-learn: Machine learning in Python. the Journal of machine Learning research, 12, 2825-2830.

Petrone, R. M., Devito, K. J., Silins, U., Mendoza, C., Brown, S. C., Kaufman, S. C., & Price, J. S. (2008). Transient peat properties in two pond-peatland complexes in the sub-humid Western Boreal Plain, Canada. Mires & Peat, 3.

Ploton, P., Mortier, F., Réjou-Méchain, M., Barbier, N., Picard, N., Rossi, V., Dormann, C., Cornu, G., Viennois, G., Bayol, N., Lyapustin, A., Gourlet-Fleury, S., & Pélissier, R. (2020). Spatial validation reveals poor predictive performance of large-scale ecological mapping models. Nature communications, 11(1), 4540.

R Core Team. (2024). R: a language and environment for statistical computing.

Risk, C., & James, P. M. A. (2022). Optimal Cross-Validation Strategies for Selection of Spatial Interpolation Models for the Canadian Forest Fire Weather Index System. Earth and Space Science, 9(2), e2021EA002019.

Roberts, D. R., Bahn, V., Ciuti, S., Boyce, M. S., Elith, J., Guillera-Arroita, G., Hauenstein, S., Lahoz-Monfort, J. J., Schroder, B., Thuiller, W., Warton, D. I., & Dormann, C. F. (2017). Cross-validation strategies for data with temporal, spatial, hierarchical, or phylogenetic structure. Ecography, 40(8), 913-929.

Schratz, P., Muenchow, J., Iturritxa, E., Richter, J., & Brenning, A. (2019). Hyperparameter tuning and performance assessment of statistical and machine-learning algorithms using spatial data. Ecological Modelling, 406, 109-120.

Sörensen, R., Zinko, U., & Seibert, J. (2006). On the calculation of the topographic wetness index: evaluation of different methods based on field observations. Hydrology and Earth System Sciences, 10(1), 101-112.

Stocks, B. J., Mason, J. A., Todd, J. B., Bosch, E. M., Wotton, B. M., Amiro, B. D., Flannigan, M. D., Hirsch, K. G., Logan, K. A., Martell, D. L., & Skinner, W. R. (2002). Large forest fires in Canada, 1959–1997. Journal of Geophysical Research: Atmospheres, 107(D1), FFR-5.

Thompson, D. K., & Waddington, J. M. (2014). A Markov chain method for simulating bulk density profiles in boreal peatlands. Geoderma, 232, 123-129.

Turetsky, M. R., Amiro, B. D., Bosch, E., & Bhatti, J. S. (2004). Historical burn area in western Canadian peatlands and its relationship to fire weather indices. Global Biogeochemical Cycles, 18(4).

Turetsky, M. R., Benscoter, B., Page, S., Rein, G., Van Der Werf, G. R., & Watts, A. (2015). Global vulnerability of peatlands to fire and carbon loss. Nature Geoscience, 8(1), 11-14.

Turetsky, M. R., & St. Louis, V. L. (2006). Disturbance in boreal peatlands. In Boreal peatland ecosystems (pp. 359-379). Berlin, Heidelberg: Springer Berlin Heidelberg.

Turetsky, M., Wieder, K., Halsey, L., & Vitt, D. (2002). Current disturbance and the diminishing peatland carbon sink. Geophysical Research Letters, 29(11), 1526. https://doi.org/10.1029/2001GL014000

Van Wagner, C. E. (1987). Development and structure of the Canadian forest fire weather index system (No. 35).

Van der Werf, G. R., Randerson, J. T., Giglio, L., Collatz, G. J., Mu, M., Kasibhatla, P. S., Morton, D. C., DeFries, R, S., Jin, Y. V., & van Leeuwen, T. T. (2010). Global fire emissions and the contribution of deforestation, savanna, forest, agricultural, and peat fires (1997–2009). Atmospheric chemistry and physics, 10(23), 11707-11735.

Vitt, D. H., & Short, P. (2020). Peatlands. In Wetlands and Habitats (pp. 27-36). CRC Press.

Vitt, D. H., & Wieder, R. K. (2006). Boreal peatland ecosystems (pp. 9-24). Springer-Verlag Berlin Heidelberg.

Waddington, J. M., Thompson, D. K., Wotton, M., Quinton, W. L., Flannigan, M. D., Benscoter, B. W., ... & Turetsky, M. R. (2012). Examining the utility of the Canadian Forest Fire Weather Index System in boreal peatlands. Canadian Journal of Forest Research, 42(1), 47-58.

Weltzin, J. F., Bridgham, S. D., Pastor, J., Chen, J., & Harth, C. (2003). Potential effects of warming and drying on peatland plant community composition. Global Change Biology, 9(2), 141-151.

Wieder, R. K., Scott, K. D., Kamminga, K., Vile, M. A., Vitt, D. H., Bone, T., Xu, B. I. N., Benscoter, B. W., & Bhatti, J. S. (2009). Postfire carbon balance in boreal bogs of Alberta, Canada. Global Change Biology, 15(1), 63-81.

Wilkinson, S. L., Moore, P. A., & Waddington, J. M. (2019). Assessing drivers of cross-scale variability in peat smoldering combustion vulnerability in forested boreal peatlands. Frontiers in Forests and Global Change, 2, 84.

Wilkinson, S. L., Moore, P. A., Flannigan, M. D., Wotton, B. M., & Waddington, J. M. (2018). Did enhanced afforestation cause high severity peat burn in the Fort McMurray Horse River wildfire?. Environmental Research Letters, 13(1), 014018.

Wilkinson, S. L., Tekatch, A. M., Markle, C. E., Moore, P. A., & Waddington, J. M. (2020). Shallow peat is most vulnerable to high peat burn severity during wildfire. Environmental Research Letters, 15(10), 104032.

Wilkinson, S. L., Verkaik, G. J., Moore, P. A., & Waddington, J. M. (2020). Threshold peat burn severity breaks evaporation-limiting feedback. Ecohydrology, 13(1), e2168.

Wood, S. (2022). mgcv: Mixed GAM Computation Vehicle with Automatic Smoothness Estimation. R package version 1.8-41, https://cran.r-project.org/web/packages/mgcv/mgcv.pdf.

Wood, S. (2017). Generalized additive models: an introduction with R (Second Edition). Boco Raton: CRC Press.

Wotton, B. M., Stocks, B. J., & Martell, D. L. (2005). An index for tracking sheltered forest floor moisture within the Canadian Forest Fire Weather Index System. International Journal of Wildland Fire, 14(2), 169-182.

Zoltai, S. C., Morrissey, L. A., Livingston, G. P., & Groot, W. D. (1998). Effects of fires on carbon cycling in North American boreal peatlands. Environmental Reviews, 6(1), 13-24.

Zoltai, S. C., & Vitt, D. H. (1995). Canadian wetlands: environmental gradients and classification. Vegetatio, 118(1), 131-137.

CHAPTER 5: DISPROPORTIONATE SOIL CARBON LOSS AND ECOTONE SENSITIVITY IN BOREAL PEATLAND WILDLAND FIRES: INSIGHTS FROM LIDAR AND FIELD DATA

5.1 Abstract

Peatlands play a critical role in the global carbon (C)-climate cycle, acting as vast, long-term stores of disproportionately large quantities of C relative to their land area. In recent decades, climate-driven shifts in fire regimes have occurred across Canada's boreal regions driven by higher temperatures, increased evapotranspiration, and longer drought periods. This has increased concerns about the vulnerability of peatland C to combustion losses. Understanding the magnitude and vulnerability of C released to the atmosphere during wildland fires in peatlands is therefore essential, but it is highly uncertain.

This study was conducted in the Athabasca Oil Sands Region of Alberta's Boreal Plains. C losses from peatlands during the 2016 Horse River Wildfire were estimated based on field-collected soil C data and pre- and post-fire airborne lidar data. C Losses were quantified across peatland types and ecotones and separated into above- and below-ground combustion. Soil C losses were nearly an order of magnitude greater than vegetation C losses (2.11 ± 5.09 kg m^{-2} vs. -0.38 ± 0.32 kg m^{-2}, respectively). Bog ecotones were zones of significant soil C loss, with average losses of 16.5 kg m^{-2}. Lidar-derived burned area and C losses were compared with the spectral burn severity index, dNBR. A binary burned/unburned classification showed strong agreement in bogs (88%) but poor in swamps (48%). Vegetation C loss correlated moderately well with dNBR strength, while the relationship between soil C loss and dNBR was very weak. Comparisons between lidar-derived soil C losses with estimates of C loss based on the fire disturbance module of

national C loss model, the Canadian Model for Peatlands, indicated that C losses from bogs were greater than expected, particularly when ecotones were included, while fens and swamp C losses were on the low end of model expectations.

5.2 Introduction

Peatlands are a globally important carbon (C) sink, storing nearly one-third of the world's soil C, despite covering only 2–3% of the Earth's surface (Gorham, 1991; Vitt & Short, 2020). In Canada, C-dense boreal peatlands cover approximately 12% of the land area (Tarnocai, 2006). As a result of the wet, anoxic conditions, decomposition in peatlands is slower than the accumulation of organic matter, resulting in greater C associated with this important atmospheric C sink (Turetsky et al., 2015; Wieder et al., 2006). Boreal peatlands include bogs, fens, and swamps. Bogs are ombrogenous, receiving water exclusively from precipitation, and support vegetation such as sphagnum (*Sphagnum* spp.) moss and black spruce (*Picea mariana*) trees. Fens, on the other hand, are minerotrophic and receive both ground water and surface water. They are often dominated by sedges and brown mosses (Elmes et al., 2018; Ingram, 1983; Vitt et al., 2000; Zoltai & Vitt, 1995). Swamps, like fens, receive hydrological inputs from both ground and surface water and are, by definition, treed or forested (Zoltai & Vitt, 1995). Historically, peatlands have been resilient to wildland fire due to their typically waterlogged conditions (Zoltai et al., 1998); however, recent warming, drying, shrubification, and changing fire regimes are resulting in increased fire behaviour in peatlands, threatening the capacity of this C sink (e.g., Kettridge et al., 2015; Wilkinson et al., 2023).

In recent decades, the boreal fire regime has shifted dramatically (Flannigan et al., 2013; Kettridge et al., 2015). This trend is attributed to higher temperatures, increased evapotranspiration, and longer drought periods (e.g., Flannigan *et al*., 2009, 2016; Wotton *et al*., 2010) – especially in the Western Boreal Plain (WBP), where evapotranspiration often exceeds precipitation (Wang et al., 2014; Elmes et al., 2018). Drought conditions

result in a drop in the water table, exposing deep layers of peat to oxic conditions and making them susceptible to smouldering combustion (Waddington et al., 2012; Turetsky et al., 2011). This slow-burning, flameless combustion can persist for long periods through cold and wet conditions and can result in significant C loss by burning through peat layers that have accumulated for up to thousands of years (Rein et al., 2008; Frandsen, 1997). For example, Lukenbach et al., (2015) and Waddington et al., (2012) show that reductions/lowering of the water table can increase the depth and severity of peat combustion, resulting in higher C loss from fire and longer post fire moss and vegetation recovery times. Lower water tables may also increase the flammability of vegetation, enhancing C losses during fire (e.g., Turetsky et al., 2015). Further, lower or more fluctuating water tables can promote encroachment of shrub and deciduous trees into peat environments (Nelson et al., 2021; Weltzin et al., 2003; Chapter 2), increasing above-ground fuel that can further increase fire severity. Conversely, this increased productivity can enhance net ecosystem production, increasing C sequestration (e.g., Loisel & Yu, 2013; Nelson et al., 2021; Chapter 2).

The vulnerability of boreal peatlands and the increased frequency and intensity of fire during high to extreme fire weather periods associated with increased fuel availability from drying poses a risk to local ecosystems, which may experience significant ecological impacts (high severity) of fire (e.g., Bourgeau-Chavez et al., 2020). Fires in peatlands alter vegetation composition, favoring the growth of fire-adapted ericaceous shrubs and deciduous tree species (e.g., *Betula spp.*, *Populus spp.*), enhancing fuel loads and flammability, while reducing the dominance of keystone species such as sphagnum moss, which plays a crucial role in maintaining the surface moisture, hydrology, and C balance

of these ecosystems (Turetsky et al., 2011; Kettridge et al., 2015). Furthermore, deep-burning peat fires can cause long-lasting damage to the soil structure, lowering the water-holding capacity of the peat, enhancing shrubification and making it more vulnerable to fires (Bourgeau-Chavez et al., 2020; Jones *et al*., 2022). The susceptibility of peatlands to combustion and subsequent C losses likely varies between peatland classes (bogs, fens, and swamps) because of differences in hydrology, dominant vegetation, and hydrogeological connectivity to the broader landscape (e.g., Wilkinson et al., 2019). Peatland ecotones, the transition zones between peatland cores and adjacent ecosystems such as uplands or other peatland types, are likely especially vulnerable (e.g., Dimitrov et al., 2014; Lukenbach et al., 2015). These areas often experience greater hydrological fluctuations, and subsequently increased bulk density – conditions that promote shrubification (increasing above-ground fuel loads) and enhanced peat combustion (e.g., Lukenbach et al., 2015; Hokanson et al., 2016; Nelson et al., 2021; Chapter 2).

Warming and drying influence C loss from both above- and below-ground fuels. Lower water tables and increased fragmentation results in greater soil combustion while simultaneously enhancing conditions for shrubification, increasing fuel loads (e.g., Nelson et al., 2021; Weltzin et al., 2000; Chapter 2). This not only adds available fuel, but can further water table declines and increases in peat bulk density, reinforcing a local, ecohydrological positive feedback that further increases soil combustion (Nelson et al., 2021; Chapter 2). As fire return intervals shorten, C released from both above- and below-ground combustion may also contribute to a broader, positive C-climate feedback loop where enhanced combustion increases atmospheric C, increasing atmospheric forcing towards a warmer atmosphere and greater drying potential, further increasing peatland

vulnerability to fire (Nelson et al., 2021; Chapter 2). Such changes may also result in peatlands shifting from a C sink to a C source (Turetsky et al., 2015).

Above- and below-ground fuels contribute to peatland C loss during wildland fire, but their relative contributions are markedly different, and both are highly variable. Below-ground combustion typically dominates C losses, accounting for ~70-90% of total C losses from fires occurring in North American boreal forests and peatlands (e.g. Rogers et al., 2014; Hokanson et al., 2016; Walker et al., 2018). Reported soil C losses vary substantially, even within studies. For example, Rogers et al. (2014) found soil C losses between 0.12 and 5.14 kg m^{-2} (mean: 2.06 kg m^{-2}) across boreal organic forests, Hokanson et al. (2016) reported peatland soil C losses ranging from 0.5 to 6.5 kg m^{-2}, and Wilkinson et al. (2018) found soil C losses of 0.63 to 6.74 kg m^{-2} in sites with varying degrees of anthropogenic drainage. Above-ground C losses are smaller, but also highly variable. Boby et al. (2010) estimated that Alaskan boreal forest vegetation lost ~0.37 kg C m^{-2} during combustion, while Zoltai et al. (1998), reports average above-ground C losses of 0.16 kg C m^{-2} across northern bogs and fens, but up to 2.4 kg C m^{-2} in forested swamps. These wide ranges reflect the high ecological variability of these ecosystems, highlighting the need for high resolution, spatially continuous C loss estimates.

Despite measurement variability and known differences in combustion controls between peatland types and ecotones, understanding of peatland-C dynamics under a changing fire regime remains limited. In particular, there is a lack of spatially explicit quantification of peat combustion and C losses across peatland types and ecotones, leaving a critical gap in understanding fire-driven C emissions. As a result of methodological limitations including access to remote peatlands, a changing climate, and drying peatlands,

there remains uncertainty as to the current contribution of boreal peatland wildfires to global atmospheric C. Multispectral remote sensing such as Landsat can be used to assess burn severity via vegetation condition, often assessed through indices such as the differenced Normalized Burn Ratio (dNBR; Key & Benson, 2006). However, optical approaches cannot directly quantify soil loss (French et al., 2020) and burn severity indices such as dNBR may relate poorly to peat combustion due to canopy occlusion and the high moisture content of peatland soils, which dampen SWIR reflectance (Lobell & Asner, 2002). Conversely, changes in peat surface moisture due to hydrological fluctuations between image acquisitions can produce false, high burn severity signals even if no combustion occurred (e.g., Miller & Thode, 2007). Studies examining the relationship between dNBR and soil combustion have produced mixed results: Hoy et al. (2008) found poor correlation between dNBR and soil combustion, while Chasmer et al. (2017) reported moderate agreement, but noted reduced performance in transitional ecotones. Understanding how dNBR relates to above- and below-ground combustion in peatlands is therefore important for providing context on the reliability of dNBR and other optical indices in representing burn severity and associated C losses from peatlands.

Airborne lidar technology measures ground surface elevations over broad spatial extents, thereby reducing uncertainties in elevation data, and measuring spatial variability in depth of burn when pre- and post-fire datasets are compared (Alonzo et al., 2017; Chasmer et al., 2017; Reddy et al., 2015). Lidar data can also be used to scale field plot measurements by providing detailed measurements of vegetation structure and topography. High resolution, 3D bitemporal airborne scanning lidar data can be used to overcome methodological limitations of quantifying depth of peat burn by spatializing pre-fire ground

surface and post-fire elevation changes, thus improving understanding of peat combustion (Chasmer et al., 2017). Information from pre- and post-fire lidar data and field-based sampling approaches can thus be used to better understand C loss, spatial variability, and the contribution of boreal peatlands to atmospheric C. As burn severity indices derived from optical remote sensing data are often used in wildland fire research (e.g., Miller & Thode, 2007), understanding how well these products reflect above- and below-ground combustion in peatlands is important.

This study investigates the spatial variability of C losses from boreal peatlands during the 2016 Horse River Wildfire in northeastern Alberta using field and airborne lidar data and evaluates how well these estimates compare with broad-scale modelled C loss outputs (from the Canadian Model for Peatlands, CaMP) that inform national greenhouse gas (GHG) reporting. Specifically, it addresses the following questions:

a) How much above- and below-ground C is lost across a broad range of peatlands during wildland fire, and what is the relative contribution of these pools to direct atmospheric C emissions?

b) How does total C loss and patterns of C loss differ between peatland types (bogs, fens, and swamps) and their ecotones, and what does this suggest about their relative vulnerabilities to C losses during wildland fire?

c) How well does remotely sensed burn severity based on the differenced Normalized Burn Ratio (dNBR) from Landsat, commonly applied in forested ecosystems (e.g.,

Keeley, 2009), represent above- and below-ground C losses in peatlands, and does this relationship vary between peatland types and their ecotones?

d) How do field to lidar-derived C loss estimates compare to those of a large-scale peatland C loss model; what does this indicate about how the Horse River Wildfire was representative of, or differed from, expected conditions; and what are the implications for Canada's forest area greenhouse gas reporting?

5.3 Methods

5.3.1 Study Area

This study was conducted over a 12,254-hectare area located approximately 30 km south of Fort McMurray, Alberta (centered at 56.526818, -111.293123; Figure 5.1). The region is part of the Athabasca Oil Sands Region within Canada's Boreal Plains ecozone (Ecoregions Working Group, 1989; Elmes et al., 2021; Downing & Pettapiece, 2006). Although the study area does not encompass open-pit oil extraction zones, it contains numerous seismic lines, cut lines, oil and gas well sites, and access roads (e.g., Abib et al., 2019; Dabros et al., 2022). The climate in the region is subhumid, with an average annual temperature of 1°C (Elmes et al., 2021) and approximately 420 mm of annual precipitation (ECCC, 2019). Potential evapotranspiration (PET) frequently exceeds precipitation, leading to moisture deficits (Marshall et al., 1999; Devito et al., 2012). Despite this, the region is heavily dominated by wetlands (predominantly peatlands), covering up to 50% of the landscape (Ferone & Devito, 2004; Ficken et al., 2019). Within the study area, peatlands are comprised of 37% bog, 6% bog ecotone, 22% fen, 10% fen ecotone, 14%

swamp, and 11% swamp ecotone (Figure 5.1). These peatlands are considered to be near their climatic limit and are, therefore, highly sensitive to climatic changes and disturbances (Wilkinson et al., 2019; Devito et al., 2012).

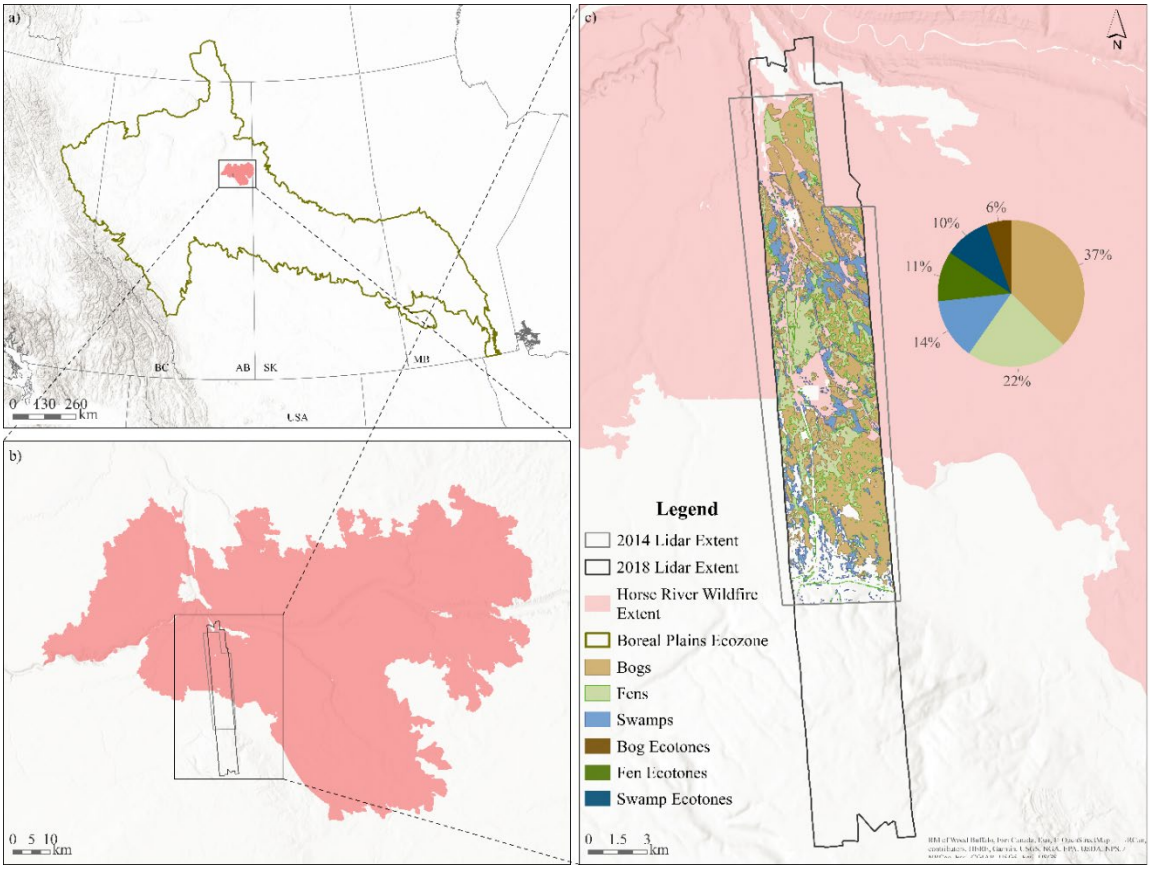

Figure 5.1. Study area map indicating a) extent of the Boreal Plains Ecozone and relative area of the Horse River Wildfire, b) Horse River Wildfire perimeter and lidar coverage, and c) the study area within overlapping lidar zones with peatland type, derived from Bourgeau-Chavez et al. (2017), shown. Proportional area of each peatland type is represented by the pie chart.

The Boreal Plains is a relatively flat region underlain by a variety of glacial materials ranging from lacustrine clay to coarse glaciofluvial substrates (Devito et al., 2012; Hokanson et al., 2016). Upland soils in the area consist of gray luvisols, gleysols, and organic soils, while lowland soils are primarily organic with peat depths exceeding 40 cm in peatlands (Jean et al., 2020; Halsey et al., 2003). Vegetation in the upland areas

includes trembling aspen (*Populus tremuloides*), balsam poplar (*Populus balsamifera*), black spruce (*Picea mariana*), white spruce (*Picea glauca*), balsam fir (*Abies balsamea*), and jack pine (*Pinus banksiana*; Downing & Pettapiece, 2006). The peatlands, primarily treed or forested, are dominated by black spruce, tamarack (*Larix laricina*), bog birch (*Betula pumila*), dwarf birch (*Betula glandulosa*), willow (*Salix spp.*), sphagnum moss, feather mosses (*Pleurozium shreberi*, *Hylocomium splendens*), lichen (*Bryoria* spp.), sedges (*Carex* spp.), alders (*Alnus rugosa*), and Labrador tea (*Ledum groenlandicum*; Smith et al., 2007).

The Horse River Wildfire, which burned the study area, ignited on May 1, 2016, under hot, dry, and windy conditions about 7 km southwest of Fort McMurray (Alberta Agriculture and Forestry & MNP, 2017). Temperatures on the day of ignition exceeded 25°C, with relative humidity below 20% and there were abnormally high winds. Over the next four days, fire weather became more severe, with temperatures rising to 30°C, relative humidity dropping to 15%, and wind speeds reaching 25 km/h (Alberta Agriculture and Forestry & MNP, 2017). These weather conditions, combined with the second warmest winter in 20 years (Elmes et al., 2018), dry spring conditions, and unflushed vegetation, resulted in rapid fire spread (Kochtubajda et al., 2017). The study area (Figure 5.1) burned from May 4 to May 16, 2016 (Alberta Agriculture and Forestry & MNP, 2017). The fire ultimately burned over 589,000 hectares (Natural Resources Canada, 2017) and was declared under control on July 4, 2016 (Alberta Agriculture and Forestry & MNP, 2017).

5.3.2 Data Acquisition

5.3.2.1 Field Data

In July 2018, field data were collected in conjunction with airborne lidar data (Section 2.2.2) for calibration and validation purposes. Sample sites consisted of 18 burned and 6 unburned "reference" peatlands, which were selected as proxies for pre-fire peatland conditions. At each site, transects approximately 30 m long were established, running from the transition zone into the middle of the peatland. Global Navigation Satellite System (GNSS) stations were set up at the beginning and end of each transect, collecting data for a minimum of one hour (Figure 5.2). Plots were placed at intervals of one meter in burned sites and two meters in unburned sites. Ground surface elevations were measured at each plot location using a level (n=708) and later referenced to the GNSS station elevations to validate lidar-derived digital terrain models (DTMs). Additionally, Post Processed Kinematic (PPK) GNSS measurements were collected (n=2655) along two road surfaces. With limited elevation variability, vegetation interference, or temporal changes, road surfaces provided a reliable "tie" for eliminating offsets between lidar datasets.

Within plots along unburned transects, peat samples of approximately 8 cm^2 (measured precisely in the field for subsequent lab-based bulk density and C analyses) were collected at 10 cm depth increments to a maximum depth of 40 cm (confined by the height of the water table). Litter was removed from the sample location and samples were

extracted using a serrated blade and pruning snips. Samples were placed in paper bags to dry until they could be processed.

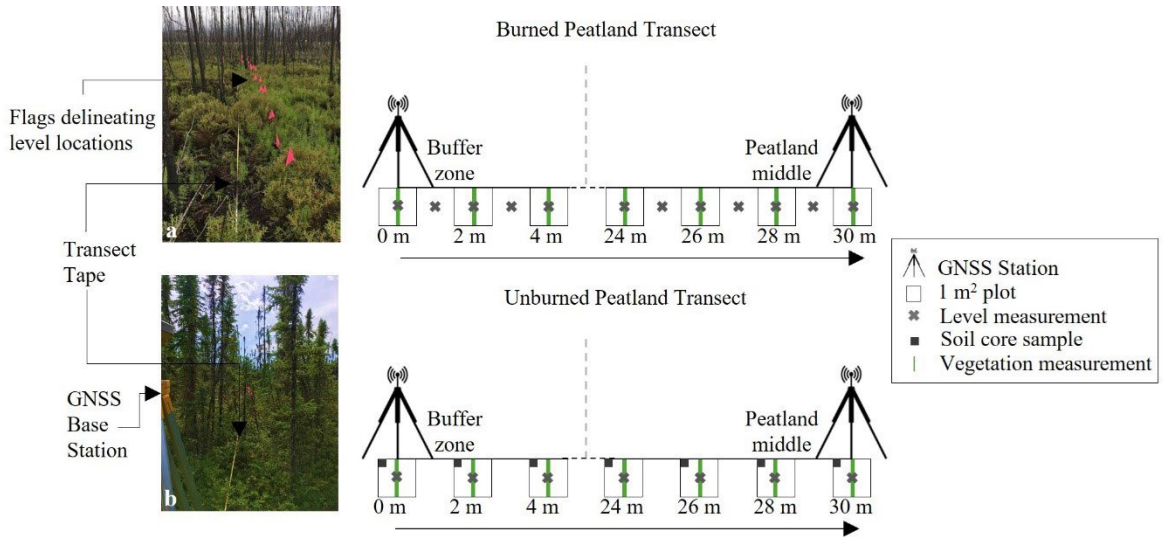

Figure 5.2. Field photos and schematic of field transects in a) burned sites and b) unburned sites.

Tree measurements were used to determine above-ground biomass (AGB) from forest mensuration plots (n=83) based on Lambert et al. (2005) and used for development of lidar-based AGB models. All plots were established coincidently with lidar data collected between 2002 and 2023 across multiple campaigns across the northern boreal and southern taiga plains. Forest mensuration within plots included species, density, diameter at breast height, and tree height. Understory plots of $1m^2$ or 3.99 m radius were measured within 37 of the 83 plots, including those presented in Flade et al. (2020, 2021) and within forest mensuration plots measured at the start of each non-burned transect in this study. Within stand estimates were also included from Gower et al. (1997), also used in Hopkinson et al. (2016a). Flade et al. (2020, 2021) and Gower et al. (1997) developed allometric equations used to estimate understory biomass based on biomass volume through destructive

sampling. Understory biomass was scaled to plot area and added to canopy biomass to determine total AGB per plot.

5.3.2.2 Lidar Data

Pre-fire lidar data were collected in May 2014 by Airborne Imaging Inc. (Canada) using a Leica ALS70 system (Leica Geosystems, Switzerland) with an emission wavelength of 1064 nm (near-infrared). Data were collected from a flight height of 1550 meters, using a pulse repetition frequency of 300 kHz and scan angles of ±25 degrees with a 50% flightline overlap, resulting in a point density of 7.2 points per square meter. Post-fire lidar data, coincident with fieldwork, were collected in July 2018 by the University of Lethbridge ARTeMiS Lab using a Titan multispectral lidar (Teledyne Optech Inc., Canada), which emits/receives laser pulses at two and three wavelengths respectively: 532 nm (green) (received), 1064 nm (near-infrared), and 1550 nm (shortwave infrared), respectively (see Hopkinson et al. 2016b). The data were collected at a flight height of 1000 meters, with a pulse repetition frequency of 300 kHz (100 kHz per wavelength) and a scan angle of ±25 degrees, resulting in a combined point density of 11.1 points per square meter.

5.3.3 Data Processing & Analysis

5.3.3.1 Laboratory Analysis

All peat core samples were oven-dried at 105°C to determine the dry weight (Carter & Gregorich, 2008a). Samples were weighed incrementally and were dried until the weight was unchanged. Dry weight and soil volume from time of collection were then used to calculate peat bulk density using equation (5.1) (Carter & Gregorich, 2008a).

$$\text{Bulk density (g/cm}^3\text{)} = \text{Dry soil weight (g)} / \text{Soil volume (cm}^3\text{)} \quad (5.1)$$

Once dry, samples were stratified within each site by transition zone and peatland based on their distance along the transect and were separated to account for differences in C densities. Samples collected between 4–12 m either side of the division between the transition zone and peatland were analysed for total organic C (TOC) content (n = 208) using loss on ignition. C density was then calculated using equation 5.2 (Carter & Gregorich, 2008b).

$$\text{C density (g/cm}^3\text{)} = \text{Bulk density (g/cm}^3\text{)} * (\text{TOC (\%)} / 100\%) \quad (5.2)$$

5.3.3.2 Lidar Data Processing

Pre- and post-fire lidar datasets were co-registered to road surface measurements obtained through PPK GNSS surveys to eliminate mean offsets between datasets using Bentley Microstation TerraSolid Terrascan software (Terrasolid, Helsinki, Finland; Axelsson, 2000). Isolated points were removed, and lidar points were classified as ground or non-ground (vegetation) using optimal classification parameters identified in Nelson et al. (2022; Chapter 3). Digital terrain models (DTMs) were created at a resolution of 1 m from ground points for both pre- and post-fire datasets using LAStools' las2dem function (RapidLasso GmbH, Germany). Canopy closure and vegetation height metrics were calculated using lascanopy at a resolution of 5 m.

5.3.3.3 GIS Analysis

All GIS analyses were conducted using ArcGIS Pro (Esri, California, U.S.). All analyses were conducted within the Horse River Wildfire perimeter, obtained from Alberta Forestry and Parks Historical Wildfire Perimeter Data. Depth of peat burn was calculated by subtracting the 2014 DTM from the 2018 DTM. To mitigate noise in the lidar data, the

resulting map was aggregated from 1 m (1 m^2) to 5 m (25 m^2) resolution using the mean. By aggregating positive and negative elevation changes, depth of burn will be conservative, due to the assumption of positive elevation change within a given aggregated pixel is likely due to noise, an unburned area of peat (for example, hummocks often do not burn during wildland fire (Benscoter & Wieder, 2003; Benscoter et al., 2015)), or is positive due to peat expansion (hydrology) and/or peat accumulation between the two lidar data collections. This also means that small areas of deep burning ("hot spots") may be underrepresented due to spatial averaging. However, the potential underestimation of these deeply burned areas, as a tradeoff for reducing high-resolution noise, mitigates the risk of over-estimating depth of burn and subsequent C losses due to outliers (Nelson et al., 2022; Chapter 3). As a result, DOB and subsequent C loss estimates are likely conservative. All vegetation canopy and height metrics were aligned with the DTM pixels.

Peatland types were mapped using the object-based classification system from Bourgeau-Chavez et al. (2017), which categorizes land cover into several wetland types (bog, open fen, treed fen, swamp, and marsh), upland classes (deciduous and coniferous forests), and other categories (water, barren/logged, and recently burned) with an overall classification accuracy of 93%. Based on this classification, bogs, fens, and swamps were then manually delineated to correct classification errors and refine boundaries. Transition zones were then delineated by identifying changes in tree height and elevation with increasing distance from the peatland edge using the method of Jones et al. (2024).

Within the fire perimeter, the proportion of each peatland/ecotone type that burned was calculated based on the proportion of pixels with depth of burn > 0, and DOB was quantified within these pixels. This approach ensured that burned areas represented

combustion, as opposed to spectral changes. Remotely sensed indices such as dNBR can misclassify burned and unburned areas in peatlands due to spectral changes resulting from vegetation regrowth or moisture variability over the time of the fire (e.g., Goodwin & Collett, 2014; Miller & Thode, 2007); therefore, dNBR was only used for comparisons with lidar-derived C losses, and not defining burned area.

Peatland forms were classified into forested, treed, or open categories based on 5 m resolution, lidar-derived canopy cover and tree height. Forested peatlands were defined as >25% canopy cover and mature trees ≥5 m in height; treed peatlands had 10-25% canopy cover and mature trees <5 m in height; and open peatlands had <10% canopy cover and mature trees <5 m in height. These classifications align with the Kyoto Protocol and Marrakesh Accords within the United Nations Framework Convention on Climate Change and are utilized by CaMP (Bona et al., 2020) for national forested peatland GHG reporting within the National Forest Carbon Monitoring Accounting and Reporting System for Canada (NFC-MARS). Initial classification was based on average canopy cover and tree height per peatland. If peatlands did not fall into one category using this threshold combination, maximum tree height and proportions of forested, treed, and open pixels were used. If results were still ambiguous, canopy cover took precedence over tree height.

To calculate the differenced Normalized Burn Ratio (dNBR) pre- and post-fire Landsat data were accessed through the USGS Earth Explorer. Pre-fire, cloud-free Landsat 8 OLI Collection (C) 2 Level (L) 2 data from April 10, 2016, were selected. Post-fire, Landsat 7 ETM+ C2 L2 data from June 21, 2016, were used, as they were collected shortly after the fire on a cloud-free day. While utilizing different sensors may result in minor differences in NBR (Koutsias & Pleniou, 2015), C2 L2 products have been atmospherically

corrected, and the datasets were checked for alignment to minimize any discrepancies. C loss rasters were aggregated to 30-m resolution to match Landsat pixel size.

The Near Infrared (NIR) and Shortwave Infrared (SWIR) bands were used in equation (5.3) to calculate dNBR: bands 5 (NIR) and 7 (SWIR) for Landsat 8 and bands 4 (NIR) and 5 (SWIR) for Landsat 7 (U.S. Geological Survey, n.d; Key & Benson, 2006).

(5.3)

Burn severity was then categorized based on the dNBR thresholds established by Hall et al. (2008): unburned ($dNBR \leq 0.04$), low severity ($0.04 < dNBR \leq 0.283$), moderate severity ($0.283 < dNBR \leq 0.513$), and high severity ($dNBR \geq 0.514$; does not exist within study area). To evaluate differences in burned area extent as detected by optical versus lidar-based methods, burn masks were created from both datasets at 30 m resolution. Pixels were classified as burned if lidar-derived DOB exceeded 0 cm and if dNBR exceeded 0.04 (following Hall et al., 2008). The proportion of peatland area within the fire perimeter that was classified as burned using each method was calculated, as well as percentage of overlap and non-overlap.

5.3.3.4 Carbon Calculations

A soil C loss raster was generated based on depth of burn and C density values derived from soil samples collected from hollows and flats (samples from hummocks were excluded, as they are typically left unburned or only lightly burned; Benscoter et al., 2011, 2015). For each peatland type, a power-law equation was fit to raw C density data to model C density with depth. This equation was then integrated to model cumulative C content

with depth (Equation 5.4), where C is cumulative carbon content (kg m^{-2}) at depth z (cm), and a and b were estimated from the raw C density power-law function.

(5.4)

Equation 5.4 was then applied to each pixel of t

he depth of burn raster to map soil C losses. Soil C cores were not collected in swamps, so, due to their similar geogenous and minerotrophic characteristics, fen and fen ecotone cumulative C depth functions were applied to swamps and swamp ecotone pixels.

Vegetation C loss from the fire was modelled using pre- and post-fire lidar data and field plot tree and shrub measurements (see Figure 5.3 for workflow). To determine pre-fire above-ground biomass (AGB) 84 vegetation mensuration plots of 11.28 and 3.99 m radius were measured for tree height and diameter at breast height (DBH), species and stem density. These plots were dispersed through the Fort McMurray region, the Utikuma region of Alberta, and central Saskatchewan. Species-specific equations from Lambert et al. (2005) were used to determine plot-based tree biomass, as well as the foliage-only canopy fuel load (CFL). Plots that included understory biomass measurements (n=48) were used to determine a species-specific shrub multiplier (based on Flade et al., 2021), based on tree species composition and age. Understory vegetation was assumed to combust fully. To convert foliage CFL to total above-ground canopy fuel load (AGFL), a fine branch multiplier of 2.36 was applied (foliage CFL*2.36) derived from measurements of Stocks et al. (2004). The shrub biomass was then added to determine full pre-fire AGFL (Equation 5.5)

(5.5)

To model the relationship between plot-specific lidar structural metrics and field-based biomass, total AGB was linearly regressed against lidar height metrics, of which the 90^{th} percentile height of ground normalized lidar returns was optimal (derived via lascanopy; LAStools; Isenburg, 2023; AGB = 0.67 * P90; R^2 = 0.86). This regression model was then used to produce a pre-fire lidar-based AGB map. Because the AGB map is dominated by stems (which do not burn much, if at all), the field, plot-based AGB and AGFL data was used to determine the relationship between AGB and AGFL ($y = 0.88x^{0.58}$; R^2 = 0.56). This was then applied to the pre-fire AGB map, producing a map of pre-fire AGFL – the biomass that would be combusted during a fire.

To determine the AGFL that was lost due to combustion, pre- and post-fire lidar-derived gap fractions were determined as percentages via lascanopy by taking the inverse of the ratio of first returns above 0.5 m to the total number of first returns. The change in gap fraction (canopy openness) between pre- and post-fire lidar data was then inverted (to canopy cover), multiplied by 0.01 to provide a value between 1 (no loss) to 0 (100% loss) and then multiplied by the pre-fire AGFL. Because lidar returns reflect from unburned stems and other materials, 100% combustion does not occur, except in cells with only shrub/understory biomass, or those where trees have fallen. To ensure that pre- and post-fire canopy cover did not vary as a result of differences in lidar point density between 2014 and 2018 surveys, canopy cover was compared in relatively unchanging, unburned conifer stands across a range of tree heights and canopy openness using randomly selected points. The offset between the two years was under 3%, which could be accounted for due to differences in precipitation and temperature, and so no correction factor was applied. Vegetation C content was assumed to be 50% of the biomass (e.g., Ma et al., 2018).

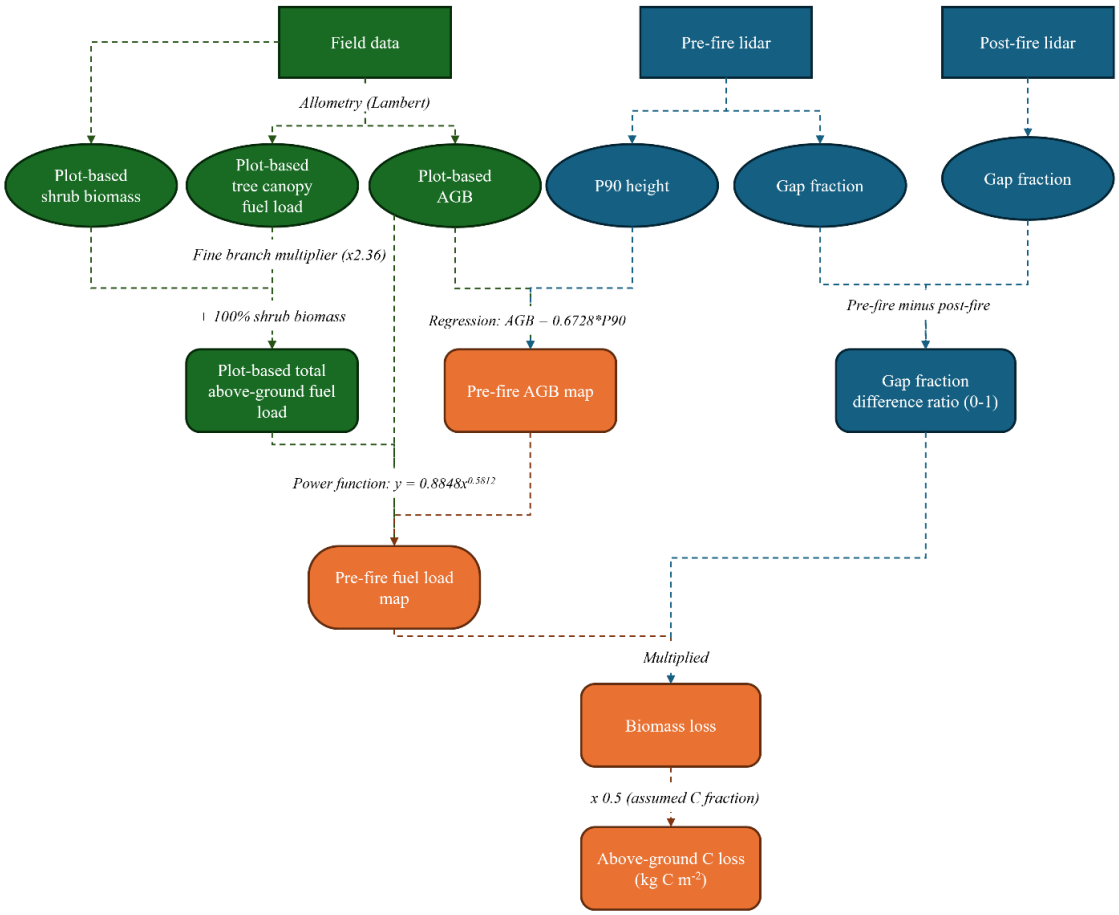

Figure 5.3. Workflow for above-ground C loss estimation from field- and lidar-data.

Random points were distributed throughout each peatland and ecotone type (n=15,474) using a proportional stratified random sampling approach followed by disproportional random sampling of two points per individual peatland. This ensured spatial representation based on peatland size, while also ensuring inclusion of smaller peatlands, and retention of data from potentially unique peatlands. C losses and canopy metrics were then extracted from each point.

5.3.3.5 CaMP Parameterization

The fire disturbance C loss equations that underpin the fire module in the Canadian Model for Peatlands (CaMP v2.0; Bona et al., 2020) were used as comparative benchmarks for

the lidar-based estimates of soil C loss. These equations estimate soil C consumption during wildland fire as a function of peatland type, pre-fire water table depth, and the C density of the oxic layer. CaMP models water table depth as a linear function of Drought Code with peatland/canopy-specific intercepts (WT = -0.045*DC + $intercept$; Bona et al., 2020), which defines the oxic layer depth. Cumulative C with depth was then estimated using a power function $C(z) = az^b$, where a and b are peatland/canopy type coefficients published in Bona et al. (2020). CaMP assumes set proportions of the oxic layers are consumed during combustion (11.4% in fens and 12.5% in bogs); these were applied to the cumulative C contents at depths. Because the DC at the time of the Horse River Wildfire was uncertain due to complex overwinter and snowmelt moisture dynamics, the four DC scenarios presented in Elmes et al. (2018) were used, adjusted based on day of burn. The lowest (DC = 287) and the highest (DC = 432) values of these scenarios were then used to bracket the estimated range of C consumption.

CaMP does not parameterize water tables for swamps, so treed and forested rich fen values were used as a proxy. Rich versus poor fens were not isolated from one another in classifying peatland canopy type. Therefore, in parameterizing the model, rich fen values were used to represent the study area. The CaMP does not make distinctions for peatland cores versus ecotones, so two analyses were conducted: one using just cores, and one with core and ecotone samples combined.

5.3.3.6 Statistical Analysis

All statistical analyses were completed using R version 4.4.3 (R Core Team, 2024). The data distributions were highly skewed, with many low C loss values and a small number of very high values that pulled the means upward. Non-parametric tests that rely on

medians were used for rigorous statistical analysis; however, it is recognized that C losses from areas of deep burning are important in representing C loss distributions across the landscape. Additionally, including means allows for comparison with other studies, where C loss is often expressed as an average. Means have therefore also been included in the results.

To determine differences in soil C densities with depth between peatland types, a linear mixed-effects model was used after log-transforming depth. Due to the right-skewed nature of the data, significance of C loss differences between peatland types, between burn severity categories, and between canopy types, were determined using Kruskal-Wallis tests followed by post-hoc Dunn's tests. The relationships between soil and vegetation C losses with dNBR across peatland types were determined using Spearman's rank correlation coefficient and Theil-Sen regressions. When comparing lidar-derived C loss estimates with CaMP outputs, means and 95% confidence intervals (CIs) were utilized to optimally represent the full scope of the landscape-scale C loss.

5.4 Results

5.4.1 Carbon Distribution Across the Landscape

5.4.1.1 Field-Based Soil Carbon Content with Peat Depth

Based on the soil cores collected in the field, soil C density increased non-linearly with depth across all peatland types (Figure 5.4a). In bogs and fens, C density increased more gradually with depth, while ecotones showed a more rapid increase in carbon density in the upper layers of peat; however, results from a linear mixed-effects model revealed that while C density did increase significantly with depth, there were no significant differences

in C density between peatland types. Figure 5.4b highlights the cumulative effect of increased C density with depth, where all peatland types saw an accelerating pattern. Bog and fen ecotones had more rapid increases in cumulative C content compared to interior peatlands, indicating that ecotones store more carbon per volume unit.

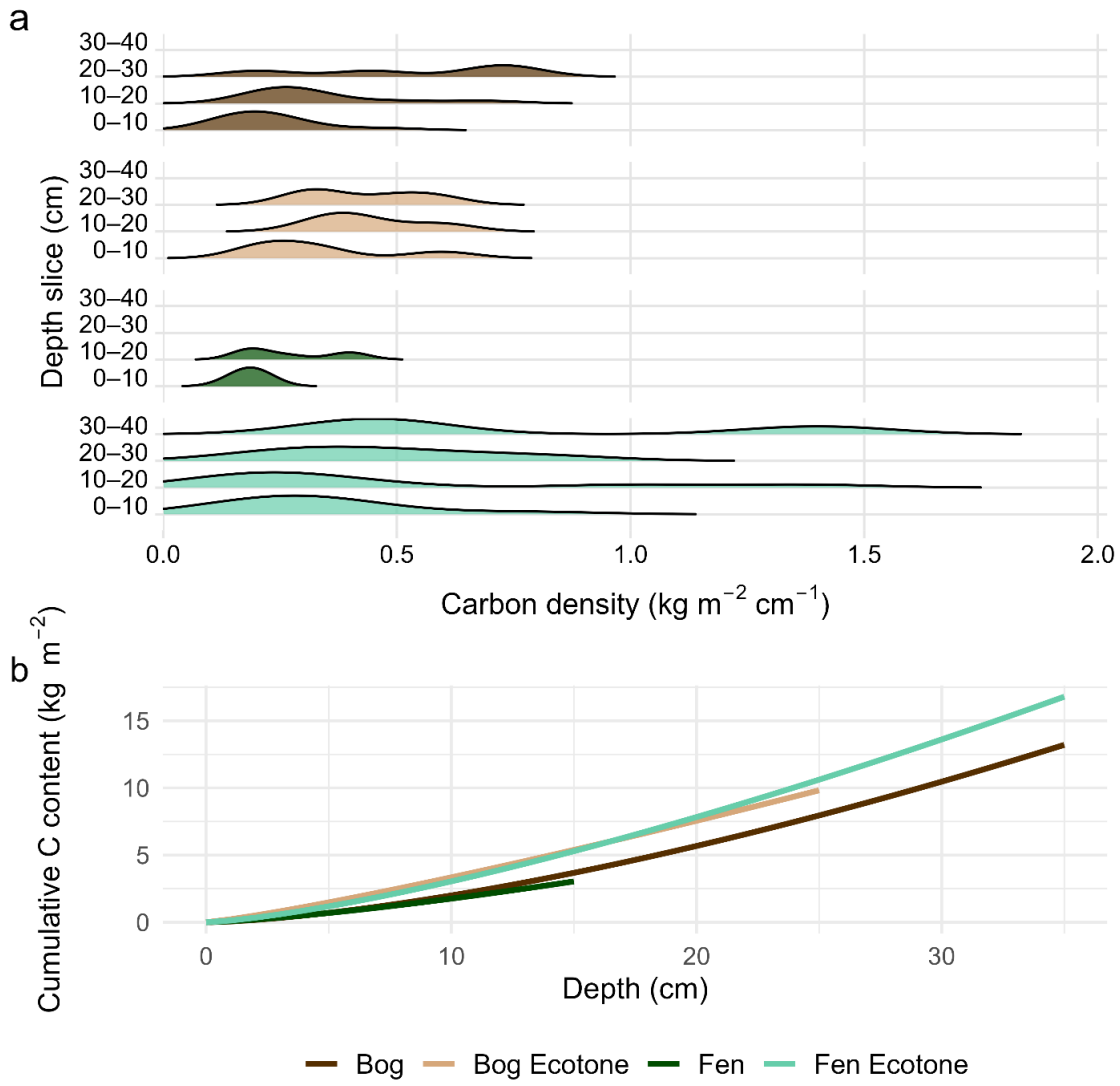

Figure 5.4a. Slice-level soil C density (kg m^{-2} cm^{-1}) with depth (cm) from field samples across peatland types. Density distributions are normalized within each peatland type to demonstrate relative distribution rather than sample size; 5.4b. Cumulative soil C content (kg m^{-2}) with depth (cm), estimated by integrating power-law functions fit to the raw data in panel a. Curves are shown over the range of depths sampled for each peatland type.

5.4.1.2 Lidar-Based Above Ground Carbon Distribution

Pre-fire vegetation (tree, shrub) C content varied between peatland types and their ecotones (Figure 5.5). Bogs ecotones contained the highest mean C density on average (2.05 kg m^{-2}), while fens had the lowest (1.48 kg m^{-2}). Peatland cores all had lower mean and median C densities than their ecotones. Ecotones exhibited greater variability in C density than core peatlands, demonstrated by larger interquartile ranges and whiskers (5^{th} to 95^{th} percentiles; Figure 5.5), suggesting greater spatial heterogeneity. This pattern was particularly pronounced in swamp ecotones, where, despite similar means and medians, the 95^{th} percentile C density was nearly 30% greater than in bog or fen ecotones. Across all peatland types, mean values were consistently higher than medians, reflecting a skewed distribution, driven by a small number of peatlands with considerably more aboveground vegetation C.

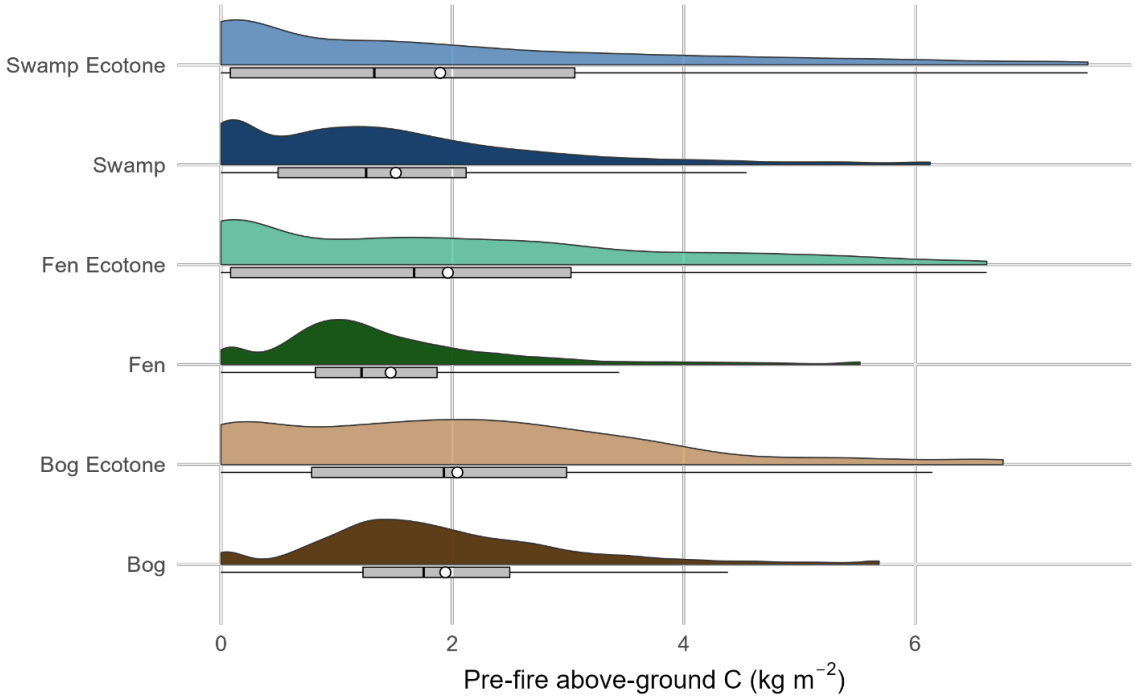

Figure 5.5. Pre-fire aboveground vegetation C content (kg m^{-2}) distribution across the study area by peatland type. Half-violins show kernel density; boxes represent median line and

inter-quartile range (IQR) with whiskers represent 5th and 95th percentiles; dots represent means.

5.4.2 Soil and Vegetation Carbon Losses by Peatland Type

Mean soil C losses consistently exceeded mean vegetation C losses across all peatland types (Figure 5.6; Figure 5.7), and averaged across peatland types, mean soil C loss was approximately an order of magnitude greater than that of vegetation, at -2.11 ± 5.09 kg m^{-2} versus -0.38 ± 0.32 kg m^{-2}. Spearman's rank correlation between soil and vegetation C losses was weak; significant ($p < 0.001$), likely due to the large sample size, but with a low rho value of 0.07, indicating no meaningful relationship.

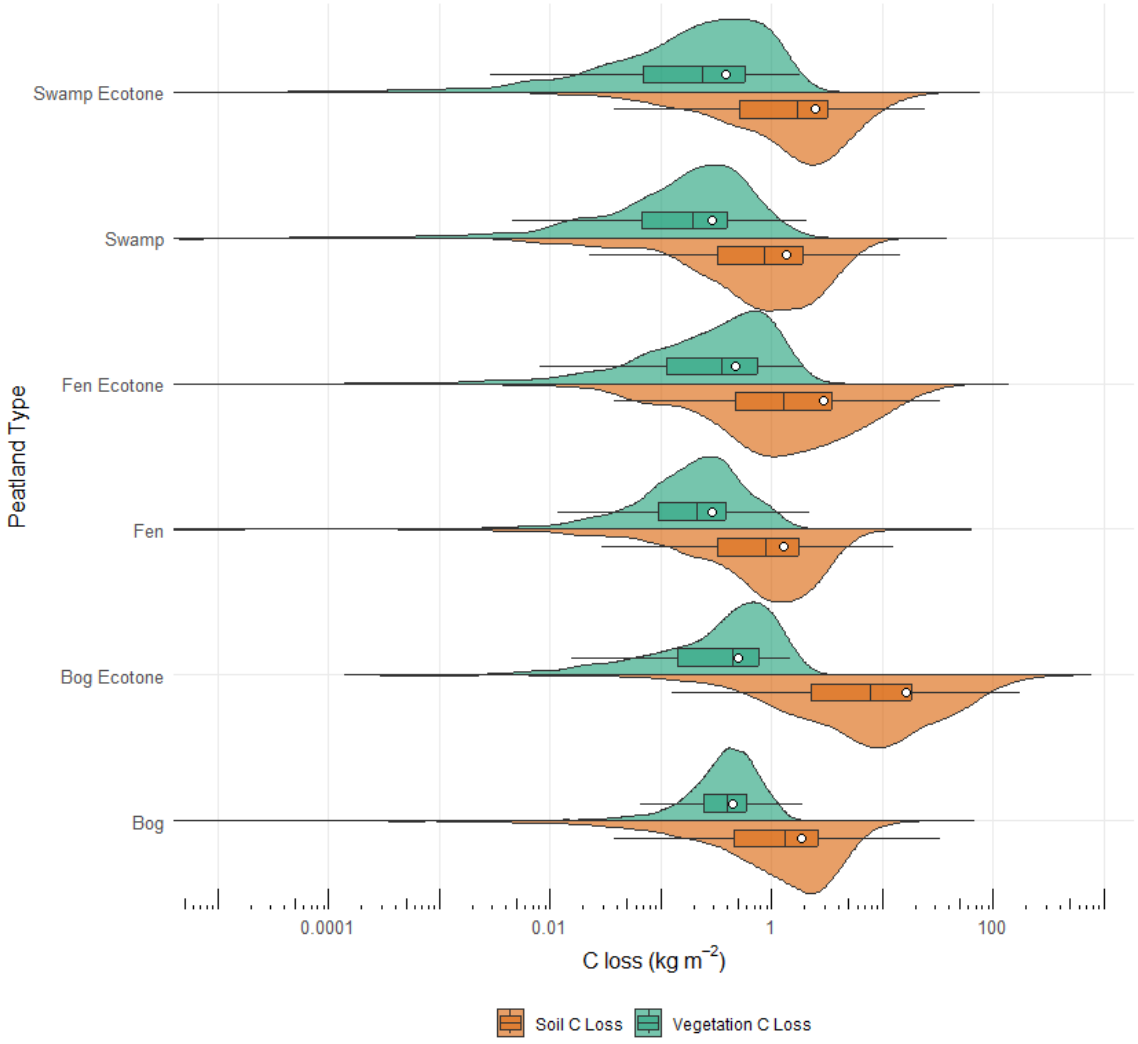

Figure 5.6. Split violin plots with embedded boxplots showing the distribution of vegetation (upper; green) and soil (lower; orange) C losses (kg m^{-2}) by peatland type. White circles represent the mean. Y-axis is on a $\log_{10}$ scale.

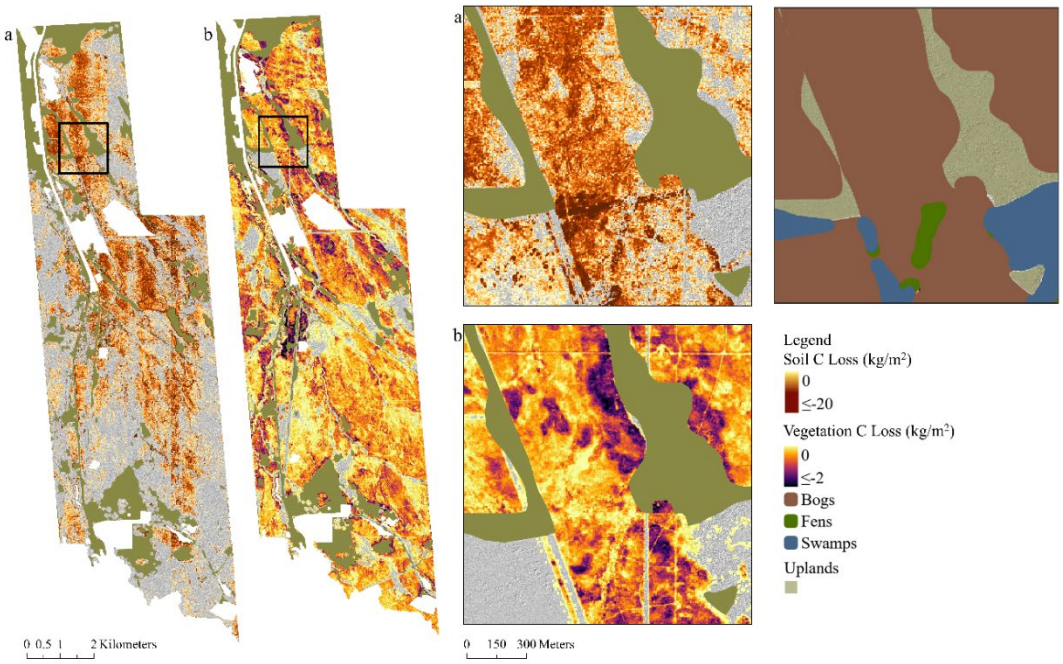

Figure 5.7. Map showing spatial distribution of (a) soil and (b) vegetation C loss across peatlands within the study area, derived from field to lidar informed models. Higher C losses are represented by darker colours (brown for vegetation and red for soil). Inset areas are denoted by black rectangles.

Carbon losses differed significantly between peatland types for both soil (Kruskal-Wallis $\chi^2 = 406.7$, $p < 0.001$; Figure 5.7a) and vegetation (Kruskal-Wallis $\chi^2 = 1246.5$, $p < 0.001$; Figure 5.7b). A post-hoc Dunn's test revealed that each ecotone lost significantly more soil C than its core counterpart ($P<0.001$). Bog ecotones were critical hotspots of soil and vegetation C loss, suggesting these margin zones are especially vulnerable to combustion (mean: -16.5 kg m^{-2}; median: -7.81 kg m^{-2}). Of the peatland core types, bogs experienced the greatest soil C loss (mean: -1.84 kg m^{-2}; median: -1.31 kg m^{-2}). Fens and swamps, on the other hand, tended to have lower soil C losses and their ecotones saw more muted effects compared to bog ecotones.

Vegetation C losses followed a similar pattern, though less extreme (Figure 5.6; Figure 5.7). In general, C loss was greater in peatland ecotones than in their corresponding cores; however, this was only significant in fens and swamps. Within core peatland types, bogs experienced the greatest vegetation C losses (mean: -0.45 kg m^{-2}; median: -0.40 kg m^{-2}). The violin plots in Figure 5.7 and the discrepancies between mean and median C losses highlight the disproportionate impact that a small number of deep-burning hotspots have on C losses – in particular from soil.

Area burned, as defined by lidar-measured DOB, as well as the contribution of total C loss varied across peatland and ecotone types (Table 5.1). Area burned ranged from 33% to 62%, with bogs and bog ecotones experiencing the greatest proportion of burned area. Fens and swamps lost a proportionally small amount of C relative to their area. In contrast, bog ecotones, despite comprising only ~6% of the burned area, accounted for ~25% of total C loss, highlighting their vulnerability to significant C losses.

Table 5.1. Proportion of total area within the fire perimeter, percent area burned (based on lidar-derived depth of burn > 0 cm), and percent contribution to total C loss for each peatland/ecotone type.

Peatland Type	% Area	% Area Burned	% of Total C Loss
Bogs	37	62	40
Fens	22	45	11
Swamps	14	34	4
Bog Ecotones	6	48	25
Fen Ecotones	10	36	10
Swamp Ecotones	11	33	9

5.4.3 Do Optical Burn Severity Metrics (dNBR) Reflect Above- and Belowground Carbon Losses?

5.4.3.1 Soil and Vegetation Carbon Loss Spatial Trends with dNBR Burn Severity

Agreement between lidar-derived versus dNBR-classified burned areas within the fire perimeter varied between peatland and ecotone classes (Table 5.2). Overall agreement of burned and unburned pixels was best in bogs (88%) and fens (84%) but declined in ecotones and was poorest in swamps (48%). Within the area identified as burned by either DOB, dNBR, or both, false positives by dNBR, where combustion was not detected by lidar (i.e. no measurable elevation loss in lidar-derived ground surfaces), occurred in 13% of pixels, ranging from 8 to 29% depending on peatland class (Table 5.2). Pixels were classified as burned only by lidar-derived DOB (i.e. measurable elevation loss), but missed by dNBR, in 12% of pixels, ranging from 3 to 37% depending on peatland class (Table 2). These misalignments were greatest in ecotones and swamps.

Table 5.2. Agreement between DOB- and dNBR-classified burned and unburned pixels. The first three columns show the percentage of total pixels where burned/unburned classifications agreed. Columns 4 and 5 show the percentage of pixels that were classified as burned by only DOB or only dNBR of the total peatland area (/Total). Columns 6 and 7 show the percentage of pixels classified as burned by only DOB or only dNBR of the total area that was classified as burned by either DOB, dNBR, or both (/Burned).

	Unburned Agree	Burned Agree	Total Agree	dNBR Only (/Total)	DOB Only (/Total)	dNBR Only (/Burned)	DOB Only (/Burned)
Bogs	1.0	87.0	88.0	8.6	3.3	8.7	3.4
Fens	4.1	80.3	84.4	8.2	7.4	8.5	7.7
Swamps	12.1	35.4	47.5	15.7	36.8	17.8	41.9
Bog Ecotones	5.4	69.5	74.9	9.6	15.4	10.1	16.3
Fen Ecotones	12.6	48.4	61.0	29.0	10.1	33.2	11.5
Swamp Ecotones	13.3	43.9	57.2	20.0	22.9	23.0	26.4
All Peatlands	6.2	68.6	74.7	13.4	11.9	14.2	12.7

The presence and strength of the association between burn severity, estimated using the often-used index dNBR, and C loss differed depending on peatland type and whether the loss occurred from vegetation or soil carbon pools (Spearman rank correlation; Table 5.3). Vegetation C loss had consistently stronger correlations with dNBR than soil C loss, across peatland types ($\rho = 0.26 – 0.70$), indicating that peatlands that experienced greater burn severity, as indicated by dNBR, also experienced greater vegetation C loss. While all relationships between vegetation C loss and dNBR were significant ($p < 0.001$), this was likely influenced by the large sample size. The magnitude of the relationship, however, varied. The associations were weak in bogs and fens, but moderate to strong in swamps and all peatland ecotone types, with the strongest correlation existing between bog ecotones and dNBR ($\rho = 0.70$; Table 5.3; Figure 5.8). When all peatland types were combined, the

relationship between vegetation C loss and dNBR was weak-to-moderate, but significant ($\rho = 0.44$), highlighting the importance of peatland type-specific analysis. Soil C loss was only weakly correlated with dNBR in bogs, fens, and their respective ecotones ($\rho = 0.09 – 0.20$, $p < 0.05$). There was no significant association, even weakly, between dNBR and soil C loss in swamps or swamp ecotones ($\rho = 0.005 – 0.03$, $p > 0.1$) and when all peatland types were combined, the relationship between soil C loss and dNBR, while significant, was very weak ($\rho = 0.08$).

Table 5.3. Spearman's rank correlation between vegetation C losses (kg m^{-2}) and soil C losses (kg m^{-2}) with dNBR for each peatland type. Values are designated as significant using asterisks (P<0.001 = ***; P<0.05 = **; P<0.1 = *).

Correlation of dNBR with Vegetation and Soil C Losses (kg m^{-2}) by Peatland Type					
Peatland Type	Spearman ρ (vegetation)	p-value	Spearman ρ (soil)	p-value	n
Bog	0.26***	<0.001	0.09***	<0.001	5683
Bog Ecotone	0.70***	<0.001	0.13**	<0.05	307
Fen	0.32***	<0.001	0.03***	<0.001	3383
Fen Ecotone	0.60***	<0.001	0.20***	<0.001	605
Swamp	0.53***	<0.001	0.005	>0.1	1724
Swamp Ecotone	0.53***	<0.001	0.03	>0.1	945
All Peatland Types	0.44***	<0.001	0.08**	<0.001	12647

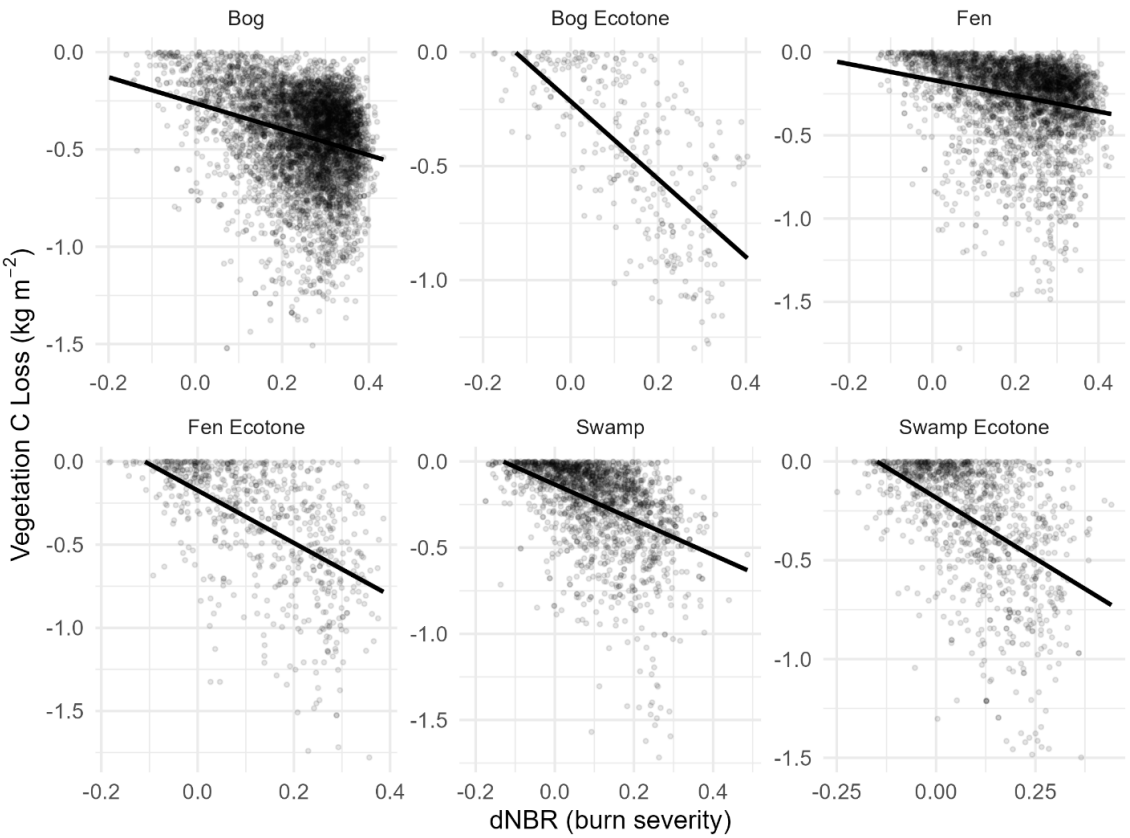

Figure 5.8. Scatter plots of vegetation C loss (kg m^{-2}) versus burn severity (dNBR) for each peatland type. Points represent individual sample estimates. Lines represent Theil-Sen regressions.

5.4.3.2 Soil and Vegetation Carbon Loss Trends with Burn Severity Categories

Figure 5.9 shows how soil and vegetation C losses vary across dNBR-defined burn severity classes (Hall et al., 2008): unburned (dNBR ≤ 0.04), low severity (0.04 < dNBR ≤0.283), and moderate severity (0.283 < dNBR ≤0.513). It is important to note that the "unburned" class reflects low dNBR values and does not necessarily indicate a lack of combustion. This category includes areas where lidar-based C loss estimates indicate combustion did occur, but dNBR signal was low.

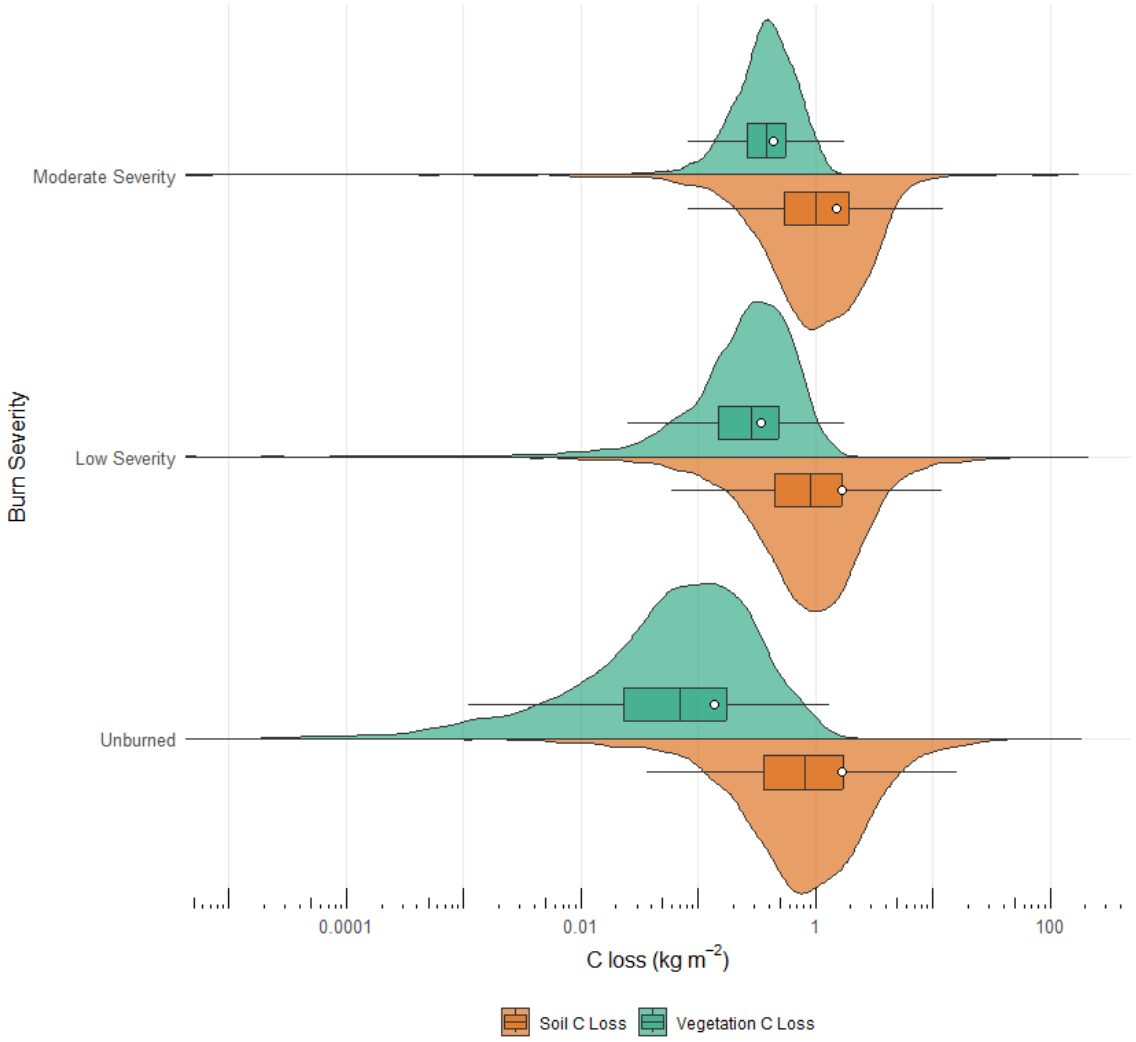

Figure 5.9: Split violin plots with embedded boxplots of vegetation (upper; green) and soil (lower; orange) C losses (kg m^{-2}) by burn-severity category. White circles represent the mean. X-axis is on a $\log_{10}$ scale. Sample sizes for unburned, low, and moderate are n = 3363, 5109, and 4684, respectively.

Median soil C loss differences were minimal, but significant between burn severity classes (Kruskal-Wallis: $\chi^2 = 68.77$, $p < 0.001$; Figure 5.9). A Post-hoc Dunn's test revealed that there were significant differences in soil C losses between all burn severity categories, and that as burn severity category increased, soil C loss also increased significantly ($P < 0.01$) from -0.81 kg m^{-2} C loss in unburned classes to -0.91 kg m^{-2} in low severity classes to -1.02 kg m^{-2} in moderate severity classes. By contrast, mean soil C losses did not follow

this trend and were -1.68 kg m^{-2}, -1.68 kg m^{-2}, and -1.50 kg m^{-2} in unburned, low severity, and moderate severity classes, respectively.

Vegetation C losses differed significantly between all burn severity classes (Kruskal-Wallis: $\chi^2 = 2362.9$, $p < 0.001$; Figure 5.9). A Dunn's test demonstrated that as burn severity category increased, so did vegetation C loss ($p < 0.001$), increasing from a median value of 0.07 kg m^{-2} C loss in areas classified as unburned to 0.29 kg m^{-2} in low severity areas to 0.39 kg m^{-2} in moderate severity areas. Mean C losses followed the same pattern, of -0.14 kg m^{-2}, -0.35 kg m^{-2}, and -0.44 kg m^{-2}, respectively.

The response of soil C loss to burn severity was mixed depending on peatland type (Figure 5.10). Post-hoc Dunn's tests revealed that bogs had significant median soil C loss increases between every burn severity class (-0.90 to -1.01 to -1.16 kg m^{-2} from unburned to low to moderate; $p < 0.05$). In bog ecotones, there were significantly greater soil C losses in unburned areas (-5.35 kg m^{-2}) than in low or moderate severity areas (-9.16, -5.70 kg m^{-2}, respectively; $p < 0.05$); however, no significant difference between low and moderate severity areas. Fens lost significantly more C in low severity areas than unburned (-0.56 to -0.68 kg m^{-2}, unburned to low; $p < 0.05$) and less than moderate (-0.68 to -0.78 kg m^{-2}, low to moderate; $p < 0.05$), with no significant difference between unburned and moderate. There were no significant differences in soil C losses between burn severity classes in fen ecotones (median: -0.67, -1.27, -1.11 kg m^{-2}; unburned, low, moderate, respectively). In swamps, every pair of burn severities differed significantly ($p < 0.05$), but losses did not increase with burn severity (median: -0.69 to -0.75 to -0.45 kg m^{-2}; unburned to low to moderate, respectively). Finally, swamp ecotones saw significantly greater C losses in

moderate than low burn severity (median: -0.84 to -1.39 kg m^{-2}; $p < 0.05$), but not between unburned (-1.30 kg m^{-2}) and low or moderate severity.

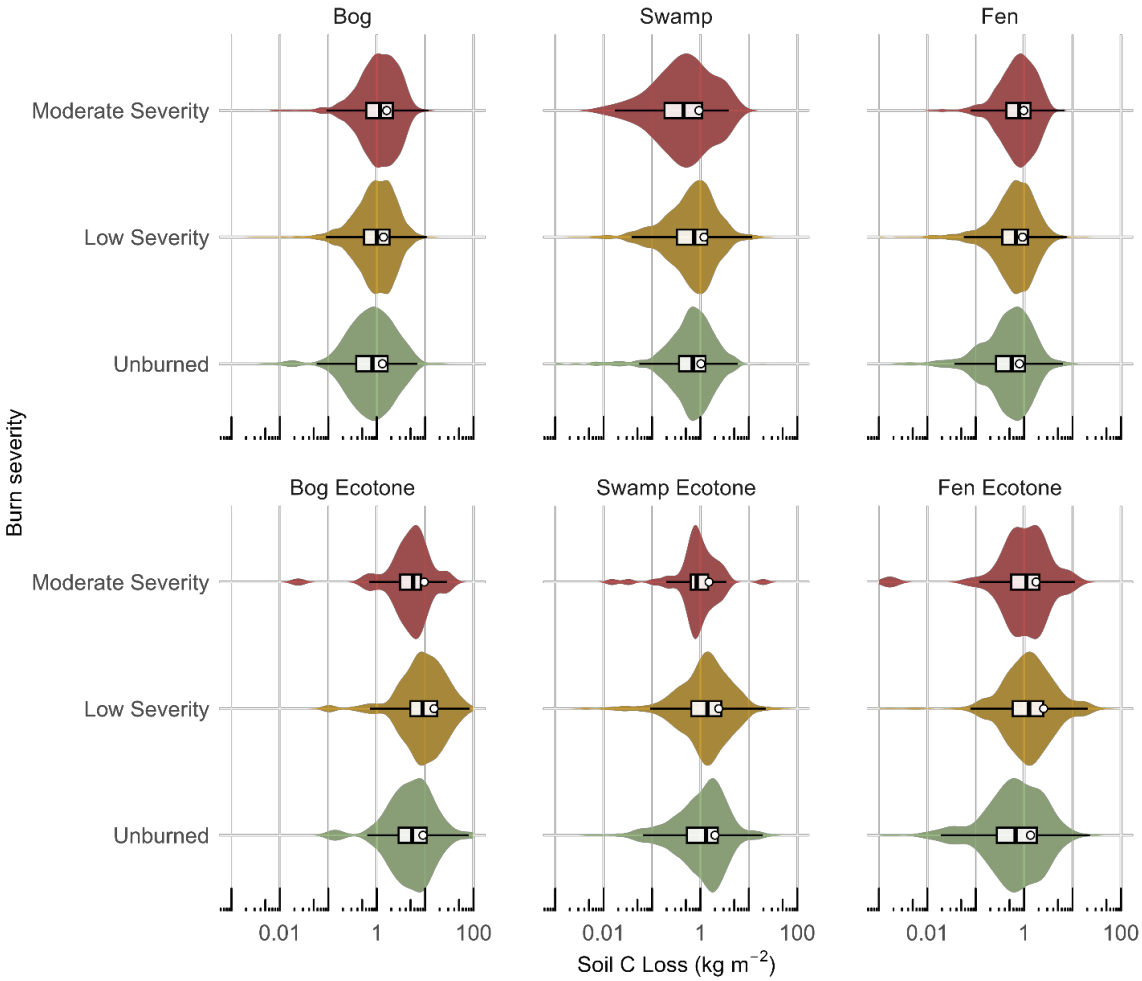

Figure 5.10: Violin plots of soil C loss (kg m^{-2}) by peatland type across three burn severity classes (unburned/regrowth, low, and moderate). Violins show data distribution, boxplots show interquartile range with whiskers to 5th and 95th percentiles, and mean is denoted by black circle embedded in boxplot. Plots have been cut off at 0.001 kg m^{-2} to improve data visualization. Sample sizes (n) for each peatland-severity combination range from 49 to 3001. X-axis is on a $\log_{10}$ scale.

Across peatland types, Kruskal-Wallis tests demonstrated significant differences between peatland types within unburned, low, and moderate severity classes (χ^2 = 253.03, 682.14, 295.7, respectively; $p < 0.001$; Figure 5.10). Bog ecotones consistently had the

greatest soil C losses under all severities, whereas fens experienced the lowest in unburned and low severity areas, while in moderate severity burns, swamps had the lowest.

Unlike with soil C losses, vegetation C loss increased systematically with burn severity in every peatland type (Figure 5.11). This was significant in all pairwise post-hoc Dunn's tests of burn severities in all peatland types ($p < 0.001$ in all peatland types except swamp ecotones where $p < 0.05$). Median C losses increased from -0.15 to -0.37 to -0.43 kg m^{-2} in bogs; -0.07 to -0.53 to -0.74 kg m^{-2} in bog ecotones; -0.07 to -0.20 to -0.25 kg m^{-2} in fens; -0.07 to -0.34 to -0.66 kg m^{-2} in fen ecotones; -0.06 to -0.21 to -0.40 kg m^{-2} in swamps; and -0.06 to -0.30 to -0.47 kg m^{-2} in swamp ecotones.

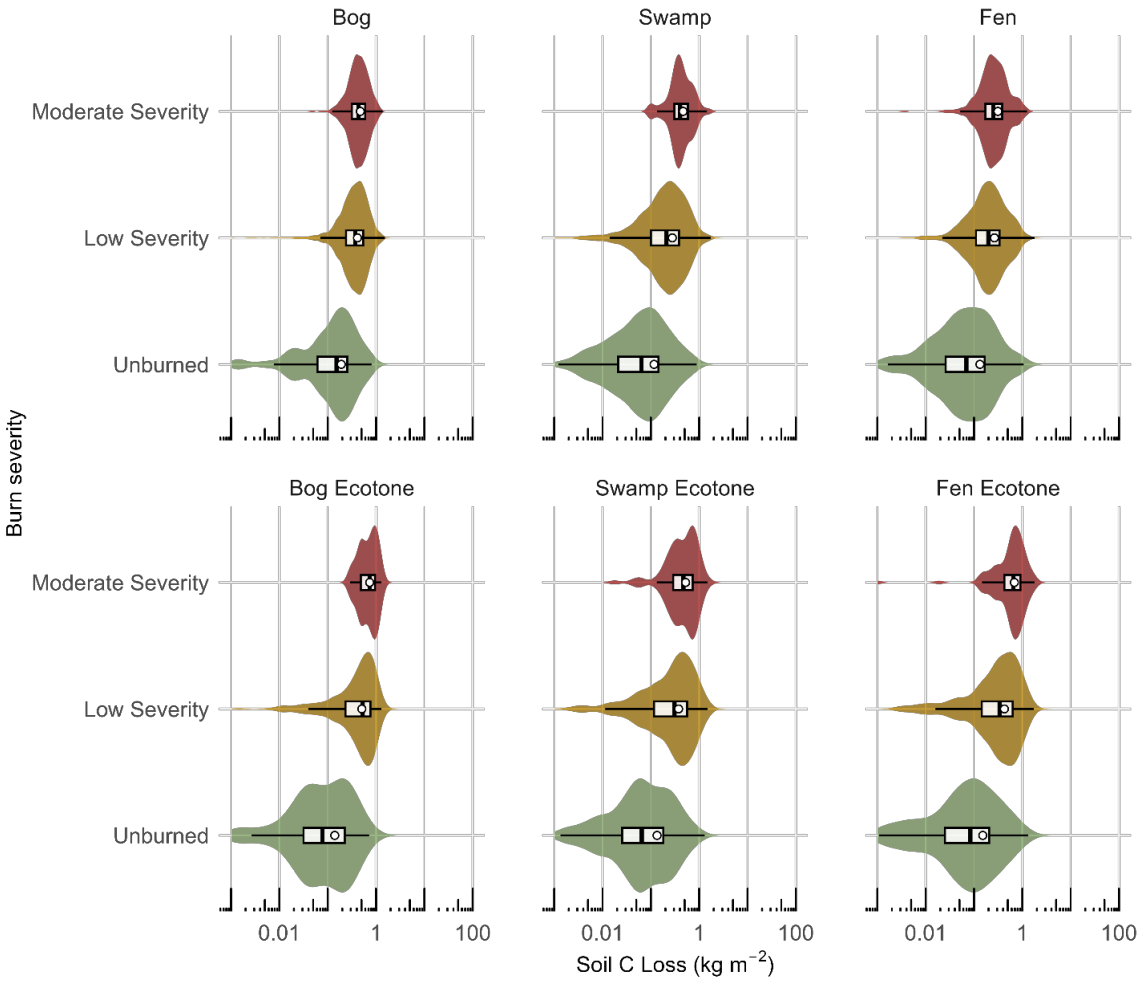

Figure 5.11: Violin plots of vegetation C loss (kg m^{-2}) by peatland type across three burn severity classes (unburned/regrowth, low, and moderate). Violins show data distribution, boxplots show interquartile range with whiskers to 5th and 95th percentiles, and mean is denoted by black circle embedded in boxplot. Plots have been cut off at 0.001 kg m^{-2} to improve data visualization. Sample sizes (n) for each peatland-severity combination range from 48 to 2995. X-axis is on a $\log_{10}$ scale.

As with soil C losses, vegetation C loss was significantly different between peatland types within each severity class (Kruskal-Wallis χ^2 = 649.71, 813.91, 48.41, for unburned, low severity, and moderate severity, respectively; $p < 0.001$; Figure 5.11). Again, bog ecotones experienced the greatest vegetation C losses across low and moderate severity classes, but bogs experienced greatest vegetation C loss in areas classified as unburned.

Fens had the lowest vegetation C loss in low or moderate severity burns, and swamps experienced the lowest C loss in areas classified as unburned.

5.4.4 Linking High-Resolution Lidar-Derived Carbon Loss Estimates to Broad Scale Model Outputs (CaMP)

Building on the spatially explicit, stratified patterns of C losses across peatland and ecotone types, lidar-derived soil C loss estimates were compared with CaMP outputs under bracketed drought scenarios to provide context for how the Horse River Wildfire aligns with modelled outcomes. CaMP outputs generated under low (DC = 287) and high (DC = 432) Drought Code scenarios aligned well overall with lidar-derived soil C loss estimates (means ± 95% CIs), though the level of agreement varied among predefined strata (peatland and canopy types as well as ecotone inclusion; Table 5.4). In open bogs, the inclusion of ecotones had little impact on lidar-derived estimates, and CaMP estimates under the high DC fell within the CIs of both core-only and combined datasets. In treed bogs, the high DC scenario also aligned best, but only when ecotones were excluded; including ecotones in these peatland types substantially increased C loss values beyond CaMP outputs. Forested bogs (with ecotone) and both swamp types aligned well with the low DC scenario. Treed fen C losses were overestimated by CaMP under both DC scenarios regardless of ecotone inclusion, and forested fens aligned with the low DC scenario once ecotones were accounted for. Open fens, uniquely, had lidar-derived estimates exceeding both CaMP scenarios, even when ecotones were included.

Table 5.4: Means and 95% CIs of lidar-derived soil C losses and CaMP outputs using low (DC = 287) and high (DC = 432) DCs, by peatland canopy type. Values are reported first for core-only data, with combined core-and-ecotone values shown in parentheses. Superscripts indicate how CaMP estimates compare to lidar-derived CIs: c = within core-only CI; e = within core-and-ecotone CI; c,e = within both; c/e = between core-only and core-and-ecotone CIs; l = low (below both); h = high (above both).

Peatland Type	Mean	Lower CI	Upper CI	CaMP; Low DC	CaMP; High DC
Open Bog	-1.17 (-1.17)	-1.01 (-1.01)	-1.34 (-1.34)	-0.94 [l]	-1.25 [c,e]
Treed Bog	-1.99 (-3.87)	-1.77 (-3.25)	-2.20 (-4.67)	-1.75 [l]	-2.11 [c]
Forested Bog	-1.47 (-1.95)	-1.43 (-1.84)	-1.52 (-2.08)	-2.05 [e]	-2.43 [h]
Open Fen	-1.17 (-1.23)	-1.01 (-1.07)	-1.36 (-1.40)	-0.32 [l]	-0.65 [l]
Treed Fen	-0.94 (-0.98)	-0 90 (-0.94)	-0.98 (-1.01)	-1.08 [h]	-1.46 [h]
Forested Fen	-0.89 (-1.29)	-0.83 (-1.17)	-0.95 (-1.41)	-1.34 [e]	-1.74 [h]
Treed Swamp	-1.10 (-1.38)	-1.02 (-1.28)	-1.19 (-1.50)	-1.14 [c]	-1.55 [h]
Forested Swamp	-1.13 (-1.64)	-1.00 (-1.48)	-1.30 (-1.80)	-1.41 [e/e]	-1.85 [h]

In assessing how canopy closure (open, treed, forested) influenced soil C loss in core-only peatlands, Kruskal-Wallis tests identified significant differences between canopy types within bogs ($\chi^2 = 8.62$, $p \leq 0.05$; Figure 5.12) and fens ($\chi^2 = 24.71$, $p \leq 0.001$), but not swamps ($\chi^2 = 0.59$, $p > 0.05$). A post-hoc Dunn's test revealed that in bogs, treed types lost significantly more C than open ($p \leq 0.01$), as did forested ($p \leq 0.05$). There was no significant difference between treed and forested bogs. In fens, forested types lost significantly more C than treed ($p \leq 0.001$), with no significant differences involving open fens.

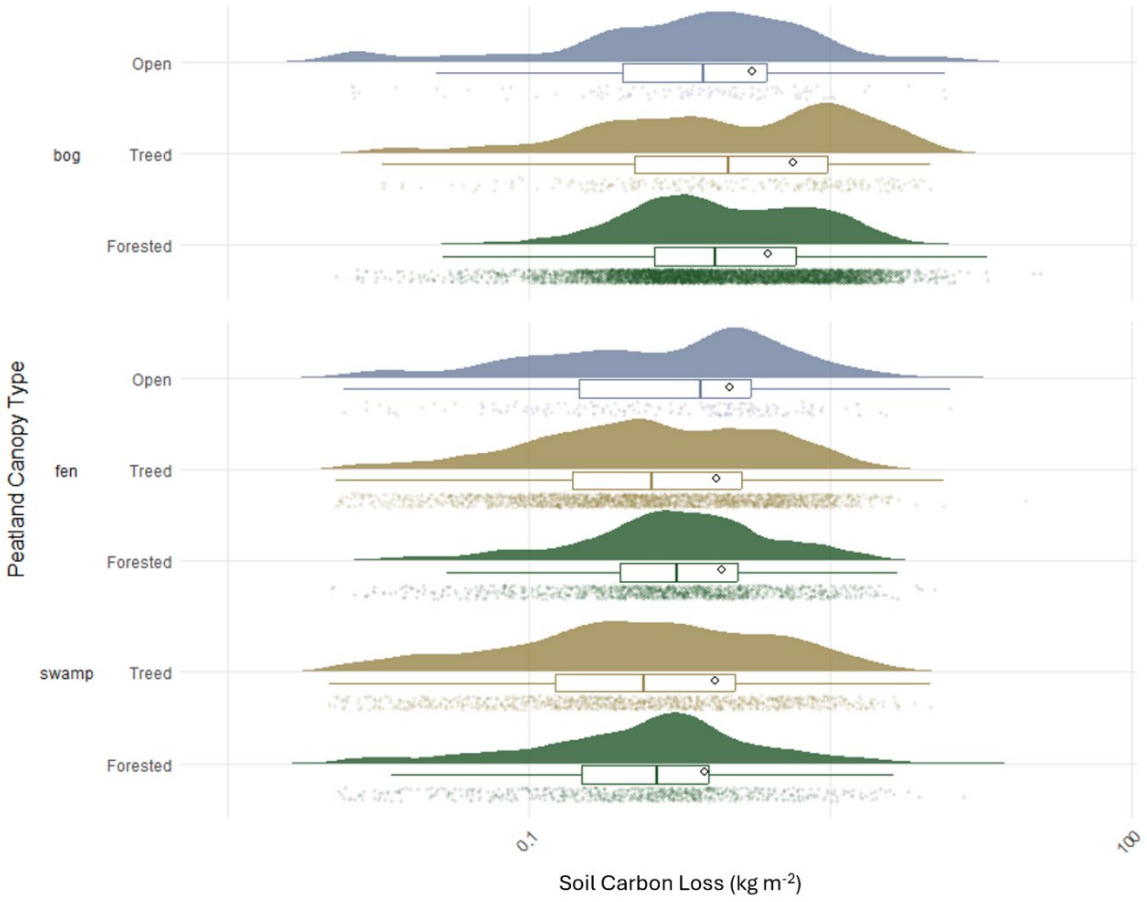

Figure 5.12: Distribution of soil C loss (kg m^{-2}) in core-only peatlands by peatland type and canopy type as defined by CaMP. Half violins show point distribution, boxplots show interquartile range with whiskers to 5th and 95th percentiles, and points show individual values. Means are denoted by black circles embedded in boxplots. Sample sizes (n) for each peatland-canopy combination range from 101 to5524. X-axis is on a $\log_{10}$ scale.

The combined core-ecotone analysis (Supplementary Figure S5.1) yielded similar patterns but with stronger differences between bog canopy types, where treed types had greater C loss than both open ($p \leq 0.001$) and forested ($p \leq 0.001$), and forested had greater C loss than open ($p \leq 0.05$). In fens, forested still lost more C than treed types ($p \leq 0.001$), while other comparisons were non-significant. Swamps, again, showed no canopy-type effect.

5.5 Discussion

5.5.1 Carbon Distribution Across the Landscape

Understanding how soil C is distributed across the landscape is essential for estimating C losses from wildland fire combustion. In unburned peatlands (as a proxy for pre-fire conditions), soil C content increased nonlinearly with depth, following a power-law relationship. The rate of increase accelerated with depth, reflecting dense carbon stores in deeper layers of peat. These results align well with C densities from other soil cores collected throughout Alberta (Bauer et al., 2024). In bogs, bog transition zones, and fens, C densities were slightly lower-than-average in the top 10-20 cm of peat but increased slightly more rapidly with depth. In contrast, fen transitions had slightly higher-than-average C densities in the top 10 cm of peat, but increased more gradually with depth.

Although soil C differences between peatland types were not statistically significant, there were notable patterns. In both bog and fen ecotones, C density was higher in the upper layers of peat and increased more rapidly with depth compared to their peatland core counterparts. This aligns with what would be expected based on results of bulk density from Lukenbach et al. (2015) and Hokanson et al. (2016) and what is known about peatland dynamics. Ecotones tend to have greater hydrologic fluctuations and subsequently increased bulk density, resulting in greater C density (e.g., Lukenbach et al., 2015; Whittington & Price, 2006).

Understanding the pre-fire distribution of aboveground C is also critical for understanding C losses during combustion. Average aboveground biomass C content ranged from 1.48 kg m^{-2} in fens to 2.05 kg m^{-2} in bog ecotones. Above ground biomass of

peatlands is highly variable with a considerable range not only regionally, but between individual peatlands (Gorham, 1991). These estimates fall in the mid-range of other published values. For example, Beaulne et al. (2021) found averages of 2.3 – 4.5 kg C m^{-2} in boreal peatlands in Quebec, while a study done in Manitoba by Reader and Stewart (1972) found values ranging from 0.50 kg m^{-2} in a treed bog, to 1.25 kg m^{-2} in a shrubby fen, to 2.33 kg m^{-2} in a forested bog (Zoltai et al., 1998).

The higher quantity of above ground biomass in bogs than in fens is interesting (Figure 5.5). While fens are typically higher in nutrient status due to their minerotrophic nature (Vitt, 1994) and have greater herbaceous vegetation biomass (Vitt & Chee, 1990; Vitt, 2006; Warner & Asada, 2006), greater groundwater flow/connectivity can result in wet conditions that limit tree growth, while the bogs are more appropriate for black spruce and other woody vegetation (Johnston et al., 2015). The deciduous vegetation more prevalent in fens may also have lower biomass than the dense black spruce typically found in forested or treed bogs (e.g., Depante et al., 2019). Peatland ecotones have greater above-ground biomass than their peatland core counterparts, as would be expected (Figure 5.5). Ecotones tend to be drier, and more supportive of tree growth than peatland middles (Wilkinson et al., 2019; Hartshorn et al., 2003). Typically, swamps would be expected to have greater above ground biomass than bogs or fens; however, swamp vegetation C was lower than that of bogs. This could be due to hydrological constraints that are limiting tree growth due to high water levels and therefore increased wetness. It is also possible that some peatlands with lower vegetation cover were misclassified as swamps, resulting in this discrepancy.

5.5.2 Soil and Vegetation Carbon Losses by Peatland Type

The results show that soil C losses were significantly greater than vegetation losses across all peatland types, a dynamic that is widely supported by studies (e.g. Amiro et al., 2001; Walker et al., 2018). On average, ~85% of the total C loss was from soil combustion, comparable to results from Amiro et al. (2001) (~85%; forest fires across Canada) and Walker et al. (2018) (~90%; boreal forest fire). This is likely due to the deep organic material and large below-ground C stores that exist in peatlands (e.g., Magnan et al., 2020; Yu, 2012), and the propensity of peat for smouldering combustion (e.g., Frandsen, 1987; Rein et al., 2008).

Median soil C losses ranged from -0.89 kg m^{-2} in fens to -7.81 kg m^{-2} in bog ecotones (means of -1.27 ± 1.45 kg m^{-2} and 16.5 ± 24.4 kg m^{-2}, respectively). Average soil C loss across all peatland types was -2.11 ± 5.09 kg m^{-2}. This large standard deviation highlights the substantial variability in combustion across the study area. The average soil C loss aligns well with findings from other studies. For example, Turetsky et al. (2011) found average soil C losses of 2.0 kg C m^{-2} in a boreal fen, Wilkinson et al. (2018) found average soil C loss to be 0.63 – 6.74 kg m^{-2} in boreal peatlands at various stages of drainage, Benscoter and Wieder (2003) found average soil C losses of 2.1 kg m^{-2} in a boreal bog, and Hokanson et al. (2016) found highly variable soil C losses of 0.5 kg m^{-2}, 0.6 kg m^{-2}, and 6.5 kg m^{-2} depending on the hydrogeological setting.

The largest soil C losses occurred in bog ecotones. Bogs are ombrogenous, hydrologically isolated from ground water, and therefore typically experience greater water table fluctuations, resulting in greater bulk density and vulnerability to deep burning (Nelson et al., 2021; Chapter 2). These fluctuations are exaggerated along the margins,

where increased bulk density, steeper hydrological gradients, and mixed peatland and upland vegetation may coexist, enhancing bog ecotone vulnerability to deep burning (Nelson et al., 2021; Chapter 2). These patterns of increased bulk density, lower and more fluctuating water tables, and increased upland vegetation closely resemble those of drained bogs, and estimated soil C losses from bog ecotones in this study were comparable to those reported for drained bogs in Wilkinson et al. (2018).

While soil C losses from fen and swamp ecotones did not differ significantly from one another, they did lose significantly more soil C than their respective cores (Figure 5.6). The two core types also do not differ significantly from one another. Fens and swamps are similar hydrologically, in that they are minerotrophic (Elmes et al, 2021), and lateral groundwater flow likely reduces hydrological fluctuations and draw-downs, particularly in the interior of the peatlands, reducing combustion. Around the margins, however, reduced soil moisture and increased bulk density result in greater soil combustion than in the cores (though significantly less than in bog margins). These results emphasize the sensitivity of peatland ecotones to deep combustion and high soil C loss, demonstrating a need to approach peatland ecotones, particularly in bogs, as critical areas for mitigating C losses.

Average vegetation C losses ranged from -0.29 ± 0.28 kg m^{-2} in fens to -0.50 ± 0.39 kg m^{-2} in bog ecotones (Figure 5.6) and averaged -0.38 ± 0.32 kg m^{-2} across all peatlands. This falls within the range of results from other studies (e.g., ~0.19 kg m^{-2} (Amiro et al., 2001); ~0.69 kg m^{-2} (French et al., 2000)). Vegetation C loss was greatest in bog ecotones and lowest in fens and swamps (Figure 5.6). Bog ecotones are high in pre-fire biomass (Figure 5.5) and are more geographically and ecologically related to uplands than their core counterparts (e.g., Hokanson et al., 2016; Ingram et al., 2019). Due to their ombrotrophic

nature, they often have lower soil moisture, particularly during dry conditions (e.g., Ferone & Devito, 2004), and are typically dominated by black spruce, a fire-adapted and flammable tree species (Johnston et al., 2015). Fens, on the other hand, had low pre-fire biomass and typically have greater hydrologic connectivity and subsequently higher moisture levels (Thompson et al., 2019). Swamps, like fens, are hydrologically connected and permanently or seasonally saturated, which can limit combustion (Ducks Unlimited Canada, 2015; National Wetlands Working Group [NWWG], 1997). While deciduous species in their leafless phase (more common in fens and swamps) are readily capable of sustaining fire spread during the "spring window", the period between snowmelt and leaf-out (Parisien et al., 2023), they are less flammable after deciduous leaf-out (Parisien et al., 2011). The generally higher flammability of conifer-dominated ecosystem is furthered during the "spring dip", where their foliage has low moisture content (Parisien et al., 2023).

The variability found in soil and vegetation C losses has several key implications. The dominance of soil C loss highlights the critical nature of peatlands as a long-term C store and emphasizes the risk of C loss through increased fire activity. Unlike upland forests, where C loss is predominantly from above ground biomass, peatlands are uniquely vulnerable to large volume belowground C loss, raising concerns about their potential to shift from a C sink to a C source (e.g., Turetsky et al., 2011; Wieder et al., 2009). At the landscape-scale, total C losses were also highly variable between peatland and ecotone types. Despite only occupying 6% of the burned area, bog ecotones contributed 25% of the total C loss (Table 5.1). This highly disproportionate C loss highlights the need to account for ecotones – particularly bogs – in C accounting and land management strategies for C loss mitigation.

The increased combustion in ecotones may reinforce positive feedback loops where more severe combustion results in greater hydrological fluctuations and reduced connectivity, altering vegetation composition (increased broadleaf recruitment). These shifts can reduce peat accumulation, altering hydrological and subsequent fire dynamics and long-term C storage (Jones et al., 2022; Mayner et al., 2024; Nelson et al., 2021; Chapter 2). This emphasizes the importance of maintaining peatland connectivity, particularly in areas at risk of land use change – highly fragmented peatlands will have a higher proportion of ecotone area. This critical role of hydrological connectivity is further highlighted by the fact that bogs, which are hydrologically isolated, had higher soil and vegetation C losses than even the ecotones around fens or swamps.

5.5.3 Evaluating the Remotely Sensed Burn Severity Index (dNBR) as an Indicator of Carbon Loss in Boreal Peatlands

Vegetation C loss was well-correlated with remotely sensed burn severity (dNBR), whereas soil C loss showed negligible to weak correlations, and instead exhibited high C losses even under low-severity conditions (Figure 5.9). Binning dNBR into burn severity categories of unburned/regrowth, low, and moderate severity classes improved the relationship between soil C loss and burn severity, and nonparametric tests concluded that there were significant differences in soil C loss between burn severity classes, with greater soil C loss increasing with burn severity class. However, mean soil C losses did not follow this pattern, suggesting that burn severity class may be indicative of general soil combustion trends, but excludes areas of deep soil combustion that can occur in areas classified as low severity (Figure 5.10). Comparisons of dNBR- and lidar-derived burn

masks revealed overall moderate to strong agreements overall, but poor agreement in ecotones and swamps (Table 5.2), likely driven by high moisture content and heterogenous vegetation.

This has important implications in post-fire modelling and carbon assessments, where reliance on optical remote sensing products may result in an underestimation of total C loss. Further, areas classified as “unburned or regrowth” were not necessarily unburned. The imagery timing (April to June) likely captured vegetation “greenup” (Parisien et al., 2023), reducing the contrast between pre- and post-fire data and limiting the ability of dNBR to detect combustion.

The response of individual peatland types to burn severity was highly variable. Only in bogs did soil C loss increase systematically with burn severity (Figure 5.10), whereas other peatland types had variations in soil C losses that did not follow the pattern of increased severity. For example, fen ecotones did not differ significantly across severity classes, and swamps showed a varied response (Figure 5.10). These findings suggest that hydrologically isolated peatlands may be more influenced by above-ground burn severity, while areas such as fen ecotones, with strong lateral ground water flows are more resilient to these effects. In such areas, substantial soil combustion can occur even in areas where spectral indices indicate low or no burn, due to subsurface smouldering that is not detected spectrally. This highlights a limitation of relying on dNBR or other spectral indices for estimating the impacts of wildland fire, especially in complex peatland ecosystems.

In contrast, vegetation C loss increased systematically with dNBR and burn severity category across all peatland types. The correlation with dNBR was strongest in peatland ecotones. These areas tend to exhibit characteristics of upland ecosystems (e.g., Hokanson

et al., 2016; Ingram et al., 2019), and have greater pre-fire biomass (Figure 5.6), which can enhance the difference between pre- and post-fire spectral signatures (Key & Benson, 2006). Core peatlands, by contrast, tend to have higher moisture content (Hokanson et al., 2016), which can reduce the extent of canopy combustion by inhibiting ignition and flame spread, particularly in crown fires (Thompson et al., 2015). Further, even when vegetation is combusted, high moisture content can dampen reflectance in the NIR and SWIR wavelengths (Lobell & Asner, 2002) weakening the contrast captured by dNBR.

The weak relationship between dNBR and burn severity classes with soil C loss, as opposed to the tight correlation with vegetation C loss, is reflective of both the spectral characteristics of dNBR and the hydrology, geology, and ecology of peatlands. Because dNBR measures changes in the ratio of surface and green vegetation reflectance, it readily captures loss of canopy and presence of surface char. However, this is not necessarily reflective of soil combustion – high pre-fire moisture content in peatlands could be erroneously captured as similar to burned areas (Alcaras et al., 2022), further reducing dNBR. Most importantly, peat fires can smoulder well below the surface (e.g., Frandsen, 1987; Rein et al., 2008), making it difficult for optical sensors like Landsat to detect combustion during the event. Even post-fire, the lack of vegetation change or charring can result in low dNBR values despite significant belowground C losses. This highlights the utility of pre- and post-fire lidar data, which are less affected by surface moisture and canopy occlusion and can capture data across large spatial extents at a relatively fine scale.

5.5.4 Contextualizing High-Resolution Carbon Losses with Broad-Scale CaMP Estimates

There are few models that estimate total C loss, including soil and vegetation components, from peatlands during combustion. The CaMP, which estimates greenhouse gas removal

and emissions from peatlands in Canada, plays a key role in national greenhouse gas reporting, and includes estimations of C losses during wildland fire (Bona et al., 2020). However, due to its high-level function and broad-scale application, it is expected that there will be complexities and variability between individual fires that it does not capture. By placing lidar-derived estimates of C loss due to wildland fire combustion in the context of CaMP outputs, it becomes possible to evaluate the extent to which C losses from the Horse River Wildfire align with what would largely be expected, nationally, and where they diverge. These divergences provide insight into the specific conditions that may drive higher C losses, identifying patterns that may signal shifts in fire-peatland dynamics under a changing climate.

Results from lidar-derived soil C loss estimates aligned well with CaMP outputs, particularly in bogs, though this was dependent on canopy type and whether ecotones were included (Figure 5.12; Table 5.4). Open and treed bogs aligned closely with CaMP estimates under high DC conditions (DC = 432). Forested bogs, however, only aligned with CaMP outputs when ecotones were included, and even then, only under low DC conditions (DC = 287). This indicates that the increase in C loss expected from forested bogs by CaMP was not observed here.

Fens and swamps saw optimal alignment between lidar-derived and CaMP-estimated C losses under low DC scenarios, particularly with the inclusion of ecotones. However, open fens exhibited greater C losses than CaMP outputs, even under a high DC scenario (DC = 432). One explanation may be due to the occurrence of high winds and temperatures that occurred in the days preceding the fire (Alberta Agriculture and Forestry & MNP, 2017). Without the wind- and radiation-blocking effect of trees, open fens may

have experienced disproportionately high evapotranspiration of surface and near-surface water (e.g., Kettridge et al., 2013). This could result in drier-than-expected conditions, and subsequently deeper combustion than would be expected under the typical moisture conditions used in the CaMP.

The inclusion of ecotones consistently increased lidar-derived C loss estimates, but the resulting impact on alignment with CaMP outputs varied by peatland and canopy type. In cases such as forested fens and swamps, adding ecotones improved alignment with CaMP (under low DC), while in treed bogs, ecotone inclusion increased the mean C loss and CIs above CaMP projections, even under high DC scenarios. Ecotones typically have lower soil moisture and higher bulk density, as well as increased vegetation, all of which can enhance peat combustion (Nelson et al., 2021; Chapter 2). This highlights the importance of separating core peatlands from ecotones when looking at impacts of wildland fire, as they may not respond the same way during combustion. With climate change, peatlands are expected to undergo enhanced drying and encroachment of woody vegetation (e.g., Weltzin et al., 2003; Waddington et al, 2015; Thompson et al., 2019), possibly expanding ecotones or transforming core peatlands to resemble them. This shift would make a greater proportion of the boreal ecosystem vulnerable to deep burning and elevated C losses. As such, incorporating the core versus ecotone variability in fire response into carbon-wildfire models is essential in understanding future C emissions and ecosystem impacts.

5.5.5 Uncertainties and Future Research

While this study provides insight into C losses from boreal peatlands during wildland fire, there are important limitations that must be noted, and which may be used to guide further

research. First, while the use of pre- and post-fire airborne lidar is a strength of this study, as it allowed for the estimation of depth of burn and subsequently, soil C loss, across a large spatial extent, it also has limitations. Dense surface vegetation or standing water can inhibit laser pulses from measuring the true ground surface, impacting the reliability of DTMs. These impacts were mitigated by optimizing ground classifications following Nelson et al. (2022; Chapter 3), providing confidence in lidar elevation measurements when averaged (field-validated offsets of 0 cm in areas of low vegetation regeneration and 1 cm in areas of high regeneration); however, point-specific measurements may be erroneous. Further, when subtracting pre- and post-fire DTMs, co-registration errors may arise where even small misalignments in some areas may be represented as peat growth or loss.

Changes on the landscape beyond the fire likely occurred between lidar data collections. Between the pre-fire survey and post-fire lidar data collection, some peat accumulation and vegetation regeneration (post-fire) likely would have occurred, likely leading to an underestimation of depth of burn. Peatlands may have also shrunken or swelled during this time due to hydrological fluctuations, resulting in either missed combustion or erroneously including areas as combustion that did not burn. Comparisons of elevation change in burned versus unburned peatlands were not conducted, as they would likely introduce additional uncertainties, as opposed to reducing them. Fire through peatland environments can have significant impact on peatland hydrology and bulk density, as well as ecohydrological functions such as an increase in hydrophobicity (e.g., Nelson et al., 2021; Chapter 2). Because of this, burned peatland systems do not necessarily respond to hydrological conditions such as drought or flooding in the same way as unburned. It would be erroneous, therefore, to measure peat surface elevation changes in unburned areas

and extrapolate those to burned areas. Instead, to reduce the noise associated with peat fluctuations, data were aggregated to 25 m^2. However, many of the very small depth of burn point estimates (i.e. < 1 cm) may not represent true combustion. The high frequency of these small values would lower both median and mean estimates, likely leading to an underestimation of C loss.

Finally, aboveground C loss estimates did not include downed woody debris, as it was not measured in the biomass field plots. However, these fuels typically contribute a small fraction of total C losses during combustion in the boreal. For example, Johnston et al. (2015) found that coarse woody debris contributed less than 2% of total C losses. It is unlikely that their exclusion significantly influenced the estimates presented here.

Lidar acquisitions immediately post-fire would substantially reduce uncertainties in future research by reducing the influence of vegetation growth and vertical peat fluctuations. Including additional pools of potential C loss or storage, such as woody debris and pyrogenic C, would also improve C loss estimates. Finally, expanding this study across multiple fires along spatial and temporal gradients would enhance generalizability of findings and provide increased confidence in estimates of C loss during boreal peatland fires.

This study area represents only a small portion of a single fire. While it includes a range of peatlands (bogs, fens, swamps and their ecotones) and canopy types, these are not inherently representative of the broader boreal peatland structure. Ducks Unlimited Canada (2017) identified fens as the dominant peatland type across Alberta's boreal region, whereas bogs dominate the present study area. This area is also highly anthropogenically altered with access roads and cutlines. The degree of peatland fragmentation, ecotone

extent and microtopography is expected to vary substantially across the boreal. As such, while patterns identified in this study provide important insights into peatland vulnerability to combustion, extrapolation of numerical estimates should be approached cautiously. Finally, the analysis of lidar-derived C losses and CaMP outputs presented here provides a high-level comparison into how C losses from the Horse River Wildfire diverged from modelled expectations. However, differences in fire severity, peatland composition, and particularly ecotone extent, are likely to impact agreement between fine- and broad-scale estimates. Future research should examine multiple fires across spatial and temporal gradients to strengthen confidence in C loss estimates, improve parameterization of C models such as CaMP, and guide GHG reporting.

5.6 Conclusion

Soil C losses were consistently and substantially greater than vegetation C losses across all peatland types, highlighting the vast belowground C storage of peatlands and the susceptibility of these deep organic layers to significant C loss during smouldering combustion. Ecotones experienced the greatest C losses – both above- and below-ground, emphasizing the importance of maintaining hydrological connectivity and minimizing fragmentation of peatlands. Of note, bog ecotones contributed disproportionately to total C losses, with soil C losses comparable to those observed in drained bogs from the same fire event, reported by Wilkinson et al. (2018), highlighting their vulnerability and critical nature in C-fire dynamics. These findings reinforce the need to distinguish between peatland cores and ecotones when assessing landscape-scale C losses, particularly for C accounting. Overlooking this distinction would risk underestimating C losses and landscape vulnerability.

While remotely sensed burn severity had a strong relationship with above-ground C losses, it was a poor predictor of soil C loss, particularly in core peatlands. Below-ground combustion resulted in approximately six times the C loss of above-ground, and so metrics such as dNBR are unable to infer total C losses, or indicate ecosystem impacts to below-ground properties.

In comparing field to lidar-derived C loss estimates with CaMP estimates, it was clear that including ecotones both increased C loss estimates and shifted the degree of alignment between lidar-derived and CaMP-estimated C losses. This reinforces the importance of isolating ecotones when analysing combustion impacts, given their unique geophysical and hydrological properties.

This research highlights the importance of boreal peatland soil as a long-term C store. Maintaining this requires a focus on maintaining hydrological connectivity and reducing fragmentation, both of which are essential for reducing ecotonal extent and mitigating against increased C loss during wildland fire.

5.7 Acknowledgements

Field data collection was supported by Dr. Linda Flade, Emily Jones, and Dr. Craig Mahoney. Lidar data collection and assistance with processing was provided by Maxim Okhrimenko. Quinn Barber (Natural Resources Canada) contributed fire weather and day-of-burn data. This research was supported by funding from several sources. Dr. Laura Chasmer's funding from Natural Sciences and Engineering Research Council (NSERC) Discovery Grant, the Canada Wildfire NSERC SPG-N, and University of Lethbridge Start-Up Funding. Dr. Chris Hopkinson's funding from the Western Economic Diversification

Canada Funding (purchase of Teledyne Optech Inc. Titan multispectral lidar), an NSERC Discovery Grant, and a Canadian Foundation for Innovation grant (Hopkinson and Chasmer). Kailyn Nelson received funding from an NSERC Canada Graduate Scholarship, Alberta Innovates Graduate Student Scholarship, the Nexen Fellowship in Water Research, Canada Wildfire (NSERC SPG-N), and the University of Lethbridge School of Graduate Studies.

5.8 References

Abib, T. H., Chasmer, L., Hopkinson, C., Mahoney, C., & Rodriguez, L. C. (2019). Seismic line impacts on proximal boreal forest and wetland environments in Alberta. Science of the Total Environment, 658, 1601-1613.

Alberta Agriculture and Forestry & MNP LLP. (2017). A review of the 2016 Horse River wildfire.

Alcaras, E., Costantino, D., Guastaferro, F., Parente, C., & Pepe, M. (2022). Normalized Burn Ratio Plus (NBR+): A New Index for Sentinel-2 Imagery, Remote Sens. 2022, 14, 1727.

Alonzo, M., Morton, D. C., Cook, B. D., Andersen, H. E., Babcock, C., & Pattison, R. (2017). Patterns of canopy and surface layer consumption in a boreal forest fire from repeat airborne lidar. Environmental Research Letters, 12(6), 065004.

Amiro, B. D., Todd, J. B., Wotton, B. M., Logan, K. A., Flannigan, M. D., Stocks, B. J., Mason, J. A., Martell, D. L., & Hirsch, K. G. (2001). Direct carbon emissions from Canadian forest fires, 1959-1999. Canadian Journal of Forest Research, 31(3), 512-525.

Axelsson, P. (2000). DEM generation from laser scanner data using adaptive TIN models. In International Archives of Photogrammetry and Remote Sensing, Proceedings of the ISPRS, Amsterdam, The Netherlands, 16–23 July 2000; Volume 33, Part B4/1, pp. 110–117.

Bauer, I.E., Davies, M.A., Bona, K.A., Hararuk, O., Shaw, C.H., Thompson, D.K., Kurz, W.A., Webster, K.L., Garneau, M., McLaughlin, J.W., Packalen, M.S., Prystupa, E., Sanderson, N.K., and Tarnocai, C., 2024, Peat profile database from peatlands in Canada.

Beaulne, J., Garneau, M., Magnan, G., & Boucher, É. (2021). Peat deposits store more carbon than trees in forested peatlands of the boreal biome. Scientific Reports, 11(1), 2657.

Benscoter, B. W., Greenacre, D., & Turetsky, M. R. (2015). Wildfire as a key determinant of peatland microtopography. Canadian Journal of Forest Research, 45(8), 1132-1136.

Benscoter, B. W., Thompson, D. K., Waddington, J. M., Flannigan, M. D., Wotton, B. M., De Groot, W. J., & Turetsky, M. R. (2011). Interactive effects of vegetation, soil moisture and bulk density on depth of burning of thick organic soils. International Journal of Wildland Fire, 20(3), 418-429.

Boby, L. A., Schuur, E. A., Mack, M. C., Verbyla, D., & Johnstone, J. F. (2010). Quantifying fire severity, carbon, and nitrogen emissions in Alaska's boreal forest. Ecological Applications, 20(6), 1633-1647.

Bourgeau-Chavez, L. L., Endres, S., Powell, R., Battaglia, M. J., Benscoter, B., Turetsky, M., ... & Banda, E. (2017). Mapping boreal peatland ecosystem types from multitemporal radar and optical satellite imagery. Canadian Journal of Forest Research, 47(4), 545-559.

Bourgeau-Chavez, L. L., Grelik, S. L., Billmire, M., Jenkins, L. K., Kasischke, E. S., & Turetsky, M. R. (2020). Assessing boreal peat fire severity and vulnerability of peatlands to early season wildland fire. Frontiers in Forests and Global Change, 3, 20.

Chasmer, L. E., Hopkinson, C. D., Petrone, R. M., & Sitar, M. (2017). Using multitemporal and multispectral airborne lidar to assess depth of peat loss and correspondence with a new active normalized burn ratio for wildfires. Geophysical Research Letters, 44(23), 11-851.

Depante, M., Morison, M. Q., Petrone, R. M., Devito, K. J., Kettridge, N., & Waddington, J. M. (2019). Hydraulic redistribution and hydrological controls on aspen transpiration and establishment in peatlands following wildfire. Hydrological Processes, 33(21), 2714–2728. https://doi.org/10.1002/hyp.13522.

Devito, K., Mendoza, C., & Qualizza, C. (2012). Conceptualizing water movement in the Boreal Plains. Implications for watershed reconstruction.

Downing, D. J., & Pettapiece, W. W. Natural Regions and Subregions of Alberta; No. T/852; Government of Alberta Publish: Edmonton, AB, Canada, 2006; 264p.

Ducks Unlimited Canada. (2015). Field guide: Boreal wetland classes in the boreal plains ecozone of Canada.

Ducks Unlimited Canada. (2017). Boreal Wetlands and Climate Change: Key findings to support the development of Alberta's Climate Change Adaptation Strategy. Retrieved from: https://abnawmp.ca/wp-content/uploads/2020/09/Boreal-Science-Summary-Final_web.pdf

Dabros, A., Higgins, K. L., & Pinzon, J. (2022). Seismic line edge effects on plants, lichens and their environmental conditions in boreal peatlands of Northwest Alberta (Canada). Restoration Ecology, 30(4), e13468.

Dimitrov, D. D., Bhatti, J. S., & Grant, R. F. (2014). The transition zones (ecotone) between boreal forests and peatlands: Ecological controls on ecosystem productivity along a transition zone between upland black spruce forest and a poor forested fen in central Saskatchewan. Ecological modelling, 291, 96-108.

ECCC. (2019). Canadian Climate Normals - Fort McMurray A. Environment and Climate Change Canada. Available at: https://climate.weather.gc.ca/climate_normals/index_e.html. (Accessed February 2023).

Ecological Stratification Working Group. 1995. A National ecological framework for Canada. Agriculture and Agri-Food Canada and Environment Canada.

Ecoregions Working Group. (1989). Ecoclimatic regions of Canada. Ecological Land Classification Series No. 23. Environment Canada.

Elmes, M. C., Thompson, D. K., Sherwood, J. H., & Price, J. S. (2018). Hydrometeorological conditions preceding wildfire, and the 10 subsequent burning of a fen watershed in Fort McMurray, Alberta, Canada.

Elmes, M. C., Davidson, S. J., & Price, J. S. (2021). Ecohydrological interactions in a boreal fen–swamp complex, Alberta, Canada. Ecohydrology, 14(7), e2335.

Ferone, J. M., & Devito, K. J. (2004). Shallow groundwater–surface water interactions in pond–peatland complexes along a Boreal Plains topographic gradient. Journal of Hydrology, 292(1-4), 75-95.

Ficken, C. D., Cobbaert, D., Rooney, R.C. (2019). Low extent but high impact of human land use on wetland flora across the boreal oil sands region. Sci. Total Environ. 693, 133647.

Flade, L., Hopkinson, C., & Chasmer, L. (2020). Allometric equations for shrub and short-stature tree aboveground biomass within boreal ecosystems of northwestern Canada. Forests, 11(11), 1207.

Flade, L., Hopkinson, C., & Chasmer, L. (2021). Aboveground biomass allocation of boreal shrubs and short-stature trees in northwestern Canada. Forests, 12(2), 234.

Flannigan, M., Cantin, A. S., De Groot, W. J., Wotton, M., Newbery, A., & Gowman, L. M. (2013). Global wildland fire season severity in the 21st century. Forest Ecology and Management, 294, 54-61.

Flannigan, M., Stocks, B., Turetsky, M., & Wotton, M. (2009). Impacts of climate change on fire activity and fire management in the circumboreal forest. Global change biology, 15(3), 549-560.

Flannigan, M. D., Wotton, B. M., Marshall, G. A., De Groot, W. J., Johnston, J., Jurko, N., & Cantin, A. S. (2016). Fuel moisture sensitivity to temperature and precipitation: climate change implications. Climatic Change, 134, 59-71.

Frandsen, W. H. (1987). The influence of moisture and mineral soil on the combustion limits of smoldering forest duff. Canadian Journal of Forest Research, 17(12), 1540-1544.

Frandsen, W. H. (1997). Ignition probability of organic soils. Canadian Journal of Forest Research, 27(9), 1471-1477.

French, N. H., Graham, J., Whitman, E., & Bourgeau-Chavez, L. L. (2020). Quantifying surface severity of the 2014 and 2015 fires in the Great Slave Lake area of Canada. International journal of wildland fire, 29(10), 892-906.

Groot, A., Carlson, D.W., Fleming, R.L., Wood, J.E., 1997. Small openings in trembling aspen forest: microclimate and regeneration of white spruce and trembling aspen. NODA/NFP Technical Report TR-47 31 pgs. (ISBN 0-662-25461-9)

Goodwin, N. R., & Collett, L. J. (2014). Development of an automated method for mapping fire history captured in Landsat TM and ETM+ time series across Queensland, Australia. Remote Sensing of Environment, 148, 206-221.

Gorham, E. (1991). Northern peatlands: role in the carbon cycle and probable responses to climatic warming. Ecological applications, 1(2), 182-195.

Gower, S. T., Vogel, J. G., Norman, J. M., Kucharik, C. J., Steele, S. J., & Stow, T. K. (1997). Carbon distribution and aboveground net primary production in aspen, jack

pine, and black spruce stands in Saskatchewan and Manitoba, Canada. Journal of Geophysical Research: Atmospheres, 102(D24), 29029-29041.

Guêné-Nanchen, M., LeBlanc, M. C., & Rochefort, L. (2022). Post-fire peatland vegetation recovery: a case study in open rich fens of the Canadian boreal forest. Botany, 100(5), 435-447.

Hall, R. J., Freeburn, J. T., De Groot, W. J., Pritchard, J. M., Lynham, T. J., & Landry, R. (2008). Remote sensing of burn severity: experience from western Canada boreal fires. International Journal of Wildland Fire, 17(4), 476-489.

Halsey, L., Vitt, D., Beilman, D., Crow, S., Mehelcic, S., and Wells, R. (2003). Alberta Wetlands Inventory Standards, Version 2.0.

Hartshorn, A. S., Southard, R. J., & Bledsoe, C. S. (2003). Structure and function of peatland-forest ecotones in southeastern Alaska. Soil Science Society of America Journal, 67(5), 1572-1581.

Hokanson, K. J., Lukenbach, M. C., Devito, K. J., Kettridge, N., Petrone, R. M., & Waddington, J. M. (2016). Groundwater connectivity controls peat burn severity in the boreal plains. Ecohydrology, 9(4), 574-584.

Hopkinson, C., Chasmer, L., Barr, A. G., Kljun, N., Black, T. A., & McCaughey, J. H. (2016a). Monitoring boreal forest biomass and carbon storage change by integrating airborne laser scanning, biometry and eddy covariance data. Remote Sensing of Environment, 181, 82-95.

Hopkinson, C., Chasmer, L., Gynan, C., Mahoney, C., & Sitar, M. (2016b). Multisensor and multispectral LiDAR characterization and classification of a forest environment. Canadian journal of remote sensing, 42(5), 501-520.

Hoy, E. E., French, N. H., Turetsky, M. R., Trigg, S. N., & Kasischke, E. S. (2008). Evaluating the potential of Landsat TM/ETM+ imagery for assessing fire severity in Alaskan black spruce forests. International Journal of Wildland Fire, 17(4), 500-514.

Ingram, H. A. P.: Hydrology, in: Ecosystems of the World 4A. Mires: Swamp, bog, fen and moor, edited by: Gore, A. J. P., Elsevier, Amsterdam, 67–224, 1983.

Ingram, R. C., Moore, P. A., Wilkinson, S., Petrone, R. M., & Waddington, J. M. (2019). Postfire soil carbon accumulation does not recover boreal peatland combustion loss in some hydrogeological settings. Journal of Geophysical Research: Biogeosciences, 124(4), 775-788.

Isenburg, M. (2023). LAStools: Efficient LiDAR processing tools (Version 230816) [Software]. Rapidlasso GmbH.

Jean, S. A., Pinno, B. D., & Nielsen, S. E. (2020). Early regeneration dynamics of pure black spruce and aspen forests after wildfire in boreal Alberta, Canada. Forests, 11(3), 333.

Johnston, D. C., Turetsky, M. R., Benscoter, B. W., & Wotton, B. M. (2015). Fuel load, structure, and potential fire behaviour in black spruce bogs. Canadian Journal of Forest Research, 45(7), 888-899.

Jones, E. A., Chasmer, L. E., Devito, K. J., & Hopkinson, C. D. (2024). Shortening fire return interval predisposes west-central Canadian boreal peatlands to more rapid vegetation growth and transition to forest cover. Global Change Biology, 30(2), e17185.

Jones, E., Chasmer, L., Devito, K., Rood, S., & Hopkinson, C. (2022). Ecological impacts of shortening fire return intervals on boreal peatlands and transition zones using integrated in situ field sampling and lidar approaches. Ecohydrology, 15(3), e2403.

Keeley, J. E. (2009). Fire intensity, fire severity and burn severity: a brief review and suggested usage. International journal of wildland fire, 18(1), 116-126.

Key, C. H., & Benson, N. C. (2006). Landscape assessment (LA). In: Lutes, Duncan C.; Keane, Robert E.; Caratti, John F.; Key, Carl H.; Benson, Nathan C.; Sutherland, Steve; Gangi, Larry J. 2006. FIREMON: Fire effects monitoring and inventory system. Gen. Tech. Rep. RMRS-GTR-164-CD. Fort Collins, CO: US Department of Agriculture, Forest Service, Rocky Mountain Research Station. p. LA-1-55, 164.

Kettridge, N., Turetsky, M. R., Sherwood, J. H., Thompson, D. K., Miller, C. A., Benscoter, B. W., Flannigan, M. D., Wotton, B. M., & Waddington, J. M. (2015). Moderate drop in water table increases peatland vulnerability to post-fire regime shift. Scientific reports, 5(1), 8063.

Kochtubajda, B., Brimelow, J., Flannigan, M., & Morrow, B. (2017). The extreme 2016 wildfire in Fort McMurray, Alberta, Canada. Bulletin of the American Meteorological Society, 98(8).

Koutsias, N., & Pleniou, M. (2015). Comparing the spectral signal of burned surfaces between Landsat 7 ETM+ and Landsat 8 OLI sensors. International Journal of Remote Sensing, 36(14), 3714-3732.

Lambert, M. C., Ung, C. H., & Raulier, F. (2005). Canadian national tree aboveground biomass equations. Canadian Journal of Forest Research, 35(8), 1996-2018.

Landsat Spectral Indices products courtesy of the U.S. Geological Survey Earth Resources Observation and Science Center.

Lobell, D. B., & Asner, G. P. (2002). Moisture effects on soil reflectance. Soil Science Society of America Journal, 66(3), 722-727.

Loisel, J., & Yu, Z. (2013). Recent acceleration of carbon accumulation in a boreal peatland, south central Alaska. Journal of Geophysical Research: Biogeosciences, 118(1), 41-53.

Lovitt, J., Rahman, M. M., Saraswati, S., McDermid, G. J., Strack, M., & Xu, B. (2018). UAV remote sensing can reveal the effects of low-impact seismic lines on surface morphology, hydrology, and methane (CH4) release in a boreal treed bog. Journal of Geophysical Research: Biogeosciences, 123(3), 1117-1129.

Lukenbach, M. C., Hokanson, K. J., Moore, P. A., Devito, K. J., Kettridge, N., Thompson, D. K., Wotton, B. M., Petrone, R. M., & Waddington, J. M. (2015). Hydrological controls on deep burning in a northern forested peatland. Hydrological Processes, 29(18), 4114-4124.

Lukenbach, M. C., Hokanson, K. J., Devito, K. J., Kettridge, N., Petrone, R. M., Mendoza, C. A., Granath, G., & Waddington, J. M. (2017). Post-fire ecohydrological conditions at peatland margins in different hydrogeological settings of the Boreal Plain. Journal of Hydrology, 548, 741-753.

Ma, S., He, F., Tian, D., Zou, D., Yan, Z., Yang, Y., Zhou, T., Huang, K., Shen, H. and Fang, J., (2018). Variations and determinants of carbon content in plants: a global synthesis. Biogeosciences, 15(3), 693-702.

Magnan, G., Garneau, M., Le Stum-Boivin, É., Grondin, P., & Bergeron, Y. (2020). Long-term carbon sequestration in boreal forested peatlands in eastern Canada. Ecosystems, 23(7), 1481-1493.

Marra, G., & Wood, S. (2011). Practical variable selection for generalized additive models. Computational Statistics & Data Analysis, 55, 2372–2387.

Marshall, I. B., Schut, P., & Ballard, M. (1999). A national ecological framework for Canada: Attribute data. Environmental Quality Branch, Ecosystems Science Directorate, Environment Canada and Research Branch, Agriculture and Agri-Food

Canada, Ottawa/Hull. http://sis.agr.gc.ca/cansis/nsdb/ecostrat/1999report/index.html (Accessed February 2023).

Miller, J. D., & Thode, A. E. (2007). Quantifying burn severity in a heterogeneous landscape with a relative version of the delta Normalized Burn Ratio (dNBR). Remote sensing of Environment, 109(1), 66-80.

National Wetlands Working Group (NWWG). (1997). In B. G. Warner & C. D. A. Rubec (Eds.), The Canadian wetland classification system (2nd ed.). National Wetlands Working Group, Wetlands Research Branch, University of Waterloo.

Natural Resources Canada. (2017). The State of Canada's Forests—Annual Report 2017; Government of Canada: Ottawa, ON, Canada.

Nelson, K., Thompson, D., Hopkinson, C., Petrone, R., & Chasmer, L. (2021). Peatland-fire interactions: A review of wildland fire feedbacks and interactions in Canadian boreal peatlands. Science of the total environment, 769, 145212.

Nelson, K., Chasmer, L., & Hopkinson, C. (2022). Quantifying Lidar Elevation Accuracy: Parameterization and Wavelength Selection for Optimal Ground Classifications Based on Time since Fire/Disturbance. Remote Sensing, 14(20), 5080.

Parisien, M. A., Parks, S. A., Miller, C., Krawchuk, M. A., Heathcott, M., & Moritz, M. A. (2011). Contributions of ignitions, fuels, and weather to the spatial patterns of burn probability of a boreal landscape. Ecosystems, 14(7), 1141-1155.

Parisien, M. A., Barber, Q. E., Flannigan, M. D., & Jain, P. (2023). Broadleaf tree phenology and springtime wildfire occurrence in boreal Canada. Global Change Biology, 29(21), 6106-6119.

Pedersen, E. J., Miller, D. L., Simpson, G. L., & Ross, N. (2019). Hierarchical generalized additive models in ecology: an introduction with mgcv. PeerJ, 7, e6876.

Petrone, R. M., Devito, K. J., Silins, U., Mendoza, C., Brown, S. C., Kaufman, S. C., & Price, J. S. (2008). Transient peat properties in two pond-peatland complexes in the sub-humid Western Boreal Plain, Canada. Mires & Peat, 3.

R Core Team. (2024). R: a language and environment for statistical computing.

Reader, R. J., & Stewart, J. M. (1972). The relationship between net primary production and accumulation for a peatland in southeastern Manitoba. Ecology, 53(6), 1024-1037.

Reddy, A. D., Hawbaker, T. J., Wurster, F., Zhu, Z., Ward, S., Newcomb, D., & Murray, R. (2015). Quantifying soil carbon loss and uncertainty from a peatland wildfire using multi-temporal LiDAR. Remote Sensing of Environment, 170, 306-316.

Rein, G., Cleaver, N., Ashton, C., Pironi, P., & Torero, J. L. (2008). The severity of smouldering peat fires and damage to the forest soil. Catena, 74(3), 304-309.

Rogers, B. M., Veraverbeke, S., Azzari, G., Czimczik, C. I., Holden, S. R., Mouteva, G. O., Sedano, F., Treseder, K. K., & Randerson, J. T. (2014). Quantifying fire-wide carbon emissions in interior Alaska using field measurements and Landsat imagery. Journal of Geophysical Research: Biogeosciences, 119(8), 1608-1629.

Smith, K.B., C.E. Smith, S.F. Forest, and A.J. Richard. 2007. A Field Guide to the Wetlands of the Boreal Plains Ecozone of Canada. Ducks Unlimited Canada, Western Boreal Office: Edmonton, Alberta. 98 pp.

Tarnocai, C. (2006). The effect of climate change on carbon in Canadian peatlands. Global and planetary Change, 53(4), 222-232.

Thompson, D. K., Baisley, A. S., & Waddington, J. M. (2015). Seasonal variation in albedo and radiation exchange between a burned and unburned forested peatland: Implications for peatland evaporation. Hydrological Processes, 29(14), 3227–3235. https://doi.org /10.1002/hyp.10436.

Thompson, D. K., Simpson, B. N., Whitman, E., Barber, Q. E., & Parisien, M. A. (2019). Peatland hydrological dynamics as a driver of landscape connectivity and fire activity in the boreal plain of Canada. Forests, 10(7), 534.

Thompson, D. K., Wotton, B. M., & Waddington, J. M. (2014). Estimating the heat transfer to an organic soil surface during crown fire. International Journal of Wildland Fire, 24(1), 120-129.

Turetsky, M. R., Benscoter, B., Page, S., Rein, G., Van Der Werf, G. R., & Watts, A. (2015). Global vulnerability of peatlands to fire and carbon loss. Nature Geoscience, 8(1), 11-14.

Turetsky, M. R., Donahue, W., & Benscoter, B. W. (2011). Experimental drying intensifies burning and carbon losses in a northern peatland. Nature communications, 2(1), 514.

U.S. Geological Survey. (n.d.). Landsat Normalized Burn Ratio (NBR). U.S. Department of the Interior. https://www.usgs.gov/landsat-missions/landsat-normalized-burn-ratio

Vitt, D. H. (1994). An overview of factors that influence the development of Canadian peatlands. The Memoirs of the Entomological Society of Canada, 126(S169), 7-20.

Vitt, D. H., Halsey, L. A., Bauer, I. E., & Campbell, C. (2000). Spatial and temporal trends in carbon storage of peatlands of continental western Canada through the Holocene. Canadian Journal of Earth Sciences, 37(5), 683-693.

Vitt, D. H. (2006). Functional characteristics and indicators of boreal peatlands. In Boreal peatland ecosystems (pp. 9-24). Berlin, Heidelberg: Springer Berlin Heidelberg.

Vitt, D. H., & Chee, W. L. (1990). The relationships of vegetation to surface water chemistry and peat chemistry in fens of Alberta, Canada. Vegetatio, 89, 87-106.

Vitt, D. H., & Short, P. (2020). Peatlands. In Wetlands and Habitats (pp. 27-36). CRC Press.

Waddington, J. M., Thompson, D. K., Wotton, M., Quinton, W. L., Flannigan, M. D., Benscoter, B. W., Baisley, S. A., & Turetsky, M. R. (2012). Examining the utility of the Canadian Forest Fire Weather Index System in boreal peatlands. Canadian Journal of Forest Research, 42(1), 47-58.

Waddington, J. M., Morris, P. J., Kettridge, N., Granath, G., Thompson, D. K., & Moore, P. A. (2015). Hydrological feedbacks in northern peatlands. Ecohydrology, 8(1), 113-127.

Walker, X. J., Rogers, B. M., Baltzer, J. L., Cumming, S. G., Day, N. J., Goetz, S. J., Johnstone, J. F., Schuur, E. A., Turetsky, M. R., & Mack, M. C. (2018). Cross-scale controls on carbon emissions from boreal forest megafires. Global Change Biology, 24(9), 4251-4265.

Wang, Y., Hogg, E. H., Price, D. T., Edwards, J., & Williamson, T. (2014). Past and projected future changes in moisture conditions in the Canadian boreal forest. The Forestry Chronicle, 90(5), 678-691.

Warner, B. G., & Asada, T. (2006). Biological diversity of peatlands in Canada. Aquatic Sciences, 68, 240-253.

Weltzin, J. F., Bridgham, S. D., Pastor, J., Chen, J., & Harth, C. (2003). Potential effects of warming and drying on peatland plant community composition. Global Change Biology, 9(2), 141-151.

Weltzin, J. F., Pastor, J., Harth, C., Bridgham, S. D., Updegraff, K., & Chapin, C. T. (2000). Response of bog and fen plant communities to warming and water-table manipulations. Ecology, 81(12), 3464-3478.

Whittington, P. N., & Price, J. S. (2006). The effects of water table draw-down (as a surrogate for climate change) on the hydrology of a fen peatland, Canada. Hydrological Processes, 20(17), 3589-3600.

Wieder, R. K., Scott, K. D., Kamminga, K., Vile, M. A., Vitt, D. H., Bone, T., Xu, B. I. N., Benscoter, B. W., & Bhatti, J. S. (2009). Postfire carbon balance in boreal bogs of Alberta, Canada. Global Change Biology, 15(1), 63-81.

Wieder, R. K., Vitt, D. H., & Benscoter, B. W. (2006). Peatlands and the boreal forest. In Boreal peatland ecosystems (pp. 1-8). Berlin, Heidelberg: Springer Berlin Heidelberg.

Wilkinson, S. L., Moore, P. A., Flannigan, M. D., Wotton, B. M., & Waddington, J. M. (2018). Did enhanced afforestation cause high severity peat burn in the Fort McMurray Horse River wildfire?. Environmental Research Letters, 13(1), 014018

Wilkinson, S. L., Moore, P. A., & Waddington, J. M. (2019). Assessing drivers of cross-scale variability in peat smoldering combustion vulnerability in forested boreal peatlands. Frontiers in Forests and Global Change, 2, 84.

Wilkinson, S. L., Andersen, R., Moore, P. A., Davidson, S. J., Granath, G., & Waddington, J. M. (2023). Wildfire and degradation accelerate northern peatland carbon release. Nature Climate Change, 13(5), 456-461.

Wood, S. (2022). mgcv: Mixed GAM Computation Vehicle with Automatic Smoothness Estimation. R package version 1.8-41, https://cran.r-project.org/web/packages/mgcv/mgcv.pdf.

Wood, S. (2017). Generalized additive models: an introduction with R (Second Edition). Boco Raton: CRC Press.

Wotton, B. M., Nock, C. A., & Flannigan, M. D. (2010). Forest fire occurrence and climate change in Canada. International Journal of Wildland Fire, 19(3), 253-271.

Zoltai, S. C., & Vitt, D. H. (1995). Canadian wetlands: environmental gradients and classification. Vegetation, 118(1), 131-137.

Zoltai, S. C., Morrissey, L. A., Livingston, G. P., & Groot, W. D. (1998). Effects of fires on carbon cycling in North American boreal peatlands. Environmental Reviews, 6(1), 13-24.

Yu, Z. C. (2012). Northern peatland carbon stocks and dynamics: a review. Biogeosciences, 9(10), 4071-4085.

CHAPTER 6: CONCLUSION

This thesis advances understanding of boreal peat combustion and carbon (C) loss during boreal peatland fires – an area of high uncertainty in global C budgets and Earth systems models (e.g., Bona et al., 2024; Lin et al., 2021; Loisel et al., 2021; Schuur et al., 2022). It uses integrated field measurements, bi-temporal airborne lidar data, and statistical modelling and analyses to quantify depth of burn and above- and below-ground C losses across peatland types and ecotones of the Boreal Plains. It builds on this by identifying ecological and biophysical conditions that drive variability in below-ground combustion, providing insights into conditions that enhance or reduce boreal peatland resiliency to wildland fire. By providing high-resolution, spatially continuous estimates of peat combustion across a range of peatlands and linking these with drivers, this thesis reduces uncertainty of combustion-related C loss estimates and provides a foundation for improved representation of boreal peatland fires in regional, national and global C budgets and models.

6.1 Summary and Conclusions

Four main research questions, each with several specific objectives, are addressed in this thesis through the manuscript-based Chapters 2-5. A synthesis of these research questions, how they were addressed, and key findings is presented below.

6.1.1 Research Questions and Answers

How do peatland-fire feedbacks and ecological mechanisms impact the resiliency of boreal peatlands to wildland fire and C loss?

To address this question, Chapter Two synthesizes existing literature to identify key pre- and post-fire feedbacks and processes that regulate or enhance burn severity or post-fire ecosystem change. Pre-fire, soil moisture and peat bulk density are dominant controls on peat combustion (Benscoter et al., 2011; Kohlenberg et al., 2018; Rein et al., 2008). These are regulated through negative feedback mechanisms such as hydrological connectivity which attenuates water table fluctuations, which in turn reduces bulk density, both contributing to reduced burn severity. Conversely, these can be dysregulated through positive feedbacks between peatland drying (or drainage), fluctuating water tables, and increased bulk density, leading to enhanced burn severities, which further dysregulates systems and increases C loss through combustion and decomposition (Nelson et al., 2021; Chapter 2). A positive feedback mechanism also exists where drier peatlands with higher bulk densities are more prone to shrubification (Weltzin et al., 2003), which subsequently lowers water tables through increased evapotranspiration and interception of precipitation (though it is moderated somewhat by increased shading; e.g., Nelson et al., 2021; Thompson et al., 2014; Waddington et al., 2015; Chapter 2). *Sphagnum fuscum* mosses, which are naturally fire-resistant and moisture-retaining, exist in a negative feedback with low burn severity; however, under drying or drained peatland conditions, a shift to more flammable mosses such as feathermoss can occur (Wilkinson et al., 2018), shifting to a positive feedback system that enhances burn severity (Nelson et al., 2021; Chapter 2).

Post-fire, peatlands may exist in either regulating or reinforcing feedback cycles depending on pre-fire conditions. If peatlands are hydrologically connected or undrained, water tables recover more rapidly to pre-fire levels (Kettridge et al., 2015; Lukenbach et al., 2017), supporting *Sphagnum* regeneration (Clymo and Duckett, 1986), and maintaining

ecosystem resiliency (Nelson et al., 2021; Chapter 2). In contrast, severe burns, or combustion in peatlands that are hydrologically disconnected or drained, can increase water table fluctuations and promote drying (Lukenbach et al., 2017; Sherwood et al., 2013; Thompson et al., 2014). Severe burns can alter microtopography, reducing hummocks and their moisture-retaining species and promoting shrub encroachment (Benscoter et al., 2005).

While the negative and positive feedbacks that regulate peat combustion are complex, varied, and can balance one another out on a local scale, the cumulative impacts of climate change and increased burn severities reinforce predominantly positive feedbacks that promote drying and long-term C loss, and amplify the impacts of combustion on boreal peatlands (Nelson et al., 2021; Chapter 2).

How accurately can airborne lidar measure ground surface elevations of burned and unburned peatlands across a continuum of vegetation growth, and what wavelength(s) and classification parameters optimize this accuracy?

Chapter 3 compares lidar ground-classified elevations with field-measured ground elevations across roads, burned peatlands with low, moderate, and tall vegetation regeneration, and unburned peatlands. It identifies optimal classification parameters and emission wavelengths (532 nm, 1064 nm, 1550 nm, and their combinations), as well as the impact of vegetation regeneration, through an iterative test of 230 differently classified ground surfaces. Optimal classification parameters and optimal wavelength(s) varied depending on vegetation growth status, highlighting the importance of optimizing

processing routines for land cover types. Mean offsets of lidar-derived ground surfaces from field-validated ground measurements were calculated to be 0.00 m in burned areas, regardless of vegetation regeneration status, and 0.01 m in unburned areas. Point-based RMSE ranged from 0.09 m in burned peatlands with low vegetation regeneration to 0.19 m in unburned areas (Nelson et al., 2022; Chapter 3).

These results highlight the utility of lidar data for depth of burn analyses, and suggest that if carefully parameterized, lidar data collected up to three years post-fire can be utilized without significant differences in cumulative errors compared to using data collected immediately post-fire (Nelson et al., 2022; Chapter 3). This upholds lidar as a robust ground-surface measurement tool, even within vegetated landscapes or small elevation changes, and expands the capacity for further research using airborne lidar in the years following wildland fire.

How deeply do boreal peatlands and ecotones burn, what is the spatial variability of this, and what are the antecedent conditions that are associated with variability in peat combustion?

Using pre- and post-fire lidar data, Chapter 4 quantifies peat combustion across bogs, fens, swamps, and their ecotones. The analysis found an average DOB (DOB) of 8.1 ± 6.2 cm across all peatlands and ecotones, with bog ecotones exhibiting the greatest DOB (9.3 ± 7.3 cm), and fens the lowest (7.0 ± 5.2 cm). Generalized Additive Models (GAMs) and Random Forest (RF) models were used to identify the most influential, remotely measured predictors associated with peat combustion within bogs, fens, and swamps from an initial

pool of 84 topographic, morphological, vegetation, hydrological, anthropogenic, and fire-weather covariates. GAMs explained 39-45% of the deviance when spatial covariates were included and 24-29% when they were excluded, and convergence between GAM and RF model results increased confidence in drivers identified. Across peatland types, bottom-up predictors associated with DOB dominated models, indicating that ecohydrological properties of peatlands are more strongly associated with peat combustion than external fire-weather variables. Top predictive variables varied by peatland type, with DOB in bogs associated predominantly with topographic and morphological variables, including peatland area, perimeter length, and distance to peatland edge. Relationships indicated that large bogs are likely to burn more deeply towards the edges, while small bogs, which may be drier, burn more deeply towards the middle. In fens, vegetation and anthropogenic disturbances were strongly associated with depth of burn (DOB) variability, with the top variables identified as Normalized Difference Vegetation Index (NDVI), flow accumulation, distance to seismic lines, Topographic Position Index (TPI), and vegetation structure (lidar-derived p25 and p50). The top predictor category in swamps was hydrology, predominantly Modified Normalized Difference Water Index (MNDWI). These variables can act as indicators for peatland vulnerability to wildland fire and C loss. These findings emphasize the importance of peatland-specific fire and landscape management and C loss mitigation strategies for the enhanced resilience of these ecosystems.

How much above- and below-ground C is lost during boreal peatland fires, how does this vary spatially, and how well is this captured by a) remotely sensed burn severity indices and b) national-scale operational C models?

By integrating lidar-derived DOB measurements with field-derived soil C density models, Chapter 5 investigates the variability of above- and below-ground C loss across bogs, fens, swamps, and their ecotones. Results show that soil C losses were nearly an order of magnitude greater than those of vegetation (-2.11 ± 5.09 kg m^{-2} versus -0.38 ± 0.32 kg m^{-2}), and that ecotones lost significantly more soil C than their corresponding peatland cores. Bog ecotones experienced particularly significant soil C losses, averaging -16.5 kg m^{-2}. Together, bogs and bog ecotones accounted for 65% of the total C loss, despite comprising only 43% of peatland area.

Lidar-derived combustion extent and C loss were compared with those estimated from dNBR. Agreement in burned versus unburned extent varied by peatland and ecotone type, with the strongest agreement (88%) in bogs and the weakest (48%) in swamps. The relationship between dNBR and vegetation C loss was much stronger than with soil C loss, and results emphasized that deep combustion could occur even in areas classified as low severity or even unburned by dNBR. Lidar-derived C losses were also compared with estimates based on the Canadian Model for Peatlands (CaMP) fire disturbance equations under low and high Drought Code (DC) scenarios, which revealed peatland-, ecotone-, and canopy-specific differences. In bogs, agreement was best under high DC conditions, indicating that lidar-derived C losses were on the higher end of what modelled outputs would suggest, while outputs from fens and swamps aligned better under low DC scenarios, indicating that lidar-derived C losses in these peatland types were on the low end of what models would suggest. This indicates that within the study area, bogs may have been particularly vulnerable to combustion, and suggests that with climate change, bogs may

experience even greater C losses, while fens and swamps may shift towards more bog-like behaviour/combustion potential.

6.1.2 Collective Impact

Collectively, the results of this thesis indicate the importance of hydrological connectivity, topography, vegetation structure, and anthropogenic disturbance patterns on peatland resiliency or vulnerability to wildland fire (Chapters 2, 4, 5). Bogs and bog ecotones, which are ombrogenous and therefore more susceptible to water table fluctuations, were the peatland ecosystems that were most vulnerable to deep combustion and C losses. Fens and swamps, on the other hand, which are geogenous and, in the case of swamps, at times fully inundated with water, burned less deeply and had lower proportions of burned area (Chapters 4, 5). Clear patterns emerged in which environmental drivers of combustion were distinct across peatland types (Chapter 4), revealing how ecohydrological conditions and context within the landscape influence patterns of combustion.

This thesis advances understanding of boreal peatland fire dynamics by quantifying spatially explicit C losses and driving mechanisms. It reduces uncertainties in C loss estimates at a high spatial resolution across hundreds of peatlands and provides indicators of peatland vulnerability that can be measured remotely, and thus mapped, providing important insights for modelling, monitoring, and managing peatland C losses in a changing climate.

6.2 Recommendations and Outlook

Expanding upon the results generated within the scope of this thesis, several opportunities emerge for further research in peatland-wildland fire research. Future work could further

improve methodological approaches to measuring soil combustion, improve the robustness of C loss estimates, and identify how drivers of peat combustion vary across space, time, and fire intensity. Pre- and post-fire lidar data can be a powerful tool to overcome methodological challenges in quantifying peat combustion, but because of the error that can be introduced during lidar ground classification (Aguilar & Mills, 2008), developing adaptable, transferable classification routines would improve accuracy while reducing time and cost barriers of exploratory classifications. Expanding the combustion and C loss analyses presented here to other fires and peatland complexes will improve generalizability of findings and strengthen C loss estimates. Scaling models from lidar-derived C losses to more readily accessible satellite-based datasets would also improve the transferability of findings. Finally, expanded driver analyses across spatial and temporal scales would improve robustness of findings and strengthen their transferability into terrestrial C models. In addition to the scope of research, there is a need to utilise these findings in applied contexts to identify and mitigate peatlands most vulnerable to deep combustion and improve how peatland C losses are included in national C frameworks.

6.2 References

Aguilar, F. J., & Mills, J. P. (2008). Accuracy assessment of LiDAR-derived digital elevation models. Photogrammetric Record, 23(122), 148–169.

Benscoter, B. W., Thompson, D. K., Waddington, J. M., Flannigan, M. D., Wotton, B. M., De Groot, W. J., & Turetsky, M. R. (2011). Interactive effects of vegetation, soil moisture and bulk density on depth of burning of thick organic soils. International Journal of Wildland Fire, 20(3), 418-429. https://doi.org/10.1071/WF08183.

Benscoter, B. W., Kelman Wieder, R., & Vitt, D. H. (2005). Linking microtopography with post-fire succession in bogs. Journal of Vegetation Science, 16(4), 453-460. https://doi.org /10.1111/j.1654-1103.2005.tb02385.x.

Bona, K. A., Webster, K. L., Thompson, D. K., Hararuk, O., Zhang, G., & Kurz, W. A. (2024). Using the Canadian Model for Peatlands (CaMP) to examine greenhouse gas emissions and carbon sink strength in Canada's boreal and temperate peatlands. Ecological Modelling, 490, 110633.

Clymo, R. S., & Duckett, J. (1986). Regeneration of Sphagnum. New Phytologist, 102(4), 589–614. https://doi.org/10.1111/j.1469-8137.1986.tb00834.x.

Kettridge, N., Turetsky, M. R., Sherwood, J. H., Thompson, D. K., Miller, C. A., Benscoter, B. W., Flannigan, M. D., Wotton, B. M., & Waddington, J. M. (2015). Moderate drop in water table increases peatland vulnerability to post-fire regime shift. Scientific Reports, 5, 8063. https://doi.org/10.1038/srep08063.

Kohlenberg, A. J., Turetsky, M. R., Thompson, D. K., Branfireun, B. A., & Mitchell, C. P. (2018). Controls on boreal peat combustion and resulting emissions of carbon and mercury. Environmental Research Letters, 13(3), 035005.

Lin, S., Liu, Y., & Huang, X. (2021). Climate-induced Arctic-boreal peatland fire and carbon loss in the 21st century. Science of the Total Environment, 796, 148924.

Loisel, J., Gallego-Sala, A. V., Amesbury, M. J., Magnan, G., Anshari, G., Beilman, D. W., ... & Wu, J. (2021). Expert assessment of future vulnerability of the global peatland carbon sink. Nature climate change, 11(1), 70-77.

Lukenbach, M. C., Hokanson, K. J., Devito, K. J., Kettridge, N., Petrone, R. M., Mendoza, C. A., Granath, G., & Waddington, J. M. (2017). Post-fire ecohydrological conditions at peatland margins in different hydrogeological settings of the boreal plain. Journal of Hydrology, 548, 741–753. https://doi.org/10.1016/j.jhydrol.2017.03.034.

Nelson, K., Chasmer, L., & Hopkinson, C. (2022). Quantifying LiDAR elevation accuracy: Parameterization and wavelength selection for optimal ground classifications based on time since fire/disturbance. *Remote Sensing*, *14*(20), 5080.

Nelson, K., Thompson, D., Hopkinson, C., Petrone, R., & Chasmer, L. (2021). Peatland-fire interactions: A review of wildland fire feedbacks and interactions in Canadian boreal peatlands. Science of the total environment, 769, 145212.

Rein, G., Cleaver, N., Ashton, C., Pironi, P., & Torero, J. L. (2008). The severity of smouldering peat fires and damage to the forest soil. Catena, 74, 304–309. https://doi.org/10.1016
/j.catena.2008.05.008.

Sherwood, J. H., Kettridge, N., Thompson, D. K., Morris, P. J., Silins, U., & Waddington, J. M. (2013). Effect of drainage and wildfire on peat hydrophysical properties. Hydrological Processes, 27(13), 1866–1874. https://doi.org/10.1002/hyp.9820.

Schuur, E. A., Abbott, B. W., Commane, R., Ernakovich, J., Euskirchen, E., Hugelius, G., Grosse, G., Jones, M., Koven, C., Leshyk, V., & Turetsky, M. (2022). Permafrost and climate change: carbon cycle feedbacks from the warming Arctic. Annual Review of Environment and Resources, 47(1), 343-371.

Thompson, D. K., Benscoter, B. W., & Waddington, J. M. (2014). Water balance of a burned and unburned forested boreal peatland. Hydrological Processes, 28(24), 5954–5964. https://doi.org/10.1002/hyp.10074.

Waddington, J. M., Morris, P. J., Kettridge, N., Granath, G., Thompson, D. K., & Moore, P. A. (2015). Hydrological feedbacks in northern peatlands. Ecohydrology, 8, 113–127. https://doi.org/10.1002/eco.1493.

Weltzin, J. F., Bridgham, S. D., Pastor, J., Chen, J., & Harth, C. (2003). Potential effects of warming and drying on peatland plant community composition. Global Change Biology, 9, 141–151. https://doi.org/10.1046/j.1365-2486.2003.00571.x.

Wilkinson, S. L., Moore, P. A., Flannigan, M. D., Wotton, B. M., & Waddington, J. M. (2018a). Did enhanced afforestation cause high severity peat burn in the Fort McMurray Horse River wildfire? Environmental Research Letters, 13(1), 014018.

APPENDICES

Supplementary material Chapter 3

Table S3.1. Ground classification results based on different laser pulse emission wavelengths (Green, NIR, SWIR), software used, and the classification parameters, described in Tables 1 and 2. Here I also show the difference in elevation (abs. avg. dz), standard deviation of the returns, and root mean squared error (RMSE).

Wavelength(s)	Software	Classification	Land Cover Type	Points/m2	Abs. Avg. dz	St. Dev.	RMSE
SWIR	TerraScan	9	Burned	0.48	0.06	0.13	0.14
SWIR	TerraScan	9	Burned High Regen	0.48	0.04	0.16	0.17
SWIR	TerraScan	9	Burned Low Regen	0.48	0.08	0.09	0.12
SWIR	TerraScan	9	Road	0.48	0.01	0.05	0.05
SWIR	TerraScan	9	Unburned	0.48	0.03	0.19	0.19
SWIR	TerraScan	14	Burned	0.78	0.04	0.13	0.14
SWIR	TerraScan	14	Burned High Regen	0.78	0.01	0.17	0.17
SWIR	TerraScan	14	Burned Low Regen	0.78	0.06	0.09	0.11
SWIR	TerraScan	14	Road	0.78	0.01	0.05	0.05
SWIR	TerraScan	14	Unburned	0.78	0.06	0.19	0.20
SWIR	TerraScan	19	Burned	1.07	0.01	0.13	0.13
SWIR	TerraScan	19	Burned High Regen	1.07	0.01	0.17	0.17
SWIR	TerraScan	19	Burned Low Regen	1.07	0.04	0.09	0.10
SWIR	TerraScan	19	Road	1.07	0.01	0.05	0.05
SWIR	TerraScan	19	Unburned	1.07	0.09	0.19	0.21
SWIR	TerraScan	24	Burned	1.23	0.00	0.14	0.14
SWIR	TerraScan	24	Burned High Regen	1.23	0.03	0.17	0.17
SWIR	TerraScan	24	Burned Low Regen	1.23	0.03	0.09	0.10
SWIR	TerraScan	24	Road	1.23	0.01	0.05	0.05
SWIR	TerraScan	24	Unburned	1.23	0.10	0.19	0.21
SWIR	TerraScan	1	Burned	0.85	0.03	0.14	0.14
SWIR	TerraScan	1	Burned High Regen	0.85	0.01	0.17	0.17
SWIR	TerraScan	1	Burned Low Regen	0.85	0.06	0.09	0.11
SWIR	TerraScan	1	Road	0.85	0.01	0.05	0.05
SWIR	TerraScan	1	Unburned	0.85	0.07	0.19	0.20
SWIR	TerraScan	2	Burned	0.85	0.03	0.14	0.14
SWIR	TerraScan	2	Burned High Regen	0.85	0.01	0.17	0.17
SWIR	TerraScan	2	Burned Low Regen	0.85	0.06	0.09	0.11
SWIR	TerraScan	2	Road	0.85	0.01	0.05	0.05
SWIR	TerraScan	2	Unburned	0.85	0.07	0.19	0.20
SWIR	TerraScan	3	Burned	0.85	0.03	0.14	0.14
SWIR	TerraScan	3	Burned High Regen	0.85	0.01	0.17	0.17
SWIR	TerraScan	3	Burned Low Regen	0.85	0.06	0.09	0.11
SWIR	TerraScan	3	Road	0.85	0.01	0.05	0.05
SWIR	TerraScan	3	Unburned	0.85	0.07	0.19	0.20
SWIR	TerraScan	4	Burned	0.85	0.03	0.14	0.14
SWIR	TerraScan	4	Burned High Regen	0.85	0.01	0.17	0.17
SWIR	TerraScan	4	Burned Low Regen	0.85	0.06	0.09	0.11

SWIR	TerraScan	4	Road	0.85	0.01	0.05	0.05
SWIR	TerraScan	4	Unburned	0.85	0.07	0.19	0.20
SWIR	TerraScan	5	Burned	0.85	0.03	0.14	0.14
SWIR	TerraScan	5	Burned High Regen	0.85	0.01	0.17	0.17
SWIR	TerraScan	5	Burned Low Regen	0.85	0.06	0.09	0.11
SWIR	TerraScan	5	Road	0.85	0.01	0.05	0.05
SWIR	TerraScan	5	Unburned	0.85	0.07	0.19	0.20
SWIR	TerraScan	6	Burned	0.85	0.03	0.14	0.14
SWIR	TerraScan	6	Burned High Regen	0.85	0.01	0.17	0.17
SWIR	TerraScan	6	Burned Low Regen	0.85	0.06	0.09	0.11
SWIR	TerraScan	6	Road	0.85	0.01	0.05	0.05
SWIR	TerraScan	6	Unburned	0.85	0.07	0.19	0.20
SWIR	TerraScan	7	Burned	0.85	0.03	0.14	0.14
SWIR	TerraScan	7	Burned High Regen	0.85	0.01	0.17	0.17
SWIR	TerraScan	7	Burned Low Regen	0.85	0.06	0.09	0.11
SWIR	TerraScan	7	Road	0.85	0.01	0.05	0.05
SWIR	TerraScan	7	Unburned	0.85	0.07	0.19	0.20
SWIR	TerraScan	8	Burned	0.85	0.03	0.14	0.14
SWIR	TerraScan	8	Burned High Regen	0.85	0.01	0.17	0.17
SWIR	TerraScan	8	Burned Low Regen	0.85	0.06	0.09	0.11
SWIR	TerraScan	8	Road	0.85	0.01	0.05	0.05
SWIR	TerraScan	8	Unburned	0.85	0.07	0.19	0.20
SWIR	TerraScan	10	Burned	0.48	0.06	0.13	0.14
SWIR	TerraScan	10	Burned High Regen	0.48	0.04	0.16	0.17
SWIR	TerraScan	10	Burned Low Regen	0.48	0.09	0.10	0.13
SWIR	TerraScan	10	Road	0.48	0.01	0.05	0.05
SWIR	TerraScan	10	Unburned	0.48	0.03	0.19	0.19
SWIR	TerraScan	11	Burned	0.48	0.06	0.13	0.14
SWIR	TerraScan	11	Burned High Regen	0.48	0.04	0.16	0.17
SWIR	TerraScan	11	Burned Low Regen	0.48	0.08	0.09	0.12
SWIR	TerraScan	11	Road	0.48	0.01	0.05	0.05
SWIR	TerraScan	11	Unburned	0.48	0.03	0.19	0.19
SWIR	TerraScan	12	Burned	0.48	0.06	0.13	0.14
SWIR	TerraScan	12	Burned High Regen	0.48	0.04	0.16	0.17
SWIR	TerraScan	12	Burned Low Regen	0.48	0.08	0.09	0.12
SWIR	TerraScan	12	Road	0.48	0.01	0.05	0.05
SWIR	TerraScan	12	Unburned	0.48	0.03	0.19	0.19

SWIR	TerraScan	13	Burned	0.48	0.06	0.13	0.14
SWIR	TerraScan	13	Burned High Regen	0.48	0.04	0.16	0.17
SWIR	TerraScan	13	Burned Low Regen	0.48	0.08	0.09	0.12
SWIR	TerraScan	13	Road	0.48	0.01	0.05	0.05
SWIR	TerraScan	13	Unburned	0.48	0.03	0.19	0.19
SWIR	TerraScan	15	Burned	0.78	0.04	0.13	0.14
SWIR	TerraScan	15	Burned High Regen	0.78	0.01	0.17	0.17
SWIR	TerraScan	15	Burned Low Regen	0.78	0.06	0.09	0.11
SWIR	TerraScan	15	Road	0.78	0.01	0.05	0.05
SWIR	TerraScan	15	Unburned	0.78	0.06	0.19	0.20
SWIR	TerraScan	16	Burned	0.78	0.04	0.13	0.14
SWIR	TerraScan	16	Burned High Regen	0.78	0.01	0.17	0.17
SWIR	TerraScan	16	Burned Low Regen	0.78	0.06	0.09	0.11
SWIR	TerraScan	16	Road	0.78	0.01	0.05	0.05
SWIR	TerraScan	16	Unburned	0.78	0.06	0.19	0.20
SWIR	TerraScan	17	Burned	0.78	0.04	0.13	0.14
SWIR	TerraScan	17	Burned High Regen	0.78	0.01	0.17	0.17
SWIR	TerraScan	17	Burned Low Regen	0.78	0.06	0.09	0.11
SWIR	TerraScan	17	Road	0.78	0.01	0.05	0.05
SWIR	TerraScan	17	Unburned	0.78	0.06	0.19	0.20
SWIR	TerraScan	18	Burned	0.78	0.04	0.13	0.14
SWIR	TerraScan	18	Burned High Regen	0.78	0.01	0.17	0.17
SWIR	TerraScan	18	Burned Low Regen	0.78	0.06	0.09	0.11
SWIR	TerraScan	18	Road	0.78	0.01	0.05	0.05
SWIR	TerraScan	18	Unburned	0.78	0.06	0.19	0.20
SWIR	TerraScan	20	Burned	1.07	0.01	0.13	0.14
SWIR	TerraScan	20	Burned High Regen	1.07	0.01	0.17	0.17
SWIR	TerraScan	20	Burned Low Regen	1.07	0.04	0.09	0.10
SWIR	TerraScan	20	Road	1.07	0.01	0.05	0.05
SWIR	TerraScan	20	Unburned	1.07	0.09	0.19	0.21
SWIR	TerraScan	21	Burned	1.07	0.01	0.13	0.13
SWIR	TerraScan	21	Burned High Regen	1.07	0.01	0.17	0.17
SWIR	TerraScan	21	Burned Low Regen	1.07	0.04	0.09	0.10
SWIR	TerraScan	21	Road	1.07	0.01	0.05	0.05
SWIR	TerraScan	21	Unburned	1.07	0.09	0.19	0.21
SWIR	TerraScan	22	Burned	1.07	0.02	0.13	0.13
SWIR	TerraScan	22	Burned High Regen	1.07	0.01	0.17	0.17

SWIR	TerraScan	22	Burned Low Regen	1.07	0.04	0.09	0.10
SWIR	TerraScan	22	Road	1.07	0.01	0.05	0.05
SWIR	TerraScan	22	Unburned	1.07	0.09	0.19	0.21
SWIR	TerraScan	23	Burned	1.07	0.02	0.13	0.13
SWIR	TerraScan	23	Burned High Regen	1.07	0.01	0.17	0.17
SWIR	TerraScan	23	Burned Low Regen	1.07	0.04	0.09	0.10
SWIR	TerraScan	23	Road	1.07	0.01	0.05	0.05
SWIR	TerraScan	23	Unburned	1.07	0.09	0.19	0.21
SWIR	TerraScan	25	Burned	1.23	0.00	0.14	0.14
SWIR	TerraScan	25	Burned High Regen	1.23	0.03	0.17	0.18
SWIR	TerraScan	25	Burned Low Regen	1.23	0.03	0.09	0.10
SWIR	TerraScan	25	Road	1.23	0.01	0.05	0.05
SWIR	TerraScan	25	Unburned	1.23	0.10	0.19	0.22
SWIR	TerraScan	26	Burned	1.23	0.00	0.14	0.14
SWIR	TerraScan	26	Burned High Regen	1.23	0.03	0.17	0.17
SWIR	TerraScan	26	Burned Low Regen	1.23	0.03	0.09	0.10
SWIR	TerraScan	26	Road	1.23	0.01	0.05	0.05
SWIR	TerraScan	26	Unburned	1.23	0.10	0.19	0.21
SWIR	TerraScan	27	Burned	1.23	0.00	0.14	0.14
SWIR	TerraScan	27	Burned High Regen	1.23	0.03	0.17	0.17
SWIR	TerraScan	27	Burned Low Regen	1.23	0.03	0.09	0.10
SWIR	TerraScan	27	Road	1.23	0.01	0.05	0.05
SWIR	TerraScan	27	Unburned	1.23	0.10	0.19	0.21
SWIR	TerraScan	28	Burned	1.23	0.00	0.14	0.14
SWIR	TerraScan	28	Burned High Regen	1.23	0.03	0.17	0.17
SWIR	TerraScan	28	Burned Low Regen	1.23	0.03	0.09	0.10
SWIR	TerraScan	28	Road	1.23	0.01	0.05	0.05
SWIR	TerraScan	28	Unburned	1.23	0.10	0.19	0.21
SWIR & NIR	TerraScan	9	Burned	0.59	0.07	0.13	0.15
SWIR & NIR	TerraScan	9	Burned High Regen	0.59	0.05	0.17	0.17
SWIR & NIR	TerraScan	9	Burned Low Regen	0.59	0.09	0.10	0.14
SWIR & NIR	TerraScan	9	Road	0.59	0.02	0.05	0.05
SWIR & NIR	TerraScan	9	Unburned	0.59	0.01	0.20	0.19
SWIR & NIR	TerraScan	14	Burned	1.03	0.04	0.13	0.14
SWIR & NIR	TerraScan	14	Burned High Regen	1.03	0.02	0.16	0.16
SWIR & NIR	TerraScan	14	Burned Low Regen	1.03	0.07	0.10	0.12
SWIR & NIR	TerraScan	14	Road	1.03	0.01	0.05	0.05

SWIR & NIR	TerraScan	14	Unburned	1.03	0.05	0.19	0.20
SWIR & NIR	TerraScan	19	Burned	1.54	0.02	0.13	0.13
SWIR & NIR	TerraScan	19	Burned High Regen	1.54	0.00	0.17	0.17
SWIR & NIR	TerraScan	19	Burned Low Regen	1.54	0.05	0.09	0.10
SWIR & NIR	TerraScan	19	Road	1.54	0.01	0.05	0.05
SWIR & NIR	TerraScan	19	Unburned	1.54	0.08	0.19	0.20
SWIR & NIR	TerraScan	24	Burned	1.88	0.01	0.13	0.13
SWIR & NIR	TerraScan	24	Burned High Regen	1.88	0.02	0.17	0.17
SWIR & NIR	TerraScan	24	Burned Low Regen	1.88	0.04	0.09	0.10
SWIR & NIR	TerraScan	24	Road	1.88	0.00	0.04	0.04
SWIR & NIR	TerraScan	24	Unburned	1.88	0.09	0.19	0.21
SWIR & NIR	TerraScan	1	Burned	1.15	0.04	0.13	0.14
SWIR & NIR	TerraScan	1	Burned High Regen	1.15	0.01	0.16	0.16
SWIR & NIR	TerraScan	1	Burned Low Regen	1.15	0.06	0.10	0.11
SWIR & NIR	TerraScan	1	Road	1.15	0.00	0.04	0.04
SWIR & NIR	TerraScan	1	Unburned	1.15	0.06	0.19	0.20
SWIR & NIR	TerraScan	2	Burned	1.15	0.04	0.13	0.14
SWIR & NIR	TerraScan	2	Burned High Regen	1.15	0.01	0.16	0.16
SWIR & NIR	TerraScan	2	Burned Low Regen	1.15	0.06	0.10	0.11
SWIR & NIR	TerraScan	2	Road	1.15	0.00	0.04	0.04
SWIR & NIR	TerraScan	2	Unburned	1.15	0.06	0.19	0.20
SWIR & NIR	TerraScan	3	Burned	1.15	0.04	0.13	0.14
SWIR & NIR	TerraScan	3	Burned High Regen	1.15	0.01	0.16	0.16
SWIR & NIR	TerraScan	3	Burned Low Regen	1.15	0.06	0.10	0.11
SWIR & NIR	TerraScan	3	Road	1.15	0.00	0.04	0.04
SWIR & NIR	TerraScan	3	Unburned	1.15	0.06	0.19	0.20
SWIR & NIR	TerraScan	4	Burned	1.15	0.04	0.13	0.14
SWIR & NIR	TerraScan	4	Burned High Regen	1.15	0.01	0.16	0.16
SWIR & NIR	TerraScan	4	Burned Low Regen	1.15	0.06	0.10	0.11
SWIR & NIR	TerraScan	4	Road	1.15	0.00	0.04	0.04
SWIR & NIR	TerraScan	4	Unburned	1.15	0.06	0.19	0.20
SWIR & NIR	TerraScan	5	Burned	1.15	0.04	0.13	0.14
SWIR & NIR	TerraScan	5	Burned High Regen	1.15	0.01	0.16	0.16
SWIR & NIR	TerraScan	5	Burned Low Regen	1.15	0.06	0.10	0.11
SWIR & NIR	TerraScan	5	Road	1.15	0.00	0.04	0.04
SWIR & NIR	TerraScan	5	Unburned	1.15	0.06	0.19	0.20
SWIR & NIR	TerraScan	6	Burned	1.15	0.04	0.13	0.14

SWIR & NIR	TerraScan	6	Burned High Regen	1.15	0.01	0.16	0.16
SWIR & NIR	TerraScan	6	Burned Low Regen	1.15	0.06	0.10	0.11
SWIR & NIR	TerraScan	6	Road	1.15	0.00	0.04	0.04
SWIR & NIR	TerraScan	6	Unburned	1.15	0.06	0.19	0.20
SWIR & NIR	TerraScan	7	Burned	1.15	0.04	0.13	0.14
SWIR & NIR	TerraScan	7	Burned High Regen	1.15	0.01	0.16	0.16
SWIR & NIR	TerraScan	7	Burned Low Regen	1.15	0.06	0.10	0.11
SWIR & NIR	TerraScan	7	Road	1.15	0.00	0.04	0.04
SWIR & NIR	TerraScan	7	Unburned	1.15	0.06	0.19	0.20
SWIR & NIR	TerraScan	8	Burned	1.15	0.04	0.13	0.14
SWIR & NIR	TerraScan	8	Burned High Regen	1.15	0.01	0.16	0.16
SWIR & NIR	TerraScan	8	Burned Low Regen	1.15	0.06	0.10	0.11
SWIR & NIR	TerraScan	8	Road	1.15	0.00	0.04	0.04
SWIR & NIR	TerraScan	8	Unburned	1.15	0.06	0.19	0.20
SWIR & NIR	TerraScan	10	Burned	0.59	0.07	0.13	0.15
SWIR & NIR	TerraScan	10	Burned High Regen	0.59	0.05	0.17	0.17
SWIR & NIR	TerraScan	10	Burned Low Regen	0.59	0.09	0.10	0.14
SWIR & NIR	TerraScan	10	Road	0.59	0.02	0.05	0.05
SWIR & NIR	TerraScan	10	Unburned	0.59	0.01	0.19	0.19
SWIR & NIR	TerraScan	11	Burned	0.59	0.07	0.13	0.15
SWIR & NIR	TerraScan	11	Burned High Regen	0.59	0.05	0.17	0.17
SWIR & NIR	TerraScan	11	Burned Low Regen	0.59	0.09	0.10	0.14
SWIR & NIR	TerraScan	11	Road	0.59	0.02	0.05	0.05
SWIR & NIR	TerraScan	11	Unburned	0.59	0.01	0.20	0.19
SWIR & NIR	TerraScan	12	Burned	0.59	0.07	0.13	0.15
SWIR & NIR	TerraScan	12	Burned High Regen	0.59	0.05	0.17	0.17
SWIR & NIR	TerraScan	12	Burned Low Regen	0.59	0.09	0.10	0.14
SWIR & NIR	TerraScan	12	Road	0.59	0.02	0.05	0.05
SWIR & NIR	TerraScan	12	Unburned	0.59	0.01	0.20	0.19
SWIR & NIR	TerraScan	13	Burned	0.59	0.07	0.13	0.15
SWIR & NIR	TerraScan	13	Burned High Regen	0.59	0.05	0.17	0.17
SWIR & NIR	TerraScan	13	Burned Low Regen	0.59	0.09	0.10	0.14
SWIR & NIR	TerraScan	13	Road	0.59	0.02	0.05	0.05
SWIR & NIR	TerraScan	13	Unburned	0.59	0.01	0.20	0.19
SWIR & NIR	TerraScan	15	Burned	1.04	0.04	0.13	0.14
SWIR & NIR	TerraScan	15	Burned High Regen	1.04	0.02	0.16	0.16

SWIR & NIR	TerraScan	15	Burned Low Regen	1.04	0.07	0.10	0.12
SWIR & NIR	TerraScan	15	Road	1.04	0.01	0.05	0.05
SWIR & NIR	TerraScan	15	Unburned	1.04	0.05	0.19	0.20
SWIR & NIR	TerraScan	16	Burned	1.03	0.04	0.14	0.13
SWIR & NIR	TerraScan	16	Burned High Regen	1.03	0.02	0.16	0.16
SWIR & NIR	TerraScan	16	Burned Low Regen	1.03	0.07	0.10	0.12
SWIR & NIR	TerraScan	16	Road	1.03	0.01	0.05	0.05
SWIR & NIR	TerraScan	16	Unburned	1.03	0.05	0.19	0.20
SWIR & NIR	TerraScan	17	Burned	1.03	0.04	0.13	0.14
SWIR & NIR	TerraScan	17	Burned High Regen	1.03	0.02	0.16	0.16
SWIR & NIR	TerraScan	17	Burned Low Regen	1.03	0.07	0.10	0.12
SWIR & NIR	TerraScan	17	Road	1.03	0.01	0.05	0.05
SWIR & NIR	TerraScan	17	Unburned	1.03	0.05	0.19	0.20
SWIR & NIR	TerraScan	18	Burned	1.03	0.04	0.13	0.14
SWIR & NIR	TerraScan	18	Burned High Regen	1.03	0.02	0.16	0.16
SWIR & NIR	TerraScan	18	Burned Low Regen	1.03	0.07	0.10	0.12
SWIR & NIR	TerraScan	18	Road	1.03	0.01	0.05	0.05
SWIR & NIR	TerraScan	18	Unburned	1.03	0.05	0.19	0.20
SWIR & NIR	TerraScan	20	Burned	1.54	0.02	0.13	0.13
SWIR & NIR	TerraScan	20	Burned High Regen	1.54	0.00	0.17	0.16
SWIR & NIR	TerraScan	20	Burned Low Regen	1.54	0.05	0.09	0.10
SWIR & NIR	TerraScan	20	Road	1.54	0.00	0.04	0.04
SWIR & NIR	TerraScan	20	Unburned	1.54	0.08	0.19	0.20
SWIR & NIR	TerraScan	21	Burned	1.54	0.02	0.13	0.13
SWIR & NIR	TerraScan	21	Burned High Regen	1.54	0.00	0.17	0.17
SWIR & NIR	TerraScan	21	Burned Low Regen	1.54	0.05	0.09	0.10
SWIR & NIR	TerraScan	21	Road	1.54	0.01	0.05	0.05
SWIR & NIR	TerraScan	21	Unburned	1.54	0.08	0.19	0.20
SWIR & NIR	TerraScan	22	Burned	1.54	0.02	0.13	0.13
SWIR & NIR	TerraScan	22	Burned High Regen	1.54	0.00	0.17	0.17
SWIR & NIR	TerraScan	22	Burned Low Regen	1.54	0.05	0.09	0.10
SWIR & NIR	TerraScan	22	Road	1.54	0.01	0.05	0.05
SWIR & NIR	TerraScan	22	Unburned	1.54	0.08	0.19	0.20
SWIR & NIR	TerraScan	23	Burned	1.54	0.02	0.13	0.13
SWIR & NIR	TerraScan	23	Burned High Regen	1.54	0.00	0.17	0.17
SWIR & NIR	TerraScan	23	Burned Low Regen	1.54	0.05	0.09	0.10
SWIR & NIR	TerraScan	23	Road	1.54	0.01	0.05	0.05

SWIR & NIR	TerraScan	23	Unburned	1.54	0.08	0.19	0.20
SWIR & NIR	TerraScan	25	Burned	1.88	0.00	0.13	0.13
SWIR & NIR	TerraScan	25	Burned High Regen	1.88	0.02	0.17	0.17
SWIR & NIR	TerraScan	25	Burned Low Regen	1.88	0.04	0.09	0.10
SWIR & NIR	TerraScan	25	Road	1.88	0.00	0.04	0.04
SWIR & NIR	TerraScan	25	Unburned	1.88	0.09	0.19	0.21
SWIR & NIR	TerraScan	26	Burned	1.88	0.00	0.13	0.13
SWIR & NIR	TerraScan	26	Burned High Regen	1.88	0.02	0.17	0.17
SWIR & NIR	TerraScan	26	Burned Low Regen	1.88	0.04	0.09	0.10
SWIR & NIR	TerraScan	26	Road	1.88	0.00	0.04	0.04
SWIR & NIR	TerraScan	26	Unburned	1.88	0.09	0.19	0.21
SWIR & NIR	TerraScan	27	Burned	1.88	0.01	0.13	0.13
SWIR & NIR	TerraScan	27	Burned High Regen	1.88	0.02	0.17	0.17
SWIR & NIR	TerraScan	27	Burned Low Regen	1.88	0.04	0.09	0.10
SWIR & NIR	TerraScan	27	Road	1.88	0.00	0.04	0.04
SWIR & NIR	TerraScan	27	Unburned	1.88	0.09	0.19	0.21
SWIR & NIR	TerraScan	28	Burned	1.88	0.01	0.13	0.13
SWIR & NIR	TerraScan	28	Burned High Regen	1.88	0.02	0.17	0.17
SWIR & NIR	TerraScan	28	Burned Low Regen	1.88	0.04	0.09	0.10
SWIR & NIR	TerraScan	28	Road	1.88	0.00	0.04	0.04
SWIR & NIR	TerraScan	28	Unburned	1.88	0.09	0.19	0.21
SWIR, NIR & Visible	TerraScan	9	Burned	0.64	0.07	0.13	0.15
SWIR, NIR & Visible	TerraScan	9	Burned High Regen	0.64	0.05	0.17	0.17
SWIR, NIR & Visible	TerraScan	9	Burned Low Regen	0.64	0.09	0.10	0.14
SWIR, NIR & Visible	TerraScan	9	Road	0.64	0.01	0.04	0.05
SWIR, NIR & Visible	TerraScan	9	Unburned	0.64	0.01	0.19	0.19
SWIR, NIR & Visible	TerraScan	14	Burned	1.16	0.04	0.13	0.14
SWIR, NIR & Visible	TerraScan	14	Burned High Regen	1.16	0.02	0.16	0.17
SWIR, NIR & Visible	TerraScan	14	Burned Low Regen	1.16	0.07	0.10	0.12
SWIR, NIR & Visible	TerraScan	14	Road	1.16	0.01	0.04	0.05

SWIR, NIR & Visible	TerraScan	14	Unburned	1.16	0.05	0.19	0.19
SWIR, NIR & Visible	TerraScan	19	Burned	1.80	0.02	0.13	0.13
SWIR, NIR & Visible	TerraScan	19	Burned High Regen	1.80	0.01	0.17	0.17
SWIR, NIR & Visible	TerraScan	19	Burned Low Regen	1.80	0.04	0.09	0.10
SWIR, NIR & Visible	TerraScan	19	Road	1.80	0.01	0.05	0.05
SWIR, NIR & Visible	TerraScan	19	Unburned	1.80	0.08	0.19	0.20
SWIR, NIR & Visible	TerraScan	24	Burned	2.27	0.00	0.14	0.14
SWIR, NIR & Visible	TerraScan	24	Burned High Regen	2.27	0.03	0.17	0.18
SWIR, NIR & Visible	TerraScan	24	Burned Low Regen	2.27	0.03	0.09	0.10
SWIR, NIR & Visible	TerraScan	24	Road	2.27	0.01	0.05	0.05
SWIR, NIR & Visible	TerraScan	24	Unburned	2.27	0.09	0.19	0.21
SWIR, NIR & Visible	TerraScan	1	Burned	1.31	0.03	0.13	0.14
SWIR, NIR & Visible	TerraScan	1	Burned High Regen	1.31	0.01	0.17	0.17
SWIR, NIR & Visible	TerraScan	1	Burned Low Regen	1.31	0.06	0.10	0.11
SWIR, NIR & Visible	TerraScan	1	Road	1.31	0.01	0.04	0.05
SWIR, NIR & Visible	TerraScan	1	Unburned	1.31	0.06	0.19	0.20
SWIR, NIR & Visible	TerraScan	2	Burned	1.31	0.03	0.13	0.14
SWIR, NIR & Visible	TerraScan	2	Burned High Regen	1.31	0.01	0.17	0.17
SWIR, NIR & Visible	TerraScan	2	Burned Low Regen	1.31	0.06	0.10	0.11
SWIR, NIR & Visible	TerraScan	2	Road	1.31	0.01	0.04	0.05
SWIR, NIR & Visible	TerraScan	2	Unburned	1.31	0.06	0.19	0.20
SWIR, NIR & Visible	TerraScan	3	Burned	1.31	0.03	0.13	0.14

SWIR, NIR & Visible	TerraScan	3	Burned High Regen	1.31	0.01	0.17	0.17
SWIR, NIR & Visible	TerraScan	3	Burned Low Regen	1.31	0.06	0.10	0.11
SWIR, NIR & Visible	TerraScan	3	Road	1.31	0.01	0.04	0.05
SWIR, NIR & Visible	TerraScan	3	Unburned	1.31	0.06	0.19	0.20
SWIR, NIR & Visible	TerraScan	4	Burned	1.31	0.03	0.13	0.14
SWIR, NIR & Visible	TerraScan	4	Burned High Regen	1.31	0.01	0.17	0.17
SWIR, NIR & Visible	TerraScan	4	Burned Low Regen	1.31	0.06	0.10	0.11
SWIR, NIR & Visible	TerraScan	4	Road	1.31	0.01	0.04	0.05
SWIR, NIR & Visible	TerraScan	4	Unburned	1.31	0.06	0.19	0.20
SWIR, NIR & Visible	TerraScan	5	Burned	1.31	0.03	0.13	0.14
SWIR, NIR & Visible	TerraScan	5	Burned High Regen	1.31	0.01	0.17	0.17
SWIR, NIR & Visible	TerraScan	5	Burned Low Regen	1.31	0.06	0.10	0.11
SWIR, NIR & Visible	TerraScan	5	Road	1.31	0.01	0.04	0.05
SWIR, NIR & Visible	TerraScan	5	Unburned	1.31	0.06	0.19	0.20
SWIR, NIR & Visible	TerraScan	6	Burned	1.31	0.03	0.13	0.14
SWIR, NIR & Visible	TerraScan	6	Burned High Regen	1.31	0.01	0.17	0.17
SWIR, NIR & Visible	TerraScan	6	Burned Low Regen	1.31	0.06	0.10	0.11
SWIR, NIR & Visible	TerraScan	6	Road	1.31	0.01	0.04	0.05
SWIR, NIR & Visible	TerraScan	6	Unburned	1.31	0.06	0.19	0.20
SWIR, NIR & Visible	TerraScan	7	Burned	1.31	0.03	0.13	0.14
SWIR, NIR & Visible	TerraScan	7	Burned High Regen	1.31	0.01	0.17	0.17
SWIR, NIR & Visible	TerraScan	7	Burned Low Regen	1.31	0.06	0.10	0.11

SWIR, NIR & Visible	TerraScan	7	Road	1.31	0.01	0.04	0.05
SWIR, NIR & Visible	TerraScan	7	Unburned	1.31	0.06	0.19	0.20
SWIR, NIR & Visible	TerraScan	8	Burned	1.31	0.03	0.13	0.14
SWIR, NIR & Visible	TerraScan	8	Burned High Regen	1.31	0.01	0.17	0.17
SWIR, NIR & Visible	TerraScan	8	Burned Low Regen	1.31	0.06	0.10	0.11
SWIR, NIR & Visible	TerraScan	8	Road	1.31	0.01	0.04	0.05
SWIR, NIR & Visible	TerraScan	8	Unburned	1.31	0.06	0.19	0.20
SWIR, NIR & Visible	TerraScan	10	Burned	0.64	0.07	0.13	0.15
SWIR, NIR & Visible	TerraScan	10	Burned High Regen	0.64	0.05	0.17	0.17
SWIR, NIR & Visible	TerraScan	10	Burned Low Regen	0.64	0.09	0.10	0.14
SWIR, NIR & Visible	TerraScan	10	Road	0.64	0.01	0.04	0.05
SWIR, NIR & Visible	TerraScan	10	Unburned	0.64	0.01	0.19	0.19
SWIR, NIR & Visible	TerraScan	11	Burned	0.64	0.07	0.13	0.15
SWIR, NIR & Visible	TerraScan	11	Burned High Regen	0.64	0.05	0.17	0.17
SWIR, NIR & Visible	TerraScan	11	Burned Low Regen	0.64	0.09	0.10	0.14
SWIR, NIR & Visible	TerraScan	11	Road	0.64	0.01	0.04	0.05
SWIR, NIR & Visible	TerraScan	11	Unburned	0.64	0.01	0.20	0.19
SWIR, NIR & Visible	TerraScan	12	Burned	0.64	0.07	0.13	0.15
SWIR, NIR & Visible	TerraScan	12	Burned High Regen	0.64	0.05	0.17	0.17
SWIR, NIR & Visible	TerraScan	12	Burned Low Regen	0.64	0.09	0.10	0.14
SWIR, NIR & Visible	TerraScan	12	Road	0.64	0.01	0.04	0.05
SWIR, NIR & Visible	TerraScan	12	Unburned	0.64	0.01	0.19	0.19

SWIR, NIR & Visible	TerraScan	13	Burned	0.64	0.07	0.13	0.15
SWIR, NIR & Visible	TerraScan	13	Burned High Regen	0.64	0.05	0.17	0.17
SWIR, NIR & Visible	TerraScan	13	Burned Low Regen	0.64	0.09	0.10	0.14
SWIR, NIR & Visible	TerraScan	13	Road	0.64	0.01	0.04	0.05
SWIR, NIR & Visible	TerraScan	13	Unburned	0.64	0.01	0.19	0.19
SWIR, NIR & Visible	TerraScan	15	Burned	1.17	0.04	0.13	0.14
SWIR, NIR & Visible	TerraScan	15	Burned High Regen	1.17	0.02	0.17	0.17
SWIR, NIR & Visible	TerraScan	15	Burned Low Regen	1.17	0.07	0.10	0.12
SWIR, NIR & Visible	TerraScan	15	Road	1.17	0.01	0.04	0.05
SWIR, NIR & Visible	TerraScan	15	Unburned	1.17	0.05	0.19	0.20
SWIR, NIR & Visible	TerraScan	16	Burned	1.16	0.04	0.13	0.14
SWIR, NIR & Visible	TerraScan	16	Burned High Regen	1.16	0.02	0.17	0.16
SWIR, NIR & Visible	TerraScan	16	Burned Low Regen	1.16	0.07	0.10	0.12
SWIR, NIR & Visible	TerraScan	16	Road	1.16	0.01	0.04	0.05
SWIR, NIR & Visible	TerraScan	16	Unburned	1.16	0.05	0.19	0.19
SWIR, NIR & Visible	TerraScan	17	Burned	1.16	0.04	0.13	0.14
SWIR, NIR & Visible	TerraScan	17	Burned High Regen	1.16	0.02	0.16	0.17
SWIR, NIR & Visible	TerraScan	17	Burned Low Regen	1.16	0.07	0.10	0.12
SWIR, NIR & Visible	TerraScan	17	Road	1.16	0.01	0.04	0.05
SWIR, NIR & Visible	TerraScan	17	Unburned	1.16	0.05	0.19	0.19
SWIR, NIR & Visible	TerraScan	18	Burned	1.16	0.04	0.13	0.14
SWIR, NIR & Visible	TerraScan	18	Burned High Regen	1.16	0.02	0.17	0.17

SWIR, NIR & Visible	TerraScan	18	Burned Low Regen	1.16	0.07	0.10	0.12
SWIR, NIR & Visible	TerraScan	18	Road	1.16	0.01	0.04	0.05
SWIR, NIR & Visible	TerraScan	18	Unburned	1.16	0.05	0.19	0.19
SWIR, NIR & Visible	TerraScan	20	Burned	1.81	0.02	0.13	0.13
SWIR, NIR & Visible	TerraScan	20	Burned High Regen	1.81	0.01	0.17	0.17
SWIR, NIR & Visible	TerraScan	20	Burned Low Regen	1.81	0.04	0.09	0.10
SWIR, NIR & Visible	TerraScan	20	Road	1.81	0.01	0.05	0.05
SWIR, NIR & Visible	TerraScan	20	Unburned	1.81	0.08	0.19	0.20
SWIR, NIR & Visible	TerraScan	21	Burned	1.80	0.02	0.13	0.13
SWIR, NIR & Visible	TerraScan	21	Burned High Regen	1.80	0.01	0.17	0.17
SWIR, NIR & Visible	TerraScan	21	Burned Low Regen	1.80	0.04	0.09	0.10
SWIR, NIR & Visible	TerraScan	21	Road	1.80	0.01	0.05	0.05
SWIR, NIR & Visible	TerraScan	21	Unburned	1.80	0.08	0.19	0.20
SWIR, NIR & Visible	TerraScan	22	Burned	1.80	0.02	0.13	0.13
SWIR, NIR & Visible	TerraScan	22	Burned High Regen	1.80	0.01	0.17	0.17
SWIR, NIR & Visible	TerraScan	22	Burned Low Regen	1.80	0.04	0.09	0.10
SWIR, NIR & Visible	TerraScan	22	Road	1.80	0.01	0.05	0.05
SWIR, NIR & Visible	TerraScan	22	Unburned	1.80	0.08	0.19	0.20
SWIR, NIR & Visible	TerraScan	23	Burned	1.80	0.02	0.13	0.13
SWIR, NIR & Visible	TerraScan	23	Burned High Regen	1.80	0.01	0.17	0.17
SWIR, NIR & Visible	TerraScan	23	Burned Low Regen	1.80	0.04	0.09	0.10
SWIR, NIR & Visible	TerraScan	23	Road	1.80	0.01	0.05	0.05

SWIR, NIR & Visible	TerraScan	23	Unburned	1.80	0.08	0.19	0.20
SWIR, NIR & Visible	TerraScan	25	Burned	2.27	0.00	0.14	0.14
SWIR, NIR & Visible	TerraScan	25	Burned High Regen	2.27	0.03	0.17	0.18
SWIR, NIR & Visible	TerraScan	25	Burned Low Regen	2.27	0.03	0.09	0.10
SWIR, NIR & Visible	TerraScan	25	Road	2.27	0.01	0.05	0.05
SWIR, NIR & Visible	TerraScan	25	Unburned	2.27	0.09	0.19	0.21
SWIR, NIR & Visible	TerraScan	26	Burned	2.27	0.00	0.14	0.14
SWIR, NIR & Visible	TerraScan	26	Burned High Regen	2.27	0.03	0.17	0.18
SWIR, NIR & Visible	TerraScan	26	Burned Low Regen	2.27	0.03	0.09	0.10
SWIR, NIR & Visible	TerraScan	26	Road	2.27	0.01	0.05	0.05
SWIR, NIR & Visible	TerraScan	26	Unburned	2.27	0.09	0.19	0.21
SWIR, NIR & Visible	TerraScan	27	Burned	2.27	0.00	0.14	0.14
SWIR, NIR & Visible	TerraScan	27	Burned High Regen	2.27	0.03	0.17	0.18
SWIR, NIR & Visible	TerraScan	27	Burned Low Regen	2.27	0.03	0.09	0.10
SWIR, NIR & Visible	TerraScan	27	Road	2.27	0.01	0.05	0.05
SWIR, NIR & Visible	TerraScan	27	Unburned	2.27	0.09	0.19	0.21
SWIR, NIR & Visible	TerraScan	33	Burned	2.26	0.00	0.14	0.14
SWIR, NIR & Visible	TerraScan	33	Burned High Regen	2.26	0.03	0.17	0.18
SWIR, NIR & Visible	TerraScan	33	Burned Low Regen	2.26	0.03	0.09	0.10
SWIR, NIR & Visible	TerraScan	33	Road	2.26	0.01	0.05	0.05
SWIR, NIR & Visible	TerraScan	33	Unburned	2.26	0.09	0.19	0.21
SWIR, NIR & Visible	TerraScan	34	Burned	1.05	0.03	0.13	0.13

SWIR, NIR & Visible	TerraScan	34	Burned High Regen	1.05	0.00	0.17	0.17
SWIR, NIR & Visible	TerraScan	34	Burned Low Regen	1.05	0.06	0.09	0.11
SWIR, NIR & Visible	TerraScan	34	Road	1.05	0.02	0.05	0.05
SWIR, NIR & Visible	TerraScan	34	Unburned	1.05	0.07	0.19	0.20
SWIR, NIR & Visible	TerraScan	35	Burned	0.22	0.09	0.13	0.16
SWIR, NIR & Visible	TerraScan	35	Burned High Regen	0.22	0.07	0.16	0.18
SWIR, NIR & Visible	TerraScan	35	Burned Low Regen	0.22	0.11	0.10	0.15
SWIR, NIR & Visible	TerraScan	35	Road	0.22	0.02	0.04	0.05
SWIR, NIR & Visible	TerraScan	35	Unburned	0.22	0.01	0.20	0.20
SWIR, NIR & Visible	TerraScan	36	Burned	2.27	0.00	0.14	0.14
SWIR, NIR & Visible	TerraScan	36	Burned High Regen	2.27	0.03	0.17	0.18
SWIR, NIR & Visible	TerraScan	36	Burned Low Regen	2.27	0.03	0.09	0.10
SWIR, NIR & Visible	TerraScan	36	Road	2.27	0.01	0.05	0.05
SWIR, NIR & Visible	TerraScan	36	Unburned	2.27	0.09	0.19	0.21
SWIR, NIR & Visible	TerraScan	29	Burned	4.06	0.04	0.14	0.15
SWIR, NIR & Visible	TerraScan	29	Burned High Regen	4.06	0.07	0.17	0.19
SWIR, NIR & Visible	TerraScan	29	Burned Low Regen	4.06	0.01	0.09	0.09
SWIR, NIR & Visible	TerraScan	29	Road	4.06	0.00	0.05	0.05
SWIR, NIR & Visible	TerraScan	29	Unburned	4.06	0.14	0.21	0.25
SWIR, NIR & Visible	TerraScan	30	Burned	3.94	0.04	0.14	0.15
SWIR, NIR & Visible	TerraScan	30	Burned High Regen	3.94	0.06	0.17	0.18
SWIR, NIR & Visible	TerraScan	30	Burned Low Regen	3.94	0.01	0.09	0.09

SWIR, NIR & Visible	TerraScan	30	Road	3.94	0.00	0.05	0.05
SWIR, NIR & Visible	TerraScan	30	Unburned	3.94	0.13	0.21	0.25
SWIR, NIR & Visible	TerraScan	31	Burned	3.32	0.03	0.14	0.14
SWIR, NIR & Visible	TerraScan	31	Burned High Regen	3.32	0.05	0.17	0.18
SWIR, NIR & Visible	TerraScan	31	Burned Low Regen	3.32	0.01	0.09	0.09
SWIR, NIR & Visible	TerraScan	31	Road	3.32	0.01	0.05	0.05
SWIR, NIR & Visible	TerraScan	31	Unburned	3.32	0.12	0.20	0.23
SWIR, NIR & Visible	TerraScan	32	Burned	1.53	0.03	0.13	0.13
SWIR, NIR & Visible	TerraScan	32	Burned High Regen	1.53	0.01	0.16	0.16
SWIR, NIR & Visible	TerraScan	32	Burned Low Regen	1.53	0.05	0.09	0.11
SWIR, NIR & Visible	TerraScan	32	Road	1.53	0.01	0.04	0.05
SWIR, NIR & Visible	TerraScan	32	Unburned	1.53	0.07	0.19	0.20
SWIR, NIR & Visible	TerraScan	28	Burned	2.27	0.00	0.14	0.14
SWIR, NIR & Visible	TerraScan	28	Burned High Regen	2.27	0.03	0.17	0.18
SWIR, NIR & Visible	TerraScan	28	Burned Low Regen	2.27	0.03	0.09	0.10
SWIR, NIR & Visible	TerraScan	28	Road	2.27	0.01	0.05	0.05
SWIR, NIR & Visible	TerraScan	28	Unburned	2.27	0.09	0.19	0.21
NIR	TerraScan	9	Burned	0.46	0.05	0.14	0.14
NIR	TerraScan	9	Burned High Regen	0.46	0.03	0.16	0.16
NIR	TerraScan	9	Burned Low Regen	0.46	0.07	0.11	0.13
NIR	TerraScan	9	Road	0.46	0.00	0.04	0.04
NIR	TerraScan	9	Unburned	0.46	0.04	0.20	0.20
NIR	TerraScan	14	Burned	0.75	0.02	0.13	0.13
NIR	TerraScan	14	Burned High Regen	0.75	0.00	0.17	0.17
NIR	TerraScan	14	Burned Low Regen	0.75	0.05	0.10	0.11

NIR	TerraScan	14	Road	0.75	0.00	0.04	0.04
NIR	TerraScan	14	Unburned	0.75	0.06	0.20	0.21
NIR	TerraScan	19	Burned	1.03	0.01	0.14	0.14
NIR	TerraScan	19	Burned High Regen	1.03	0.03	0.16	0.17
NIR	TerraScan	19	Burned Low Regen	1.03	0.03	0.10	0.10
NIR	TerraScan	19	Road	1.03	0.00	0.04	0.04
NIR	TerraScan	19	Unburned	1.03	0.09	0.20	0.22
NIR	TerraScan	24	Burned	1.20	0.01	0.14	0.14
NIR	TerraScan	24	Burned High Regen	1.20	0.04	0.17	0.18
NIR	TerraScan	24	Burned Low Regen	1.20	0.02	0.10	0.10
NIR	TerraScan	24	Road	1.20	0.00	0.04	0.04
NIR	TerraScan	24	Unburned	1.20	0.11	0.19	0.22
NIR	TerraScan	1	Burned	0.82	0.02	0.13	0.14
NIR	TerraScan	1	Burned High Regen	0.82	0.01	0.17	0.17
NIR	TerraScan	1	Burned Low Regen	0.82	0.05	0.10	0.11
NIR	TerraScan	1	Road	0.82	0.00	0.04	0.04
NIR	TerraScan	1	Unburned	0.82	0.07	0.20	0.21
NIR	TerraScan	2	Burned	0.82	0.02	0.13	0.14
NIR	TerraScan	2	Burned High Regen	0.82	0.01	0.17	0.17
NIR	TerraScan	2	Burned Low Regen	0.82	0.05	0.10	0.11
NIR	TerraScan	2	Road	0.82	0.00	0.04	0.04
NIR	TerraScan	2	Unburned	0.82	0.07	0.20	0.21
NIR	TerraScan	3	Burned	0.82	0.02	0.13	0.14
NIR	TerraScan	3	Burned High Regen	0.82	0.01	0.17	0.17
NIR	TerraScan	3	Burned Low Regen	0.82	0.05	0.10	0.11
NIR	TerraScan	3	Road	0.82	0.00	0.04	0.04
NIR	TerraScan	3	Unburned	0.82	0.07	0.20	0.21
NIR	TerraScan	4	Burned	0.82	0.02	0.13	0.14
NIR	TerraScan	4	Burned High Regen	0.82	0.01	0.17	0.17
NIR	TerraScan	4	Burned Low Regen	0.82	0.05	0.10	0.11
NIR	TerraScan	4	Road	0.82	0.00	0.04	0.04
NIR	TerraScan	4	Unburned	0.82	0.07	0.20	0.21
NIR	TerraScan	5	Burned	0.82	0.02	0.13	0.14
NIR	TerraScan	5	Burned High Regen	0.82	0.01	0.17	0.17
NIR	TerraScan	5	Burned Low Regen	0.82	0.05	0.10	0.11
NIR	TerraScan	5	Road	0.82	0.00	0.04	0.04
NIR	TerraScan	5	Unburned	0.82	0.07	0.20	0.21

NIR	TerraScan	6	Burned	0.82	0.02	0.13	0.14
NIR	TerraScan	6	Burned High Regen	0.82	0.01	0.17	0.17
NIR	TerraScan	6	Burned Low Regen	0.82	0.05	0.10	0.11
NIR	TerraScan	6	Road	0.82	0.00	0.04	0.04
NIR	TerraScan	6	Unburned	0.82	0.07	0.20	0.21
NIR	TerraScan	7	Burned	0.82	0.02	0.13	0.14
NIR	TerraScan	7	Burned High Regen	0.82	0.01	0.17	0.17
NIR	TerraScan	7	Burned Low Regen	0.82	0.05	0.10	0.11
NIR	TerraScan	7	Road	0.82	0.00	0.04	0.04
NIR	TerraScan	7	Unburned	0.82	0.07	0.20	0.21
NIR	TerraScan	8	Burned	0.82	0.02	0.13	0.14
NIR	TerraScan	8	Burned High Regen	0.82	0.01	0.17	0.17
NIR	TerraScan	8	Burned Low Regen	0.82	0.05	0.10	0.11
NIR	TerraScan	8	Road	0.82	0.00	0.04	0.04
NIR	TerraScan	8	Unburned	0.82	0.07	0.20	0.21
NIR	TerraScan	10	Burned	0.46	0.05	0.14	0.15
NIR	TerraScan	10	Burned High Regen	0.46	0.03	0.16	0.16
NIR	TerraScan	10	Burned Low Regen	0.46	0.07	0.11	0.13
NIR	TerraScan	10	Road	0.46	0.00	0.04	0.04
NIR	TerraScan	10	Unburned	0.46	0.03	0.19	0.19
NIR	TerraScan	11	Burned	0.46	0.05	0.14	0.15
NIR	TerraScan	11	Burned High Regen	0.46	0.03	0.16	0.16
NIR	TerraScan	11	Burned Low Regen	0.46	0.07	0.11	0.13
NIR	TerraScan	11	Road	0.46	0.00	0.04	0.04
NIR	TerraScan	11	Unburned	0.46	0.04	0.20	0.20
NIR	TerraScan	12	Burned	0.46	0.05	0.14	0.14
NIR	TerraScan	12	Burned High Regen	0.46	0.03	0.16	0.16
NIR	TerraScan	12	Burned Low Regen	0.46	0.07	0.11	0.13
NIR	TerraScan	12	Road	0.46	0.00	0.04	0.04
NIR	TerraScan	12	Unburned	0.46	0.04	0.20	0.20
NIR	TerraScan	13	Burned	0.46	0.05	0.14	0.14
NIR	TerraScan	13	Burned High Regen	0.46	0.03	0.16	0.16
NIR	TerraScan	13	Burned Low Regen	0.46	0.07	0.11	0.13
NIR	TerraScan	13	Road	0.46	0.00	0.04	0.04
NIR	TerraScan	13	Unburned	0.46	0.04	0.20	0.20
NIR	TerraScan	15	Burned	0.75	0.02	0.13	0.13
NIR	TerraScan	15	Burned High Regen	0.75	0.00	0.17	0.17

NIR	TerraScan	15	Burned Low Regen	0.75	0.05	0.10	0.11
NIR	TerraScan	15	Road	0.75	0.00	0.04	0.04
NIR	TerraScan	15	Unburned	0.75	0.06	0.20	0.21
NIR	TerraScan	16	Burned	0.75	0.02	0.13	0.13
NIR	TerraScan	16	Burned High Regen	0.75	0.00	0.17	0.17
NIR	TerraScan	16	Burned Low Regen	0.75	0.05	0.10	0.11
NIR	TerraScan	16	Road	0.75	0.00	0.04	0.04
NIR	TerraScan	16	Unburned	0.75	0.06	0.20	0.21
NIR	TerraScan	17	Burned	0.75	0.02	0.13	0.13
NIR	TerraScan	17	Burned High Regen	0.75	0.00	0.17	0.17
NIR	TerraScan	17	Burned Low Regen	0.75	0.05	0.10	0.11
NIR	TerraScan	17	Road	0.75	0.00	0.04	0.04
NIR	TerraScan	17	Unburned	0.75	0.06	0.20	0.21
NIR	TerraScan	18	Burned	0.75	0.02	0.13	0.13
NIR	TerraScan	18	Burned High Regen	0.75	0.00	0.17	0.17
NIR	TerraScan	18	Burned Low Regen	0.75	0.05	0.10	0.11
NIR	TerraScan	18	Road	0.75	0.00	0.04	0.04
NIR	TerraScan	18	Unburned	0.75	0.06	0.20	0.21
NIR	TerraScan	20	Burned	1.03	0.00	0.14	0.14
NIR	TerraScan	20	Burned High Regen	1.03	0.03	0.16	0.17
NIR	TerraScan	20	Burned Low Regen	1.03	0.03	0.10	0.10
NIR	TerraScan	20	Road	1.03	0.00	0.04	0.04
NIR	TerraScan	20	Unburned	1.03	0.09	0.20	0.22
NIR	TerraScan	21	Burned	1.03	0.00	0.14	0.14
NIR	TerraScan	21	Burned High Regen	1.03	0.03	0.16	0.17
NIR	TerraScan	21	Burned Low Regen	1.03	0.03	0.10	0.10
NIR	TerraScan	21	Road	1.03	0.00	0.04	0.04
NIR	TerraScan	21	Unburned	1.03	0.09	0.20	0.22
NIR	TerraScan	22	Burned	1.03	0.00	0.14	0.14
NIR	TerraScan	22	Burned High Regen	1.03	0.03	0.16	0.17
NIR	TerraScan	22	Burned Low Regen	1.03	0.03	0.10	0.10
NIR	TerraScan	22	Road	1.03	0.00	0.04	0.04
NIR	TerraScan	22	Unburned	1.03	0.09	0.20	0.22
NIR	TerraScan	24	Burned	1.03	0.00	0.14	0.14
NIR	TerraScan	23	Burned High Regen	1.03	0.03	0.16	0.17
NIR	TerraScan	23	Burned Low Regen	1.03	0.03	0.10	0.10
NIR	TerraScan	23	Road	1.03	0.00	0.04	0.04

NIR	TerraScan	23	Unburned	1.03	0.09	0.20	0.22
NIR	TerraScan	25	Burned	1.20	0.01	0.14	0.14
NIR	TerraScan	25	Burned High Regen	1.20	0.04	0.17	0.18
NIR	TerraScan	25	Burned Low Regen	1.20	0.02	0.10	0.10
NIR	TerraScan	25	Road	1.20	0.00	0.04	0.04
NIR	TerraScan	25	Unburned	1.20	0.11	0.19	0.22
NIR	TerraScan	26	Burned	1.20	0.01	0.14	0.14
NIR	TerraScan	26	Burned High Regen	1.20	0.04	0.17	0.18
NIR	TerraScan	26	Burned Low Regen	1.20	0.02	0.10	0.10
NIR	TerraScan	26	Road	1.20	0.00	0.04	0.04
NIR	TerraScan	26	Unburned	1.20	0.11	0.19	0.22
NIR	TerraScan	27	Burned	1.20	0.01	0.14	0.14
NIR	TerraScan	27	Burned High Regen	1.20	0.04	0.17	0.18
NIR	TerraScan	27	Burned Low Regen	1.20	0.02	0.10	0.10
NIR	TerraScan	27	Road	1.20	0.00	0.04	0.04
NIR	TerraScan	27	Unburned	1.20	0.11	0.19	0.22
NIR	TerraScan	28	Burned	1.20	0.01	0.14	0.14
NIR	TerraScan	28	Burned High Regen	1.20	0.04	0.17	0.18
NIR	TerraScan	28	Burned Low Regen	1.20	0.02	0.10	0.10
NIR	TerraScan	28	Road	1.20	0.00	0.04	0.04
NIR	TerraScan	28	Unburned	1.20	0.11	0.19	0.22
Visible	TerraScan	9	Burned	0.53	0.00	0.14	0.14
Visible	TerraScan	9	Burned High Regen	0.53	0.03	0.17	0.17
Visible	TerraScan	9	Burned Low Regen	0.53	0.03	0.10	0.10
Visible	TerraScan	9	Road	0.53	0.01	0.05	0.05
Visible	TerraScan	9	Unburned	0.53	0.11	0.19	0.22
Visible	TerraScan	14	Burned	0.86	0.03	0.13	0.14
Visible	TerraScan	14	Burned High Regen	0.86	0.06	0.17	0.18
Visible	TerraScan	14	Burned Low Regen	0.86	0.00	0.09	0.09
Visible	TerraScan	14	Road	0.86	0.01	0.05	0.05
Visible	TerraScan	14	Unburned	0.86	0.14	0.19	0.24
Visible	TerraScan	19	Burned	1.12	0.05	0.14	0.15
Visible	TerraScan	19	Burned High Regen	1.12	0.07	0.17	0.18
Visible	TerraScan	19	Burned Low Regen	1.12	0.02	0.09	0.09
Visible	TerraScan	19	Road	1.12	0.01	0.05	0.05
Visible	TerraScan	19	Unburned	1.12	0.16	0.20	0.25
Visible	TerraScan	24	Burned	1.23	0.05	0.14	0.15

Visible	TerraScan	24	Burned High Regen	1.23	0.08	0.17	0.19
Visible	TerraScan	24	Burned Low Regen	1.23	0.02	0.09	0.09
Visible	TerraScan	24	Road	1.23	0.01	0.05	0.05
Visible	TerraScan	24	Unburned	1.23	0.17	0.20	0.26
Visible	TerraScan	1	Burned	0.93	0.03	0.13	0.14
Visible	TerraScan	1	Burned High Regen	0.93	0.06	0.17	0.18
Visible	TerraScan	1	Burned Low Regen	0.93	0.01	0.09	0.09
Visible	TerraScan	1	Road	0.93	0.01	0.05	0.05
Visible	TerraScan	1	Unburned	0.93	0.15	0.20	0.24
Visible	TerraScan	2	Burned	0.93	0.03	0.13	0.14
Visible	TerraScan	2	Burned High Regen	0.93	0.06	0.17	0.18
Visible	TerraScan	2	Burned Low Regen	0.93	0.01	0.09	0.09
Visible	TerraScan	2	Road	0.93	0.01	0.05	0.05
Visible	TerraScan	2	Unburned	0.93	0.15	0.20	0.24
Visible	TerraScan	3	Burned	0.93	0.03	0.13	0.14
Visible	TerraScan	3	Burned High Regen	0.93	0.06	0.17	0.18
Visible	TerraScan	3	Burned Low Regen	0.93	0.01	0.09	0.09
Visible	TerraScan	3	Road	0.93	0.01	0.05	0.05
Visible	TerraScan	3	Unburned	0.93	0.15	0.20	0.24
Visible	TerraScan	4	Burned	0.93	0.03	0.13	0.14
Visible	TerraScan	4	Burned High Regen	0.93	0.06	0.17	0.18
Visible	TerraScan	4	Burned Low Regen	0.93	0.01	0.09	0.09
Visible	TerraScan	4	Road	0.93	0.01	0.05	0.05
Visible	TerraScan	4	Unburned	0.93	0.15	0.20	0.24
Visible	TerraScan	5	Burned	0.93	0.03	0.13	0.14
Visible	TerraScan	5	Burned High Regen	0.93	0.06	0.17	0.18
Visible	TerraScan	5	Burned Low Regen	0.93	0.01	0.09	0.09
Visible	TerraScan	5	Road	0.93	0.01	0.05	0.05
Visible	TerraScan	5	Unburned	0.93	0.15	0.20	0.24
Visible	TerraScan	6	Burned	0.93	0.03	0.13	0.14
Visible	TerraScan	6	Burned High Regen	0.93	0.06	0.17	0.18
Visible	TerraScan	6	Burned Low Regen	0.93	0.01	0.09	0.09
Visible	TerraScan	6	Road	0.93	0.01	0.05	0.05
Visible	TerraScan	6	Unburned	0.93	0.15	0.20	0.24
Visible	TerraScan	7	Burned	0.93	0.03	0.13	0.14
Visible	TerraScan	7	Burned High Regen	0.93	0.06	0.17	0.18

Visible	TerraScan	7	Burned Low Regen	0.93	0.01	0.09	0.09
Visible	TerraScan	7	Road	0.93	0.01	0.05	0.05
Visible	TerraScan	7	Unburned	0.93	0.15	0.20	0.24
Visible	TerraScan	8	Burned	0.93	0.03	0.13	0.14
Visible	TerraScan	8	Burned High Regen	0.93	0.06	0.17	0.18
Visible	TerraScan	8	Burned Low Regen	0.93	0.01	0.09	0.09
Visible	TerraScan	8	Road	0.93	0.01	0.05	0.05
Visible	TerraScan	8	Unburned	0.93	0.15	0.20	0.24
Visible	TerraScan	10	Burned	0.53	0.00	0.14	0.14
Visible	TerraScan	10	Burned High Regen	0.53	0.03	0.17	0.17
Visible	TerraScan	10	Burned Low Regen	0.53	0.03	0.10	0.10
Visible	TerraScan	10	Road	0.53	0.01	0.05	0.05
Visible	TerraScan	10	Unburned	0.53	0.11	0.19	0.22
Visible	TerraScan	11	Burned	0.53	0.00	0.14	0.14
Visible	TerraScan	11	Burned High Regen	0.53	0.03	0.17	0.17
Visible	TerraScan	11	Burned Low Regen	0.53	0.03	0.10	0.10
Visible	TerraScan	11	Road	0.53	0.01	0.05	0.05
Visible	TerraScan	11	Unburned	0.53	0.11	0.19	0.22
Visible	TerraScan	12	Burned	0.53	0.00	0.14	0.14
Visible	TerraScan	12	Burned High Regen	0.53	0.03	0.17	0.17
Visible	TerraScan	12	Burned Low Regen	0.53	0.03	0.10	0.10
Visible	TerraScan	12	Road	0.53	0.01	0.05	0.05
Visible	TerraScan	12	Unburned	0.53	0.11	0.19	0.22
Visible	TerraScan	13	Burned	0.53	0.00	0.14	0.14
Visible	TerraScan	13	Burned High Regen	0.53	0.03	0.17	0.17
Visible	TerraScan	13	Burned Low Regen	0.53	0.03	0.10	0.10
Visible	TerraScan	13	Road	0.53	0.01	0.05	0.05
Visible	TerraScan	13	Unburned	0.53	0.11	0.19	0.22
Visible	TerraScan	15	Burned	0.86	0.03	0.13	0.14
Visible	TerraScan	15	Burned High Regen	0.86	0.06	0.17	0.18
Visible	TerraScan	15	Burned Low Regen	0.86	0.00	0.09	0.09
Visible	TerraScan	15	Road	0.86	0.01	0.05	0.05
Visible	TerraScan	15	Unburned	0.86	0.14	0.20	0.24
Visible	TerraScan	16	Burned	0.86	0.03	0.13	0.14
Visible	TerraScan	16	Burned High Regen	0.86	0.06	0.17	0.18
Visible	TerraScan	16	Burned Low Regen	0.86	0.00	0.09	0.09
Visible	TerraScan	16	Road	0.86	0.01	0.05	0.05

Visible	TerraScan	16	Unburned	0.86	0.14	0.20	0.24
Visible	TerraScan	17	Burned	0.86	0.03	0.13	0.14
Visible	TerraScan	17	Burned High Regen	0.86	0.06	0.17	0.18
Visible	TerraScan	17	Burned Low Regen	0.86	0.00	0.09	0.09
Visible	TerraScan	17	Road	0.86	0.01	0.05	0.05
Visible	TerraScan	17	Unburned	0.86	0.14	0.19	0.24
Visible	TerraScan	18	Burned	0.86	0.03	0.13	0.14
Visible	TerraScan	18	Burned High Regen	0.86	0.06	0.17	0.18
Visible	TerraScan	18	Burned Low Regen	0.86	0.00	0.09	0.09
Visible	TerraScan	18	Road	0.86	0.01	0.05	0.05
Visible	TerraScan	18	Unburned	0.86	0.14	0.19	0.24
Visible	TerraScan	20	Burned	1.12	0.05	0.14	0.15
Visible	TerraScan	20	Burned High Regen	1.12	0.07	0.17	0.18
Visible	TerraScan	20	Burned Low Regen	1.12	0.02	0.09	0.09
Visible	TerraScan	20	Road	1.12	0.01	0.05	0.05
Visible	TerraScan	20	Unburned	1.12	0.15	0.20	0.25
Visible	TerraScan	21	Burned	1.12	0.05	0.14	0.15
Visible	TerraScan	21	Burned High Regen	1.12	0.07	0.17	0.19
Visible	TerraScan	21	Burned Low Regen	1.12	0.02	0.09	0.09
Visible	TerraScan	21	Road	1.12	0.01	0.05	0.05
Visible	TerraScan	21	Unburned	1.12	0.16	0.20	0.25
Visible	TerraScan	22	Burned	1.12	0.05	0.14	0.15
Visible	TerraScan	22	Burned High Regen	1.12	0.07	0.17	0.19
Visible	TerraScan	22	Burned Low Regen	1.12	0.02	0.09	0.09
Visible	TerraScan	22	Road	1.12	0.01	0.05	0.05
Visible	TerraScan	22	Unburned	1.12	0.16	0.20	0.25
Visible	TerraScan	23	Burned	1.12	0.05	0.14	0.15
Visible	TerraScan	23	Burned High Regen	1.12	0.07	0.17	0.19
Visible	TerraScan	23	Burned Low Regen	1.12	0.02	0.09	0.09
Visible	TerraScan	23	Road	1.12	0.01	0.05	0.05
Visible	TerraScan	23	Unburned	1.12	0.16	0.20	0.25
Visible	TerraScan	25	Burned	1.24	0.05	0.14	0.15
Visible	TerraScan	25	Burned High Regen	1.24	0.08	0.17	0.19
Visible	TerraScan	25	Burned Low Regen	1.24	0.02	0.09	0.09
Visible	TerraScan	25	Road	1.24	0.01	0.05	0.05
Visible	TerraScan	25	Unburned	1.24	0.17	0.21	0.26
Visible	TerraScan	26	Burned	1.24	0.05	0.14	0.15

Visible	TerraScan	26	Burned High Regen	1.24	0.08	0.17	0.19
Visible	TerraScan	26	Burned Low Regen	1.24	0.02	0.09	0.09
Visible	TerraScan	26	Road	1.24	0.01	0.05	0.05
Visible	TerraScan	26	Unburned	1.24	0.17	0.20	0.26
Visible	TerraScan	27	Burned	1.23	0.05	0.14	0.15
Visible	TerraScan	27	Burned High Regen	1.23	0.08	0.17	0.19
Visible	TerraScan	27	Burned Low Regen	1.23	0.02	0.09	0.09
Visible	TerraScan	27	Road	1.23	0.01	0.05	0.05
Visible	TerraScan	27	Unburned	1.23	0.17	0.20	0.26
Visible	TerraScan	28	Burned	1.23	0.05	0.14	0.15
Visible	TerraScan	28	Burned High Regen	1.23	0.08	0.17	0.19
Visible	TerraScan	28	Burned Low Regen	1.23	0.02	0.09	0.09
Visible	TerraScan	28	Road	1.23	0.01	0.05	0.05
Visible	TerraScan	28	Unburned	1.23	0.17	0.20	0.26
SWIR	LASTools	A	Unburned	1.28	0.11	0.22	0.19
SWIR	LASTools	A	Road	1.28	0.01	0.05	0.05
SWIR	LASTools	A	Burned High Regen	1.28	0.03	0.18	0.18
SWIR	LASTools	A	Burned	1.28	0.00	0.14	0.14
SWIR	LASTools	A	Burned Low Regen	1.28	0.03	0.10	0.09
SWIR	LASTools	C	Unburned	1.28	0.10	0.22	0.20
SWIR	LASTools	C	Road	1.28	0.01	0.05	0.05
SWIR	LASTools	C	Burned High Regen	1.28	0.03	0.18	0.18
SWIR	LASTools	C	Burned	1.28	0.00	0.14	0.14
SWIR	LASTools	C	Burned Low Regen	1.28	0.03	0.10	0.09
SWIR	LASTools	B	Unburned	1.27	0.10	0.22	0.20
SWIR	LASTools	B	Road	1.27	0.01	0.05	0.05
SWIR	LASTools	B	Burned High Regen	1.27	0.03	0.18	0.18
SWIR	LASTools	B	Burned	1.27	0.00	0.14	0.14
SWIR	LASTools	B	Burned Low Regen	1.27	0.03	0.10	0.09
SWIR	LASTools	E	Unburned	1.28	0.11	0.22	0.20
SWIR	LASTools	E	Road	1.28	0.01	0.05	0.05
SWIR	LASTools	E	Burned High Regen	1.28	0.03	0.18	0.18
SWIR	LASTools	E	Burned	1.28	0.00	0.14	0.14
SWIR	LASTools	E	Burned Low Regen	1.28	0.03	0.10	0.09
SWIR	LASTools	D	Unburned	1.28	0.10	0.23	0.20
SWIR	LASTools	D	Road	1.28	0.01	0.05	0.05
SWIR	LASTools	D	Burned High Regen	1.28	0.03	0.19	0.18

SWIR	LASTools	D	Burned	1.28	0.00	0.15	0.15
SWIR	LASTools	D	Burned Low Regen	1.28	0.03	0.10	0.09
SWIR	LASTools	F	Unburned	1.32	0.10	0.22	0.20
SWIR	LASTools	F	Road	1.32	0.01	0.05	0.05
SWIR	LASTools	F	Burned High Regen	1.32	0.03	0.18	0.18
SWIR	LASTools	F	Burned	1.32	0.01	0.14	0.14
SWIR	LASTools	F	Burned Low Regen	1.32	0.03	0.09	0.09
SWIR	LASTools	H	Unburned	1.33	0.10	0.22	0.20
SWIR	LASTools	H	Road	1.33	0.01	0.05	0.05
SWIR	LASTools	H	Burned High Regen	1.33	0.03	0.18	0.17
SWIR	LASTools	H	Burned	1.33	0.01	0.14	0.14
SWIR	LASTools	H	Burned Low Regen	1.33	0.03	0.09	0.09
SWIR	LASTools	G	Unburned	1.33	0.10	0.22	0.20
SWIR	LASTools	G	Road	1.33	0.01	0.05	0.05
SWIR	LASTools	G	Burned High Regen	1.33	0.03	0.18	0.17
SWIR	LASTools	G	Burned	1.33	0.00	0.14	0.14
SWIR	LASTools	G	Burned Low Regen	1.33	0.03	0.09	0.09
SWIR	LASTools	J	Unburned	1.34	0.10	0.22	0.20
SWIR	LASTools	J	Road	1.34	0.01	0.05	0.05
SWIR	LASTools	J	Burned High Regen	1.34	0.03	0.18	0.17
SWIR	LASTools	J	Burned	1.34	0.00	0.14	0.14
SWIR	LASTools	J	Burned Low Regen	1.34	0.03	0.09	0.09
SWIR	LASTools	I	Unburned	1.34	0.10	0.22	0.20
SWIR	LASTools	I	Road	1.34	0.01	0.05	0.05
SWIR	LASTools	I	Burned High Regen	1.34	0.03	0.18	0.17
SWIR	LASTools	I	Burned	1.34	0.01	0.14	0.14
SWIR	LASTools	I	Burned Low Regen	1.34	0.03	0.09	0.09
NIR	LASTools	A	Unburned	1.24	0.11	0.23	0.20
NIR	LASTools	A	Road	1.24	0.00	0.04	0.04
NIR	LASTools	A	Burned High Regen	1.24	0.04	0.18	0.18
NIR	LASTools	A	Burned	1.24	0.02	0.15	0.15
NIR	LASTools	A	Burned Low Regen	1.24	0.01	0.10	0.10
NIR	LASTools	C	Unburned	1.24	0.10	0.22	0.20
NIR	LASTools	C	Road	1.24	0.00	0.04	0.04
NIR	LASTools	C	Burned High Regen	1.24	0.04	0.18	0.17
NIR	LASTools	C	Burned	1.24	0.02	0.14	0.14
NIR	LASTools	C	Burned Low Regen	1.24	0.01	0.10	0.10

NIR	LASTools	B	Unburned	1.24	0.09	0.21	0.19
NIR	LASTools	B	Road	1.24	0.00	0.04	0.04
NIR	LASTools	B	Burned High Regen	1.24	0.04	0.18	0.18
NIR	LASTools	B	Burned	1.24	0.02	0.14	0.14
NIR	LASTools	B	Burned Low Regen	1.24	0.01	0.10	0.10
NIR	LASTools	E	Unburned	1.24	0.10	0.22	0.19
NIR	LASTools	E	Road	1.24	0.00	0.04	0.04
NIR	LASTools	E	Burned High Regen	1.24	0.04	0.18	0.17
NIR	LASTools	E	Burned	1.24	0.02	0.14	0.14
NIR	LASTools	E	Burned Low Regen	1.24	0.01	0.10	0.10
NIR	LASTools	D	Unburned	1.24	0.10	0.22	0.20
NIR	LASTools	D	Road	1.24	0.00	0.04	0.04
NIR	LASTools	D	Burned High Regen	1.24	0.04	0.18	0.17
NIR	LASTools	D	Burned	1.24	0.02	0.14	0.14
NIR	LASTools	D	Burned Low Regen	1.24	0.01	0.10	0.10
NIR	LASTools	F	Unburned	1.28	0.11	0.23	0.20
NIR	LASTools	F	Road	1.28	0.00	0.04	0.04
NIR	LASTools	F	Burned High Regen	1.28	0.04	0.18	0.18
NIR	LASTools	F	Burned	1.28	0.02	0.14	0.14
NIR	LASTools	F	Burned Low Regen	1.28	0.01	0.10	0.10
NIR	LASTools	H	Unburned	1.30	0.11	0.23	0.21
NIR	LASTools	H	Road	1.30	0.00	0.04	0.04
NIR	LASTools	H	Burned High Regen	1.30	0.05	0.18	0.17
NIR	LASTools	H	Burned	1.30	0.02	0.14	0.14
NIR	LASTools	H	Burned Low Regen	1.30	0.01	0.09	0.09
NIR	LASTools	G	Unburned	1.30	0.11	0.23	0.20
NIR	LASTools	G	Road	1.30	0.00	0.04	0.04
NIR	LASTools	G	Burned High Regen	1.30	0.05	0.18	0.17
NIR	LASTools	G	Burned	1.30	0.02	0.14	0.14
NIR	LASTools	G	Burned Low Regen	1.30	0.01	0.09	0.09
NIR	LASTools	J	Unburned	1.31	0.11	0.23	0.20
NIR	LASTools	J	Road	1.31	0.00	0.04	0.04
NIR	LASTools	J	Burned High Regen	1.31	0.05	0.18	0.17
NIR	LASTools	J	Burned	1.31	0.02	0.14	0.14
NIR	LASTools	J	Burned Low Regen	1.31	0.01	0.09	0.09
NIR	LASTools	I	Unburned	1.30	0.11	0.23	0.20
NIR	LASTools	I	Road	1.30	0.00	0.04	0.04

NIR	LASTools	I	Burned High Regen	1.30	0.05	0.18	0.17
NIR	LASTools	I	Burned	1.30	0.02	0.14	0.14
NIR	LASTools	I	Burned Low Regen	1.30	0.01	0.09	0.09
Visible	LASTools	A	Unburned	1.30	0.17	0.26	0.20
Visible	LASTools	A	Road	1.30	0.01	0.05	0.05
Visible	LASTools	A	Burned High Regen	1.30	0.08	0.19	0.17
Visible	LASTools	A	Burned	1.30	0.06	0.15	0.14
Visible	LASTools	A	Burned Low Regen	1.30	0.03	0.09	0.09
Visible	LASTools	C	Unburned	1.30	0.17	0.26	0.20
Visible	LASTools	C	Road	1.30	0.01	0.05	0.05
Visible	LASTools	C	Burned High Regen	1.30	0.09	0.19	0.17
Visible	LASTools	C	Burned	1.30	0.06	0.15	0.14
Visible	LASTools	C	Burned Low Regen	1.30	0.03	0.09	0.09
Visible	LASTools	B	Unburned	1.30	0.16	0.26	0.20
Visible	LASTools	B	Road	1.30	0.01	0.05	0.05
Visible	LASTools	B	Burned High Regen	1.30	0.09	0.19	0.17
Visible	LASTools	B	Burned	1.30	0.06	0.15	0.14
Visible	LASTools	B	Burned Low Regen	1.30	0.03	0.09	0.09
Visible	LASTools	E	Unburned	1.30	0.16	0.26	0.20
Visible	LASTools	E	Road	1.30	0.01	0.05	0.05
Visible	LASTools	E	Burned High Regen	1.30	0.08	0.19	0.17
Visible	LASTools	E	Burned	1.30	0.06	0.15	0.14
Visible	LASTools	E	Burned Low Regen	1.30	0.03	0.09	0.09
Visible	LASTools	D	Unburned	1.30	0.17	0.26	0.20
Visible	LASTools	D	Road	1.30	0.01	0.05	0.05
Visible	LASTools	D	Burned High Regen	1.30	0.09	0.19	0.17
Visible	LASTools	D	Burned	1.30	0.06	0.15	0.14
Visible	LASTools	D	Burned Low Regen	1.30	0.03	0.09	0.09
Visible	LASTools	F	Unburned	1.32	0.17	0.26	0.20
Visible	LASTools	F	Road	1.32	0.00	0.05	0.05
Visible	LASTools	F	Burned High Regen	1.32	0.09	0.19	0.17
Visible	LASTools	F	Burned	1.32	0.06	0.15	0.14
Visible	LASTools	F	Burned Low Regen	1.32	0.03	0.09	0.09
Visible	LASTools	H	Unburned	1.33	0.17	0.26	0.20
Visible	LASTools	H	Road	1.33	0.00	0.05	0.05
Visible	LASTools	H	Burned High Regen	1.33	0.09	0.19	0.18
Visible	LASTools	H	Burned	1.33	0.06	0.15	0.14

Visible	LASTools	H	Burned Low Regen	1.33	0.03	0.09	0.09
Visible	LASTools	G	Unburned	1.33	0.17	0.26	0.20
Visible	LASTools	G	Road	1.33	0.00	0.05	0.05
Visible	LASTools	G	Burned High Regen	1.33	0.09	0.19	0.17
Visible	LASTools	G	Burned	1.33	0.06	0.15	0.14
Visible	LASTools	G	Burned Low Regen	1.33	0.03	0.09	0.09
Visible	LASTools	J	Unburned	1.33	0.17	0.26	0.20
Visible	LASTools	J	Road	1.33	0.00	0.05	0.05
Visible	LASTools	J	Burned High Regen	1.33	0.09	0.19	0.17
Visible	LASTools	J	Burned	1.33	0.06	0.15	0.14
Visible	LASTools	J	Burned Low Regen	1.33	0.03	0.09	0.09
Visible	LASTools	I	Unburned	1.33	0.17	0.26	0.20
Visible	LASTools	I	Road	1.33	0.00	0.05	0.05
Visible	LASTools	I	Burned High Regen	1.33	0.09	0.19	0.17
Visible	LASTools	I	Burned	1.33	0.06	0.15	0.14
Visible	LASTools	I	Burned Low Regen	1.33	0.03	0.09	0.09
SWIR & NIR	LASTools	A	Unburned	2.41	0.11	0.23	0.20
SWIR & NIR	LASTools	A	Road	2.41	0.00	0.05	0.05
SWIR & NIR	LASTools	A	Burned High Regen	2.41	0.03	0.18	0.18
SWIR & NIR	LASTools	A	Burned	2.41	0.01	0.14	0.14
SWIR & NIR	LASTools	A	Burned Low Regen	2.41	0.02	0.10	0.10
SWIR & NIR	LASTools	A	Unburned	2.41	0.10	0.22	0.19
SWIR & NIR	LASTools	C	Road	2.41	0.00	0.04	0.04
SWIR & NIR	LASTools	C	Burned High Regen	2.41	0.03	0.18	0.18
SWIR & NIR	LASTools	C	Burned	2.41	0.01	0.14	0.14
SWIR & NIR	LASTools	C	Burned Low Regen	2.41	0.02	0.10	0.09
SWIR & NIR	LASTools	B	Unburned	2.40	0.11	0.22	0.19
SWIR & NIR	LASTools	B	Road	2.40	0.00	0.05	0.05
SWIR & NIR	LASTools	B	Burned High Regen	2.40	0.03	0.18	0.18
SWIR & NIR	LASTools	B	Burned	2.40	0.01	0.14	0.14
SWIR & NIR	LASTools	B	Burned Low Regen	2.40	0.02	0.10	0.09
SWIR & NIR	LASTools	E	Unburned	2.42	0.11	0.23	0.20
SWIR & NIR	LASTools	E	Road	2.42	0.00	0.05	0.05
SWIR & NIR	LASTools	E	Burned High Regen	2.42	0.03	0.18	0.18
SWIR & NIR	LASTools	E	Burned	2.42	0.01	0.14	0.14
SWIR & NIR	LASTools	E	Burned Low Regen	2.42	0.02	0.09	0.09
SWIR & NIR	LASTools	D	Unburned	2.41	0.11	0.22	0.20

SWIR & NIR	LASTools	D	Road	2.41	0.00	0.05	0.05
SWIR & NIR	LASTools	D	Burned High Regen	2.41	0.03	0.18	0.18
SWIR & NIR	LASTools	D	Burned	2.41	0.01	0.14	0.14
SWIR & NIR	LASTools	D	Burned Low Regen	2.41	0.02	0.09	0.09
SWIR & NIR	LASTools	F	Unburned	2.58	0.11	0.23	0.20
SWIR & NIR	LASTools	F	Road	2.58	0.00	0.05	0.05
SWIR & NIR	LASTools	F	Burned High Regen	2.58	0.04	0.18	175.00
SWIR & NIR	LASTools	F	Burned	2.58	0.02	0.14	0.14
SWIR & NIR	LASTools	F	Burned Low Regen	2.58	0.02	0.09	0.09
SWIR & NIR	LASTools	H	Unburned	2.60	0.11	0.23	0.20
SWIR & NIR	LASTools	H	Road	2.60	0.00	0.05	0.05
SWIR & NIR	LASTools	H	Burned High Regen	2.60	0.04	0.18	0.17
SWIR & NIR	LASTools	H	Burned	2.60	0.02	0.14	0.14
SWIR & NIR	LASTools	H	Burned Low Regen	2.60	0.01	0.09	0.09
SWIR & NIR	LASTools	G	Unburned	2.60	0.11	0.23	0.20
SWIR & NIR	LASTools	G	Road	2.60	0.00	0.05	0.05
SWIR & NIR	LASTools	G	Burned High Regen	2.60	0.04	0.18	0.17
SWIR & NIR	LASTools	G	Burned	2.60	0.02	0.14	0.14
SWIR & NIR	LASTools	G	Burned Low Regen	2.60	0.01	0.09	0.09
SWIR & NIR	LASTools	J	Unburned	2.61	0.11	0.23	0.20
SWIR & NIR	LASTools	J	Road	2.61	0.00	0.05	0.05
SWIR & NIR	LASTools	J	Burned High Regen	2.61	0.04	0.18	0.18
SWIR & NIR	LASTools	J	Burned	2.61	0.02	0.14	0.14
SWIR & NIR	LASTools	J	Burned Low Regen	2.61	0.01	0.09	0.09
SWIR & NIR	LASTools	I	Unburned	2.61	0.11	0.23	0.20
SWIR & NIR	LASTools	I	Road	2.61	0.00	0.05	0.05
SWIR & NIR	LASTools	I	Burned High Regen	2.61	0.04	0.18	0.18
SWIR & NIR	LASTools	I	Burned	2.61	0.02	0.14	0.14
SWIR & NIR	LASTools	I	Burned Low Regen	2.61	0.02	0.09	0.09
SWIR, NIR & Visible	LASTools	A	Unburned	3.36	0.11	0.24	0.21
SWIR, NIR & Visible	LASTools	A	Road	3.36	0.00	0.05	0.05
SWIR, NIR & Visible	LASTools	A	Burned High Regen	3.36	0.04	0.18	0.18
SWIR, NIR & Visible	LASTools	A	Burned	3.36	0.01	0.15	0.14
SWIR, NIR & Visible	LASTools	A	Burned Low Regen	3.36	0.02	0.10	0.10

SWIR, NIR & Visible	LASTools	C	Unburned	3.34	0.12	0.23	0.20
SWIR, NIR & Visible	LASTools	C	Road	3.34	0.00	0.05	0.05
SWIR, NIR & Visible	LASTools	C	Burned High Regen	3.34	0.04	0.18	0.18
SWIR, NIR & Visible	LASTools	C	Burned	3.34	0.02	0.14	0.14
SWIR, NIR & Visible	LASTools	C	Burned Low Regen	3.34	0.01	0.10	0.10
SWIR, NIR & Visible	LASTools	B	Unburned	3.34	0.12	0.23	0.20
SWIR, NIR & Visible	LASTools	B	Road	3.34	0.00	0.05	0.05
SWIR, NIR & Visible	LASTools	B	Burned High Regen	3.34	0.04	0.18	0.18
SWIR, NIR & Visible	LASTools	B	Burned	3.34	0.02	0.14	0.14
SWIR, NIR & Visible	LASTools	B	Burned Low Regen	3.34	0.01	0.09	0.09
SWIR, NIR & Visible	LASTools	E	Unburned	3.35	0.12	0.23	0.20
SWIR, NIR & Visible	LASTools	E	Road	3.35	0.00	0.05	0.05
SWIR, NIR & Visible	LASTools	E	Burned High Regen	3.35	0.04	0.18	0.17
SWIR, NIR & Visible	LASTools	E	Burned	3.35	0.02	0.14	0.14
SWIR, NIR & Visible	LASTools	E	Burned Low Regen	3.35	0.01	0.10	0.10
SWIR, NIR & Visible	LASTools	D	Unburned	3.35	0.12	0.23	0.20
SWIR, NIR & Visible	LASTools	D	Road	3.35	0.00	0.05	0.05
SWIR, NIR & Visible	LASTools	D	Burned High Regen	3.35	0.04	0.18	0.18
SWIR, NIR & Visible	LASTools	D	Burned	3.35	0.02	0.14	0.14
SWIR, NIR & Visible	LASTools	D	Burned Low Regen	3.35	0.01	0.10	0.09
SWIR, NIR & Visible	LASTools	F	Unburned	3.70	0.12	0.24	0.20
SWIR, NIR & Visible	LASTools	F	Road	3.70	0.00	0.05	0.05
SWIR, NIR & Visible	LASTools	F	Burned High Regen	3.70	0.05	0.18	0.18

SWIR, NIR & Visible	LASTools	F	Burned	3.70	0.03	0.15	0.14
SWIR, NIR & Visible	LASTools	F	Burned Low Regen	3.70	0.00	0.09	0.09
SWIR, NIR & Visible	LASTools	H	Unburned	3.71	0.12	0.24	0.20
SWIR, NIR & Visible	LASTools	H	Road	3.71	0.00	0.05	0.05
SWIR, NIR & Visible	LASTools	H	Burned High Regen	3.71	0.06	0.18	0.17
SWIR, NIR & Visible	LASTools	H	Burned	3.71	0.03	0.14	0.14
SWIR, NIR & Visible	LASTools	H	Burned Low Regen	3.71	0.00	0.09	0.09
SWIR, NIR & Visible	LASTools	G	Unburned	3.70	0.12	0.24	0.20
SWIR, NIR & Visible	LASTools	G	Road	3.70	0.00	0.05	0.05
SWIR, NIR & Visible	LASTools	G	Burned High Regen	3.70	0.06	0.18	0.17
SWIR, NIR & Visible	LASTools	G	Burned	3.70	0.03	0.14	0.14
SWIR, NIR & Visible	LASTools	G	Burned Low Regen	3.70	0.00	0.09	0.09
SWIR, NIR & Visible	LASTools	J	Unburned	3.72	0.12	0.24	0.21
SWIR, NIR & Visible	LASTools	J	Road	3.72	0.00	0.05	0.05
SWIR, NIR & Visible	LASTools	J	Burned High Regen	3.72	0.06	0.18	0.17
SWIR, NIR & Visible	LASTools	J	Burned	3.72	0.03	0.14	0.14
SWIR, NIR & Visible	LASTools	J	Burned Low Regen	3.72	0.00	0.09	0.09
SWIR, NIR & Visible	LASTools	I	Unburned	3.71	0.12	0.24	0.20
SWIR, NIR & Visible	LASTools	I	Road	3.71	0.00	0.05	0.05
SWIR, NIR & Visible	LASTools	I	Burned High Regen	3.71	0.05	0.18	0.17
SWIR, NIR & Visible	LASTools	I	Burned	3.71	0.03	0.14	0.14
SWIR, NIR & Visible	LASTools	I	Burned Low Regen	3.71	0.00	0.09	0.09

Supplementary material Chapter 4

Table S4.1. List of candidate covariates with scales and thresholds included in Random Forest and Generalized Additive Model frameworks prior to backwards selection.

Category	Variable	Scales / height thresholds (m)
Canopy cover (lidar; 5 m)	Canopy cover	Minimum height: 1.37, 5, 10
Vegetation structural distribution (lidar; 20 m)	Height: standard deviation	Minimum height: 0.2, 0.5, 1.37, 5
	Height: skewness	Minimum height: 0.2, 0.5, 1.37, 5
	Height: kurtosis	Minimum height: 0.2, 0.5, 1.37, 5
	Height: maximum	Minimum height: 0.2, 0.5, 1.37, 5
	Height: average	Minimum height: 0.2, 0.5, 1.37, 5
	Height: P95	Minimum height: 0.2, 0.5, 1.37, 5
	Height: P75	Minimum height: 0.2, 0.5, 1.37, 5
	Height: P50	Minimum height: 0.2, 0.5, 1.37, 5
	Height: P25	Minimum height: 0.2, 0.5, 1.37, 5
Topography (lidar DEM; 5 m)	Slope	Scales: 5, 10, 100
	Aspect	Scales: 5, 10, 100
	Topographic Position Index (TPI)	Scales: 5, 10, 15, 20, 30, 50, 60, 75, 100, 150, 500
Hydrology (AB DEM; 25 m)	Flow accumulation	25, 75, 125, 250
	Topographic Wetness Index (TWI)	75, 125, 250
Landscape positioning	Distance to peatland edge	—
	Distance to nearest road	—
	Distance to nearest seismic line	—
	Distance to nearest cut line	—
	Distance to nearest industrial site	—
	Distance to nearest industrial water source	—
	Distance to nearest linear hydrological feature	—
	Distance to Gregoire Lake	—
Peatland morphology	Peatland perimeter length	—
	Peatland area	—
	Peatland length:area ratio	—
Fire weather indices	Fire Weather Index (FWI)	Scale: 90
	Duff Moisture Code (DMC)	Scale: 90
	Drought Code (DC)	Scale: 90

Category	Variable	Scales / height thresholds (m)
	Fine Fuel Moisture Code (FFMC)	Scale: 90
	Day of Burn	Scale: 90
	Buildup Index (BUI)	Scale: 90
	Initial Spread Index (ISI)	Scale: 90
	Normalized Difference Moisture Index (NDMI)	Scale: 30
Vegetation & moisture indices	Normalized Difference Vegetation Index (NDVI)	Scale: 30
	Modified NDWI (MNDWI)	Scale: 30

Table S4.2. Base seeds used for RF model runs during model parameterization, backwards selection, and model stability checks.

Run #	Seed
1	42
2	1000
3	3600
4	2025
5	5555
6	7
7	44
8	77
9	44444
10	51991

Table S4.3. RF parameters used in initial backwards selection runs and in final model runs.

Parameter	Bog-Initial	Bog-Final	Fen-Initial	Fen-Final	Swamp-Initial	Swamp-Final
Number of trees	1500	1500	1000	1500	1000	1500
Max. tree depth	20	None	25	25	23	20
Min. samples to split	2	2	2	2	2	2
Min. samples in leaf	2	1	2	2	2	2
Max. features for splits	15	sqrt	25	sqrt	15	4
Bootstrap	True	True	True	True	True	True
Min. impurity decrease	0	1e-07	0	1e-07	0	1e-06
Max. samples	None	None	None	0.9	None	None

Table S4.4. Hierarchical partitioning of covariates included in the final bog GAM from hp.gam

Predictor	Rank	% Contribution
Slope (100 m resolution)	1	23.02
Distance to peatland edge (m)	2	20.63
Peatland area (m^2)	3	11.96
Aspect (100 m resolution)	4	9.72
Vegetation height – p50 (m)	5	8.07
Peatland perimeter length (m)	6	7.47
DMC	7	5.23
Distance to industrial water (m)	8	4.63
Vegetation height – p25 (m)	9	2.99
Vegetation height – standard deviation (m)	10	2.99
Slope (10 m resolution)	11	1.49
Distance to linear hydrological features (m)	12	1.49
TPI (100 m)	13	0.30

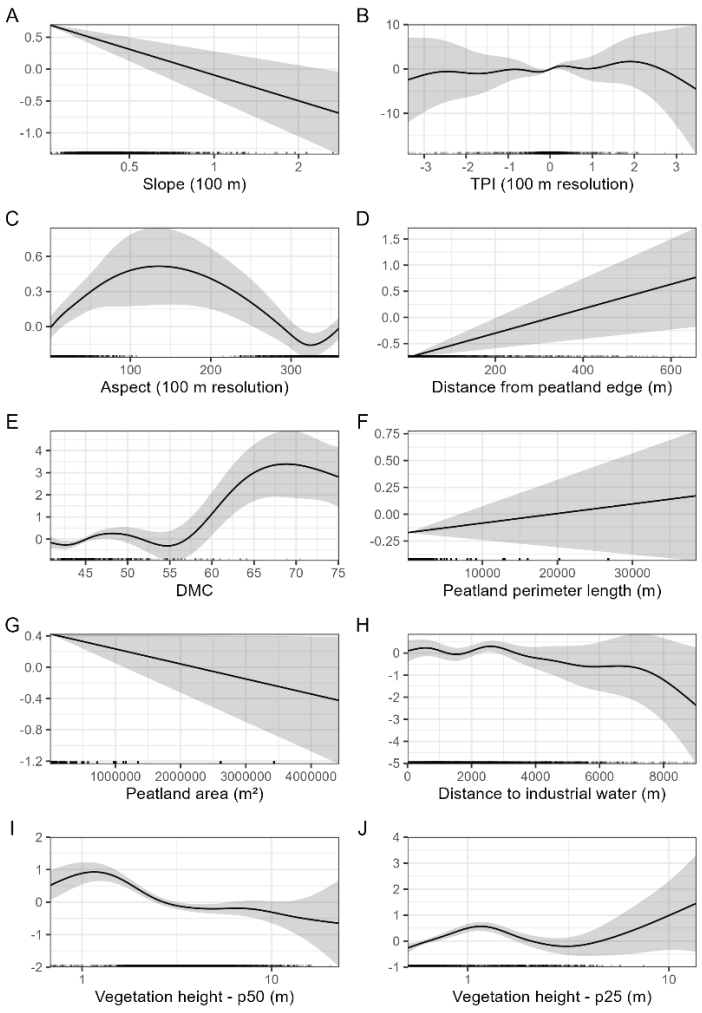

Figure S4.1. Partial-effects plots of covariate smooths retained in the final bog GAM, showing the influence of each covariate on depth of burn (link scale). Shaded regions show 95% confidence intervals.

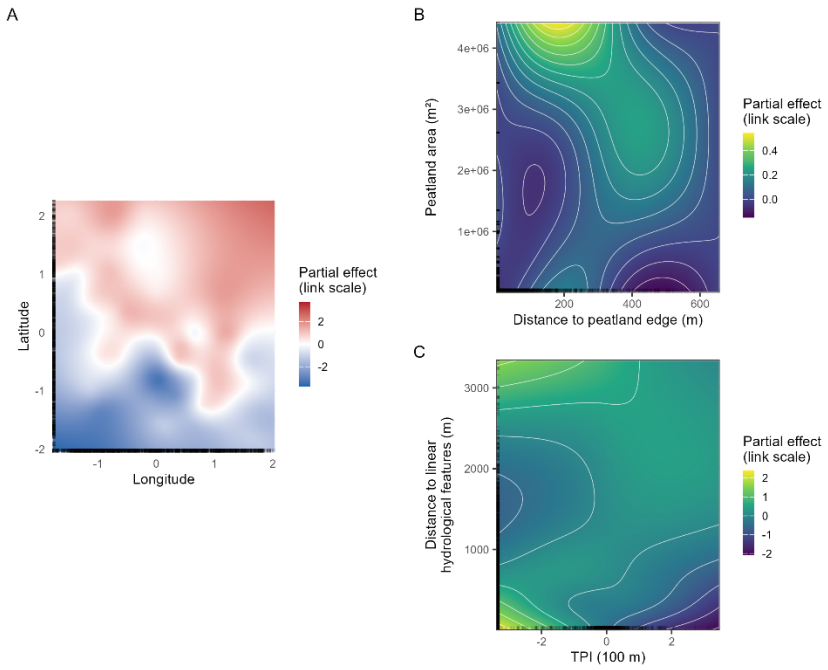

Figure S4.2. Partial-effects plots of spatial covariates and interaction terms retained in the final bog GAM.

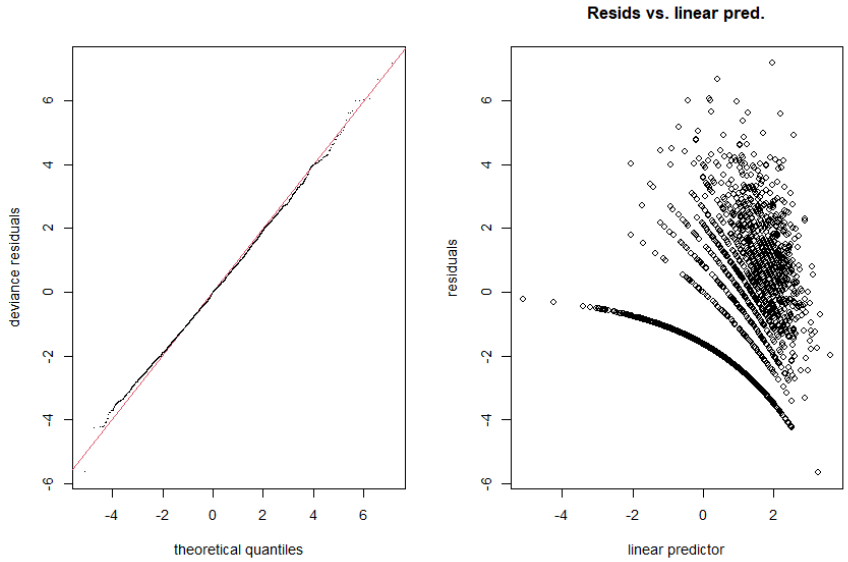

Figure S4.3. Diagnostic plots for bog GAM from gam.check(). a) shows the QQ plot of deviance residuals vs. theoretical quantiles; b) plots residuals vs. linear predictor.

Table S4.5. Hierarchical partitioning of covariates included in the final fen GAM from hp.gam

Predictor	Rank	% Contribution
NDVI	1	46.59
Distance to nearest seismic line (m)	2	22.30
Vegetation height – p50 (m)	3	7.65
Aspect (100 m resolution)	4	7.15
Length:area ratio	5	4.16
NDMI	6	3.00
Distance to nearest road (m)	7	2.83
Distance to nearest cutline (m)	8	2.50
FFMC	9	2.33
Flow Accumulation (250 m resolution)	10	0.83
TPI (30 m resolution)	11	0.67

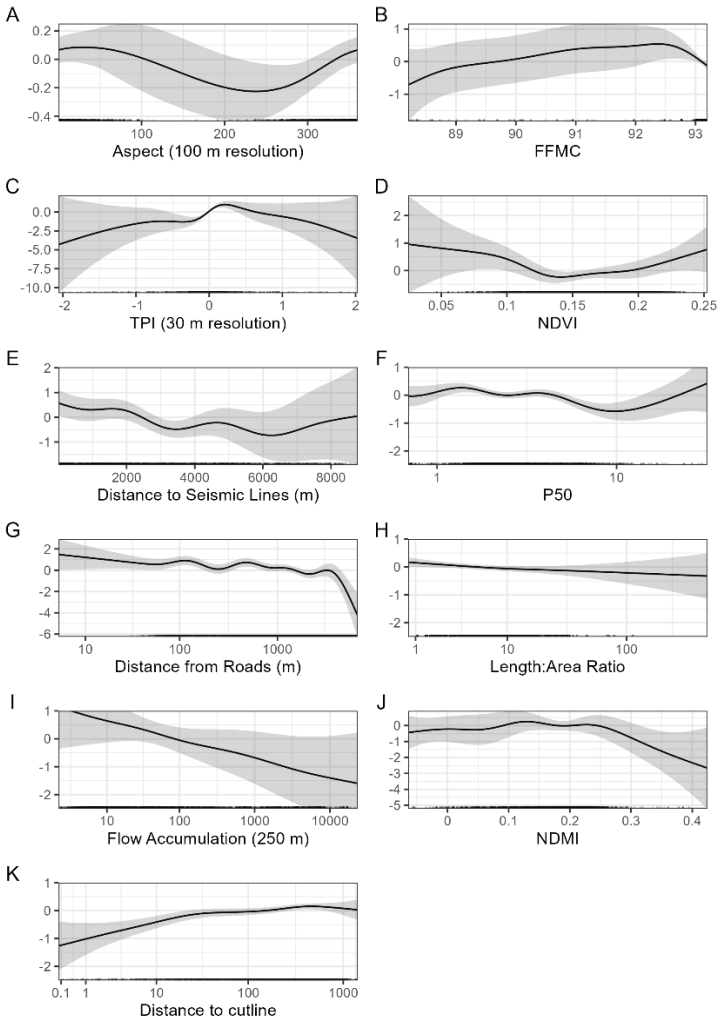

Figure S4.4. Partial-effects plots of covariate smooths retained in the final fen GAM, showing the influence of each covariate on depth of burn (link scale). Shaded regions show 95% confidence intervals.

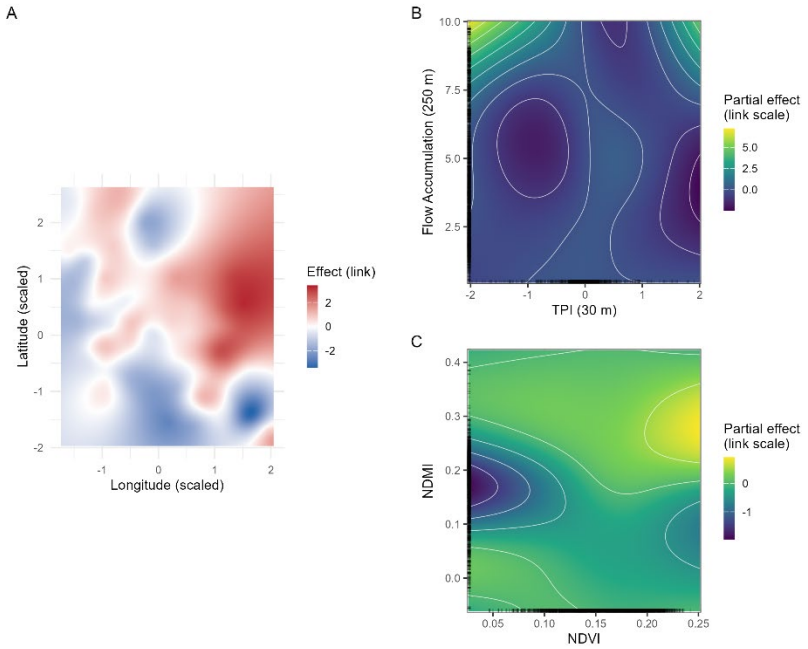

Figure S4.5. Partial-effects plots of spatial covariates and interaction terms retained in the final fen GAM.

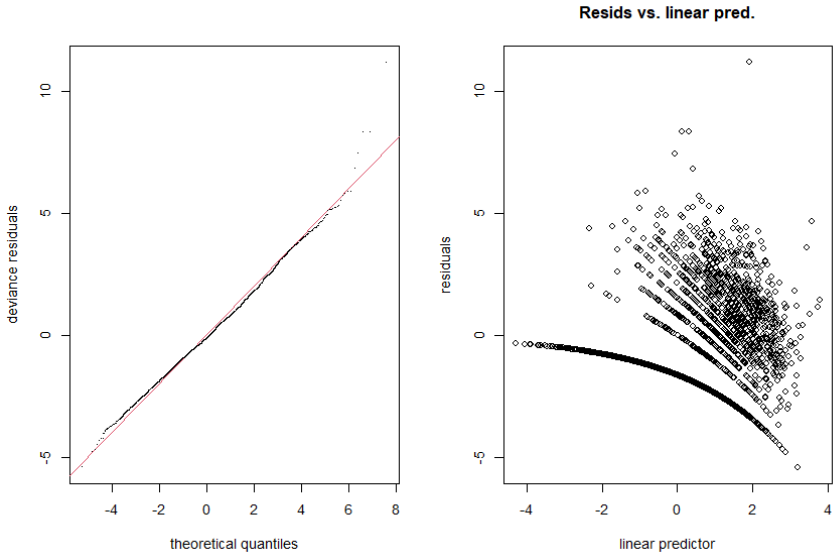

Figure S4.6. Diagnostic plots for fen GAM from gam.check(). a) shows the QQ plot of deviance residuals vs. theoretical quantiles; b) plots residuals vs. linear predictor.

Table S4.6. Hierarchical partitioning of covariates included in the final swamp GAM from hp.gam

Predictor	Rank	% Contribution
MNDWI	1	28.62
Vegetation height – p25 (m)	2	23.08
Distance to linear hydrological feature (m)	3	9.33
TPI (10 m resolution)	4	8.00
Distance to nearest road (m)	5	7.90
Distance to nearest seismic line (m)	6	6.87
Length:area ratio	7	5.23
Peatland area (m^2)	8	3.49
TPI (20 m resolution)	9	3.08
Slope (10 m resolution)	10	2.77
TPI (500 m resolution)	11	1.23
Distance to nearest cutline	12	0.41

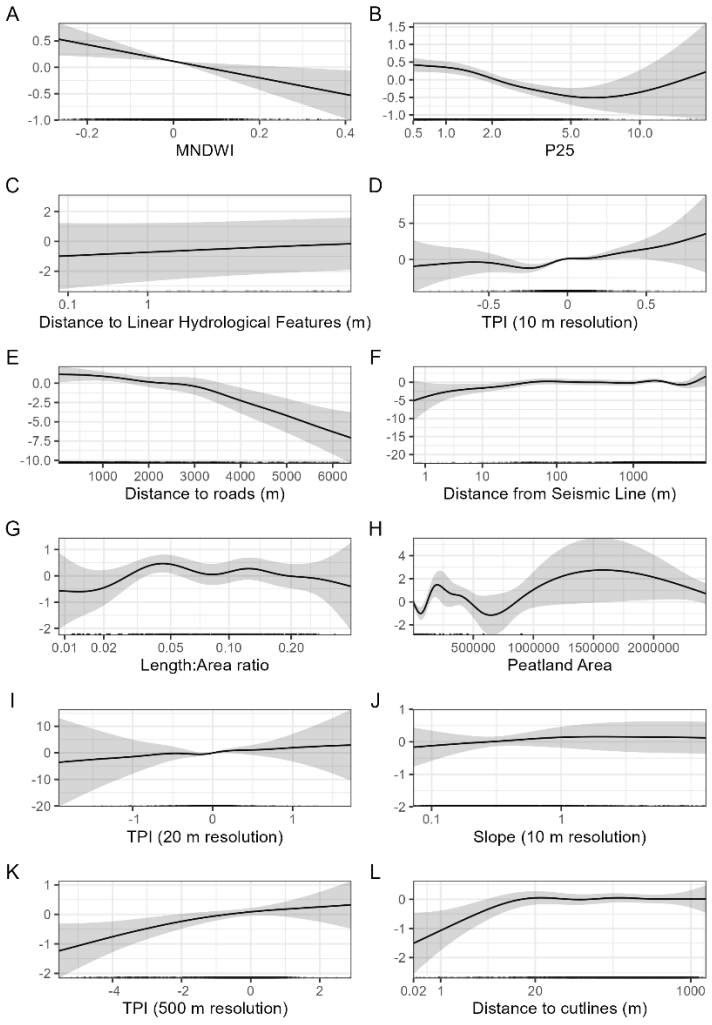

Figure S4.7. Partial-effects plots of covariate smooths retained in the final swamp GAM, showing the influence of each covariate on depth of burn (link scale). Shaded regions show 95% confidence intervals.

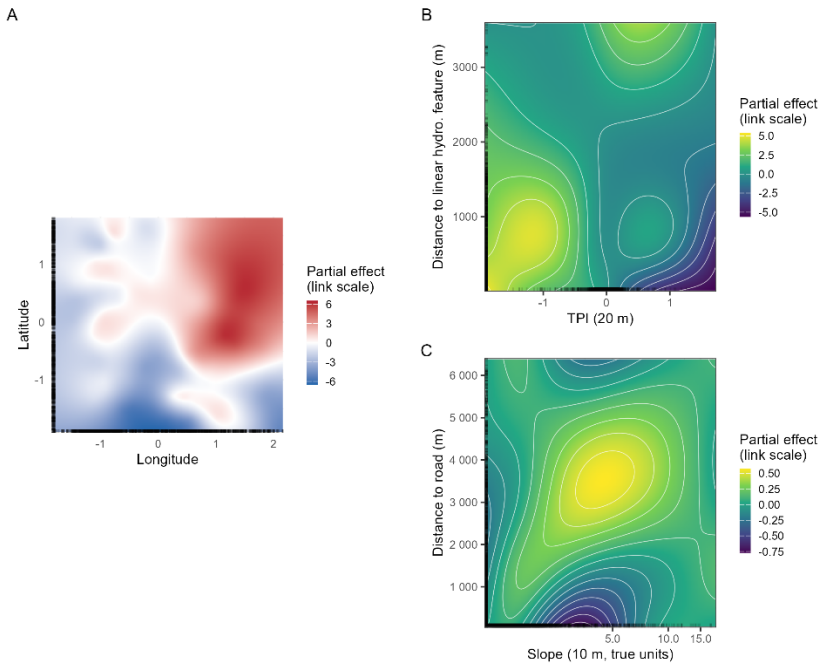

Figure S4.8. Partial-effects plots of spatial covariates and interaction terms retained in the final bog GAM.

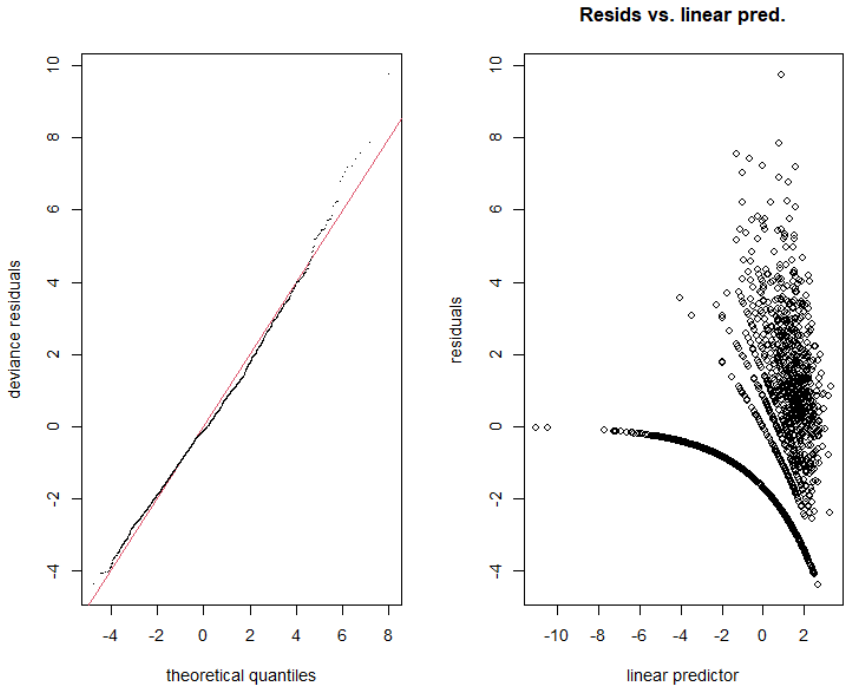

Figure S4.9. Diagnostic plots for swamp GAM from gam.check(). a) shows the QQ plot of deviance residuals vs. theoretical quantiles; b) plots residuals vs. linear predictor.

Supplementary Text:

Bog <- gam(DOB_cm ~ s(merged_0_5_std, bs = "tp") + s(log_05_p50, bs = "tp") + s(log_02_p25, bs = "tp") + s(TPI100, bs = "tp") + s(Aspect_100m, bs = "cc") + s(Slope_10m, bs = "tp") + Slope_100m + NEAR_DIST + s(NEAR_IndWater_Scaled, bs = "tp") + s(DMC, bs = "tp") + Length_Geo + Area_Geo + te(NEAR_DIST, Area_Geo, bs="tp") + te(TPI100, LinearHydro_Dist) + s(Lat_scale, Long_scale, bs="gp", k = 60, m=2), family = tw(link = "log"), data = bog_data, knots = list(Aspect_100m = c(0,360)), method = "REML")

Fen <- gam(DOB_cm ~ s(Aspect_100m, bs = "cc", k=10) + s(log_05_p50, bs = "tp") + s(log_NEAR_ROADS, bs = "tp") + s(scale_NEAR_SeismicLine, bs = "tp") + s(log_NEAR_CutLine, bs = "tp") + s(FFMC, bs = "tp") + s(TPI30, bs = "tp") + s(NDMI, bs = "tp") + s(NDVI, bs = "tp") + te(TPI30, LogFlowAc_250m, bs="tp") + s(log_LengthAreaRatio_2x100, bs = "tp") + s(LogFlowAc_250m, bs = "tp") + te(NDVI, NDMI, bs="tp") + s(Lat_scale, Long_scale, bs="gp", k = 60, m=2), family = tw(link = "log"), data = fen_data, knots = list(Aspect_100m = c(0,360)), method = "REML")

Swamp <- gam(DOB_cm ~ s(log_LengthAreaRatio_2x100, bs = "tp") + s(log_05_p25, bs = "tp") + s(scale_NEAR_ROADS, bs = "tp") + s(log_NEAR_SeismicLine, bs = "tp") +

s(LogSlope_10m, bs = "tp") + s(log_NEAR_CutLine, bs = "tp") + s(TPI20, bs = "tp") + s(TPI_10, bs = "tp") + s(TPI500, bs = "tp") + s(scale_Area_Geo, bs = "tp") + te(TPI20, LinearHydro_Dist, bs="tp") + te(LogSlope_10m, scale_NEAR_ROADS, bs="tp") + MNDWI + s(log_LinearHydro_Dist, bs = "tp") + s(Lat_scaled, Long_scaled, bs="gp", k = 60, m=2), family = tw(link = "log"), data = swamp_data, method = "REML")

Supplementary material Chapter 5

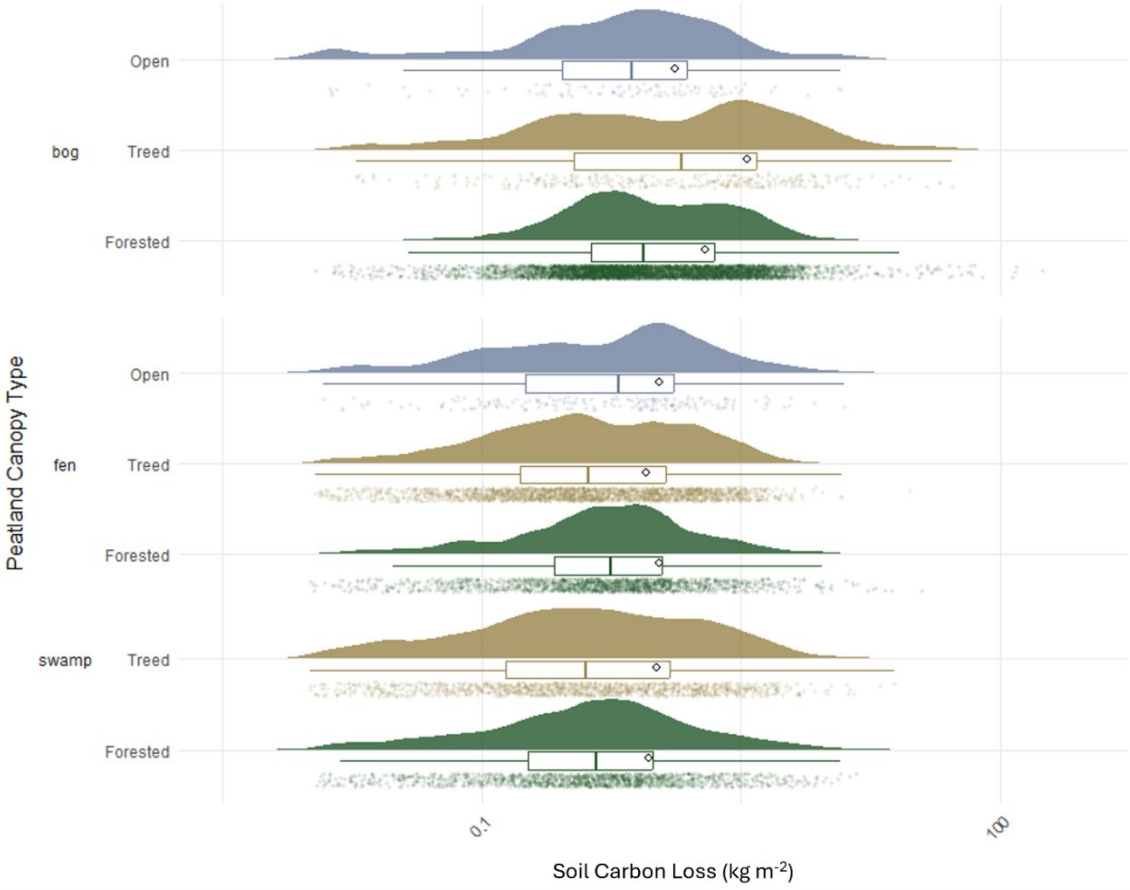

Supplementary Figure S5.1: Distribution of soil C loss (kg m^{-2}) in combined core-ecotone peatlands by peatland type and canopy type as defined by CaMP. Half violins show point distribution, boxplots show interquartile range with whiskers to 5th and 95th percentiles, and points show individual values. Means are denoted by black circles embedded in boxplots. Sample sizes (n) for each peatland-canopy combination range from 101 to5748. X-axis is on a $\log_{10}$ scale.